National Library
of Canada

Acquisitions and
Bibliographic Services Branch

395 Wellington Street
Ottawa, Ontario
K1A 0N4

Bibliothèque nationale
du Canada

Direction des acquisitions et
des services bibliographiques

395, rue Wellington
Ottawa (Ontario)
K1A 0N4

Your file Votre référence

Our file Notre référence

NOTICE

The quality of this microform is heavily dependent upon the quality of the original thesis submitted for microfilming. Every effort has been made to ensure the highest quality of reproduction possible.

If pages are missing, contact the university which granted the degree.

Some pages may have indistinct print especially if the original pages were typed with a poor typewriter ribbon or if the university sent us an inferior photocopy.

AVIS

La qualité de cette microforme dépend grandement de la qualité de la thèse soumise au microfilmage. Nous avons tout fait pour assurer une qualité supérieure de reproduction.

S'il manque des pages, veuillez communiquer avec l'université qui a conféré le grade.

La qualité d'impression de certaines pages peut laisser à désirer, surtout si les pages originales ont été dactylographiées à l'aide d'un ruban usé ou si l'université nous a fait parvenir une photocopie de qualité inférieure.

Canada

Development of Triplet Excited State Probes for Organized Media

by

Ronald Boch

A thesis presented to the

School of Graduate Studies and Research

In partial fulfillment for the degree of

Doctor of Philosophy

In the Ottawa-Carleton Chemistry Institute

Department of Chemistry

University of Ottawa

Ottawa, Ontario

Canada

UNIVERSITÉ D'OTTAWA  UNIVERSITY OF OTTAWA

National Library
of Canada

Acquisitions and
Bibliographic Services Branch

395 Wellington Street
Ottawa, Ontario
K1A 0N4

Bibliothèque nationale
du Canada

Direction des acquisitions et
des services bibliographiques

395, rue Wellington
Ottawa (Ontario)
K1A 0N4

Your file Votre référence

Our file Notre référence

ISBN 0-612-07792-6

Canada

UNIVERSITÉ D'OTTAWA
UNIVERSITY OF OTTAWA

Acknowledgements

I would like to thank all the people who assisted me during my graduate studies, especially my Ph. D. supervisor, Tito Scaiano. It was through his supervision that I was able to achieve much more than what has been written in these pages. He is truly an outstanding supervisor.

I would also like to thank the many people who I have collaborated with in the chemistry and biology departments. In particular, I would like to thank Dr. Arnason, Dr. Durst, Dr. J.C. Bradley, Yvonne Lear, Dr. Mike Whittlesey, Nadereh Mohtat and Terry Connolly for their help in rewarding and enjoyable projects over the past few years. Thanks also to Dr. Alex Fallis for convincing me to switch from biochemistry to chemistry and continue onto graduate studies. I would also like to thank Eco-Research, Stentor, Pestcon and the Ontario Graduate Fellowships for financial support over the past several years.

I would also like to thank the many people who I have worked along side with in Tito's lab over the past few years. In particular, thanks to Dr. Monica Barra who showed me the way and to Dr. Cornelia Bohne who helped me in the early stages of my graduate studies. Thanks also to Carolyn Moorlog and Krista Stefaniak whom I had the opportunity to supervise; I think I learned as much as they did. Thanks to Alain Berinstain and André Simard for keeping the laser system going; also Corinne Bensimon for the X-ray analysis, Glen Facey and Raj Capoor for the NMR studies.

I am also truly grateful to Erika, whose support has added immeasurably to every aspect of my life. I am also grateful to my family, especially my mother who have guided me through the many decisions that have brought me to this point. This thesis is dedicated to my father, who has inspired me in ways he will never know.

Table of Contents

List of Tables

List of Schemes

List of Figures

List of Abbreviations

RTP	=	room temperature phosphorescence
LFP	=	laser flash photolysis
isc	=	intersystem crossing
IR	=	infrared
PMT	=	photomultiplier tube
ΔOD	=	change in optical density
I_o	=	light intensity of the monitoring beam (transmission)
ε	=	extinction coefficient
Δr	=	change in reflectance
J_o	=	light intensity of the monitoring beam (diffuse reflectance)
ΔJ	=	change in reflectance after excitation
$O_2(^1\Delta_g)$	=	singlet oxygen
Φ_Δ	=	singlet oxygen quantum yield
GC	=	gas chromatography
MM2	=	molecular modeling (version 2)
CAChe	=	computer aided chemistry
MMX	=	molecular modeling calculations
Bz	=	*p*-methoxybenzoyl group
CD	=	cyclodextrin
GC-MS	=	gas chromatography - mass spectrometry
NMR	=	nuclear magnetic resonance
TLC	=	thin layer chromatography
TBDMS	=	tetrabutyldimethylsilyl
DMF	=	dimethylformamide
THF	=	tetrahydrofuran

m.p.	=	melting point
β-MCD	=	hepatikis (2,6-di-O-methyl)-β-cyclodextrin
α-GAV	=	α-guaiacoxyacetoveratrone
DMSO	=	dimethyl sulfoxide
SCh	=	sodium cholate
CTAB	=	cetyltrimethylammonium bromide
α-T	=	α-terthienyl
SDS	=	sodium dodecyl sulfate
e^-_{aq}	=	solvated electron
UV	=	ultraviolet
K	=	equilibrium constant
k	=	rate constant
ESR	=	electron spin resonance
ppm	=	parts per million
ppb	=	parts per billion
BSA	=	bovine serum albumin

Abstract

This thesis describes the detailed evaluation of using triplet excited states of *p*-methoxypropiophenone derivatives (**I-VI**) to probe organized media both in the solid state and in solution. The ketone triplets decay by intramolecular charge transfer β-aryl quenching of the excited carbonyl and show a high sensitivity to conformational constraints imposed by substituents or by the surrounding environment. The experience acquired with the ketone probes proved useful also in the study of α-terthienyl in protein environments, where the same type of techniques were applied.

Preliminary experiments with chiral derivatives of these triplet ketone probes in solution, showed that methyl substitution at the β-methylene position (which is not a participant in the deactivation mechanism) causes a dramatic decrease in the triplet lifetime. Further investigation with molecular mechanics calculations revealed that this effect is attributed to conformational preferences imposed by the added substituents. Methyl substitution in the β-aryl ring affects the ease of oxidation of this ring and as a result induces changes in the kinetics for intramolecular charge transfer. This conclusion is further supported by cyclic voltammetry experiments. In the solid state, X-ray structures show that the charge transfer interaction provides also an efficient mode of deactivation for the β-methylene substituted ketones but not in the unsubstituted one which crystallizes in a stretched conformation. In the case of *p*-methoxy-β-phenylbutyrophenone (**II**), the triplet lifetime in the solid state is 420 ns for the pure R and S enantiomers but 733 ns for the racemic crystals, showing an interesting case of chiral discrimination.

Powder X-ray and solid state NMR data suggest that conformational and packing differences between the enantiomers and racemic crystals are responsible for differences in the efficiency of intramolecular deactivation.

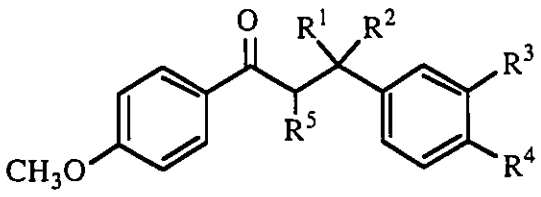

I: $R_1=R_2=R_3=R_4=R_5=H$

II: $R_1=CH_3$; $R_2=R_3=R_4=R_5=H$

III: $R_1=R_2=CH_3$; $R_3=R_4=R_5=H$

IV: $R_1=R_2=R_4=R_5=H$; $R_3=CH_3$

V: $R_1=R_2=R_3=R_5=H$; $R_4=CH_3$

VI: $R_1=R_2=R_3=R_4=H$; $R_5=OH$

Incorporation of these probes into chiral hosts such as cyclodextrins and cholate micelles lengthen the triplet lifetimes by restricting the movement of the β-phenyl ring and thus slowing down the intramolecular deactivation process. Studies using these methyl substituted ketone probes (**I-III**) in cyclodextrins provided information on intracavity mobility, inclusion geometries, and generally on the importance of steric factors in the formation and stability of cyclodextrin complexes. Intramolecular quenching, characteristic of these probes, provides further information on specific stereochemical constraints in CD complexes and magnifies the effects observed in homogeneous solution. Solid CD inclusion complexes were also prepared and the triplet behavior observed in the solid state was compared to solution. The inclusion complexes show a significant preference for inclusion of (R) *p*-methoxy-β-phenylbutyrophenone (**II**) over the S enantiomer, however this is not reflected in their respective triplet decay kinetics, either in solution or in the solid state.

In anionic micelles, the ketone probes undergo two-photon photoionization under conditions of pulsed laser excitation. Both SDS and sodium cholate micelles promoted charge separation and led to hydrated electrons (e^-_{aq}) that could be readily detected by their absorption at $\lambda > 600$ nm and through its reactions with oxygen and nitrous oxide. The lifetimes of e^-_{aq} were determined by small concentrations of aromatic ketone in the aqueous phase in equilibrium with the micelle solubilized ketone.

In the chapter 6 of this thesis, the triplet behavior of α-terthienyl photosensitizers conjugated to bovine serum albumin (BSA) was investigated. The protein conjugates were to serve as models for antibody conjugates for elucidating insect resistance to pesticides. The conjugates were prepared with varying amounts of sensitizer attached to the protein. Oxygen quenching of the conjugated α-terthienyl triplet states is approximately an order of magnitude slower in the protein environment compared to homogeneous solution. However, relatively high yields of singlet oxygen are still observed after photo-excitation of the sensitizer.

Chapter 1. Introduction

Triplet States in Microheterogeneous Environments

The study of inclusion compounds in which a guest is incorporated into a host has been traditionally carried out to gain information about the host, guest or both.[1-3] Compared to homogeneous solution, these organized assemblies have been shown to control and modify chemical reactivity and remain an area of considerable investigation.[4-6] Of particular interest to investigators are host-guest systems such as enzymes or cells and their substrates. Unfortunately, the complexity of these structures makes the study of these environments rather complex. As a result, models are used to try to best imitate these environments by eliminating many of the complexities while preserving their overall properties. This makes it possible to draw conclusions from the behavior observed and better understand the processes taking place, before attempting to probe the parent structures which the host models were originally developed to mimic.

Spectroscopic techniques have long been used as a tool to monitor guest probe molecules in a host environment. Traditionally, fluorescence has been used in which the host's or guest's fluorescent properties change upon complexation. Shifts in absorption and emission maxima, or changes in their fluorescent decay kinetics have proven to be very powerful tools, especially with today's sophisticated fluorimeters and analysis programs.[7,8] However, there exists a limitation with fluorescence techniques. Fluorescence lifetimes are very short and as a result, may not be detectable, or may occur in a shorter timescale than the phenomena

investigated. Despite these limiting factors, fluorescent probes such as pyrene have been used extensively to study diffusion processes in micelles and other host environments.[9-12]

This thesis describes probe molecules that efficiently form triplet excited states upon light activation. Triplet states are much longer lived than singlets and potentially offer more opportunity to analyze dynamic processes while in the host environment. The choice of triplet probes was not meant as a substitute for singlet fluorescent probes, but rather as tools to gain additional information that is not readily accessible with fluorescent probes. Our investigations dealt primarily with molecular aggregates that mimic some of the features of biological environments and, in later sections, we employed proteins conjugated to triplet probes. While some of the environments are structurally quite simple, suitable comparisons can still be made with their biological counterparts.

The triplet probe molecules selected must be chemically stable, show good absorption at the wavelengths of excitation, produce a suitable yield of triplet state for monitoring purposes, and have properties that will provide information about the desired environment. Triplet states can be studied spectroscopically by their phosphorescence emission or absorption. Phosphorescence emission from triplet states, like fluorescence, has been successfully used to probe the association dynamics between a host microenvironment and a guest. The long lived nature of room temperature phosphorescence (RTP) allows processes to be monitored which occur in timescales longer than microseconds.[1] However, triplet emissions are usually weak and prone to quenching making this technique of limited application. Despite these drawbacks, RTP has been used in the

determination of entry/exit rates of inclusion[3,13] and assessing the rigidity of host environments.[14,15]

The focus of this thesis is to directly monitor triplet excited states in organized media through their absorption, thus avoiding many of the problems associated with monitoring phosphorescence. In order to directly monitor triplet excited states through their absorption, a relatively large concentration of triplet states must be generated for detection purposes and, in order to facilitate kinetic analysis, these triplet states must be generated in a short period of time. The technique of choice for carrying out the studies mentioned above is known as laser flash photolysis (LFP) and has been used extensively to study short lived transient species such as triplet excited states.[16,17] Chapter 2 gives a detailed description of the LFP apparatus and techniques used in this thesis.

Monitoring triplet state absorption in host environments can provide information on dynamic interactions between the triplet guest and host. For example, exit rates of aromatic molecules from micellar hosts has been measured by monitoring their triplet absorption decay kinetics with respect to quencher concentration.[18] Pyrene can be used to probe mobility through monitoring the triplet-triplet annihilation kinetics which are manifested in the resulting excimer or monomer emission.[19] Directly monitoring pyrene triplet-triplet annihilation in reversed micelles using laser flash photolysis techniques has recently been used to differentiate inter- and intramicellar processes.[20] The ability to use these triplets for such studies hinges on pyrene's long triplet lifetime. Although this technique monitors the process through fluorescence emission, the probes of interest and the timescales accessible are in fact triplet state properties. Other triplet probes, such as xanthone, can be used to study changes in polarity of a

microenvironment. The triplet absorption spectrum of the low-lying triplet state of xanthone has a strong dependance on the polarity of the media and can be used to report on the polarity of the media; the less polar the environment is, the more red shifted the triplet absorption maximum is. Barra *et al.*[21] have used xanthone to measure association/dissociation kinetics in cyclodextrin solutions by directly monitoring the shift in the triplet absorption maximum of xanthone using laser flash photolysis techniques. In another study, carried out with solid state xanthone-cyclodextrin inclusion complexes, it was shown that the triplet decay kinetics of xanthone are dependent on the size of the cyclodextrin cavity.[22] This was the first time laser flash photolysis had been used to study cyclodextrin solid state complexes. In another recent study, the recombination kinetics of triplet radical ion pairs absorbed onto microcrystalline cellulose was studied by laser flash photolysis techniques.[23]

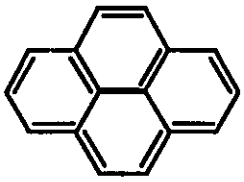

pyrene

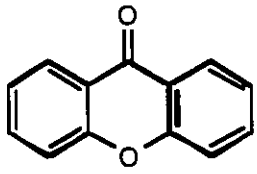

xanthone

As the potential of laser flash photolysis techniques for monitoring excited states in model host environments is being demonstrated, researchers have now began exploring more complex host systems such as living cells and proteins.[24-26] This has been accelerated by the virtual explosion of research in the use of triplet photosensitizers as potential

photochemotherapetic agents against cancer. This new clinically viable treatment employs a triplet precursor which localizes in cancerous tissue and upon excitation with light, produces high levels of singlet oxygen in the area of the tumor through the photosensitization of oxygen by the triplet state.[27-29] New photosensitizers are rapidly being developed and are being "fine tuned" through understanding their excited state dynamics in biological substrates. Again, the technique of choice to monitor these dynamics has been LFP and it is now being used to monitor excited triplet states in tissue and cells. Merocyanine dyes which are potential photodynamic drugs, have recently been directly monitored in cells using LFP techniques.[26]

An important aspect in using triplet state molecules as probes of host environments is to understand their mobility within the host. The majority of the studies involving mobility of triplet states use *intermolecular* processes as a method of detecting mobility. Using this method, a fairly unreactive triplet is formed in an environment and allowed to react with added quenchers.[3,18,30] An alternative method presented in the this thesis involves triplet probes based on *p*-methoxy-β-phenylpropiophenone (shown below) which rely on an *intramolecular* quenching mechanism; thus, they do not require the use of external quenchers. As a result, these probe derivatives are extremely sensitive to conformational constraints which can be imposed by the host environment or by the substituents attached to the probe itself. The investigation began by examining the time-resolved behavior of these probes in homogeneous solution before continuing onto more complex media, including solid crystalline media, cyclodextrins and micellar solution. In addition, a second triplet probe molecule, α-terthienyl (shown below), was investigated to establish its photosensitizing ability

when attached to a protein. The results are compared to previous solution experiments as well as associated complexes. The long term research was aimed at the development of novel antibody conjugates of α-terthienyl.

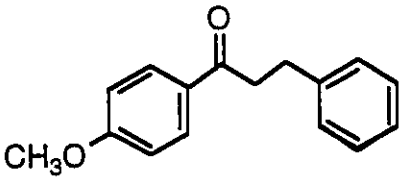

p-methoxy-β-phenylpropiophenone

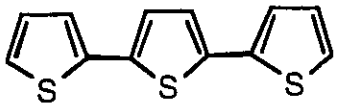

α-terthienyl

Chapter 2. Laser Techniques and General Instrumentation

2.1. Introduction

This thesis describes results using several different laser techniques to study photochemical processes in solution and in the solid state. The focus was on the characterization of excited state intermediates and their photochemical products. The goal of these studies was to better understand the interactions between excited state probes and their surrounding environment, whether that environment was the solvent or as potentially complicated as a protein. To better understand these interactions and the products that may result, a variety of techniques were used which are described below.

The intermediates that were of interest in this thesis were triplet excited states (T_1) formed from intersystem crossing (isc) from an excited singlet state (S_1). Intersystem crossing results in parallel electron spins which inefficiently relax down to the ground state (S_0) in the absence of adequate spin-orbit coupling. As a result, triplet states are relatively long lived and offer an excellent opportunity for investigation of dynamic processes that may occur during their lifetime.

Excited states, such as triplet intermediates, can be generated by laser light excitation of a precursor which results in the population of a singlet excited state (S_1) that can subsequently intersystem cross to the triplet state. Detection of the excited state is accomplished spectrophotometrically by its absorption of monitoring light. A simplified Jablonski diagram (excluding emission) describing these processes is shown Scheme 2.1. The technique used in this thesis to monitor excited

states in this way is known as laser flash photolysis (LFP) first reported by Kosonocky *et al.*[17], Lindqvist[31], Weiss *et al.*[32] and Porter.[16]

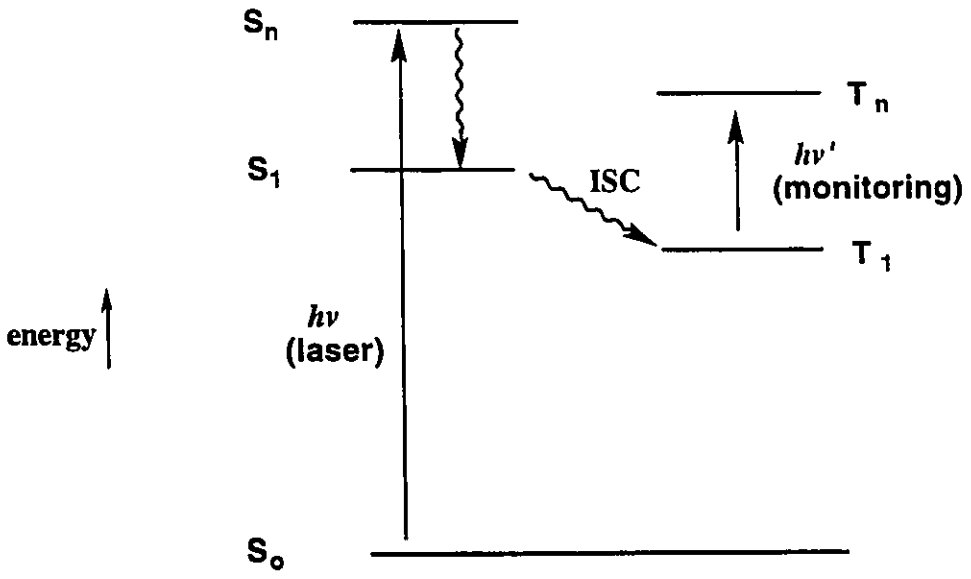

Scheme 2.1. A simplified Jablonski diagram depicting the excitation of a ground state molecule with laser irradiation ($h\nu$). The triplet state formed through intersystem crossing (isc) can be monitored through its absorption ($h\nu'$).

Methods of detecting transients in a host of environments has expanded the applications of laser flash photolysis into areas that were previously inaccessible to the photochemist. Nanosecond techniques such as time resolved conductance,[33] diffuse reflectance LFP,[34] singlet oxygen emission,[35] photoacoustic calorimetry,[36] are but a few that have been recently added to the arsenal of techniques available at the University of Ottawa. With the advent of picosecond and even shorter sources of light, there is no doubt that the number of processes able to be studied will continue to grow.

In this thesis, several of the above techniques will be used extensively, including laser flash photolysis using transmission and diffuse reflectance monitoring techniques, as well as detection of singlet oxygen near IR emission. In this chapter, I will describe in detail the techniques and instruments used during the course of the research described in this thesis. The more general experimental procedures (synthetic, analytical purification, etc.) are described in the experimental sections where they apply.

2.2. Laser Flash Photolysis

Laser flash photolysis uses a pulsed laser to generate an excited state from an appropriate precursor and a monitoring light source to analyze the transient's absorption. The laser must have a pulse duration shorter than the processes under investigation and have a high enough intensity that an appreciable amount of transient (typically 10-50 μM) is generated for detection purposes. After the laser fires, there is a change in absorptivity of the sample solution which alters the intensity of a monitoring beam as it passes through the solution. This intensity change is measured by a photomultiplier tube (PMT) detector as a function of time in order to extract spectral and kinetic information. In general, the system can be viewed as a very fast spectrophotometer with a laser as the excitation source.

There are a variety of lasers available in the laser lab at the University of Ottawa which can effectively cover wavelengths of excitation from 248 nm to 1064 nm. The lasers used primarily in these studies are the 308 nm EX 530 Lumonics excimer laser, a 337 nm Molectron UV-24 nitrogen laser and a 266 or 355 nm Surelite Nd/Yag laser with pulse

durations typically under 10 ns and energies of <100, 5, 10 and 30 mJ, respectively. The laser pulses were directed towards and concentrated (but not focused) on the samples at right angles with respect to the monitoring beam by a series of prisms and lenses. The experimental setup is shown in Figure 2.1. The lasers were usually operated at 1 Hz and shutters controlled exposure of the sample to either the monitoring or laser light sources. The energy of the lasers could be effectively attenuated with the use of calibrated neutral density filters.

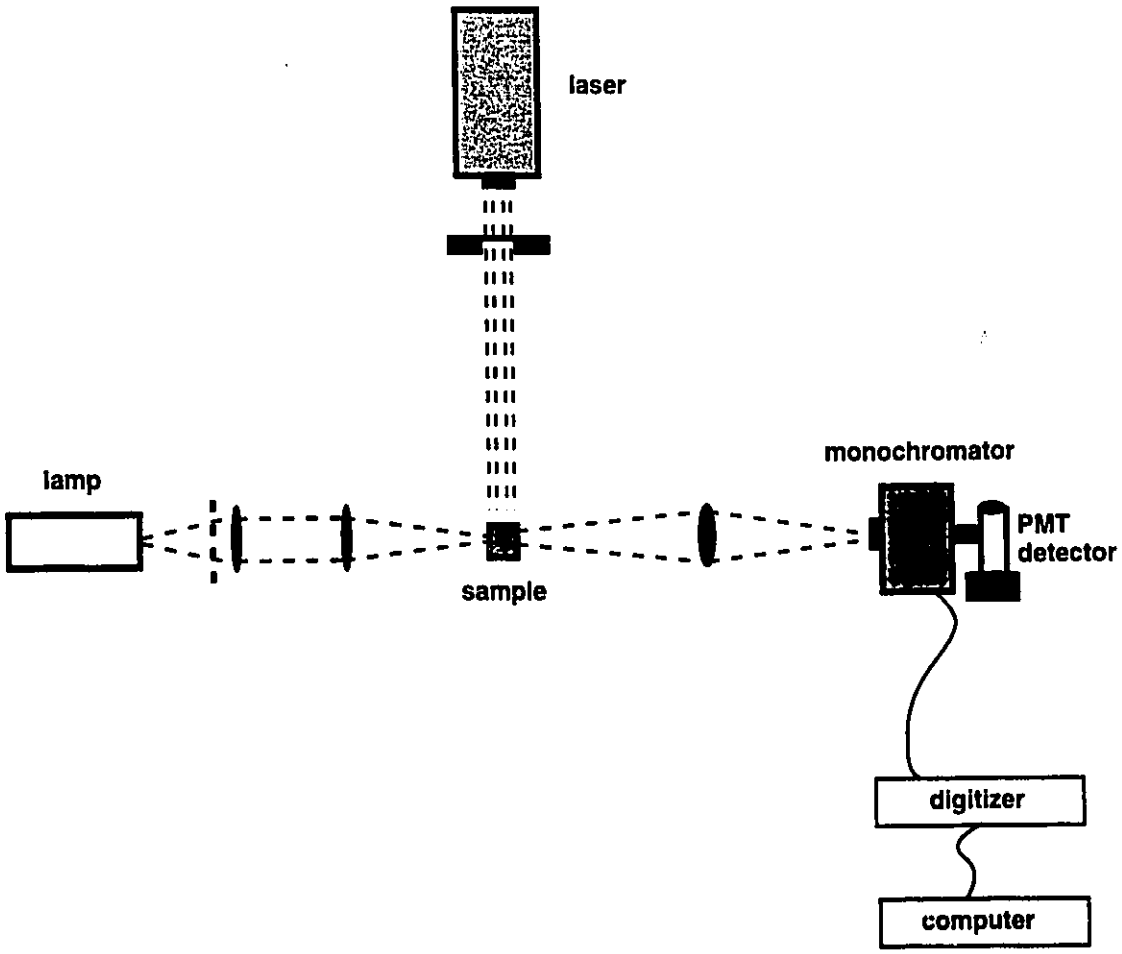

Figure 2.1. Experimental setup of a laser flash photolysis system.

Samples were prepared at concentrations that did not exceed an optical density of 0.4 at the laser wavelength to avoid shock waves or a concentration gradient of the transient species. The sample solutions were contained in cells made of 7 x 7 mm^2 Suprasil quartz tubing or could be flowed through specially constructed sample cells if a net chemical reaction occurred upon irradiation. To avoid product buildup or sample depletion in static samples, the solutions were shaken after every laser shot. Altering the gas content of the solution was achieved through bubbling with the desired gas for 15-30 min depending on the sample volume.

The monitoring/detection system consisted of a pulsed 150 Watt xenon lamp, a high intensity monochromator and a photomultiplier tube detector operating on six dynodes. The monitoring lamp was pulsed so that the intensity of the beam is increased by a factor of 5 - 20 during a few ms. This enhanced the signal to noise ratio which is especially important for small or short-lived (<100 ns) signals. The monitoring beam is focused through the sample and into a monochromator which selects the wavelength of light to be monitored. The selected wavelengths of light were detected by the PMT detector which yielded a current terminated into an appropriate load resistor (typically 93 Ohms) giving a voltage signal. The voltage signal changed with time and was captured by a Tektronix 2440 digital storage oscilloscope equipped with pre-trigger capabilities which was interfaced with Macintosh computers controlled by LabView-2.2 software. A line synchronizer coordinated the various components of the LFP system including the lasers, lamp pulser and shutters through a series of transistor-transistor linked (TTL) pulses that originated at the same point on a 60 Hz AC sine wave so that proper time sequences of events were maintained.

Figure 2.2 shows a plot of PMT output versus time for a period from one second before to one second after a particular laser pulse. At the beginning of the experiment, light from the monitoring beam is recorded before it is pulsed which causes a sharp increase in the PMT output. The laser then fires and subsequently strikes a fiber optic cable which triggers the transient digitizer to start saving data points. The signal that results is shown in the small box in Figure 2.2. The intensity of the monitoring beam, I_o, is measured on a second channel and represents the baseline from which changes in PMT voltage (sample absorption) are measured.

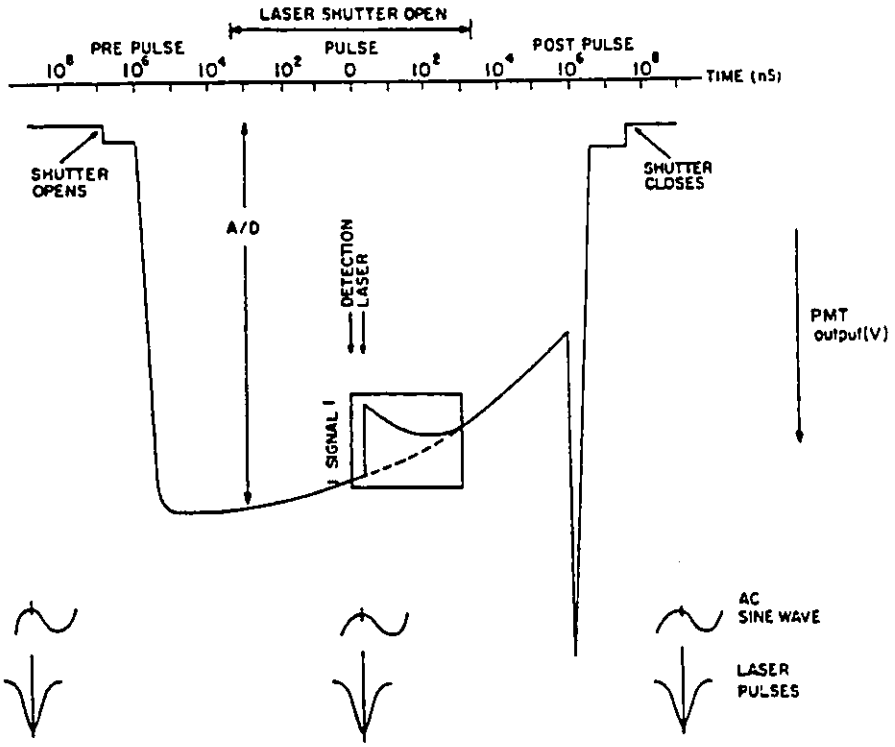

Figure 2.2. The sequence of timed events in the kinetic laser flash photolysis (LFP) experiment.

Therefore, the data from a laser flash photolysis experiment consists of a series of voltage signals converted from the PMT detector as a function of time at a particular wavelength selected by the monochromator. This raw data is processed by the computer which converts the voltage signals from the PMT to a change in absorbance (ΔOD) according to equation 2.1:

$$\Delta OD = - \log (1 - Signal / I_0) \qquad (2.1)$$

Typically, a kinetic trace was obtained by averaging the data collected from multiple laser shots. The ΔOD was then plotted against time to provide a kinetic trace like the one shown in the inset of Figure 2.3. Transient absorption spectra were constructed by acquiring kinetic traces at several wavelengths and plotting ΔOD of each kinetic trace against wavelength (Figure 2.3). In order for the signals at different wavelengths to be comparable, the I_0 values must be similar over the wavelengths measured. This was accomplished by a programmable power supply which could set the PMT output to any desirable level and maintain this level throughout the experiment.

Two-laser two-colour laser flash photolysis is a technique similar to conventional LFP described above but instead of using a single laser to generate the transient species (termed the "synthesis" laser), a second laser (termed the "photolysis" laser) was used to further excite the transient. The wavelength of the second laser were chosen so that the transient produced by the first laser, absorbs at that wavelength. The setup for two laser experiments was exactly the same as described above except the TTL signal which triggered the synthesis laser to fire was routed through a Stanford Research Systems Inc. Model DG535 4 channel digital

delay/pulse generator. The delay generator then sent a second delayed TTL signal to the second laser.

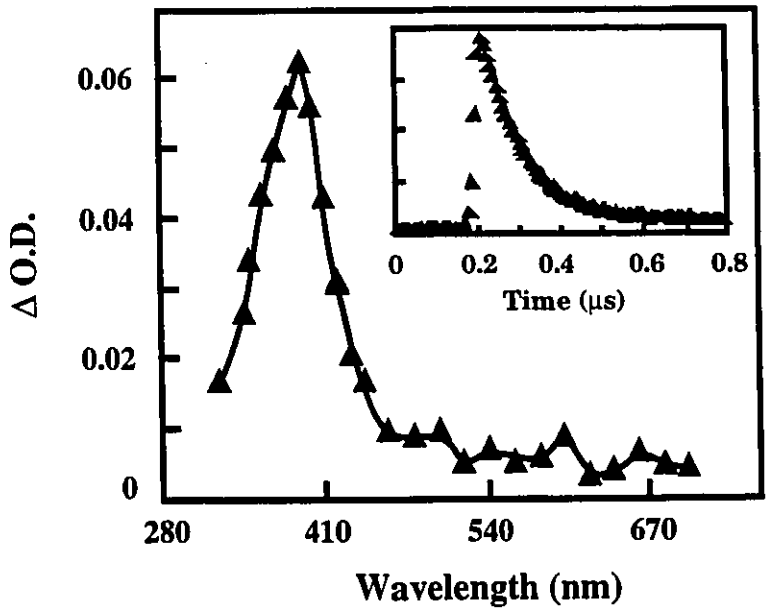

Figure 2.3. Triplet-triplet absorption spectrum for *p*-methoxy-β-phenylpropiophenone in acetonitrile monitored 20 ns after the laser pulse. Inset: Decay trace for the above sample monitored at 400 nm following 337 nm laser excitation.

2.3. Diffuse Reflectance Laser Flash Photolysis.

Opaque, light scattering samples can be studied using the laser flash photolysis technique by using the diffuse reflected light from the sample for analysis. A detailed account of the technique is given by Wilkinson.[37] The diffuse reflectance setup was much like the one described for solution experiments but the detector was arranged to capture the diffuse reflected monitoring light (see Figure 2.4) instead of transmitted light. This light had penetrated into the solid, returned to the surface and was collected in

much the same way as in the transmission experiments described above (section 2.2). However, the data collected were not treated as absorbances but with the Kubelka-Munk treatment[38] for strongly scattering samples, i.e.

$$F(R) = K/S = [(1 - R)^2] / 2R \qquad (2.2)$$

where $K = 2 \varepsilon C$, ε is the extinction coefficient and C the concentration. The fraction of reflected light absorbed by the transient (reflectance change, Δr) is $\Delta J/J_0$ where J_0 is the reflectance intensity before excitation and ΔJ is the change in the reflectance after excitation. For moderate values of reflectance change, such as observed in this thesis, this function is linear with concentration.

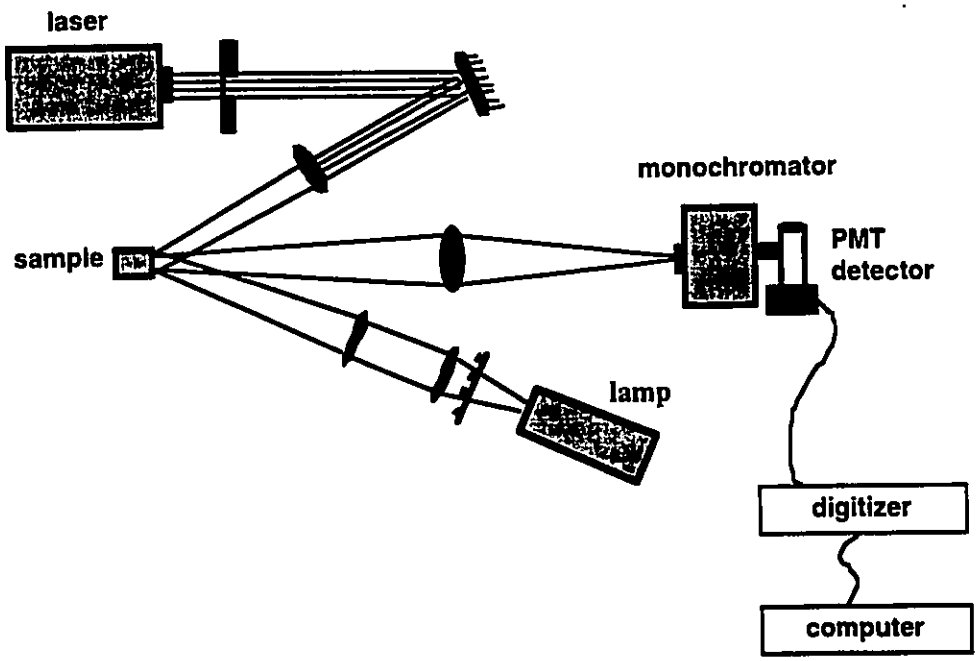

Figure 2.4. Time-resolved diffuse reflectance laser flash photolysis experimetal setup.

2.4. Singlet Oxygen Emission Detection

Energy transfer from triplet excited states to ground state oxygen occurs usually close to diffusion controlled rates provided the triplet energy of the triplet sensitizer is above the energy of singlet oxygen, $O_2(^1\Delta_g)$ of 22.4 kcal mol^{-1}.[39] The sensitized singlet oxygen can then deactivate back down to ground state by nonradiative means over a period of several microseconds to milliseconds depending on the solvent. A very small fraction (<.01) of the singlet oxygen produced can radiatively decay with emission of a photon having a wavelength of 1.27 μm.[35,40-42] The recent development of detectors able to detect this very weak luminescence has made it possible to directly monitor singlet oxygen in solution.

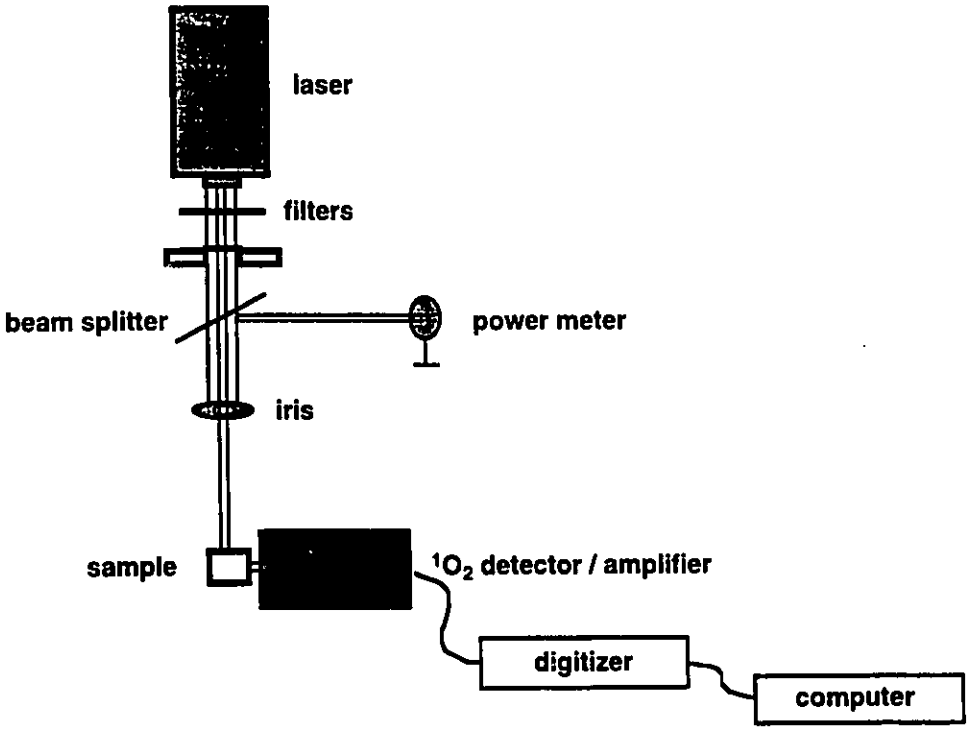

Figure 2.5. Time-resolved singlet oxygen luminescence detection apparatus.

The time-resolved infrared emission detection apparatus, used to monitor the kinetics of the relaxation of singlet oxygen, O_2 ($^1\Delta_g$), is based on detection of luminescence using a germanium photodiode. Our particular set-up, shown in Figure 2.5, employed pulses from a frequency tripled Surelite Nd/Yag laser (λ = 355 nm from a 1064 nm fundamental, 10 ns pulse, < 35 mJ / pulse) to excite oxygenated samples contained in a 10 x 10 mm path length quartz fluorescence cuvette. Before passing through the sample, the laser light was passed through a 355 nm bandpass filter (Schott) and a KG-5 short pass filter (Schott) to eliminate any residual 532 nm or 1064 nm light arising from the second harmonic generator or fundamental, respectively. An iris was used to further collimate the beam. In addition, the relative laser power was measured by diverting a small amount of the incident laser light (~4%) to a wavelength calibrated Molectron JD 2000 joulemeter ratiometer power meter using a quartz beam splitter. Detection of the luminescence emission from $O_2(^1\Delta_g)$ was carried out at right angles to the direction of the excitation beam, with an anti-reflection coated 3 mm thick silicon filter (CVI Laser Corp.) was placed between the sample and detector to remove interfering light of lower wavelengths, due to fluorescence or laser fundamental frequency (1.06 μm) scattering. The detector used was an EG&G Judson J16 8SP ROM5 (5mm) germanium photodiode, mounted on a modified BNC connector, and signals were amplified using a Stanford Research Systems low noise preamplifier (model SR560). The preamplifier was equipped with several short and long pass bandwidth filters which allowed the removal of unwanted signals generated by the laser pulse itself or scattering which is common at the detection level the system was operating at. Typical preamplfier settings were 2-5 x 10^3 gain with 10/30 KHz and 12 dB/octave

low pass filter settings. Amplified signals were captured by a Tektronix 2432 digitizer. Computer control of the experiment and data acquisition were similar to those used in laser flash photolysis work described above except that there was no monitoring beam. Figure 2.6 shows a typical singlet oxygen emission trace obtained using the above apparatus. Deuterated water (D_2O) was used instead of water because it absorbs less in the IR and the singlet oxygen is longer lived.

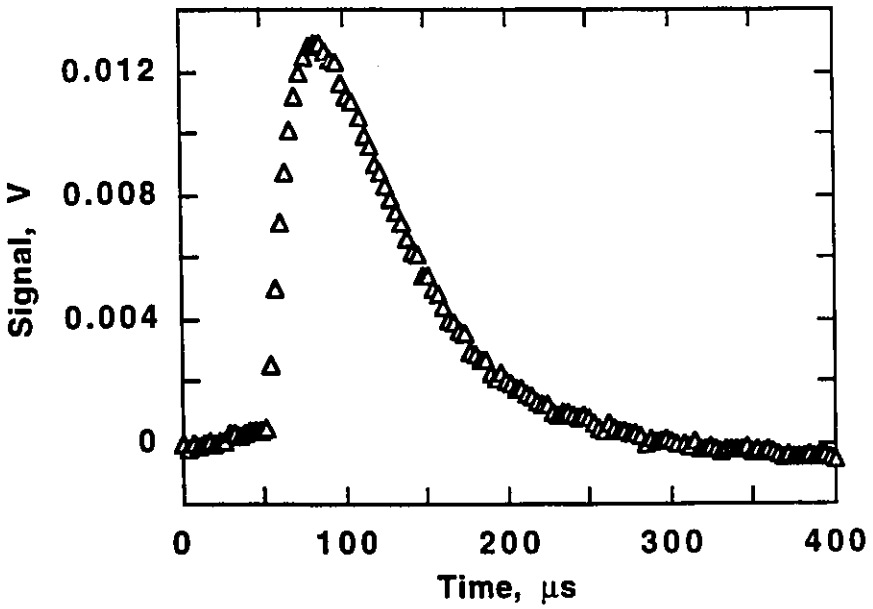

Figure 2.6. Deacy trace for O_2 ($^1\Delta_g$) emission centred at 1.27 μm generated from Rose Bengal (sensitizer) in D_2O solution using a 30 kHz low pass cutoff filter.

In order to accurately determine quantum yields (Φ_Δ) of singlet oxygen sensitization by triplet excited states, a comparative method was used whereby the energy dependence of the initial $O_2(^1\Delta_g)$ luminescence intensity (I_o) was measured for optically matched samples under study and

for a reference compound for which the Φ_Δ value was accurately known in the same solvent. Table 2.1 shows typical singlet oxygen standards used for various solvents. The power of the laser was altered by fine tuning the alignment of the third harmonic generator. By direct comparison of the slopes of the power dependence plots, the Φ_Δ value for the sample was obtained. Up to 50 shots were averaged (for the lowest laser excitation energy) for each data point. In many cases a non-linear plot was obtained due to competitive absorption by the thiophene triplet states formed during the laser pulse. In these cases a second order polynomial fit was carried out to determine the slope at zero dose (and hence, at zero triplet concentration).

Table 2.1. Singlet oxygen standards for various solvents.

Standard	Φ_Δ	Solvent
Phenazine	0.83	C_6H_6 [43]
	0.84	$CHCl_3$ [44]
	0.89	CH_2Cl_2 [44]
	0.83	CH_3CN [45]
Rose Bengal	0.80	D_2O [46,47]
Acridine	0.82	CH_3CN [44]
$Ru(bipy)_3$	0.86	CD_3OD [48]

Chapter 3. β-Phenyl Ketones as Triplet Probes

3.1. Introduction

Ketone excited states have long been a subject of photochemical investigation.[49] Depending on the substitution, they can undergo a variety of reactions leading to different transient behaviour and resulting products. The reactivity of non-conjugated aryl ketones are of particular interest. Reactions typical in these types of ketones have been outlined in Scheme 3.1. In ketones possessing a γ-hydrogen, the excited triplet carbonyl undergoes a characteristic 1,5-hydrogen shift to yield both cleavage and cyclization products in a well known Norrish Type II photoelimination, which is also referred to as a Type II reaction.[50] The result is a short lived but well characterized 1,4 biradical.[51] Ketones can also undergo photoreduction by reaction with good hydrogen donor substrates such as alcohols and amines. In some cases[52] the reaction may involve a considerable degree of charge transfer. Where the group α to the carbonyl favours Norrish Type I cleavage, two distinct radicals are produced which can undergo further reactions. In 1970, Whitten *et al.* [53], Wagner *et al.* [54] and Stermitz *et al.* [55] reported simultaneously on a different type of reactivity for the non-conjugated aryl ketones. In ketones possessing a β-aryl group, both Type I and Type II processes occurred with very low efficiency. In fact, in some experiments, irradiation of a β-phenyl ketone for up to 46 hours resulted in no photoreaction and the starting material was recovered essentially unchanged.[55] The lack of reactivity had been known for a number of years[56,57], but the three 1970 reports established the basis for this photoinduced stability.

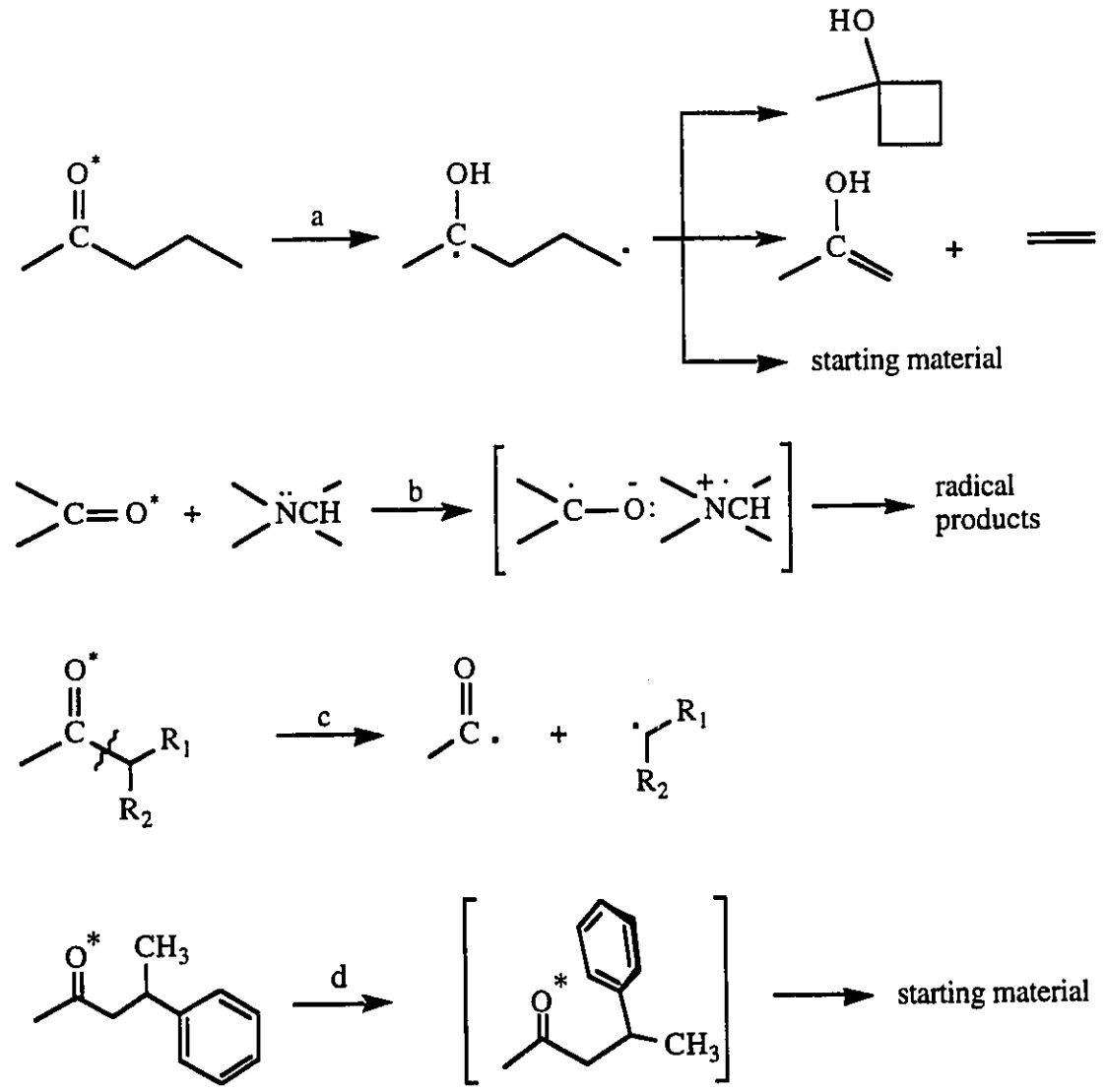

Scheme 3.1. Some reactions of triplet ketones: (a) Type II cleavage (Norrish Type II) and cyclization; (b) reaction with amines leads to charge transfer complexes; (c) α-cleavage (Type I cleavage); (d) β-phenyl quenching.

It was observed that even in the presence of an easily abstractable γ-hydrogen, such as that shown in Scheme 3.1(d), Type II photoelimination

cannot compete with this efficient deactivation process. The source of this photostability was not entirely clarified at the time but was assigned to some interaction between the carbonyl chromophore and the β-aryl substituent. It was suggested that rapid intramolecular quenching involving the β-phenyl ring was competing with the normal chemical reactivity of the n,π* triplet state.[54] It was known that carbonyl triplet quenching by aromatic rings occurred to some degree. For example, in 1963, Bell *et al.*[58] reported an anomolous short lifetime of benzophenone triplet in benzene solution. Although a low amount of ketyl radical was observed, no definite explanation was provided at that time. A series of reports followed which attempted to explain the possible interaction between the carbonyl triplet and the aromatic benzene molecule as a diradical adduct[59,60] formed from reversible hydrogen abstraction. A charge transfer complex between the aromatic quencher and the carbonyl forming an "exciplex" is now accepted as the mechanism of interaction.[61-64] Later work presented in this thesis and by other groups, provide more evidence for this charge transfer interaction.[65]

Laser flash photolysis techniques allow the investigator to directly monitor the transients of interest produced from the excited ketones. In 1983, a series of β-aryl ketones were investigated using this technique.[66] The ketones were based on the structure shown in Figure 3.1 (where X = H). No detectable transient was observed due to the highly efficient triplet deactivation process which leads to very short triplet lifetimes (< 1 ns). In later work[67], the addition of a *p*-methoxy substituent (X = MeO) was shown to dramatically increase the triplet lifetimes of these ketones, facilitating their detection.

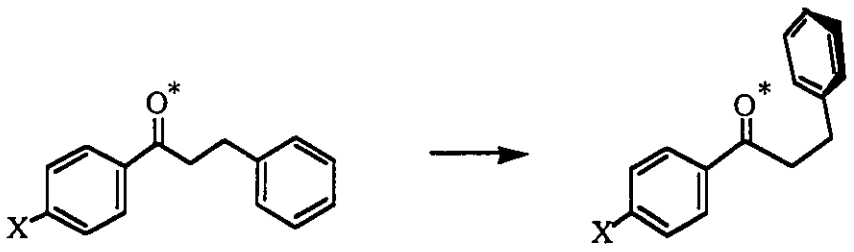

I : X = CH_3O

Figure 3.1. Intramolecular deactivation of triplet states by β-phenyl quenching.

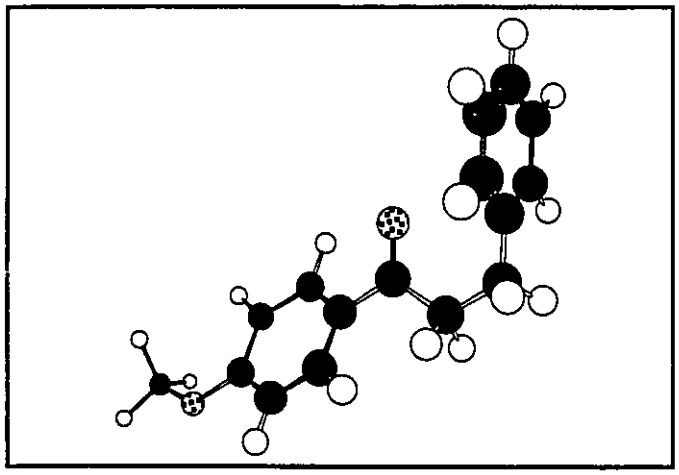

Figure 3.2. Triplet state quenching conformation in β-phenyl ketones.

The deactivation mechanism involves the movement of the β-aryl group above the carbonyl oxygen as shown in Figure 3.1. The mechanism requires the β-phenyl ring to overlap the half-vacant non-bonding (n) orbital. A specific conformation for interaction, shown in Figure 3.2 is expected from evidence of low pre-exponetial factors for the deactivation.[67] The charge transfer interaction involves the carbonyl n,π^* triplet state which may be the lowest state, or be thermally populated. In the latter

case, compounds containing a *p*-methoxy substituent, stabilization of the π,π^* triplet state results. This places more negative charge on the carbonyl oxygen and slows down the charge transfer from the aromatic ring resulting in a longer lived triplet state.[68,69] The effect of lengthening triplet lifetimes with *p*-methoxy substitution is also shown in Figure 3.3 with ketones not possessing a β-phenyl ring.

In 1984, Kilp *et al.*[69] monitored triplet states of **I** (Figure 3.1) using conventional nanosecond laser flash photolysis equipment. Without electron donating substituents, these ketones have lifetimes around 1 ns in solution[67,69], making detection of these triplet states difficult if not impossible at room temperature. The addition of a *p*-methoxy substituent significantly lengthens the triplet lifetime of **I** to around 200-300 nanoseconds which can be easily monitored. However, this slow down of β-aryl quenching does not introduce γ-hydrogen abstraction in ketones possessing an abstractable hydrogen as another competing reaction. Both Type II reactivity and β-phenyl quenching are processes that require an n,π^* state; however, the former process does not occur in any measurable extent. For example, irradiation of *p*-methoxy-β-phenylbutyrophenone (see section 3.2.1) for more than twelve hours still yields no observable products much like the earlier experiments without *p*-methoxy substituents.[53-55]

The kinetics of triplet decay of β-phenyl ketones described above is dependent on both the electronic nature of the excited state (n,π^* or π,π^*) as well as substituents that affect the conformation or movement of the deactivating β-aryl ring. In the latter case, conformational restrictions can also be imposed by the external environment such as solvent choice or incorporation into hosts. In the next sections (3.2 and 3.3) we will explore these aspects both in solution and the solid state.

The β-aryl ketones of interest in this thesis all possess a *p*-methoxy substituent (derivatives of ketone **I**) on the benzoyl moiety as seen in Figure 3.1. In studies of β-aryl ketones not possessing a *p*-methoxy substituent, the triplet lifetimes are very short due to the favourable interaction between the predominately n,π* triplet state and the β-aryl group. It is believed that the movement of the β-phenyl ring into the correct orientation for quenching becomes the rate-determining step, rather than the dynamics of the charge transfer process.[67]

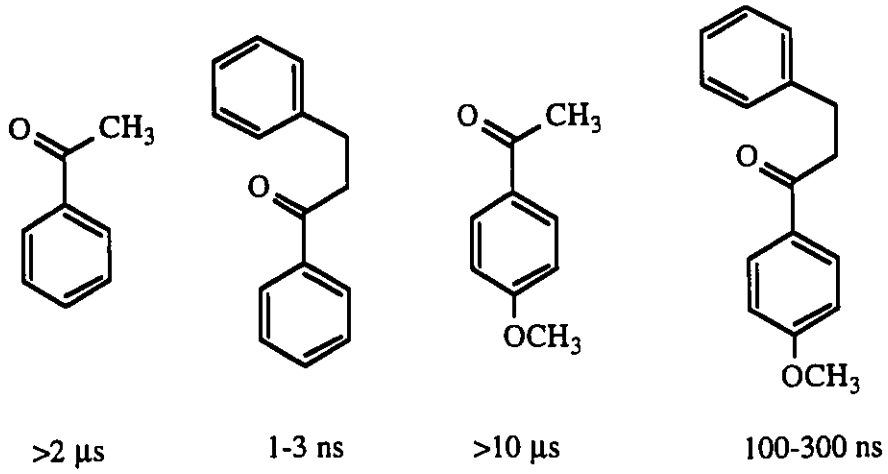

Figure 3.3. Aromatic ketones showing triplet lifetimes under nitrogen illustrating the effect of a *p*-methoxy substituent and β-phenyl group on triplet lifetimes.

Ketones lacking a *p*-methoxy group show little effect on their triplet lifetimes with various β-aryl substitutions such as methyl, methoxy and halogen groups.[67] Little effect is also seen in the triplet lifetime in the absence of ring substitution when substituents are added at the β-position.[66] For example, β-phenylpropiophenone, and β-phenylbutyrophenone have

similiar triplet lifetimes in solution of around 1-3 ns. However, the addition of a *p*-methoxy substituent can dramatically enhance these effects through significantly lengthening the triplet lifetimes by producing a low lying π,π^* triplet state. As a result, substituent effects are readily observable.

The initial interest in this thesis with these ketones focussed on their use as probes for chiral hosts. The synthesis of **II**, a chiral probe possessing a methyl group in the β-position, was expected to have different decay kinetics depending on the isomer used and the chiral host investigated. This particular ketone had never been synthesized before and the first laser flash photolysis experiments carried out were done so to compare its photobehaviour to similar ketones in other studies.

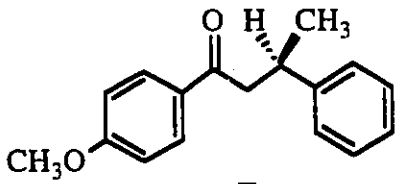

II

Preliminary experiments with **II** indicated that methyl substitution away from the reaction centre had dramatic effects on the triplet lifetime compared to the unsubstituted ketone (**I**). This observation prompted us to investigate various other methyl substituted derivatives (**III-V**) in an attempt to understand the effects of methyl substitution on the triplet lifetimes. Substitutions were made either in the β-position or on the β-phenyl ring to explore the influence of steric and redox properties. In addition, a chiral alcohol derivative (**VI**) was investigated to evaluate the possible effect of hydrogen bonding between the carbonyl and the alcohol group on the triplet lifetime.

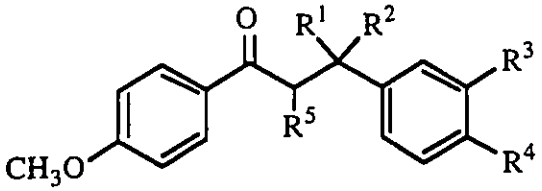

I: $R_1=R_2=R_3=R_4=R_5=H$

II: $R_1=CH_3$; $R_2=R_3=R_4=R_5=H$

III: $R_1=R_2=CH_3$; $R_3=R_4=R_5=H$

IV: $R_1=R_2=R_4=R_5=H$; $R_3=CH_3$

V: $R_1=R_2=R_3=R_5=H$; $R_4=CH_3$

VI: $R_1=R_2=R_3=R_4=H$; $R_5=OH$

In section 3.3, the triplet lifetimes of **I** and **II** are measured in the solid state. Only a limited amount of work has been done with β-aryl ketones in the solid state. In other photochemical systems, Scheffer *et al.* have reported extensive research on the influence of reaction media on the reactivity of ketones, especially in crystals.[70,71] Traditionally, the rationalization of reaction pathways has been carried out indirectly by analyzing X-ray data and product distributions to best understand photochemical mechanisms in the solid state. Monitoring directly the excited states controlling the photochemistry in the solid can be used to further complement our understanding of solid state photochemical mechanisms.

The transient behavior of lignin model compounds, also containing a β-aryl group, have been studied in the solid state, as well as on silica, zeolite and cellulose supports.[72,73] However, the observations are complicated by cleavage of the starting materials upon laser excitation to form radicals and products which also can absorb light. Ketones, such as **I** and **II**, where cleavage of the starting material is not a major process, simplify the transient solid state photochemistry.

In section 3.3, we report the effect of conformational changes on triplet lifetimes which are discussed in section 3.2 in solution, are even more prevalent in the the solid state. By using diffuse reflectance laser flash photolysis techniques on solid samples of these ketones, we are able to demonstrate that conformational effects also play a significant role in the solid state. We also demonstrate that the triplet state of ketone **II** can distinguish packing differences in crystals of pure enantiomers and racemic mixtures. These results are then rationalized through the triplet lifetimes observed along with powder and single crystal X-ray crystallography.

In this chapter, a combination of photochemical studies employing laser flash photolysis techniques, electrochemical measurements, molecular modeling calculations and X-ray data are presented along with a rationalization of the observed variations in triplet lifetimes in various *p*-methoxy-β-phenylpropiophenone derivatives both in solution and in the solid state.

3.2. Effect of Substituents in Solution

3.2.1. Results

Triplet lifetimes were determined at room temperature employing laser flash photolysis techniques. The decays showed clean monoexponential behavior, although a small amount of residual absorption was frequently observed following the completion of the triplet decay. Figure 3.4 shows a representative transient spectrum for **II** and a decay trace for the triplet monitored at 400 nm.

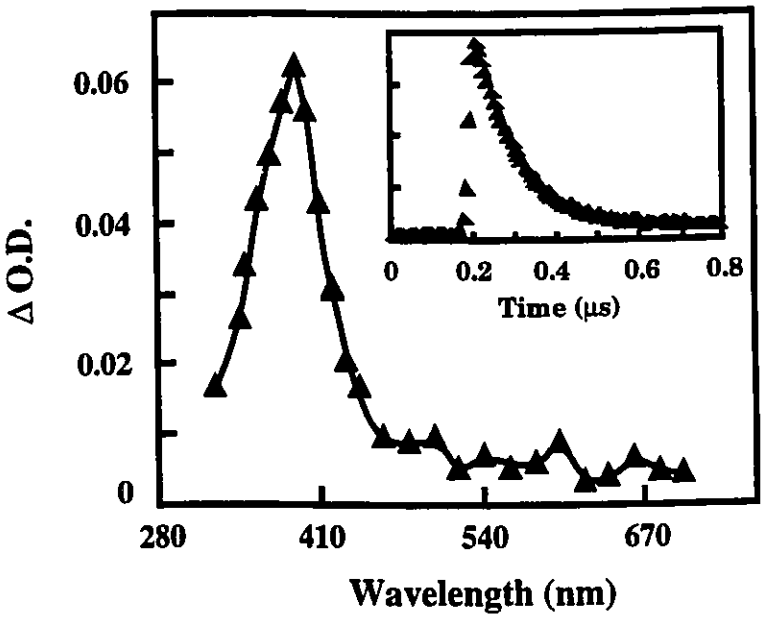

Figure 3.4. Triplet-triplet absorption spectrum for **II** in acetonitrile at room temperature monitored 20 ns after the laser pulse. Inset: Decay trace for **II** monitored at 400 nm following 337 nm laser excitation.

The triplet spectra were virtually identical regardless of methyl substitution in the β-phenyl ring or in the methylene chain, and agree well with literature spectra for ketones with the *p*-methoxybenzoyl chromophore.[67,74] In the case of **VI**, a small amount of absorption was detected around 500 nm and may be the result of some Norrish Type I cleavage. The triplet lifetimes recorded for ketones **I-VI** are given in Table 3.1.

The introduction of methyl groups in the β-position in ketones **II** and **III** had dramatic effects on the triplet lifetimes compared to the unsubstituted ketone **I**. We reasoned that since the mechanism of deactivation involves the interaction of the β-phenyl ring with the carbonyl oxygen, the introduction of methyl substituents may have induced changes in conformation and/or the ring's freedom of movement. We noted that since ketones **2** and **3** have γ-hydrogens, they could conceivably undergo the Norrish Type II reaction; Wagner et al.[54] showed that this process occurs with very low quantum yields in β-phenylbutyrophenone, thus supporting that the lifetimes are determined by β-phenyl quenching, and not chemical reactions. To further address this point, ketone **II** was irradiated at 300 nm under steady state conditions. Prior to irradiation, the samples, contained in quartz 7 x 7 mm^2 cells, were deaerated by bubbling nitrogen through the solution for forty minutes. After 12 hours of irradiation, no observable product formation was observed by GC-MS analysis. Similar irradiations of the alcohol substituted ketone (**VI**) for 12 hours in deaerated acetonitrile solution revealed a very low yield of *p*-methoxy-benzoic acid which is attributed to the oxidation of the corresponding aldehyde resulting from some α-cleavage. The low yields of product formation even after extensive irradiations, provides further evidence that the lifetimes are solely

determined by β-phenyl quenching in the case of the methyl and alcohol substituted derivatives.

Table 3.1. Kinetic data for the decay of ketone triplets at room temperature.[a]

Ketone	Lifetime[b] in nanoseconds in		
	Methanol	Acetonitrile	Benzene
I	239	50	
II	95	19	18
III	10		
IV	151	29	28
V	31	9	12
VI	64	31	60

[a] All decay traces monitored at 400 nm after 337 nm laser excitation; ketone concentrations were typically ~ 1 x 10^{-3} M.
[b] Typical errors are about 5% for lifetimes of 50 ns or longer and ca. 10% for the shorter values.

Methyl substitutions in the *meta* and especially *para* positions on the β-phenyl ring also shorten the triplet lifetime (see Table 3.1). Shorter lifetimes could be the result of changes in the oxidation potential of the ring through methyl substitution, thereby facilitating easier transfer of electrons to the carbonyl n,π* triplet during charge transfer. Electrochemical measurements (*vide infra*) were carried out in order to address this question.

The addition of an alcohol group in the α-position also shows a dramatic effect on the triplet lifetime. We reasoned that the effect may be the result of hydrogen bonding between the carbonyl oxygen and alcohol hydrogen which may "draw" the phenyl ring closer to the carbonyl for deactivation. Molecular mechanics calculations and X-ray studies were used to predict the preferred conformation of this compound. Both methods resulted in conformations that promoted β-aryl quenching through hydrogen bonding (see below).

While our studies center on methanol as solvent, a few exploratory measurements in acetonitrile and benzene (see Table 3.1) clearly suggest that our observations are quite general. The longer lifetimes in hydroxylic solvents are believed to be due to hydrogen bonding with the solvent at the carbonyl centre which restricts the access required for the deactivation to occur.[67]

Molecular mechanics calculations

In an attempt to understand the differences in triplet lifetimes (see Table 3.1), molecular mechanics calculations were performed using PCMODEL software derived from the MM2 force field of Allinger[75] to estimate the effects of conformational and steric factors of methyl substitution in the β-position. It should be noted that these calculations were performed in 1990. Since then, other more advanced molecular modeling programs have entered the market. Some of the calculations outlined below were repeated on a newer molecular mechanics program called CAChe (Computer Aided Chemistry). This program is also based on Allinger's MM2 force field and gave essentially the same results as PCMODEL.

Dihedral drivers were used in which minimizations were performed for angle increments around 3° on ketones **I-III** for rotation about bond **b** as shown in the structure below. The dihedral angle is defined by the four atoms connected by the bonds marked in bold. Figure 3.5 shows the results of these calculations. During the minimizations, no other parameters, (other than the dihedral angle) were kept constant. At the minimum and maximum energies the dihedral angle was fixed and the structure was reminimized; these positions were always very close (± 2°) to the multiples of 60°.

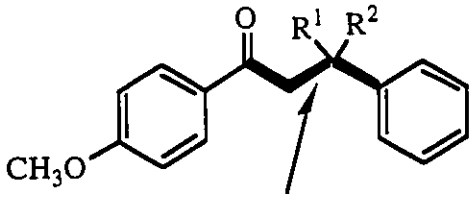

I-III

b

Ketone **I** has three lowest energy conformers having dihedral angles of about 60^0, 180^0 and 300^0 with respect to the carbonyl group each having approximately equal energies. For ketone **II** the lowest energy conformer has a dihedral angle of about 60^0. The preferred position of the deactivating phenyl ring in **II** now lies closer to the carbonyl (Figure 3.6); this explains the reduction in lifetime between ketones **I** and **II**. For ketone **III**, the situation is quite similar; the β-phenyl ring now prefers to lie at either 60° or 300° angle with respect to the carbonyl group. Combined with these conformational effects, increased methyl substitution in the β-position raises energy barriers for rotation of the phenyl group away from the carbonyl. Our calculations also suggested that in the case of **III** the distance between the carbonyl oxygen and the ring (as measured by the

distance to the *ortho*-carbons) was smaller than for **II**. However, it was clear that small changes in the position or tilt of the β-phenyl ring are not predicted very accurately at this level of calculation and any argument based on variations in this distance would be highly speculative.

The minimized structures calculated for ketones **I, II** and **VI** were very similar to the structures determined by single crystal X-ray diffraction patterns of these ketones (X-ray structural information for **I** and **II** are given in section 3.3). Ketone **III** was an oil, thus no X-ray structure was possible. The X-ray structures for **I, II** and **VI** are given in Figure 3.7. The dihedral angles for the three structures defined above, were calculated to be within 1 or 2° of the measured angles in the X-ray structures. The structure of the alcohol substituted ketone (**VI**) corresponds to the lowest energy conformation calculated for **II** and places the β-phenyl ring at 51° with respect to the carbonyl group. Hydrogen bonding reinforces this conformation making it more difficult for the phenyl group to rotate away from the carbonyl group. This effect serves to further decrease the observed triplet lifetime of this ketone as seen in Table 3.1.

Low temperature NMR studies were attempted with **II** to differentiate any conformational preferences that might arise at lower temperatures. Unfortunately, temperatures as low as -65°C in $CDCl_3$ were unsuccessful at partitioning any of the signals in either the ^{13}C or ^{1}H NMR spectra. The sample's restricted solubility at lower temperatures in solvents such as CD_3OD hindered further investigation.

Cyclic voltammetry

The electrochemistry of ketones **I, IV,** and **V** was investigated in an attempt to establish to what degree different methyl substitutions on the

phenyl ring can affect its electron donating character. The oxidative properties of aromatic rings can be substantially altered by methyl substitution. In a related piece of work, differences in standard oxidation potentials for various alkylbenzene derivatives were reported by Kochi *et al.* [76], who recorded voltammograms under acid conditions with very fast scan rates and using microvoltammetric electrodes to measure the reversible reduction of the arene cation radicals. In our work, a more traditional cyclic voltammetry set up was sufficient, since only relative irreversible oxidation voltammograms are adequate for our analysis.

Ketones **I**, **IV** and **V** all gave irreversible oxidative cyclic voltammograms, as expected. Representative voltammograms recorded at a scan speed of 10 seconds / inch are shown in Figure 3.8. For ketone **V**, which had the shortest triplet lifetime, the onset of oxidation was at a lower potential than **I** or **IV**. The same trend of oxidation potentials is also observed when comparing toluene to m- and p-xylene.[76] This lower potential is thought to be due to the para substituted β-phenyl ring. Conclusions about oxidation potential differences concerning the β-phenyl ring for ketones **I** and **IV** could not be easily made since the *p*-methoxyacetophenone moiety is oxidized at roughly the same potential as the β-phenyl ring causing overlap of the signals. The earlier onset of oxidation of ketone **V** suggests that the β-aryl ring is a better electron donor thus resulting in the shorter triplet lifetime observed.

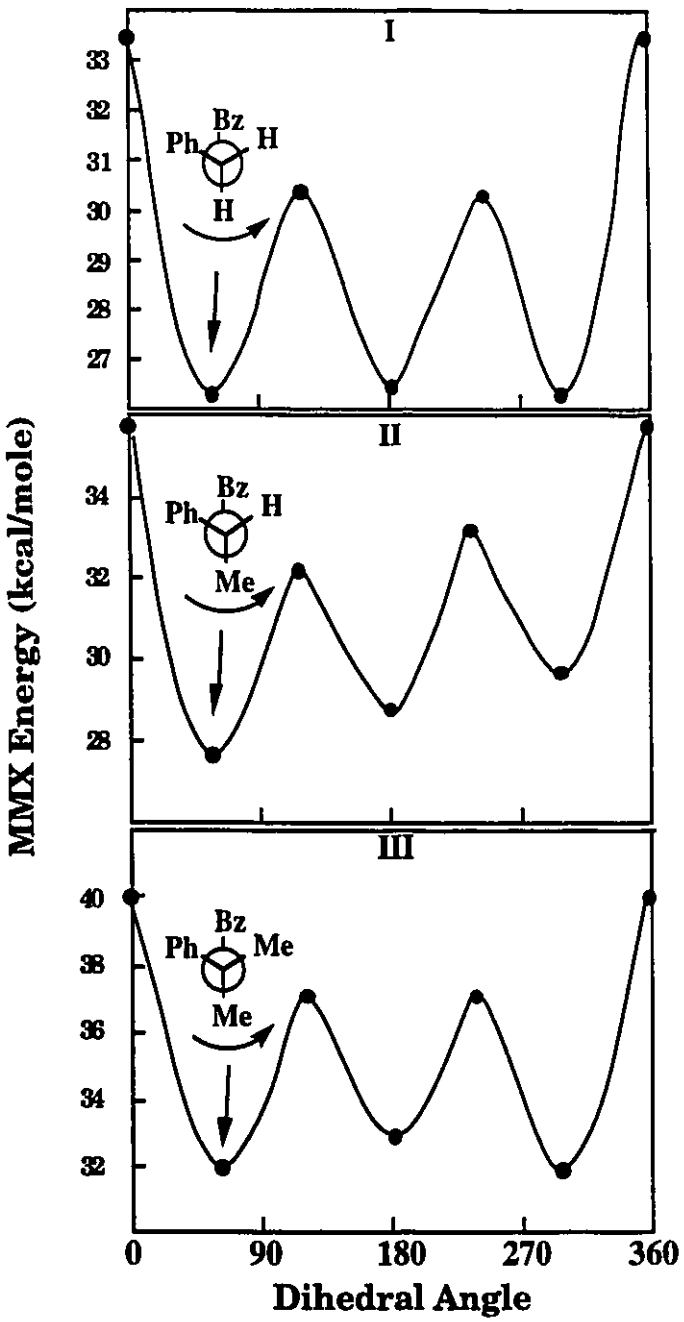

Figure 3.5. Energy barriers calculated for key conformations using MMX calculations (Absolute MMX energies for different compounds are not comparable; only energy barriers can be compared). The energies were obtained by fixing the dihedral angle but minimizing the rest of the structure. 'Bz' represents the *p*-methoxybenzoyl group; note that these are ground state structures.

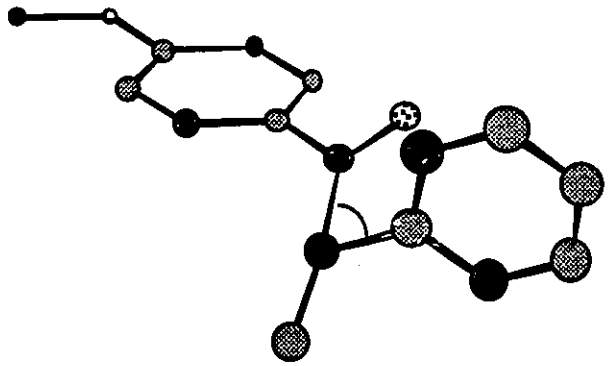

II

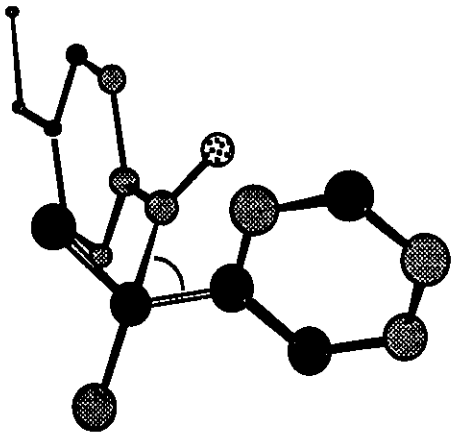

III

Figure 3.6. Minimum energy conformations for **II** and **III** obtained using MMX calculations. Note that these are ground state structures. The solid black center displays two overlapping carbon atoms (as in a Newman projection) and the arc shows the dihedral angle displayed in Figure 3.5.

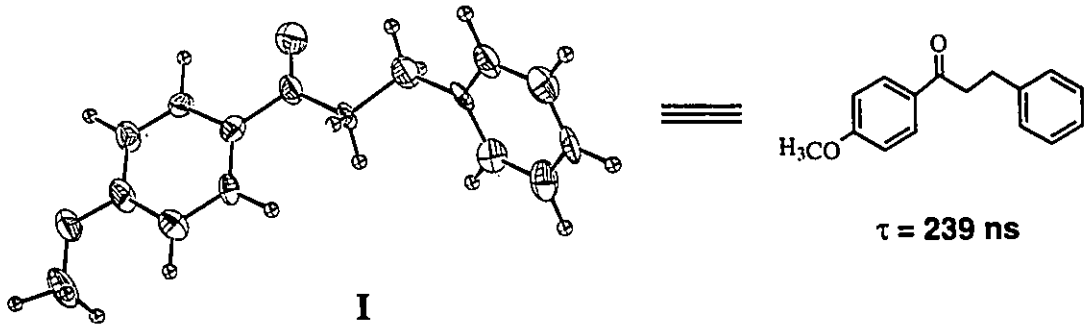

τ = 239 ns

I

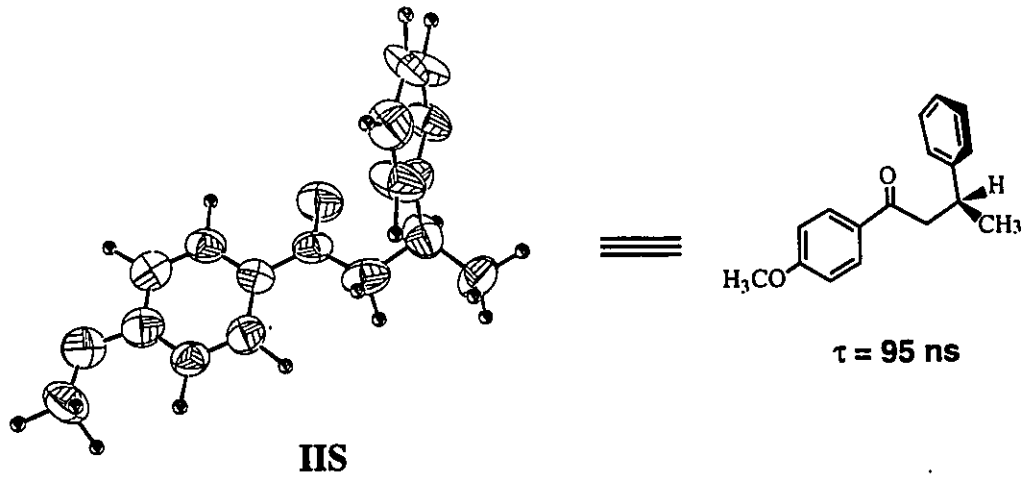

τ = 95 ns

IIS

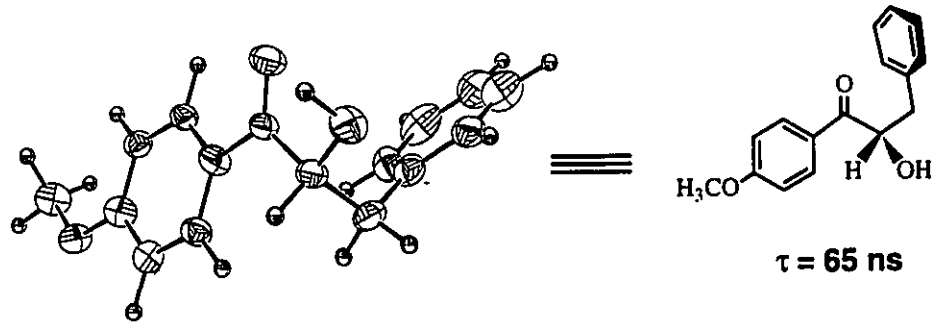

τ = 65 ns

VI

Figure 3.7. Conformations of ketones **I, II** and **VI** determined by single crystal X-ray diffraction along with the triplet lifetimes observed in methanol under a nitrogen atmosphere corresponding to Table 3.1.

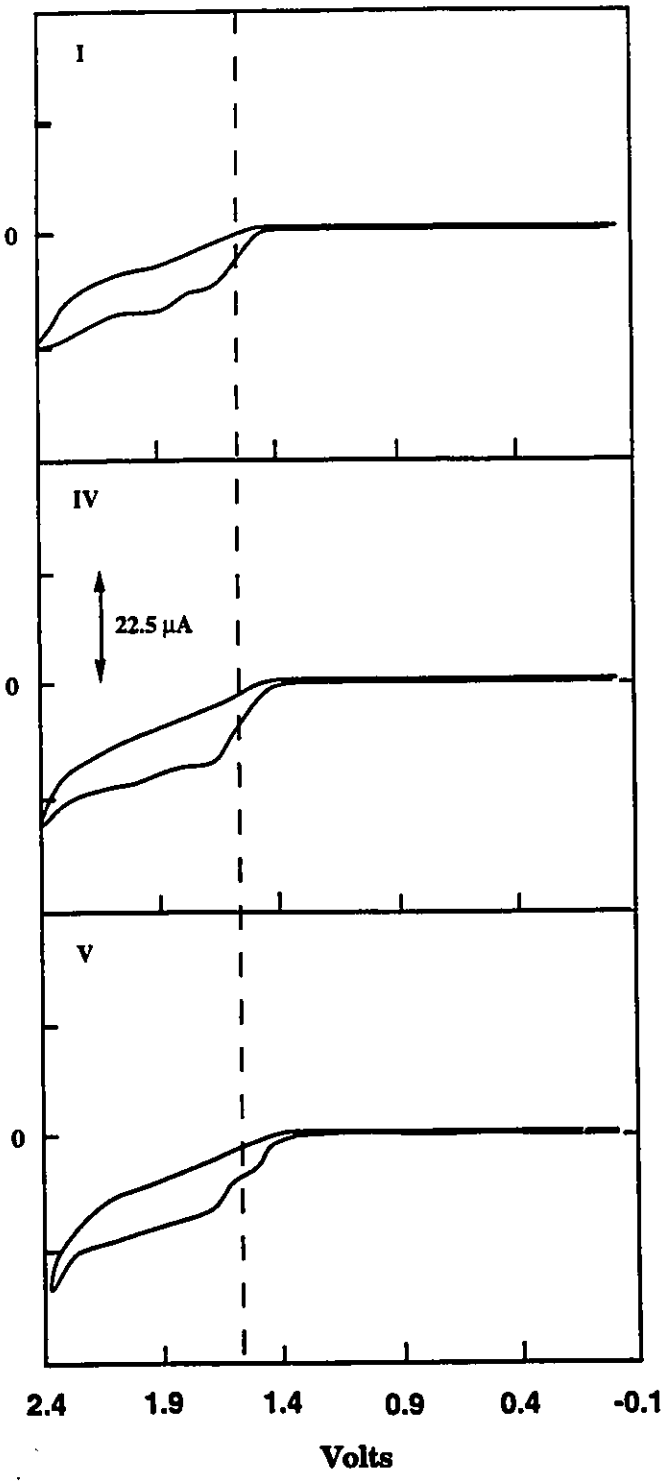

Figure 3.8. Irreversible cyclic voltammograms of **I**, **IV** and **V**. (The dashed line was added to facilitate comparison)

3.2.2. Discussion

It is well established that the mechanism for intramolecular β-aryl quenching of carbonyl triplets, such as the Norrish Type I and II reactions[77] requires n,π* triplet character[67] and adequate mobility so that the conformation for quenching can be achieved (see Figure 3.2). Conformational restrictions, imposed either by changes in the molecular structure[66], or by media (e.g. by inclusion in zeolite channels[78] or cyclodextrins[79,80]) can lead to significant increases in triplet lifetime. All the ketones examined in this work have low lying π,π* triplets as a result of *p*-methoxy substitution of the benzoyl chromophore. The deactivation mechanism requires the carbonyl n,π* triplet state which is 2-3 kcal/mol higher in energy than the corresponding stabilized π,π* state and must be thermally populated for the charge transfer interaction.[67] This leads to triplet lifetimes that are sufficiently long to be amenable for study by nanosecond laser photolysis technique. In addition, the lifetimes are sufficiently long that conformational and electronic factors can now lead to variations in these lifetimes. In contrast, in the case of β-phenylpropiophenone derivatives with no substituent on the benzoyl chromophore, the lifetimes are very short and are predominantly controlled by bond rotation.[67]

The initial work with **II** was motivated by an interest in systems with asymmetric centers. The unexpected shortening of the triplet lifetime upon introduction of a methyl group in the methylene chain was initially surprising. With hindsight, these results could be readily rationalized on the basis of conformational preferences. Earlier work comparing the lifetimes of β-phenylpropiophenones and α-phenoxyacetophenones also led

to the conclusion that steric interactions involving the linkage between the chromophore and quencher can play a crucial role in determining the triplet lifetime.[81,82] Similarly, when the α- or β- carbon atoms in the linkage are part of a small ring system the triplet lifetimes are also increased significantly.[66] In addition, conformational constraints imposed by substitution at the α-carbon of β-arylpropiophenones lead to reactivity differences towards triplet state intramolecular ε-hydrogen abstraction, which were interpreted as resulting from preferential population of the conformations necessary for reaction.[83]

The results obtained in the present studies reflect two distinct types of effects. In the case of compounds **I**, **II** and **III**, the effects are of a conformational nature, since neither the properties of the chromophore, nor those of the deactivating ring should be significantly affected by methyl substitution on the $-CH_2CH_2-$ link. Figures 3.5 and 3.6 show the results of MMX calculations, which even at this rather basic level illustrate the conformational preferences of these molecules. For ketone **I**, there are three preferred conformations with essentially the same predicted energy, whereas in the case of **II**, our MMX calculations indicate that the preferred conformation (see Figures 3.5 and 3.6) places the β-phenyl ring at ~60° with respect to the carbonyl chromophore. These conformations are consistent with the X-ray structures shown in Figure 3.7. The case of **III** is similar; now there are two energetically equivalent lowest energy conformations at 60° and 300°, increasing the probability of finding the β-phenyl ring close to the carbonyl. Besides analysing the preferred lowest energy conformations one also has to take into account the energy barriers hindering the approach to an eclipsed conformation. In a first approximation, a fully eclipsed conformation (corresponding to the vertical axis in Figure 3.5)

between the β-phenyl and the carbonyl groups was assumed to be required for quenching. The probability of reaching the conformation required for quenching is a function of the energy barrier to approach this eclipsed conformation, but it is also a function of the barrier observed for the other substituents which control the rotation of the deactivating ring away from the carbonyl. For example, an increase in the energy barrier for rotation of the β–phenyl ring away from the carbonyl is observed when substituting the β-hydrogens for methyl groups; this increase leads to a higher probability of achieving the eclipsed conformation between the β-phenyl ring and the carbonyl group. Clearly, not only are the chromophore and quencher closer in the case of **II** and **III**, but also the energy barriers predict easier intramolecular conformational interconversion leading to quenching for these compounds, as observed. In the case of **VI**, hydrogen bonding provides for a lowest energy conformation at 51°, placing the β-phenyl ring close to the carbonyl group. This structure is consistent with the X-ray crystal structure shown in Figure 3.7.

Figure 3.5 predicts ketone **I** to have three preferred minimas, each with approximately equal energy. This implies that there is no preference for anti or gauche conformations which would be highly improbable. Numerous attempts at analyzing this conclusion with our version of PC-MODEL and others in hopes of differentiating these two conformations were unsuccessful and must be a fault in the calculations. However, a calculated lower energy anti conformation in these ketones would only add our findings, and in this respect it does not conflict with our results.

It is generally believed that the mechanism for β-aryl quenching involves charge transfer from the quencher group to the excited carbonyl. Not surprisingly, in systems with low lying π,π^* states quenching involves

the more electrophilic and thermally populated n,π* state.[67] Methyl substitution at the β-aryl ring should make oxidation easier and therefore result in a reduction of the triplet lifetimes. This prediction proved correct, as shown by the lifetimes for **IV** and **V** given in Table 3.1. Cyclic voltammograms (see Figure 3.8) also confirm this expectation, the largest effect on both the lifetime and the oxidation potential being induced by para-methyl substitution. It is interesting that in the case of **V** *p*-methyl substitution essentially reverses the kinetic effect due to the low lying π,π* triplet in the *p*-methoxybenzoyl chromophore (compare the data in Table 1 with the unsubstituted substrate;[67] it is possible that in the case of **V** rotational control may play a role in determining the lifetime. Leigh *et al.*[84] have recently confirmed these results in similiar ketones using a wide variety of electron withdrawing and donating substitutents. The triplet decay rates for these derivatives show an excellent correlation with σ^+ substituent constants ($\rho^+ = -1.8 \pm 0.2$), thus verifying that the intramolecular quenching of carbonyl triplets involves charge transfer interactions and is dependant on the oxidation potential of the β-aryl ring.

3.2.3 Conclusions

In conclusion, laser photolysis studies of the triplet states of **I-VI** demonstrate the importance of conformational and redox properties in determining the kinetics for intramolecular charge transfer quenching in these molecules. The effects of substitution in the $-CH_2CH_2-$ link are quite dramatic but explain conformational preferences that can be readily rationalized by MMX molecular modeling calculations. The results also confirm the earlier proposal [67] that in the absence of the *p*-methoxy

substituent the lifetimes are too short to be amenable for direct study with nanosecond techniques and are largely controlled by bond rotation which tends to mask other effects which are readily observable in the series studied herein.

3.3 Effect of Substituents in the Solid State

3.3.1. Results

The triplet absorption spectra obtained in the solid state from ketones **I** and **II** using laser flash photolysis diffuse reflectance techniques (see Chapter 2) and were virtually identical to those obtained in homogeneous solution described in section 3.2. Both spectra had maxima at around 400 nm and can be readily assigned to the triplet state.[67] Figure 3.9 shows a typical solid state triplet absorption spectrum of ketone **IIrac** collected after 308 nm laser irradiation. Ketones **I** and **II** gave similar triplet spectra in the solid state, and the addition of oxygen had no effect on their triplet spectra or lifetimes. In solution, the triplets of these ketones are efficiently quenched by oxygen. This indicates that the penetration of oxygen through the crystal lattice is very inefficient. The lack of oxygen effect on solid state triplet lifetimes has been reported elsewhere.[72]

Comparisons of the triplet lifetimes in solution and the solid state for the ketones studied are shown in Table 3.2. The lifetimes were much longer in the solid state for all the ketones, reflecting, as expected the highly restricted mobility of the deactivating β-phenyl ring in the solid. However, ketone **II** showed only a modest increase in lifetime in the solid compared to solution. A comparison of the triplet decay traces of ketones **I** and **IIrac** monitored at 400 nm after 308 nm laser irradiation is shown in Figure 3.10. In solution, it is the β-phenyl ring which performs the deactivation of the carbonyl triplet. However, in the case of **I** in the solid state this may not be the case. Single crystal X-ray crystallography was used to determine the orientation of ketones **I** and **II** in the solid state. Figures 3.11 and 3.12 show

the crystal structures and unit cell arrangements for these two ketones. Both samples crystallized into orthorhombic unit cells having very similar dimensions. Ketone **I** had unit cell dimensions of a = 10.340(13), b = 31.00(4), c = 8.073(8) Å and a density of 1.233 g/cm^3; **IIS** had dimensions of a = 8.0283 (26), b = 31.2398(143), c = 5.6805(35) Å and a density of 1.186 g/cm^3. Despite their similar chemical properties, a distinct difference is observed in the proximity of the β-phenyl ring to the carbonyl group. Ketone **IIS** has the deactivating ring placed much closer to the carbonyl in the solid state, clearly making β-phenyl quenching a primary mechanism of triplet deactivation for this ketone. However, in the X-ray structure of ketone **I,** the β-phenyl ring is much farther away, making an intramolecular deactivation pathway highly improbable. The relative orientation of the aromatic benzoyl rings is illustrated in Figure 3.13. These are clearly too far for excimer formation mechanisms of the type that have been shown to be responsible for the decay in other systems.[73] The molecules are probably close enough for energy migration to occur, presumably leading to deactivation via defects or traps.

In section 3.2, it was shown that steady state irradiation of **I** and **II** in solution did not reveal any detectable products. The photostability in solution is attributed to a highly efficient β-aryl quenching mechanism which yields no product formation, even when an easily abstractable γ-hydrogen is present (ie. ketone **II**). This stability is also observed in steady-state irradiations of solid **I** and **IIrac** for periods of more than 100 hours at 300 nm. Again, like the solution experiments, no detectable products were observed by GC-MS analysis.

Of particular interest was the difference between the racemic crystal triplet lifetime and the pure enantiomers of **II**. We were surprised by a

triplet lifetime nearly twice as long for the racemic crystals compared to the pure enantiomers, as seen in Table 3.2. Figure 3.14 shows the actual triplet decay traces of **IIrac** compared to the pure enantiomers monitored at 400 nm after 308 nm laser irradiation. In contrast, **IIS** and **IIR** gave the same lifetime with superimposable decay traces. A number of attempts at growing crystals of **IIrac** suitable for X-ray over a period of two years were unsuccessful. Several methods, including supersaturation, slow evaporation and nucleation were attempted in various solvents and solvent mixtures. In order to gain some insight into the structure of the racemic crystals, it was necessary to use powder X-ray and solid state NMR techniques to describe the differences in the crystal structures. Figure 3.15 shows the unit cell dimensions obtained from the powder X-ray diffraction pattern of **IIS** and **IIrac**. Unit cell dimensions were calculated using PC-ITO (Visser, 1969)[85] software and calculated an orthorhombic unit cell with dimensions 8.0 x 31.3 x 5.7 Å for the pure enantiomer (**IIS**) giving a volume of 1400 A^3 and density of ca. 1.18 g/cm^3; **IIrac** was calculated to have a P2 unit cell with dimensions 16.6 x 12.9 x 14.1 $Å^3$ (α=90.0°; β=103.4°; γ=90.0°) giving a volume of 2943 $Å^3$ and corresponding density of 1.16 g/cm^3. Verification of the calculations used in determining the unit cell dimensions of **IIrac** was possible by analyzing the single crystal X-ray diffraction data obtained from **IIS** which correlated with the dimensions calculated by the PC-ITO software.

To further elucidate the structural differences between the racemic and pure enantiomer crystals, solid state ^{13}C NMR spectra of the two samples were recorded (Figure 3.16). Many of the chemical shifts for the **IIrac** carbons are shifted downfield compared to **IIS** indicating a significant difference in the surrounding environment for these carbons.

In particular, the carbonyl resonance for **IIrac** shows a downfield shift of more than 2 ppm compared to **IIS**.

To eliminate the possibility of impurities in the racemic crystals which may have caused the differences in lifetimes, a "synthetic" racemic was recrystallized from a mixture of equal portions of **IIR** and **IIS**. The newly made racemic crystals had the same properties as the "authentic" racemic including its triplet decay kinetics in the solid state. In contrast, a mechanical mixture of **IIR** and **IIS** showed typical pure enantiomer lifetimes, as expected.

The results of luminescence studies following 355 nm picosecond laser excitation have been summarized in Table 3.3. Phosphorescence was always extremely weak and the emission may incorporate delayed fluorescence. While any detailed analysis would be highly speculative, it is clear that the values for **IIS** and **IIrac** are of the same magnitude and showing the same differences as observed in the time-resolved diffuse reflectance work. Typical fluorescence lifetimes were around 300 ps with a longer (minor) component which may reflect the presence of traps or distinct surface sites.

Table 3.2. Structures of the ketones studied and their respective lifetimes (ns) in methanol solution and in the solid state.

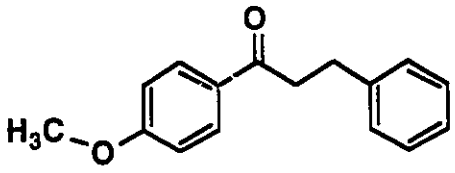

I

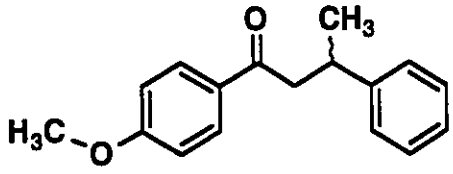

II

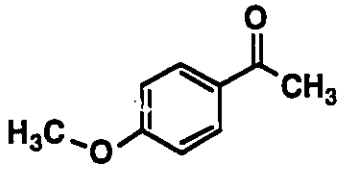

VIII

	Lifetimes (ns)[a]	
	solution[b]	solid
I	200	8000
IIrac	95	733
IIR	95	415
IIS	95	425
VIII	≥2000	1930 / 10910

[a] +/- 10%

[b] under a nitrogen atmosphere

Table 3.3. Luminescence data for various ketones in the solid state.

ketone	fluorescence [a]			phosphorescence
	λ_{max}	τ [b]	notes	τ
I	440	0.54/1.8	shift [c]	~1800
IIrac	440	0.22/1.8	shift [c]	~560
IIS	424	0.23/1.4	weak	~390
VIII	450	0.30/1.9	weak	~1600

a λ_{max} in nm and τ in ns.

b Typically the short lifetime accounts for ~80% of the decay.

c A pronouced shift to longer wavelengths with time is observed.

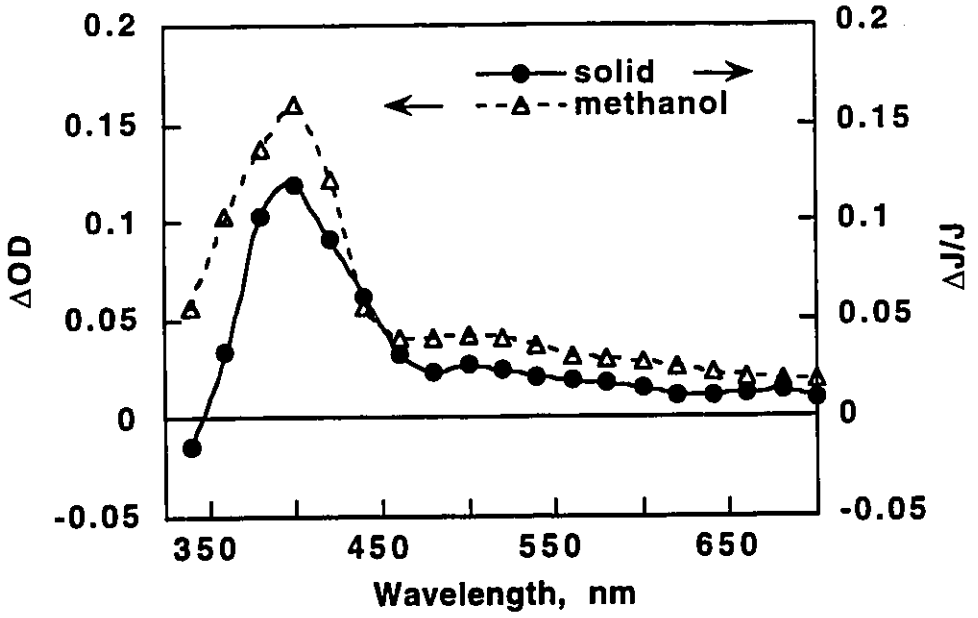

Figure 3.9. Transient absorption spectra of **IIrac** in methanol (Δ) and in the solid state (●) monitored 16 and 22 ns, respectively after 308 nm laser excitation. Expressed as ΔOD in solution and as ΔJ/J in the solid state.

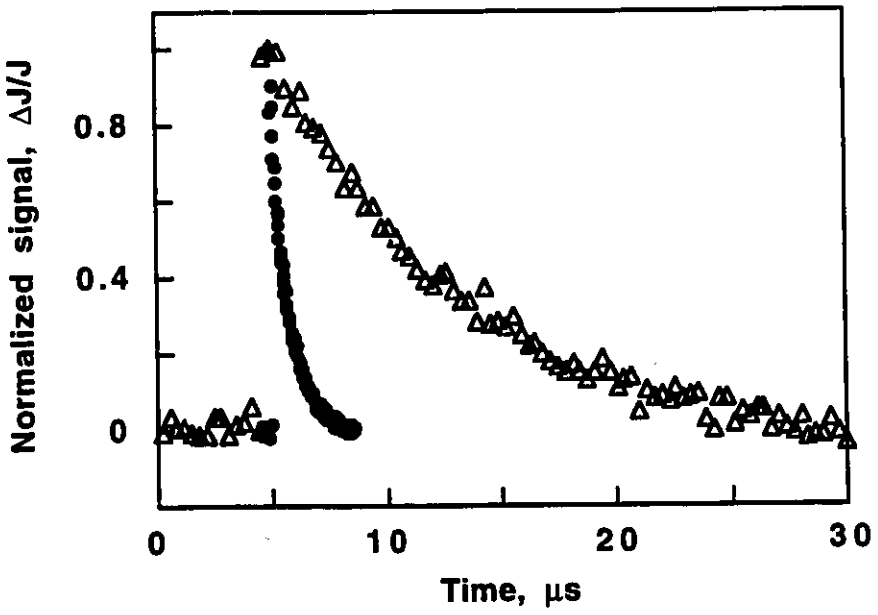

Figure 3.10. Transient absorption decays of **I** (Δ) and **IIrac** (●) in the solid state monitored at 400 nm after 308 nm laser excitation.

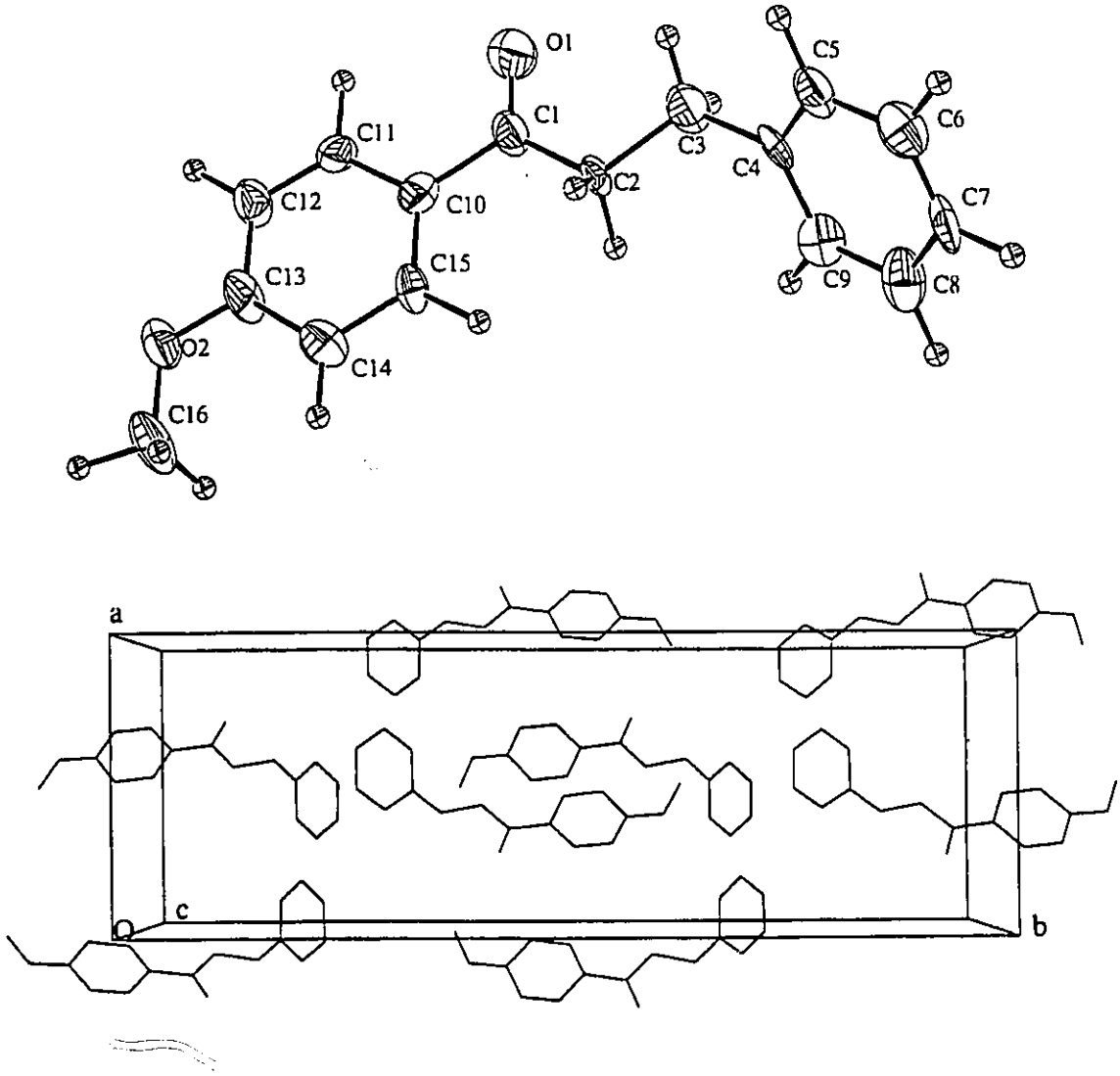

Figure 3.11. X-ray crystal structure of ketone **I** (top) and the arrangement of the molecules in the unit cell (bottom).

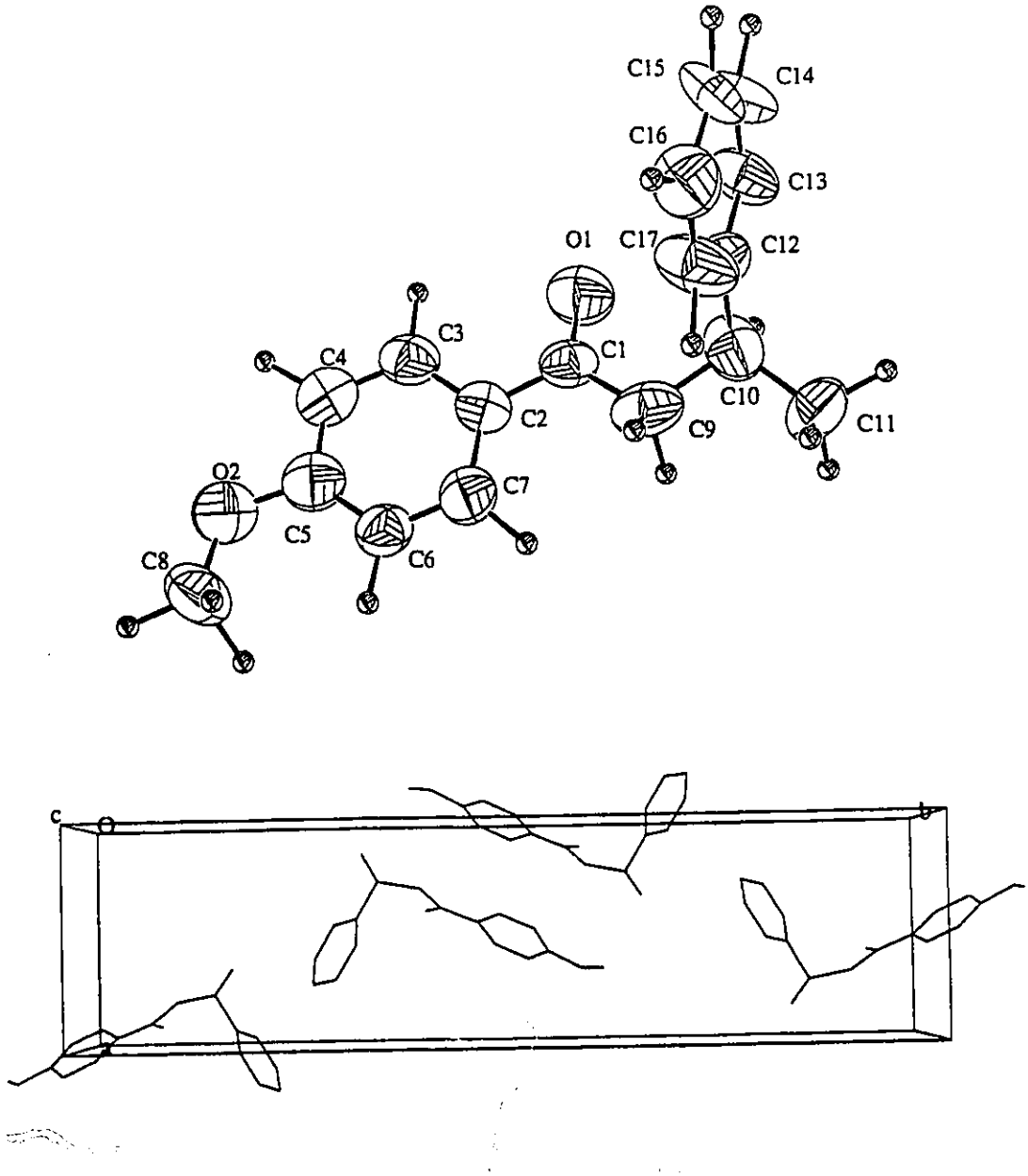

Figure 3.12. X-ray crystal structure of ketone **IIS** (top) and the arrangement of the molecules in the unit cell (bottom).

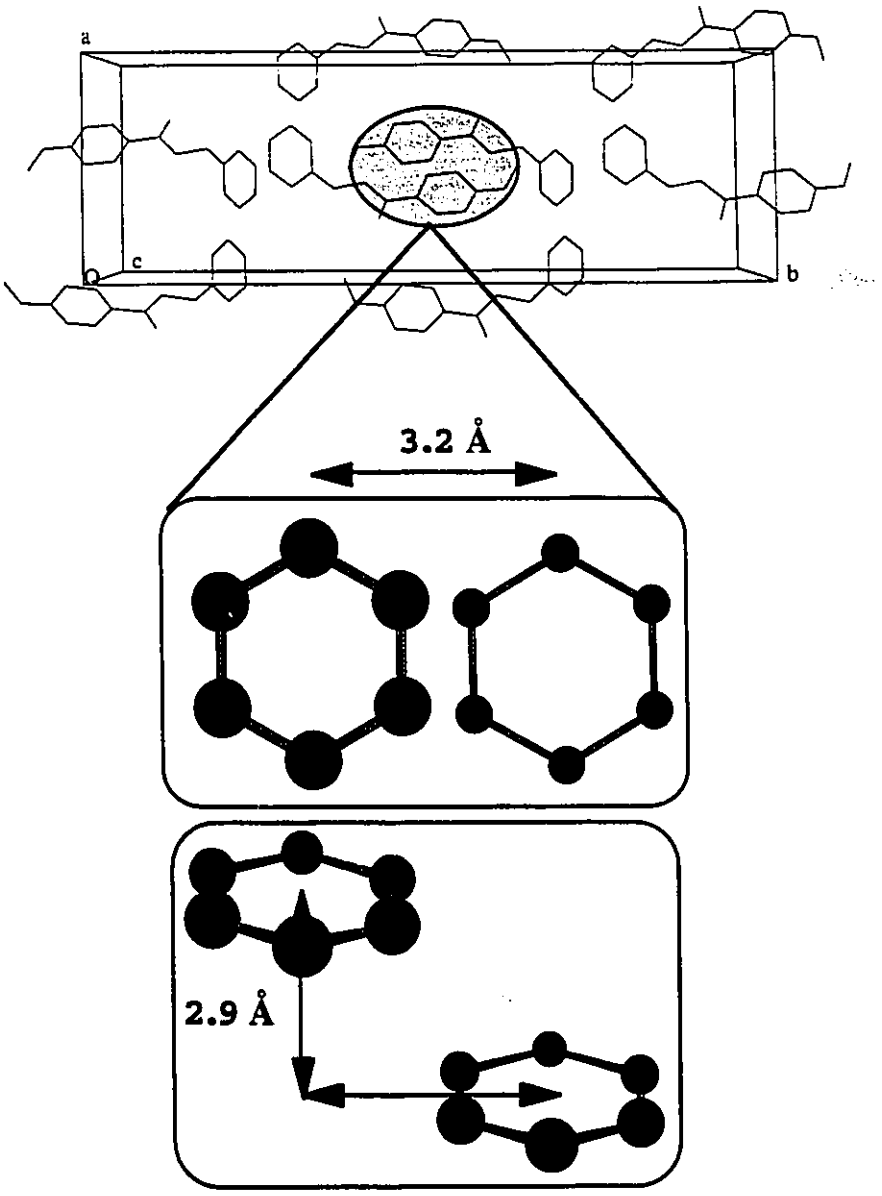

Figure 3.13. Unit cell for **I** and relative positioning of the aromatic ketone groups.

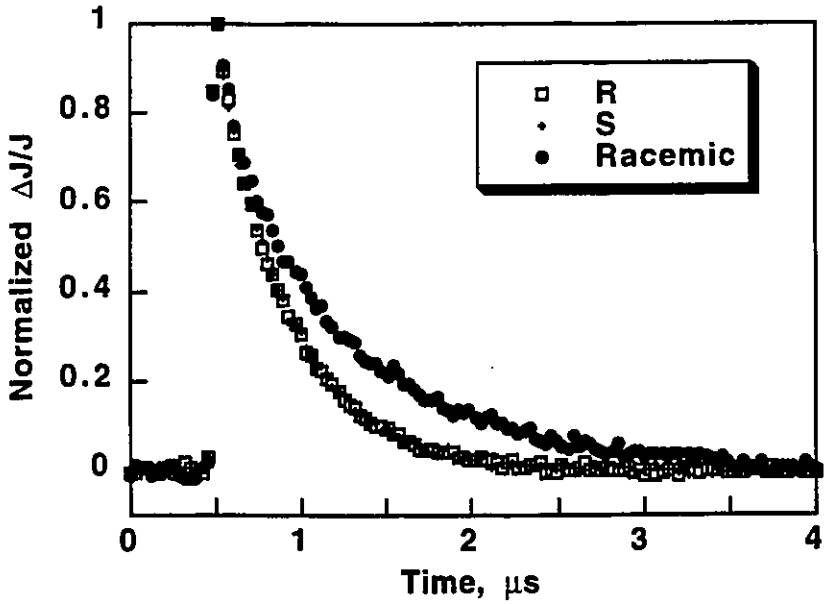

Figure 3.14. Transient absorption decay traces for **IIrac**, **IIR** and **IIS** in the solid state monitored at 400 nm after 308 nm laser excitation.

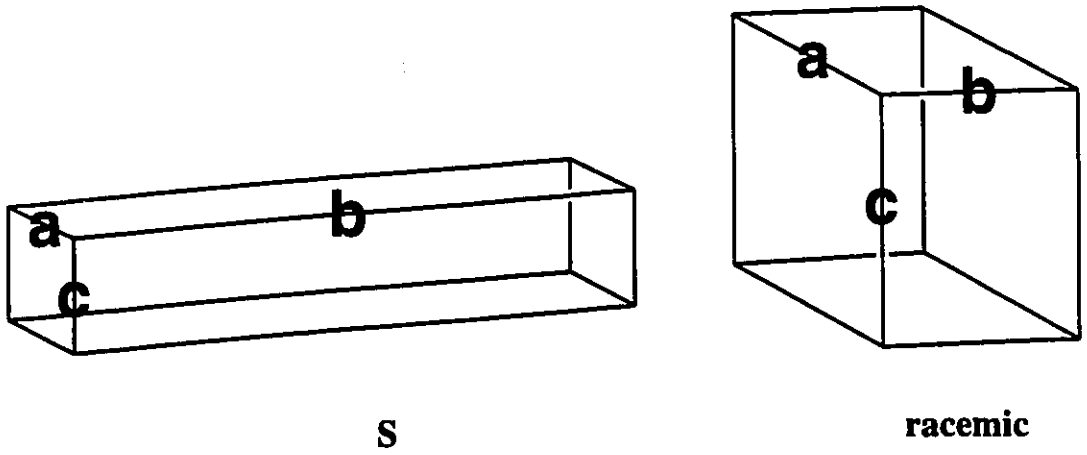

Figure 3.15. Unit cell dimensions of **IIS** (left) and **IIrac** (right) obtained from powder X-ray diffraction patterns using the PC-ITO program (Visser, 1967).[85]

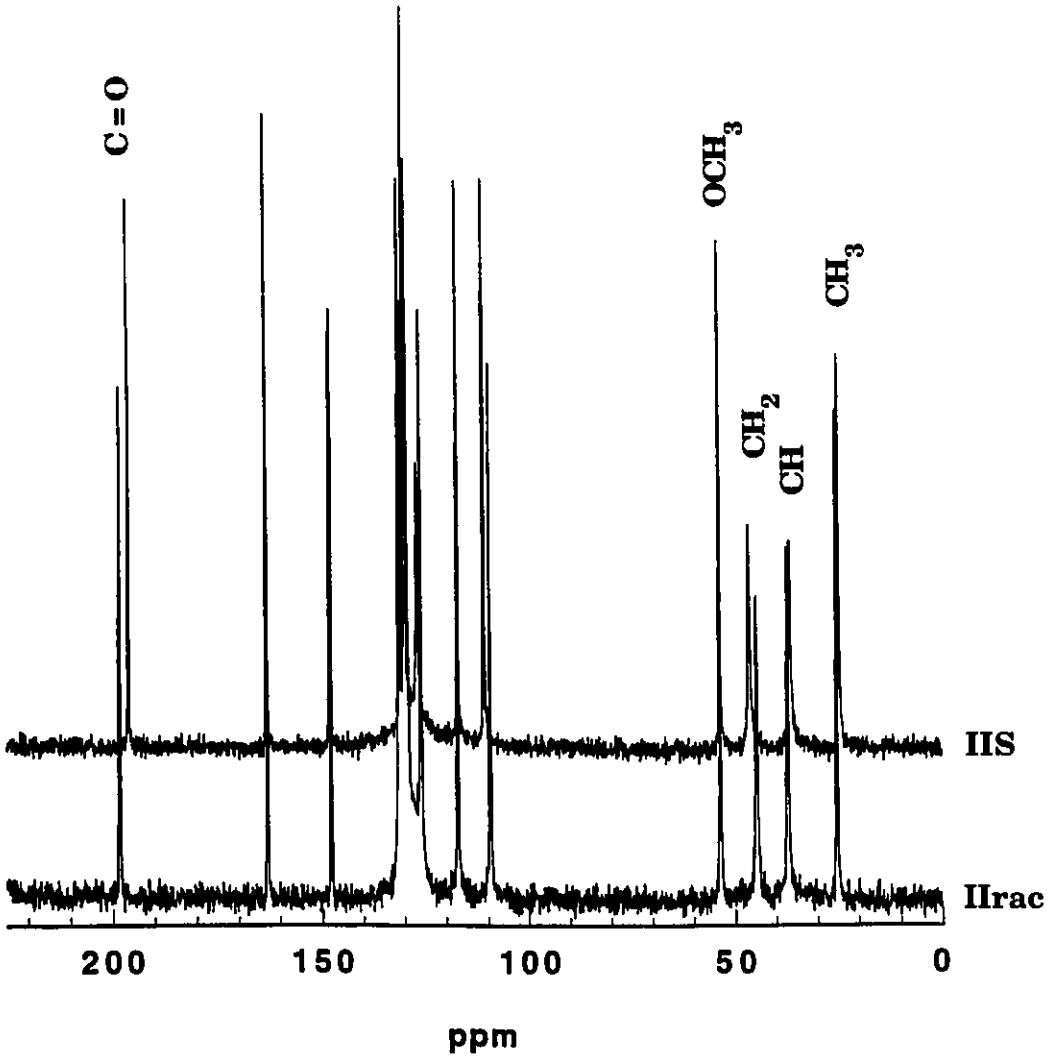

Figure 3.16. Solid state ^{13}C NMR spectra of **IIrac** and **IIS**.

3.3.2. Discussion

β-aryl ketones have been used as mobility probes in heterogeneous systems, such as cyclodextrins and zeolites because of the triplet lifetime's inherent sensitivity to mobility restrictions in confined spaces.[78,80] To effectively quench the carbonyl triplet state, a charge transfer interaction with the β-aryl ring is necessary. Confining the movement of the deactivating ring will result in longer triplet lifetimes in β-phenyl substituted ketones. Changing substituents on the molecule will also act in a similiar way by affecting the mobility of the β-aryl ring to either accelerate or slow down the decay, depending on the substitution pattern (section 3.2).

In the case of **I**, the triplet decay in solution is quite long compared to other β-phenyl ketones. This is even more pronounced in the solid state (see Table 3.2) where the triplet lifetime for **I** is extended by over an order of magnitude. Figure 3.10 shows the dramatic difference in triplet lifetimes observed. In solution, this is rationalized by the lack of steric confinements, such as methyl groups, which result in a facilitated rotation of the β-aryl ring away from the carbonyl. In the solid state, **I** and **IIS** both crystallize with orthorhombic unit cells with similar dimensions and densities. However, the crystal structure of **I**, shown in Figure 3.11, reveals a relatively flat stretched conformation with the β-aryl ring placed far away from the carbonyl, resulting in little or no intramolecular deactivation. In contrast, ketone **IIS** (Figure 3.12) has a crystal structure which places the β-aryl ring much closer to the carbonyl group, thus resulting in a solid state triplet lifetime which is only about 4-6 times longer than in solution, and more than an order of magnitude shorter than **I** in the solid state. The

close position of the β-phenyl ring to the carbonyl facilitates the charge transfer interactions required for the deactivation of the triplet state.

In the case of **I**, the β-aryl ring is quite far from the carbonyl, and triplet deactivation must occur by an alternative mechanism. A comparison of the triplet decay kinetics of *p*-methoxyacetophenone (**VIII**) with **I** reveals triplet lifetimes of similar magnitude in the solid state (Table 3.2). This leads us to believe that triplet **I** may not require an interaction of the β-aryl ring to facilitate deactivation, although we note that the decay for **VIII** is best fitted to a biexponential decay with first order lifetimes of approximately 2 and 11 μs.. The crystal packing arrangement of the molecules in the unit cell of **I** may provide an alternative deactivation pathway. Of particular interest are the two centre molecules in the unit cell shown in Figure 3.11. Their phenone moieties are aligned parallel to one another but displaced. While in other systems we have observed excimer-like deactivation mechanisms,[73] such a mode of decay appears unlikely here since a "sandwich-like" arrangement is usually required for excimer-mediated deactivation. No excimer-like emission is observed, and the relevant moieties (see Figure 3.11) are too shifted for these interactions to occur. Most likely, the crystal packing provides a channel for energy migration to traps or surface sites from where deactivation takes place. In the case of **VIII**, the longer triplet lifetime may represent deactivation through an energy migration to traps which is simlar to **I**, while the shorter decay may represent an even more efficient unidentified deactivation process.

Although the deactivation processes for solid **I** and **II** proceed through different mechanisms, both mechanisms render these compounds

remarkably photostable. No product formation was detected from either compound after more than 100 hours of 300 nm irradiation.

Relatively small differences in crystal packing can be observed from the triplet decays of the racemic compound (**IIrac**) and the pure enantiomers (**IIR, IIS**). We had suspected a difference in crystal packing judging from their respective melting points. The racemic form melts at 87°C while the pure enantiomers melt at 53°C. A more stable packing arrangement in the racemic form with greater intermolecular forces would be the cause of the elevated melting point and represents a more stable crystal lattice. Scheffer *et al.*[86] have observed different bimolecular reactivity in the solid state between dimorphs, which are defined as organic crystals of the same compound which pack in different symmetry relationships. We believe a similar phenomenon is occurring with the racemic and pure enantiomer crystals. Racemic mixtures in solution have been known to either crystallize and form a nonchiral racemic compound or undergo spontaneous resolution forming a mixture of chiral crystals. We believe that the former condition is occurring with **IIrac**, thus resulting in a different crystal structure compared to the pure enantiomers. The analysis of a solid state ^{13}C NMR spectra, indicates slight differences in the peak positions of some of the carbons. In particular, the carbonyl group in the racemic crystal is shifted upfield almost 2 ppm when compared to the pure enantiomer crystals (Figure 3.16). This would indicate a substantial difference in crystal packing and possibly the origin of chiral recognition in the case of the triplet lifetimes of **IIrac** and **IIS/IIR**.

Structural information of **IIS** was obtained from single crystal X-ray diffraction analysis of relatively easily made X-ray suitable single crystals of the pure enantiomer. A crystal large enough for single crystal X-ray

analysis could not be grown in the case of **IIrac** even after numerous attempts. Very small crystalline needles were the only result. However, the unit cell dimensions of **IIrac** were calculated from its powder X-ray diffraction pattern using PC-ITO software developed by Visser.[85] Figure 3.14, shows a scale representation of the unit cells of **IIrac** and **IIS**. The most obvious difference is the shapes of the unit cells and their respective volumes. The **IIS** unit cell is long and rectangular, nearly twice as long as the almost cubical unit cell of **IIrac**. The unit cell of **IIS** has four molecules per cell giving a density of 1.186 g/cm^3 and volume of 1400 Å^3. Based on density, there are eight molecules in the unit cell of **IIrac** giving a density of ca. 1.16 g/cm^3 and volume of 2900 Å^3. Although no conclusion can be made about the orientation of the molecules in the racemic crystal, the indirect evidence based on triplet lifetimes points toward a significant difference in crystal packing between the racemic and pure enantiomeric forms. This results in chiral discrimination in the decay kinetics of the ketones in the solid state. These changes in crystal packing must alter the position of the β-aryl ring in relation to the carbonyl in the solid state. Slightly closer packing in the racemic crystals may push the β-phenyl ring slightly away from the carbonyl, thus accounting for the longer triplet lifetime observed. This interpretation, while reasonable, must remain speculative, as there are no single crystal structural studies of **IIrac** to compare with those for **IIS**.

3.3.3. Conclusion

We have successfully measured the triplet lifetimes of several β-aryl ketones in the solid state using laser flash diffuse reflectance photolysis

techniques. Triplet absorption spectra showed little cleavage of these ketones in the solid state upon laser excitation. The triplet lifetimes in the solid state are determined by the position of the β-phenyl ring in relation to the carbonyl. We have shown that ketones having methyl substitution in the β-position will crystallize having the deactivating ring closer to the carbonyl and result in faster decay kinetics compared to unsubstituted ketones. Small packing differences in the unit cells will also be manifested in a change in triplet lifetime as seen from comparing racemic to enantiomerically pure crystals.

In the past, β-aryl ketones have proven to be excellent mobility probes in heterogeneous solution. Our research indicates that ketone **II** would be an excellent mobility probe in solid state systems as well. Small changes in the position of the deactivating β–phenyl ring results in measurable changes in triplet lifetime.

3.4. Experimental

Materials.

Solvents used for flash photolysis and synthesis (benzene, acetonitrile, cyclohexane, methanol) were obtained from BDH (Omnisolve, glass distilled) and were used without further purification.

***p*-methoxy-β-phenylpropiophenone (I)**: Ketone **I** was prepared following a synthetic procedure[87] involving conversion of the corresponding carboxylic acids (from Aldrich) into the acid chlorides by reaction with thionyl chloride. After removal of excess thionyl chloride, a Friedel-Crafts reaction[87] was carried out on the acid chlorides using anisole (Aldrich). Removal of excess anisole under reduced pressure followed by

recrystallization from ethanol gave the desired product. No *ortho*-substituted product (another possible product of the reaction) was observed. m.p. 95-97^{0}C (lit. 96-97^{0}C)[92]; ^{13}C NMR ($CDCl_3$) δ 30.35 (CH_2), 40.16(CH_2), 55.49(OCH_3), 113.74(CH), 126.11(CH), 128.45 (CH), 128.53(CH), 129.94(C), 130.32(CH), 141.48(C), 163.44(C), 197.80(CO); MS m/z (%) 240 (23, M^+), 136 (7), 135 (100), 107 (7), 92 (11), 77 (20). ^{1}H NMR ($CDCl_3$) δ 2.9-3.1 (t, 2H), 3.1-3.3 (t, 2H), 3.8 (s, 3H), 6.9 (d, 2H), 7.1-7.4 (m, 5H), 7.9 (d, 2H). IR (KBr) 1669 cm^{-1}. Anal. Found: C, 79.87; H, 6.74%. Calcd for $C_{16}H_{16}O_2$: C, 79.97; H, 6.71%.

***p*-methoxy-β-phenylbutyrophenone (II)**: Racemic, (R) and (S) phenyl butyric acid (Aldrich) were used as starting materials to make the racemic and pure isomers of **IIrac**, **IIR** and **IIS** using the same method as **I** above. m.p. 86.5-87^{0}C (**IIrac**); 53-54^{0}C (**IIR/IIS**); ^{13}C NMR ($CDCl_3$) δ 21.64 (CH_3), 35.55 (CH), 46.51 (CH_2), 55.31 (OCH_3), 113.67 (CH), 126.25 (CH), 126.89 (CH), 128.53 (CH), 128.71 (C), 130.39 (CH), 146.80 (C), 163.49 (C), 197.82 (CO); MS m/z (%) 254 (28,M^+), 239 (25), 150 (29), 135 (100), 105 (10), 92 (10), 77 (23). IR (KBr) 1668 cm^{-1}; ^{1}H NMR ($CDCl_3$) δ 1.3 (d, 3H), 3.2 (m, 2H), 3.5 (m, 1H), 3.9 (s, 3H), 6.9 (d, 2H), 7.3 (m, 5H), 7.9 (d, 2H). Anal. Found: C, 80.06; H, 7.04% and C, 80.40; H, 7.22% for **IIrac** and **IIS**, respectively. Calcd for $C_{17}H_{18}O_2$: C, 80.29; H, 7.13%. The optical rotation ($[\alpha]^{20}$) measured with the sodium D line was +15.7^{0} for **IIR** while **IIS** was -14.7^{0}. Optical purity was verified by the lack of separation of the pure enantiomers on HPLC using a chiralcel OB column (J.T. Baker Inc.) and chiral shift reagent analysis using Tris[3-(heptafluoropropyl-hydroxymethylene)-(+)-camphorato], europium (III) derivative (Aldrich) on ^{1}H NMR. The two techniques mentioned above were able to readily resolve the two enantiomers making up **IIrac**. ^{13}C (CP-MAS) NMR: **IIS** gave signals (δ, ppm): 24.8 (CH_3), 36.5 (CH), 46.5 (CH_2), 53.7

(OCH_3), 110.8 (CH), 117.1 (CH), 126.8-131.2 (unresolved C and CH), 148.1 (C), 163.3 (C) and 196.2 (CO); **IIrac** gave signals (δ, ppm): 25.4 (CH_3), 37.1 (CH), 44.7 (CH_2), 53.6 (OCH_3), 109.4 (CH), 117.2 (CH), 126.0-131.4 (unresolved C and CH), 147.8 (C), 163.0 (C) and 198.4 (CO).

***p*-methoxy-3,3-methyl-3-phenylpropiophenone (III)**: Synthesis of ketone **III** involved the initial preparation of neophyl chloride from 3-chloro-2-methylpropene (Aldrich) following a literature procedure.[88] A standard Grignard reaction was then carried out converting the neophyl chloride into its corresponding carboxylic acid.[87] The remainder of the synthesis is the same as for ketones **I** and **II**. After removal of excess anisole, the crude yellow liquid was purified by TLC on a silica gel spinning plate (Chromatotron Model 7924T). ^{13}C NMR ($CDCl_3$) δ 28.95 (CH_3), 37.39 (CH), 50.35 (CH_2), 55.29 (OCH_3), 113.49 (CH), 125.49 (CH), 125.78 (CH), 128.20 (CH), 130.44 (CH), 131,27 (C), 149.18 (C), 163.26 (C), 197.75 (CO); MS m/z (%) 268 (4,M^+), 150 (100), 135 (92), 119 (24), 91 (24), 77 (24); IR (neat) 1674 cm^{-1}; ^1H NMR ($CDCl_3$) δ 1.5 (s, 6H), 3.2 (s, 2H), 3.8 (s, 3H), 6.8 (d, 2H), 7.3 (m, 5H), 7.8 (d, 2H).

***p*-methoxy-(3'-methyl)-3-phenylpropiophenone (IV)**: Ketones **IV** and **V** were synthesized from *p*-methoxyacetophenone and 3-methylbenzyl alcohol (**IV**) or 4-methylbenzyl alcohol (**V**) by the method of Pratt and Evans.[89] m.p. 46-47°C; ^{13}C NMR ($CDCl_3$) δ 21.46 (CH_3), 30.26 (CH_2), 40.22 (CH_2), 55.46 (OCH_3), 113.71 (CH), 125.41 (CH), 126.84 (CH), 128.43 (CH), 129.26 (CH), 130.31 (CH), 129.94 (C), 138.07 (C), 141.42 (C), 163.41 (C), 197.85 (CO); MS m/z (%) 254 (25, M^+).135 (100), 77 (17); IR (KBr) 1669 cm^{-1}; ^1H NMR ($CDCl_3$) δ 2.3

(s, 3H), 3.0 (t, 2H), 3.2 (t,2H), 3.8 (s, 3H), 7.0 (m, 6H), 7.9 (d , 2H). Anal. Found: C, 80.39; H, 7.18%. Calcd for $C_{17}H_{18}O_2$: C, 80.29; H, 7.13%.

***p*-methoxy-(4'-methyl)-3-phenylpropiophenone (V)**: m.p. 64-66 ^{o}C (lit. 64-65 ^{o}C)[93]; ^{13}C NMR ($CDCl_3$) δ 21.0 (CH_3), 29.90 (CH_2), 40.29 (CH_2), 55.45 (OCH_3), 113.69 (CH), 128.29 (CH), 129.17 (CH), 130.30 (CH), 129.95 (C), 135.55 (C), 138.35 (C), 163.39 (C), 197.85 (CO); MS m/z (%) 254 (25, M^+), 135 (100), 77 (18); IR (KBr) 1669 cm^{-1}; ^{1}H NMR ($CDCl_3$) δ 2.3 (s, 3H), 3.0 (t, 2H), 3.2 (t, 2H), 3.8 (s, 3H), 6.9 (d, 2H), 7.2 (m, 4H), 7.9 (d, 2H). Anal. Found: C, 80.54; H, 7.19%. Calcd for $C_{17}H_{18}O_2$: C, 80.29; H, 7.13%.

***p*-methoxy-β-phenyl-α-hydroxypropiophenone (VI)**: Ketone **VI** was prepared by the slow dropwise addition of the Grignard reagent from 4-bromoanisole to a solution of tetrabutyldimethylsilyl (TBDMS) protected 3-phenyllactic acid chloride cooled to ~ -15 ^{o}C in an ice-salt bath. The Grignard of 4-bromoanisole was prepared following a standard synthetic procedure involving the reaction of magnesium metal (Aldrich) with 4-bromoanisole (Aldrich) in tetrahydrofuran which was distilled over sodium prior to use.[87] The TBDMS-protected acid chloride was prepared by first functionalizing the carboxylic acid and alcohol groups on (D) or (L) phenyllactic acid (Aldrich, 10g) by adding 2.2 equivalents of *tert*-butyldimethylsilyl chloride (TBDMS, Aldrich, 20 g) and imidazole (Aldrich, 17 g; recrystallized once from ethanol) to a 0.2 M solution (100 mL) of the acid in dimethylformamide (DMF, BDH Omnisolve).[90] After 48 hours stirring at room temperature and 2 hours at 40-50 ^{o}C, the reaction mixture was diluted with 300 ml water, extracted twice with ethyl acetate and the resulting organic phases combined and washed twice with a saturated

solution of sodium bicarbonate before drying over magnesium sulfate. The mixture was then filtered and the solvent removed to give the crude protected acid as an oily liquid which was subsequently dissolved in some ethyl ether and quickly passed through a plug of silica gel using ether as the eluting solvent.

The alcohol protected acid chloride was synthesized following a procedure by Wissner *et al.*[90] Approximately 10 g of the disilylated crude was combined with 30 mL of dichloromethane and 5 drops of DMF into a 100 mL 3 necked flask cooled to approximately 0 ^{o}C with an ice-salt bath. To this mixture, 280 mL of oxalyl chloride (Aldrich) was added dropwise and after the addition, the mixture was stirred for 1.5 hours at 0 ^{o}C and then 0.5 hours at room temperature. Finally, the solvent was removed leaving the crude protected acid chloride.

At this point the Grignard of 4-bromoanisole was synthesized (0.68 g magnesium turnings (Aldrich); 12 mL THF; 3.5 mL bromoanisole (Aldrich)) and then added dropwise to a solution of the protected acid chloride (0.5 g) dissolved in ~ 2 mL diethyl ether cooled to ~ 0 ^{o}C in an ice-salt bath. After the addition was complete, the resulting mixture was stirred vigorously for 1-2 hours at room temperature at which point 5 g of crushed ice was added to the flask and then 20 mL of cold 15% H_2SO_4. The aqueous and ether layers were separated and washed twice with ether and water, respectively. The combined ether layers were then washed twice with saturated soldium bicarbonate and then dryed over magnesium sulfate. The mixture was then filtered and the solvent removed to give a crude brown oil. TLC analysis revealed the presence of four products which were separated and isolated using a chromatotron spinning silica

gel plate using a 90:10 hexane:ethyl acetate solution. The largest band was identified by GC-MS as the silylated derivative of **VI**.

Removal of the silyl protecting group was accomplished with tetrabutylammonium fluoride (Aldrich; 2.5 mL of a 1 M stock solution in THF) added dropwise to a cooled solution of 1 mL of silylated product in 11 mL THF.[91] The mixture was stirred for 12 hours at room temperature after which the solvent was removed to give a crude yellow oil. The oil was then washed several times with cold hexane (~10 mL total) and then dissolved in hot ethanol and left in the freezer to recrystallize. After several days, the resulting crystals were isolated. m.p. 54-55^{o}C; ^{13}C NMR ($CDCl_3$) δ 42.2 (CH_2), 55.6 (OCH_3), 73.4 (CH), 114.1 (CH), 131.0 (CH), 129.5 (CH), 128.3 (CH), 127.0 (CH), 126.6 (C), 136.8 (C), 164.2 (C), 199.5 (CO); MS m/z (with TMS, %) 313 (3, M^+), 193 (92), 135 (20); ^{1}H NMR ($CDCl_3$) δ 2.8-3.3 (m, 2H), 3.7 (d, OH), 3.9 (s, 3H), 5.2-5.4 (m, 1H), 6.9-7.3 (m, 7H), 7.8-8.0 (m, 2H).

***p*-Methoxyacetophenone (VIII)** was purchased from Aldrich and recrystallized once from ethanol.

Molecular modeling calculations.

These calculations were carried out using a molecular modeling software program (PCMODEL version 4 from Serena Software and CAChe molecular mechanics) for the Macintosh II series of computers. The force field used is derived from the MM2 force field and MMP1 pi-VESCF routine of Allinger.[75] A dihedral driver was utilized for the rotation of bonds and calculation of energies.

Cyclic Voltammetry.

Cyclic voltammograms were generated using an air tight cell under a nitrogen atmosphere and a Bioanalytical Systems CV-1B voltammogragh instrument utilizing both platinum working (1 mm disk) and auxiliary electrodes and a silver/silver nitrate (0.1 M) reference electrode. Voltammograms were recorded on a calibrated Hewlett Packard X-Y recorder with an x-axis scale of 0.1 V/cm and Y-axis scale of 0.25 V/cm while the scan speed was 10 sec/inch. The solutions for study consisted of 50 mL purified acetonitrile (passed through an activated alumina column), tetrabutylammonium perchlorate (1.71 g, 0.1 M) recrystallized 3 times from 90% ethyl acetate/10% hexane, and a mass of analyte equalling 1mM. The solutions were deaerated with nitrogen prior to the measurements. A standard solution of sublimed ferrocene gave a reversible signal with a potential of 0.05 V.

NMR spectra.

The ^{13}C CP/MAS NMR data was collected on a Bruker ASX-200 NMR spectrometer equipped with a 7 mm MAS probe. The cross polarization technique was employed with suppression of first order spinning sidebands.[94] The ^{1}H $\pi/2$ pulse was 3.6 μsec in duration and the contact time was 1 msec and the relaxation delay was 4 seconds. The samples were spun at 5000 Hz. In all spectra 128 transients were signal averaged. Each free induction decay was collected with 3k data points which were zero filled to 16k prior to Fourier transformation. The spectral window spanned 17774 Hz. No line broadening or resolution enhancement was applied to the data. The dipolar dephasing technique[95] was used to partially assign the spectra. The dephasing delay was 40 μsec and yields spectra consisting of

only carbonyl, quaternary and methyl carbon resonances. The chemical shifts were indirectly referenced to tetramethylsilane by externally referencing to tetrakis-trimethylsilylsilane at 3.7 ppm from TMS at 0 ppm and were in good agreement with previous solution ^{13}C NMR data reported above.

Crystallographic data.

The crystals of approximate dimensions 0.2 x 0.05 x 0.2 mm, 0.2 x 0.2 x 0.2 mm and 0.2 x 0.2 x 0.2 mm for ketones **I**, **IIS** and **VI**, respectively, were mounted on a glass capillary and diffraction measurements made on a Rigaku diffractometer with Mo Ka radiation. Other apparatus and data handling details are given elsewhere.[73] Both ketones **I** and **IIS** corresponded to orthorhombic cells, the former having cell dimensions of a = 10.3193(72), b = 31.0812(90), c = 8.0179(71) Å; the latter having dimensions a = 8.0283 (26), b = 31.2398(143), c = 5.6805(35) Å. Ketones **I** and **IIS** had Z values of 15.4 and 12.0 with F.W. = 240.30 and 254.33, as well as calculated densities of 1.241 g/cm^3 and 1.186 g/cm^3, respectively. Figures 3.11 and 3.12 show the unit cells of ketones **I** and **IIS**. Ketone **VI** corresponded to a monoclinic unit cell having cell dimensions of a = 21.953(8), b = 23.183(9), c = 10.658(5) Å (beta = 102.793(5)) with a calculated density of 1.282 g/cm^3, Z value of 5.5 and F.W. = 255.29.

Powder X-ray spectra were collected using a Philips PW1827/91 X'Pert System powder X-ray diffractometer. PC-ITO (Visser, 1969)[85] software was used to index the powder X-ray diffraction patterns for **IIrac**. **IIS** was also calculated in the same way and compared to the values obtained from the single crystal X-ray data. The unit cell dimensions calculated for **IIrac** were 16.6 x 12.9 x 14.1 Å; $\alpha=\beta=90^o$; $\gamma=103^o$. All the lines

obtained in the powder X-ray pattern were accounted for. Similarly, the unit cell for **IIS** was calculated as 8.0 x 31.3 x 5.7 Å; $\alpha=\beta=\gamma=90^{o}$ with all lines accounted for and is in good agreement with the single crystal X-ray data given above.

Laser flash photolysis.

The laser flash photolysis apparatus used is described in detail in Chapter 2.

Luminescence spectroscopy.

These measurements were carried out using the third harmonic (355 nm) from a Continuum PY-61 picosecond YAG laser for excitation and a Hamamatsu fluorescence measurement system based on a Model C4334 Streakscope.

Steady state irradiations.

Steady state irradiations were performed in acetonitrile solution in 7 x 7 mm^2 cells made from Suprasil quartz tubing. The samples were deaerated by purging with a slow stream of nitrogen for 30 min. Solid samples were contained in small ~10 cc Suprasil quartz tubes which were continually rotated in the irradiation chamber to ensure homogeneous light exposure. The samples were irradiated in a reactor with nine RPR-300 nm lamps. The temperature of the irradiation chamber was in the 30-35 ^{o}C range. GC-MS analysis was carried out with a Fisons Instruments GC 8000 series with MD800 mass detector.

Chapter 4. Effect of Probe Incorporation into Cyclodextrins

4.1 Introduction

Our initial interest in incorporating chiral ketones, such as **II**, into chiral host environments centred around the possibility of observing different decay kinetics for the two enantiomers which would indicate different modes of complexation for each isomer. Our first choice of host was the cyclodextrin (CD's) family which had been previously studied using similar ketones.[80] Cyclodextrins (CDs) are cyclic oligosaccharides (Figure 4.1) that have a doughnut-like shape with a relatively hydrophobic cavity. Cyclodextrins are formed from enzymatic degradation of starch catalyzed by a group of amylases called glycosyltransferases which hydrolyze off one end of a starch helix turn, and then join its ends together.[96] Three different CDs are commonly available constructed of six (α-CD), seven (β-CD), or eight (γ-CD) glucose units joined by α(1-4)-linkages. The number of glucose units in the ring is determined by the site of enzymatic hydrolysis of the starch. The cavity is chiral since the monomers making up the structure are all D-glucose units resulting in a large characteristic α rotation. The size of the internal cavity changes with the number of sugar units; the smallest internal diameter, located within the cavity, is 4.2, 5.6 and 6.8 Å for α-, β- and γ-CD, respectively (Table 4.1). The diameter of the small and large entrances of the CD cavities are typically 1.2-1.7 Å and 4.6-5.2 Å larger than the smallest internal diameter.[97] Cyclodextrins readily form inclusion complexes with many organic and inorganic compounds.[97-101] Hydrophobicity and the size of the guest molecule are important factors in determining the equilibrium constant for complex formation. CD

complexes serve as tools in the study of weak intermolecular interactions and can be extended to model enzymatic processes through their demonstrated catalytic activity.[96]

In this chapter, probe molecules consisting of *p*-methoxy-β-phenylpropiophenones substituted at the β-position (Scheme 4.1) were used to investigate the mobility of the triplet molecules within the complex. In some of our experiments, the methylated derivative of β-CD (β-MCD: heptakis(2,6-di-O-methyl)-β-CD) was used as it is more soluable in water than the unsubstituted β-CD allowing solubilization of the more hydrophobic probe-β-CD complexes. The cavity of β-MCD is slightly longer than β-CD.

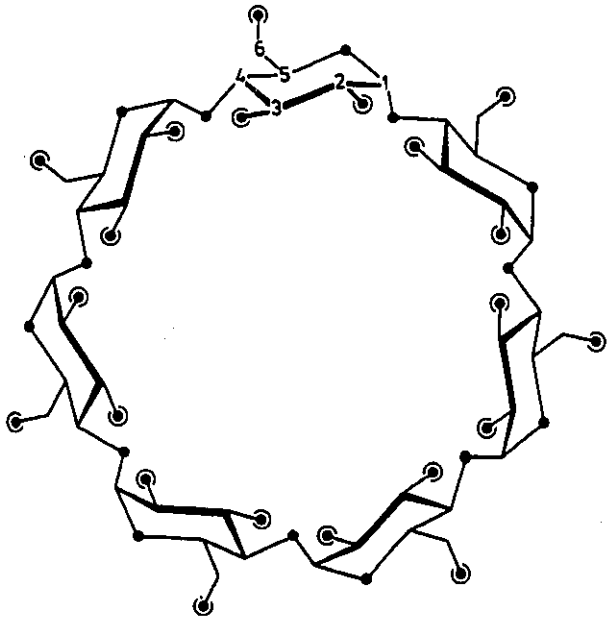

Figure 4.1. Chemical structure of β-cyclodextrin. (•) oxygen atoms, (⊙) hydroxyl groups. Adapted from Saenger.[100]

The unsubstituted ketone **I** had been used in previous studies as a mobility probe in CD's[80], zeolites[78], and liquid crystals[92,102] due to its unique

sensitivity to mobility restrictions imposed on the intramolecular triplet state deactivation by the β-aryl ring (see Chapter 3). A newly synthesized ketone mobility probe (**II**), containing a chiral centre, had never been investigated. Before a study of pure enantiomer triplet lifetimes in cyclodextrins was attempted, the effect of added methyl substitution in the β-position on probe incorporation into a CD was carried out. An interesting and perhaps useful story came out of these inital studies which helped the understanding of how these ketones are oriented in CD host environments. This will be outlined below and the chiral probe experiments will be addressed later.

Table 4.1. Cyclodextrin dimensions*.

CD	d_1: d_2: d_3 Å
α-CD	8.8: 4.2: 5.6
β-CD	10.8: 5.6: 6.8
γ-CD	12.0: 6.8: 8.0

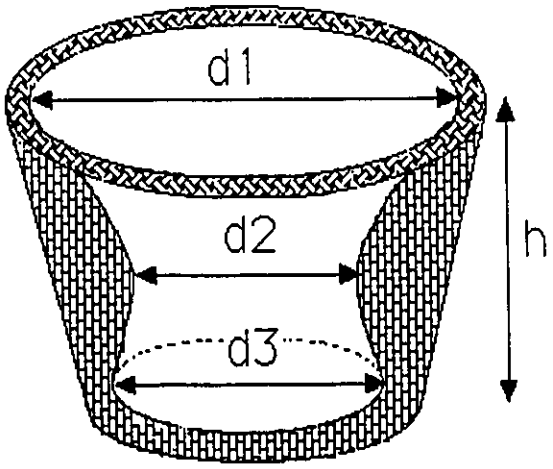

* from Saenger[100]

The solution experiments led into the analysis of the triplet states of the probe molecules in solid state CD complexes which would further restrict the mobility of the ketones. Again, the emphasis on these experiments was to restrict the mobility leading to triplet deactivation to the point where differences in complexation may be reflected in their

deactivation kinetics. In these experiments, the diffuse reflectance laser flash photolysis was used to analyse the triplet behavior of the chosen probe molecules in the solid state. The diffuse reflectance technique is described in detail in Chapter 2.

Scheme 4.1. Substituted ketones used to probe cyclodextrins.

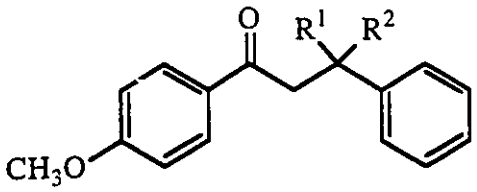

I: $R^1=R^2=H$

II: $R^1=CH_3$; $R^2=H$

III: $R^1=R^2=CH_3$

4.2 Cyclodextrin Solutions

4.2.1 Results

The triplet lifetimes for **II** and **III** in solution and complexed to CDs were measured at 400 nm and are given in Table 4.2. The decays followed first-order kinetics although a small residual absorption was observed. This behaviour had also been previously observed for **I**-CD complexes.[80] The lifetimes of the triplet of **I** in water and methanol are very similar.[80] In the case of **II** and **III** measurements in aqueous solution were not possible due to their low solubility. In the absence of aqueous data the methanol values will be used as representative of homogeneous behavior in polar solution. All triplet lifetimes increase when included in β-MCD or γ-CD, although the increase is more dramatic for the latter. The different

solution lifetimes for **I** and **II** are ascribed to different average locations of the β-phenyl ring in relation to the carbonyl moiety. Complexation with CDs will decrease the degree of rotational freedom for the β-phenyl ring. If the restriction of β-phenyl ring mobility does not allow the preferential location of the β-phenyl ring close to the carbonyl, the triplet lifetimes of **I**, **II** and **III** in a given CD should be essentially the same.

Table 4.2. Triplet lifetimes (ns) of **I**, **II** and **III** in methanol and in aqueous cyclodextrin complexes.

Compound	MeOH	β-CD or β-MCD	γ-CD
I	240 [a]	350 [a]; 293 [c]	1350 [a]
IIrac	95 [b]	212 [c]	1400
IIR		219 [c]	1394
IIS		205 [c]	1411
III	10 [b]	120 [c]	400

[a] from Netto-Ferreira *et al.*[80]

[b] from Chapter 3

[c] the methylated β-MCD was employed

4.2.2 Discussion

As discussed in section 3.1, the decay of the triplet of **I** occurs through an intramolecular deactivation process involving the motion of the β-phenyl ring over the plane of the carbonyl oxygen leading to charge

transfer of the carbonyl n,π* triplet state.[67] In the case of β-phenylpropiophenones the lowest n,π* and π,π* triplet states are very close in energy and their relative position can be altered by substitution on the aromatic rings. p-Methoxy-β-phenylpropiophenones have longer triplet lifetimes compared to β-phenylpropiophenones because the methoxy substituent leads to a low lying π,π* state.[67] Thus, reactions of n,π* state occur through its small (typically ~ 1%) thermal population.

Intramolecular quenching in **I** can be slowed down in constrained media such as the hydrophobic zeolite Silicalite[78], liquid crystals[102] and CDs.[79] In the case of CDs this effect was very dependent on the size of the cavity.[80] For β-CD only the *p*-methoxy phenyl ring is included and the β-phenyl ring is free to approach the carbonyl (Figure 4.2). In the case of γ-CD the triplet lifetime is increased by a factor of 6 relative to its solution value probably as a result of the inclusion of both rings into the CD cavity. Thus, the quenching is slowed down by restricting the movement of the β-phenyl ring. Compounds **II** and **III** were employed to investigate if methyl substitution would alter the mobility of the β-phenyl ring in CD complexes.

Studies in homogeneous solutions (section 3.2) have shown that the triplet lifetimes of **II** and **III** are shorter than that for **I** (Table 4.2). The introduction of methyl groups in the β-phenyl position changes the lowest energy conformation. MMX calculations suggest that for **II** there is a preferred conformation with minimum energy which places the β-phenyl ring at ~60^0 with respect to the carbonyl group, whereas in the case of **I** there is no preferred single conformation as the three geometries (60^0, 180^0, -60^0) have very similar energies. This effect leads to a decrease of the triplet lifetime of **II**. In the case of **III** two equivalent preferred conformations for

the β-phenyl ring (+60^0 and -60^0) in relation to the carbonyl are possible leading to a further decrease of the triplet lifetime.

The triplet lifetimes reported in Table 4.2 indicate that the size of the β-MCD cavity can only include one of the aromatic rings (Figure 4.2). The increase in lifetime is not sufficient to suggest inclusion of the β-phenyl ring but rather that some restriction of the mobility of this ring leads to longer triplet lifetimes. The much larger increase observed for γ-CD complexes is believed to be due to the inclusion of both rings into the cavity (Figure 4.2).[80] Similar arguments have been recently used by Leigh *et al.*[103] to explain the photochemistry of included *p*-(4-hydroxyphenyl)ethoxyacetophenone.

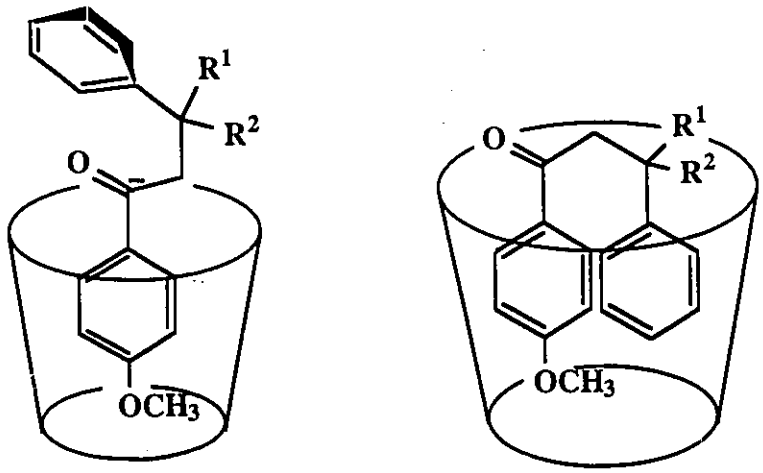

β-CD γ-CD

Figure 4.2. Schematic representation of complexes of *p*-methoxy-β-phenylpropiophenone derivatives with β- and γ-CD (adapted from Netto-Ferriera *et al.*)[80]

Complexes of both β-CD and β-MeCD with the least hydrophobic ketone (**I**) can be prepared and comparisons of the triplet lifetimes can be made (Table 4.1). A slight decrease in triplet lifetime is observed with complexes of β-MeCD reflecting less conformational restriction. The addition of methoxy substituents in β-MeCD may result in less hydrogen bonding with the included ketone, thus allowing more freedom of movement for deactivation. Complexes of β-CD and ketones **II** and **III** could not be made due to their larger hydrophobicity, thus β-MeCD was used instead.

The fact that almost the same lifetime is observed for **I** and **II** in γ-CD indicates that the mobility of the β-phenyl ring is rate limiting and that the methyl substitution at the β-position of **II** does not alter the interaction of the probe molecule with the γ-CD. The relative increase in triplet lifetime observed upon complexation of **III** with β- and γ-CD is larger than those observed for **I** and **II**. This reflects the very short lifetime of **III** in homogeneous solution due to the higher probability of having the β-phenyl ring close to the carbonyl oxygen. Inclusion into CDs clearly does not favor these conformations. Although the increase of lifetime for **III** is dramatic, the absolute values are smaller than the ones observed for complexes with **I** and **II**. This is specially true in the case of γ-CD. This suggests differences in the complexation site for **III** and for **I** or **II**. The presence of two methyl groups at the β-carbon probably creates stereochemical crowding at this position and results in an inclusion complex in which the β-phenyl ring has a higher probability of exiting the cavity. In the β-MCD-**III** system the entire molecule is probably located closer to the aqueous environment. In the case of the **III**-γ-CD complex, there are two possibilities for inclusion

which would lead to a shorter lifetime than those observed for **I** or **II**. The β-phenyl ring could be excluded from the γ-CD cavity forming a complex similar to **I** (or **II**)-β-CD in which only one of the aromatic rings is contained in the CD cavity. Alternatively, both aromatic rings in **III** are incorporated into the γ-CD cavity but they would not be located as deeply as the proposed **I** or **II**-γ-CD complexes.

In the case of incorporating the pure enantiomers of **II** into α, β or γ-CD, the same triplet lifetime was observed as indicated in Table 1. This would lead us to believe that the two ketone isomers are not being complexed differently by the cyclodextrin and as a result, no difference in the triplet lifetimes are observed. The longer cavity associated with the β-MeCD may not allow significant interaction between the ketone and the chiral rim of the CD. This may also be the case in γ-CD where significant probe incorporation is taking place as depicted in Figure 4.2. The origin of the CD's chirality lies on the rim of the larger side where the chiral hydroxyls of the D-glucose groups are located. The lack of chiral discrimination observed may reflect an inner cavity that is not very asymmetric resulting in minimal interaction between the chiral rim and the included ketones.

4.2.3 Conclusion

In conclusion, these studies have shown that the interaction of the probe molecule with the cyclodextrin affects intramolecular quenching by restricting the mobility of the molecule. A substantial increase in triplet lifetime is observed in CD complexes compared to homogeneous solution; complexes with γ-CD show the largest effect. Inclusion complexes of **I**-β-

CD have slightly longer triplet lifetimes compared to complexes of **I**-β-MeCD. The absence of additional hydrogen bonding associated with methoxy substitution in β-MeCD allows more conformational freedom in the cavity resulting in the shorter triplet lifetime observed compared to complexes of β-CD. At this point, we cannot establish if, for quenching to occur, the excited state has to exit completely the CD cavity or if the appropriate conformation can occur with partial exposure of the probe molecule to the aqueous phase. The addition of methyl substituents in the β-position of the included ketones results in an triplet lifetime that is proportionally shorter with increased substitution. This effect is due to increased stereochemical crowding at this position resulting in an inclusion complex in which the β-phenyl ring has a higher probability of exiting the cavity. Similar triplet lifetimes were observed when comparing CD complexes of **IIR** and **IIS** enantiomers which suggests that inclusion results in little interaction with the chiral rim of the CD.

In the next section, these studies on inclusion complexes were extended into the solid state.

4.3 Solid Cyclodextrin Complexes

4.3.1 Results

Incorporating the probes molecules into cyclodextrin solutions showed that significant complexation was occurring, as indicated by the increase in triplet lifetime of the complexed guest. The complexation in solution can be viewed as dynamic behavior in which the guest has freedom of movement inside the host and equilibrates with the guest concentration in the aqueous phase. Evidence presented in Chapter 5 shows that equilibration is also observed in micellar solutions as small concentrations of ketones present in the aqueous phase effectively quench solvated electrons. The monitoring technique used observes an ensemble of all the triplet states absorbing at the monitoring wavelength. As a result, small differences in triplet lifetimes arising from complexation differences may not be observed due the "mixture" of triplet signals monitored, representing complexed guest molecules in equilibrium with those in the surrounding media.

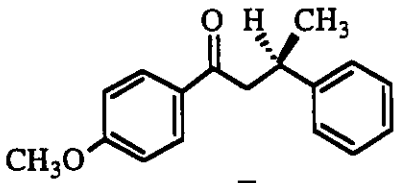

II

The decision was then made to isolate solid cyclodextrin inclusion complexes of the R, S and racemic forms of **II** (**IIR**, **IIS** and **IIrac**, respectively) and analyze their triplet decay kinetics using diffuse reflectance laser flash photolysis techniques (see Chapter 2) to probe the

behavior of the ketones complexed in the cyclodextrins. In this way, only the complexed ketones are monitored and no interference by probes in the aqueous media is possible. Differences in the degree or mode of complexation arising from chiral discrimination would be reflected in the decay kinetics of the triplet signals observed. Thus, it may be possible to directly monitor chiral discrimination of these triplet probes.

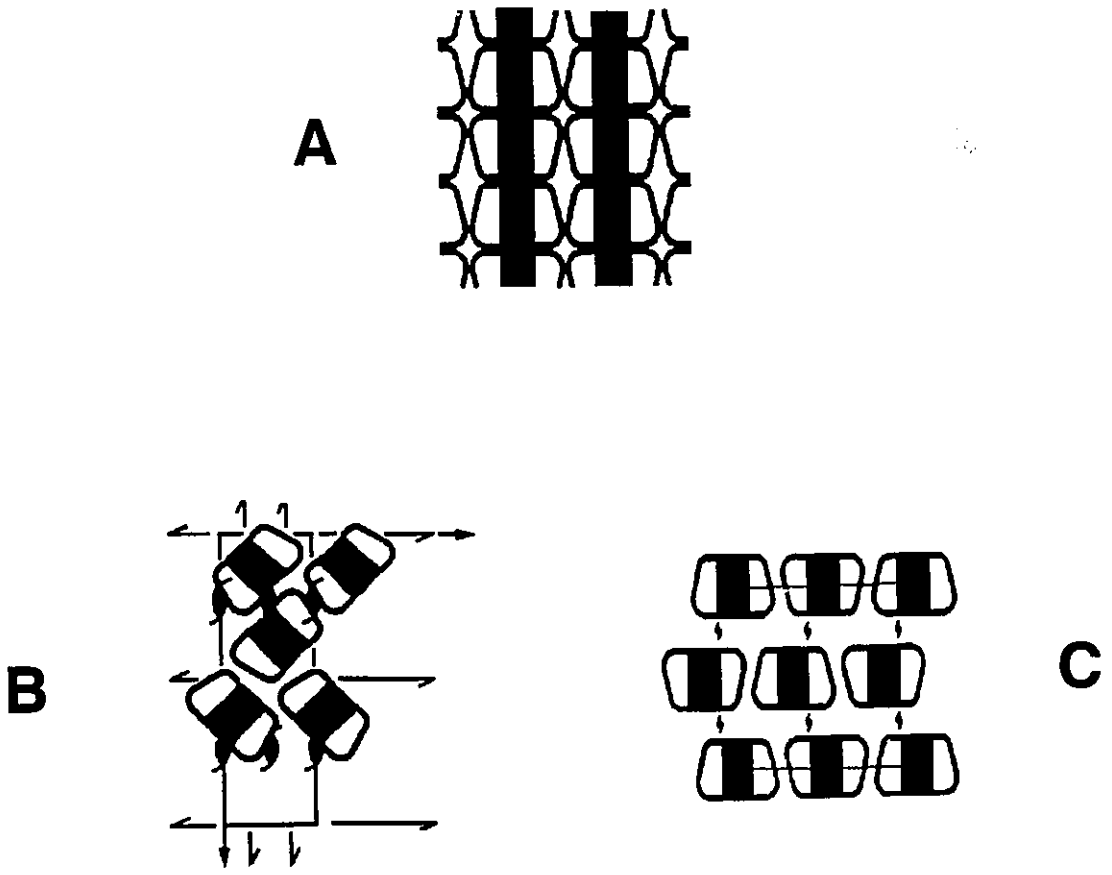

Figure 4.3. Types of solid cyclodextrin complexes.[96] (A) channel; (B) cage; (C) brick-like complexes.

Cyclodextrins can be crystallized to form inclusion complexes having various solid organized structures as shown in Figure 4.3.[96] One of the

three structures shown can be expected in crystallized CD complexes. The type of CD crystal structure is known to depend on the guest molecule.[96] Figure 4.3 shows a channel-like structure (A), a cage structure (B) and a less common brick-like arrangement (C).

Solid cyclodextrin complexes have been prepared using a technique where a saturated solution of cyclodextrin in prepared and an organic solvent containing the probe is layered on top of the cyclodextrin solution.[100] Figure 4.4 shows a schematic representation of the technique employed. This biphasic system is allowed to stand for a week or so, whereby the cyclodextrin complexes precipitate out of solution driven by incorporation of the organic solvent molecules and probe. The result is a solid consisting of cyclodextrin-probe complexes and an excess of cyclodextrin-solvent complexes. Structure A, shown in Figure 4.3 is anticipated when using ether as the precipitating solvent. This method was used to incorporate **IIR**, **IIS** and **IIrac** into α-, β-, and γ-CD's. Special sealed flasks were used to contain the mixture over the week to ensure minimal evaporation of the solvent. The precipitated complexes were filtered, washed and then dried to constant weight to remove most of the solvent leaving a complex with a large excess of empty CD cavities and a few occupied ones. In this way, the probes are effectively isolated from each other, analogous to complexes of organic molecules in zeolites.

Transient signals were then generated by laser irradiation and their subsequent absorptions monitored through diffuse reflectance in the nanosecond to microsecond timescales. Figure 4.5 shows a typical diffuse reflectance absorption spectrum obtained from **IIrac**-α-CD after 308 nm laser irradiation under air equilibrated conditions. Deaerating the complexes with nitrogen did not change the spectra. Similar spectra were

obtained with all the ketones incorporated (**IIR**, **IIS** and **IIrac**) into either α-, β- or γ-CD's. While the signals are weaker than in previous homogeneous solution experiments, the absorption centred at λ = 400 nm can be readily assigned to the ketone triplet state, comparable to earlier experiments in homogeneous solution (see section 3.2).

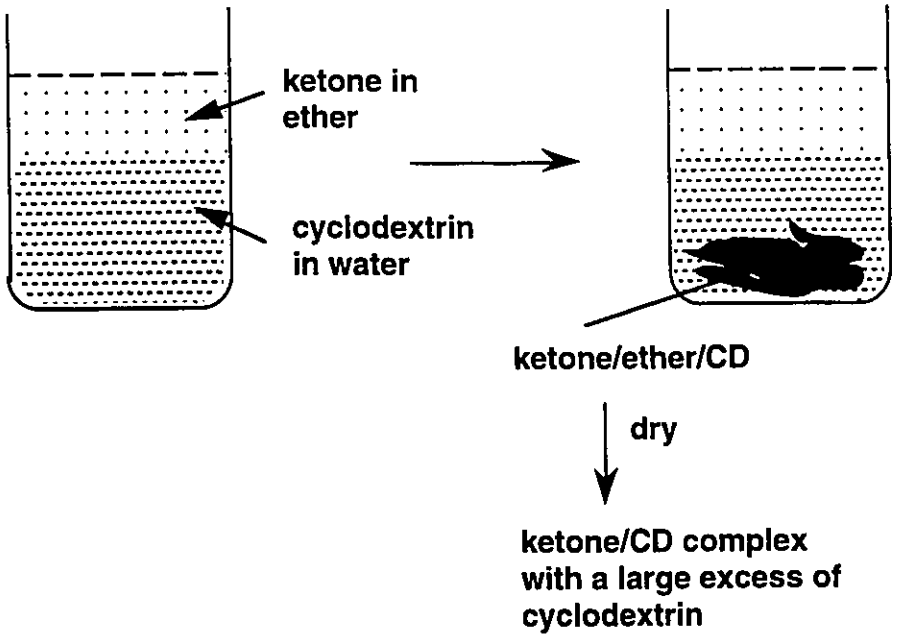

Figure 4.4. Cyclodextrin-probe complex preparation.[100]

Figure 4.6 shows typical decay traces of **IIR**, **IIS** included into α-CD under air equilibrated conditions monitored at 400 nm using the diffuse reflectance technique. Deaerating the complexes with nitrogen prior to irradiation did not affect the decays observed. The decays appear complex in nature, and may incorporate other deactivation processes in addition to β-phenyl quenching. The decay kinetics are similar for the two incorporated enantiomers indicating that conformational differences in the **IIR**-α-CD and **IIS**-α-CD inclusion complexes may not be reflected in their

triplet decay kinetics. Similar results were obtained with all the ketone-α-CD inclusion complexes studied.

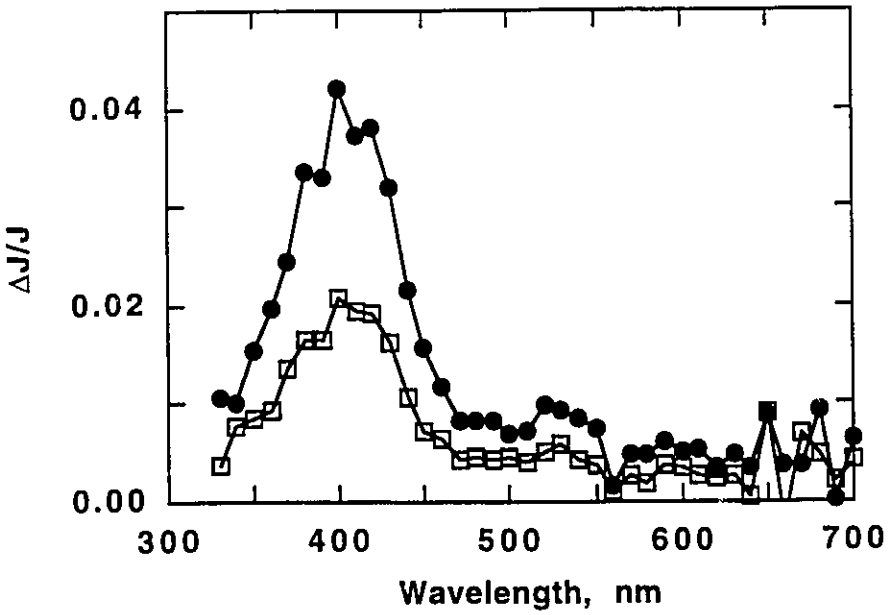

Figure 4.5. Diffuse reflectance spectra obtained 1 (●) and 4 μs (□) after 308 nm laser excitation of solid **IIrac**-α-CD complexes.

Verification of chiral discrimination was carried out using a technique in which a known mass of complex was solubilized and the absorption of the ketone guest was measured in a known concentration of complex. By knowing the extinction coefficient of the ketones, the concentration of the guest can be calculated. This method was used to measure the ketone concentration in α-, β, and γ-CD's. Table 4.3 shows significant chiral discrimination in the solid state CD complexes of **IIR** and **IIS**; **IIR** being selectively retained 1.5:1 and 1.6:1 in α-, and β-CD complexes, respectively versus **IIS** while γ-CD shows little selectivity. In

the case of α-CD, there is 25% less complexation occurring for **IIrac** but is the same in the larger γ-CD.

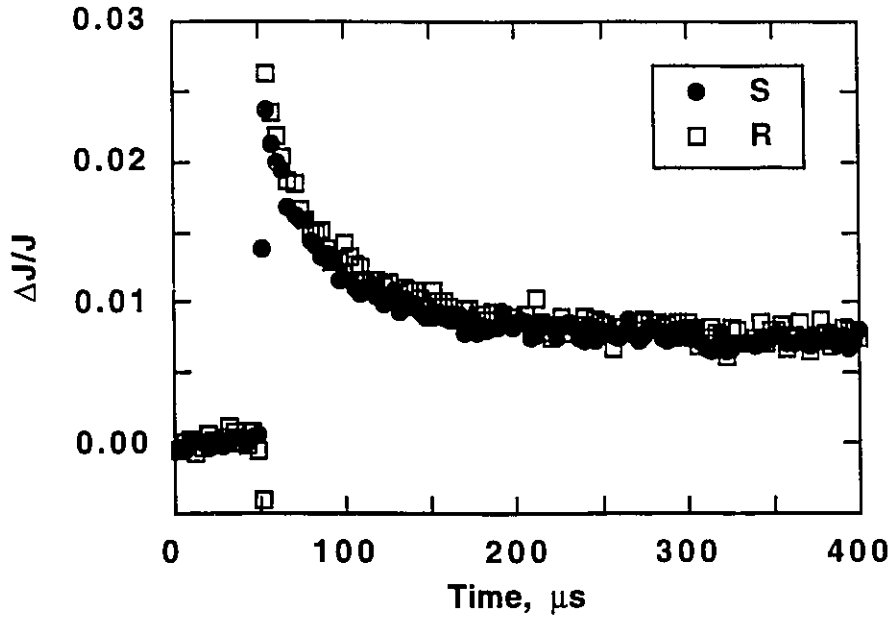

Figure 4.6. Diffuse reflectance transient triplet decays of solid **IIR**-α-CD (□) and **IIS**-α-CD (●) inclusion complexes monitored at 400 nm after 308 nm laser excitation.

GC-MS analysis of socklet extracted α- and β-CD inclusion complexes which were irradiated for 24-48 hours at 300 nm, revealed mostly the ketone starting material along with small amounts of photochemical products. A small amount of p-methoxyacetophenone was identified which probably results from Norrish Type II reactions or hydrogen abstraction from the CD and subsequent cleavage. Complexes of γ-CD showed more loss of ketone starting material with corresponding larger amounts of photochemical products.

Table 4.3. Number of cyclodextrins per ketone.

Complex	#CDs/ketone		
	IIR	**IIS**	**IIrac**
α-CD	159	239	887
β-CD	119	188	-
γ-CD	120	112	107

4.3.2 Discussion

The triplet states of **II** monitored in solid CD complexes are much longer lived than in aqueous CD complexes, (see section 4.2) or in pure crystalline states. In addition, triplet decay kinetics of **II** in CD solutions and in the crystalline state follow monoexponential kinetics (see section 4.2 and 3.3, respectively). However, inclusion complexes of **II** with CD's results in complex decay patterns, as seen in Figure 4.6. This may represent a significant conformation change in the inclusion complexes which does not allow efficient triplet deactivation by the β-aryl ring. The complex decays observed in Figure 4.6 point toward alternative deactivation pathways for the triplet states which may be occurring in conjunction with

β-aryl quenching. In a recent report, similar triplet spectra and decays were observed with lignin model compounds such as α-guaiacoxyacetoveratrone (α-Gav) which also possesses a β-phenyl ring. The ketones were studies on silica, Na-X zeolite and cellulose.[72] The complex triplet decay patterns observed for α-Gav on these solid supports represented a distribution of triplet decays on the surface. The authors suggested a mixture of β-aryl quenching, self-quenching, reaction with the host and β-cleavage as triplet decay pathways. It is conceivable that similar deactivation mechanisms are present in the complexes under investigation in this study.

The presence of oxygen had no effect on the decay kinetics observed. The lack of oxygen effect on triplets in crystalline solids of ketones **I** and **II** was demonstrared in section 3.3 (and other accounts)[72] and shows that oxygen does not penetrate the crystal lattice efficiently.

Complexation differences between the enantiomers of **II** are implied by the results shown in Table 4.3. The **IIR** enantiomer is definitely selected for by α and β-CDs but equal distributions are seen when the larger γ-CD is used as the host. The slightly larger triplet signal observed for **IIR**-α-CD inclusion complexes shown in Figure 4.6 reflects a greater **IIR** concentration in α-CD. In the case of γ-CD, its larger cavity is probably not able to differentiate between the two enantiomers, likely due to its larger size compared to α– and β-CDs and may not allow extensive complexation of the ketone guests compared to the smaller CD's. An interesting observation is seen with the complexed racemic ketone concentration seen in Table 4.3. A significantly smaller ratio of ketone is incorporated into the CD's when a racemic mixture is injected. Although speculative, this is likely due to an aggregation effect of the ketones when injected into the CD

solutions which is more prevalent in the racemic than the pure enantiomer solutions. As a result of this aggregation, less racemic ketone guest is incorporated into the CD's.

Figure 4.5 shows that the incorporated ketones have similar triplet decay kinetics, regardless of the CD, or the optical isomer used. Table 4.3 shows a significant preference for the incorporation of **IIR** into both α- and β-CD's. However, the preference for **IIR** does not lead to a measurable change in either the intermolecular or intramolecular triplet deactivation processes. The implications of this observation can have several meanings. For instance, the ketones may be oriented in different conformations but these conformations do not permit any significant intramolecular quenching. The complex decay patterns observed in Figure 4.6 may represent significant hydrogen abstraction from the CD with subsequent conjugation of the ketone guest to the CD itself. This reaction product would not be extracted and as a result, would not be detectable by GC-MS analysis. In addition, the detection of small amounts of *p*-methoxyacetophenone as a product may represent some intramolecular Norrish Type II reactivity. The complexes of γ-CD showed a noticably higher disappearance of the ketone starting material and may reflect a higher susceptability for hydrogen abstraction reactions to occur due to its larger cavity. Although these mechanisms are mere speculation at this point, one cannot infer any complexation differences between the enantiomers or racemic mixtures from their respective triplet decay kinetics.

4.3.3 Conclusion

Both α- and β-CD's have been shown by ground state absorption studies to display chiral selectivity when incorporating either **IIR** or **IIS**. The cyclodextrin selectively incorporates **IIR** in 1.5:1 and 1.6:1 ratios into α- and β-CD's, respectively over the **IIS** enantiomer. The incorporation into the larger γ-CD showed no chiral selection. The triplet states of the ketone guests were readily monitored by diffuse reflectance laser flash photolysis techniques and revealed complex decay kinetics for the included ketones. Reaction with the host and Norrish Type II reactivity are believed to be the dominant deactivation pathways for these ketones in CD solid state complexes. Product analysis of the CD complexes show some Norrish Type II product formation in the CD complexes. In addition, complexes of γ-CD show a higher consumption of ketone starting material compared to either the α-CD or β-CD complexes. The triplet decay kinetics of **IIR** and **IIS** in various CD inclusion complexes showed little difference in their kinetics. Incorporation of racemic mixtures of **II** (**IIrac**) was less than its respective enantiomers in α-CD's and may be due to aggregation during the formation of the inclusion complexes.

4.4 Experimental

Ketones **I-III** were synthesized according to a procedure outlined in section 3.4. The aqueous CD-ketone complexes were made by the "injection method" in which small aliquotes (0.5 μl) of a concentrated solution of the probe (25 mg/ml in methanol) were injected into the aqueous cyclodextrin solutions (α-CD, Heptakis(2,6-di-O-methyl)-β-cyclodextrin and γ-

cyclodextrin were from Aldrich and used as received). The solution was briefly shaken on a Vortex mixer between subsequent injections. Probes were injected into the solution until an optical density of 0.3 at the laser wavelength (308 nm) was achieved. The methylated β-CD (β-MCD) was used as it is more soluble in water than the unsubstituted β-CD.

The solid ketone-CD complexes were precipitated from a saturated CD aqueous solution that was overlayed by ethyl ether containing the ketone. The mixture was allowed to sit for a week until precipitation of the complexes was complete. The crystals were washed and then dried under vacuum until constant weight.[100] The ketone:CD ratios were calculated by measuring the ground state absorption at 308 nm of a known concentration of complex dissolved in dimethyl sulfoxide (Aldrich). The concentration of ketones in the CD inclusion complexes was calculated from the measured extinction coefficient in dimethyl sulfoxide (DMSO) at 274 nm (16350 $M^{-1}cm^{-1}$). Details on the laser flash photolysis system used are given in Chapter 2.

Steady state irradiations of the solid CD complexes were carried out in the same way as described in section 3.4. Starting material and products were extracted with 6 hours of socklet extraction using dichloromethane.

Chapter 5. Cholates and SDS Micelles

5.1. Introduction

Cyclodextrins showed no chiral selectivity in terms of the triplet lifetimes of the two chiral ketones when incorporated in cyclodextrin complexes either in solution or the solid state. Thus, we decided to try a variety of other chiral hosts. Among these, bile salts are chiral and are known to readily form small micelles in aqueus media. They contain a relatively hydrophobic cavity into which our probe molecules could be incorporated. Cholates are natural components of bile acids and have a relatively unusual structure compared with other micelle-forming molecules which typically have a long hydrocarbon chain and a polar head group (e.g. SDS). Sodium cholate (SCh) and other bile salts consist of a steroid nucleus, three α-hydroxy groups (C-3, C-7 and C-12 positions) and a hydrophilic carboxyl head group at the C-24 position.[104]

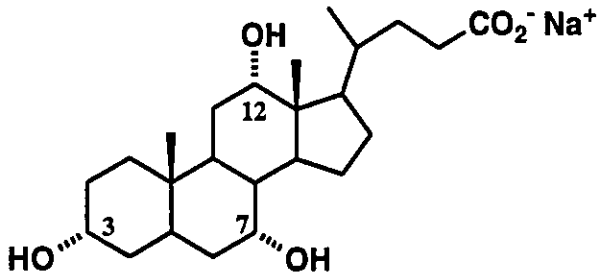

SCh

Again, as in earlier experiments, preliminary studies focussed on characterizing the triplet behavior of probe molecule (**II**) in this new environment. The initial experiments revealed the presence of an additional species along with the expected triplet. The long wavelength absorbing species was tentatively assigned as a solvated electron and

further studies were carried out to see if photoionization was specific to this ketone and/or type of micelle.

Photoionization of organic molecules, especially aromatic hydrocarbons has been shown to occur in a number of systems. For example, pyrene photoionizes under conditions of one- or two-photon excitation, depending on the nature of the environment (solution, micelles, zeolites, etc).[105-108] Two-photon ionization is a relatively common process under conditions of pulsed laser excitation. In a recent study, Hashimoto and Thomas[109] have shown that a number of substituted biphenyls undergo two-photon ionization in micellar solution following absorption of the second photon by the triplet state of these molecules. Photoionization in micellar systems is usually observed with anionic surfactants (e.g. sodium dodecyl sulfate, SDS) since in these systems, repulsive interactions favor charge separation; in addition, hydrated electrons are relatively long lived and readily detectable in these aqueous systems. The yield of photoionization is markedly reduced in cationic micelles, such as cetyltrimethylammonium bromide (CTAB) compared to anionic micelles. This is due to the positive micellar surface charge which promotes recombination of the electron-cation pairs thus preventing the release of electrons into the surrounding aqueous solution.[109]

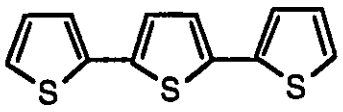

alpha-terthienyl
(α-T)

For example, photoionization of alpha-terthienyl (α-T) can be readily observed in cholate micelles. Figure 5.1, shows that three distinct absorptions can be readily detected in the transient absorption spectrum

recorded following laser excitation; these correspond to the triplet state which in turn photoionizes to give the radical cation and a solvated electron.

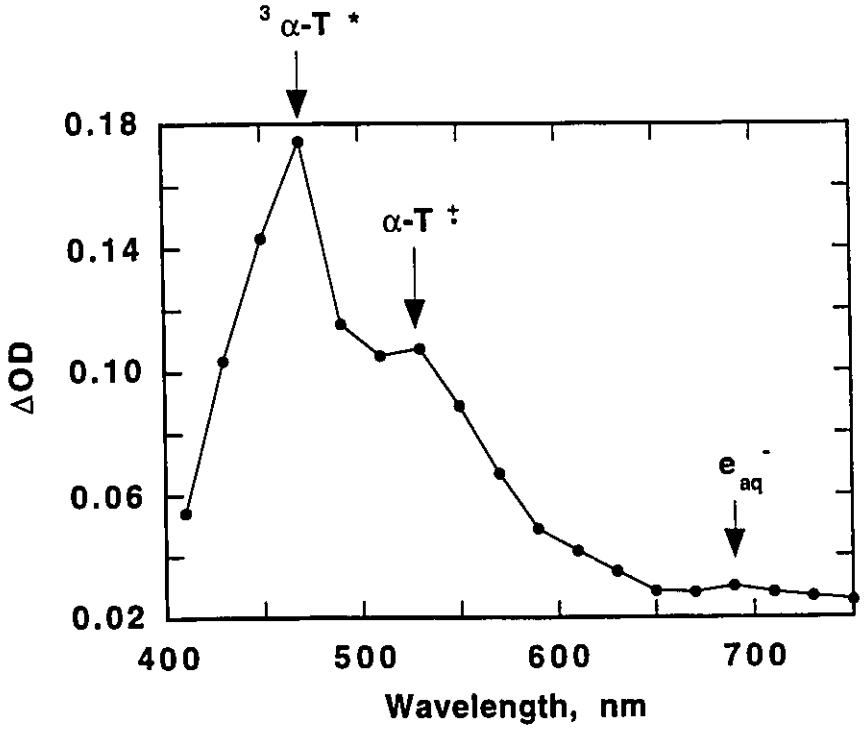

Figure 5.1. Transient absorption spectrum of 2.5 x 10^{-5} M α-T in 30 mM cholate collected 200 ns after 355 nm excitation under nitrogen saturated conditions.

The triplet state of α-T has a λ_{max} of 460 nm while its radical cation shows a λ_{max} of 550 nm.[110,111] These correspond to the large absorptions observed in Figure 5.1. The small but reproducible absorption centred around 700 nm is assigned to hydrated electrons which are known to absorb in this region.[112] Figure 5.2 shows a transient absorption decay signal of the solvated electron collected at 700 nm which can be readily quenched by the addition of nitrous oxide (N_2O) according to reaction 5.1. The absorption

of the solvated electron appears weak in Figure 5.1 compared to the very strong α-T triplet and radical cation signals observed but is still readily detected as shown in Figure 5.2.

$$N_2O + e^-_{aq} \xrightarrow[H_2O]{k = 9.6 \times 10^9\ L mol^{-1} s^{-1}} N_2 + OH^{\cdot} + OH^- \qquad (5.1)$$

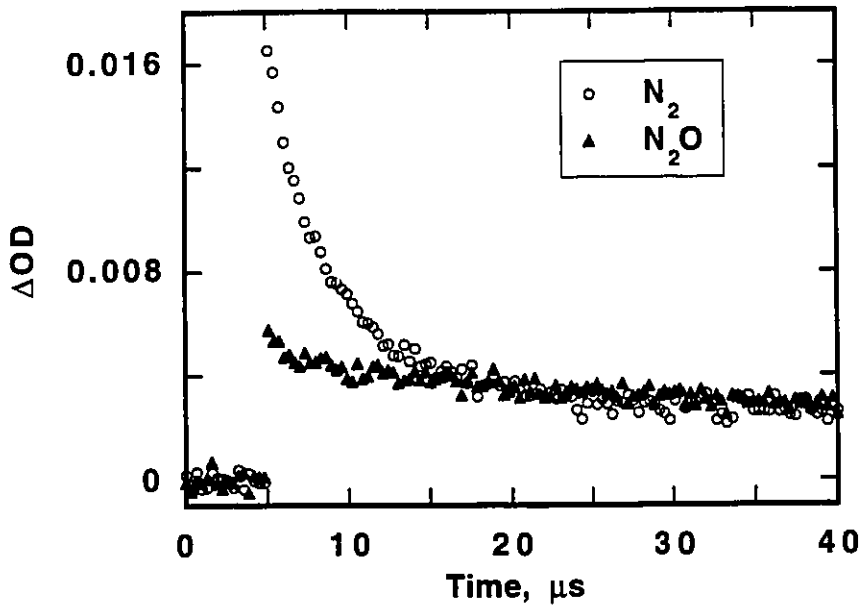

Figure 5.2. Transient absorption traces monitored at 700 nm from a solution of 2.5 x 10^{-5} M α-T in 30 mM cholate collected after 355 nm laser excitation under nitrogen (O) and nitrous oxide (N_2O) saturated conditions (▲). The residual absorption is due to α-T radical cation absorption which overlaps with the solvated electron in this region.

Photoionization of ketones is not well studied, although two-photon ionization of benzophenone in aqueous solution has been reported.[113] A

recent publication[114] shows that several aromatic ketones photoionize in SDS micelles. The technique used involved time-resolved electron spin resonance (ESR) to detect the spin polarized hydrated electron in micellar solution. A biphotonic ionization process through the excited triplet state was proposed for the formation of the solvated electrons, but their lifetimes were unusually short compared to some of the systems that were under investigation in our studies. This prompted us to report on our studies in this field and to add benzil (**XV**) to the list of ketones under study. Our work in this area was initiated by the accidental observation of the formation of hydrated electrons in ketone studies, and independently during work related to the photodegradation of lignin model compounds that were under investigation by Dr. M.K. Whittlesey.[115] This chapter reports the results of work in which these initial observations were pursued by carrying out work on SDS and sodium cholate micelles. The results of these experiments show that ketone photoionization is a common and facile process under conditions of laser excitation. Further, these studies provide an explanation for the anomalous short lifetimes for hydrated electrons generated from the photolysis of aromatic ketones in micellar solution reported by Kuwata et al.[114]

5.2 Results

Figure 5.3 shows the structures of the molecules studied in this work.

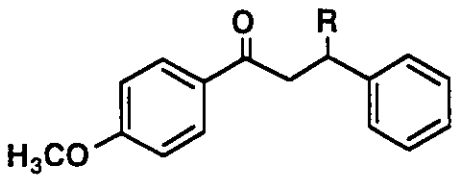

I; R = H
II; R =CH_3

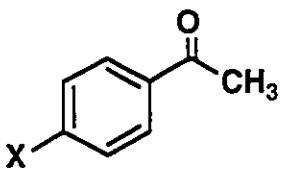

VII; X=H
VIII; X=CH_3O

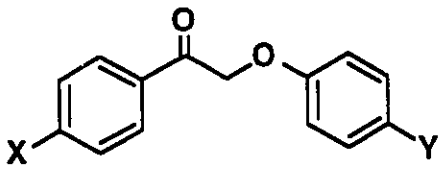

IX; X = H; Y = H
X; X = CH_3O; Y = H
XI; X = H; Y = CH_3O
XII; X = CH_3O; Y = CH_3O

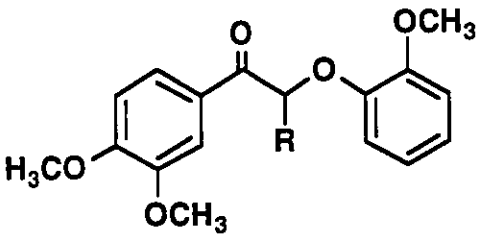

XIII; R = H
XIV; R = CH_2OH

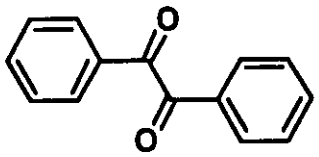

XV

Figure 5.3. Ketones used for photoionization experiments.

The ketones in Figure 5.3 were incorporated into either SDS or sodium cholate micelles and irradiated with the 308 nm pulses from an excimer laser.

SDS micelles have an aggregation number of approximately ~60, a critical micelle concentration of ~8.2 mM[116], and represent typical medium size micelles. Sodium Cholates have a critical micelle concentration near 13 mM and small aggregation numbers (~2-8).[117]

Figure 5.4 shows the spectra recorded following excitation of ketone **II** in 30 mM sodium cholate solution under nitrogen and nitrous oxide. The maximum at ~390 nm is common to both samples and can be readily

assigned to the triplet state of the ketone. A second absorption band, at λ>600 nm, is present only under nitrogen in the micellar solution. We assign this band to hydrated electrons, e^-_{aq}, which are well known to absorb in this region.[112] Both O_2 and N_2O quenched the long wavelength absorption readily, as expected for e^-_{aq}.[118] The reaction of e^-_{aq} with oxygen and N_2O (reaction 5.1) occurs with rate constants in water at room temperature of 1.9 x 10^{10} L·mol^{-1}·s^{-1} and 9.6 x 10^9 L·mol^{-1}·s^{-1}, respectively. The same qualitative observations were made in sodium taurocholate solutions.

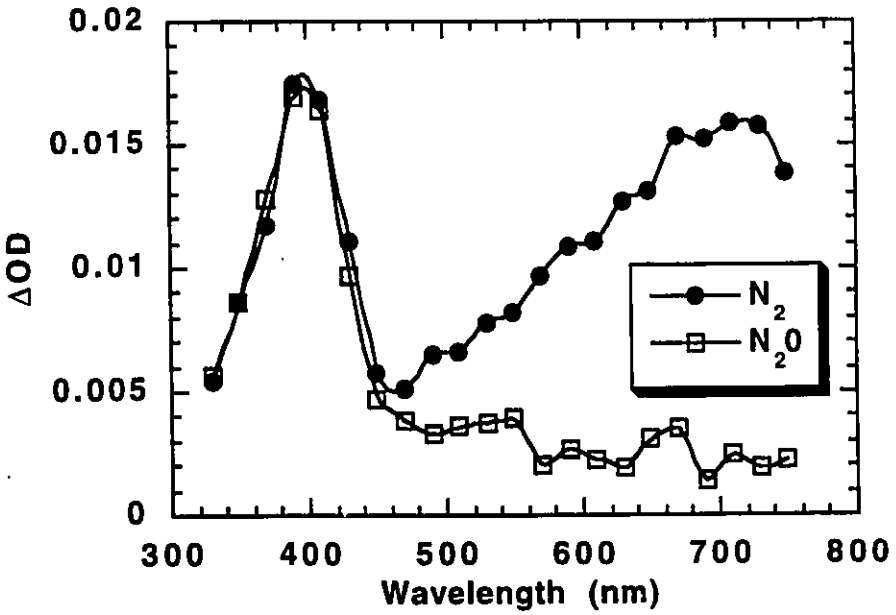

Figure 5.4. Transient absorption spectra for **II** (1.4 x 10^{-4} M) in 30 mM sodium cholate solution under nitrogen (●) and under N_2O (□), recorded ~280 ns following 308 nm laser excitation.

Both bands in Figure 5.4 form within the duration of the laser pulse (~6 ns) and decay by simple first order kinetics with a lifetime of 130 ns at 400 nm and 1.3 μs at 700 nm for 1.4 x 10^{-4} M ketone **II**. Bubbling N_2O had

no effect on the lifetime at 400 nm (as expected for the triplet state) but the lifetime at 700 nm was reduced to < 100 ns. The effect reflects electron scavenging according to reaction 5.1.

Our results for **II** and other ketones are summarized in Table 5.1. In particular, ketones **IX-XIV** are samples in lignin-related work.[115] Ketones **VII** and **VIII** were added to the series to see if a second aromatic ring was required, or had any significant effect on the photoionization reactions. In fact photoionization was observed with all the substrates in Figure 5.3.

The triplet lifetimes of the ketones **I, II,** and **IX-XIV** in Figure 5.3 are frequently controlled by intramolecular quenching by the β-aryl ring, a process initially reported for **I**,[54,55] and is now well characterized in many other systems including those in Figure 5.3.[115] Note however that in this study some of the lifetimes could be shortened by triplet-triplet annihilation; naturally, this is an unavoidable problem in studies of multiphoton phenomena since high laser doses are required. In a few instances triplet formation and electron ejection were accompanied by some β C-O cleavage which leads to readily detectable radical fragments (e.g. phenoxyl radicals).[115] This is common with ketones **XI** to **XIV**.

Table 5.1. Decay of hydrated electrons in micellar systems containing photoionizable ketones.

Compound	Surfactant[3]	[Ketone], M	τ, ns	
			N_2	air
I	Cholate	1.25×10^{-4}	1950	190
	SDS	1.26×10^{-4}	6700	250
II	Cholate	1.38×10^{-4}	1300	340
VII	Cholate[1]	2.43×10^{-3}	≤20	≤13
	SDS[1]	2.43×10^{-3}	54	47
VIII	Cholate[1]	1.48×10^{-4}	570	150
	SDS[1]	1.48×10^{-4}	1330	200
	SDS	1.2×10^{-4}	6900	180
IX	SDS	2.4×10^{-3}	410	160
X	SDS	3.0×10^{-3}	1050	230
XI	SDS	1.0×10^{-3}	730	185
XII	Cholate[1]	1.8×10^{-4}	510	131
	SDS[1]	1.8×10^{-4}	1000	
XIII	Cholate[1]	9.0×10^{-5}	850	170
	SDS[2]	8.3×10^{-5}	2200	160
XIV	SDS	9.0×10^{-5}	240	180
XV	SDS[2]	4.8×10^{-5}	10000	

[1] Based on a double exponential fit to the data.

[2] Measured at 750 nm.

[3] SDS concentration was 0.1 M; sodium cholate concentration was 30 mM.

5.3 Discussion

A key question in any system involving photionization is the number of photons required for electron ejection to occur. In principle, a simple plot of electron signal (ΔOD) against laser dose should correspond to a linear function if the process is monophotonic, and to a parabola if two photons are required, i.e.:

Monophotonic	$\Delta OD_{700} \propto$ Dose	(5.2)
Two photon	$\Delta OD_{700} \propto Dose^2$	(5.3)

While simple, this approach is not always the most reliable. This is largely due to the assumption that monophotonic processes *always* give linear behavior when ΔOD is plotted against the laser dose. There are, however, numerous cases where this is not strictly true. Deviations from linearity (downward curvature) can reflect (among other causes) saturation effects due to ground state depletion, or screening effects due to UV absorption by the transient. In fact, the latter is a necessary condition for stepwise two photon absorption to take place. If an experimental variable can be found that can reliably reflect monophotonic behavior, then the hydrated electron signals can be plotted against this variable and a parabolic curve should be a clear indication of the occurrence of two photon processes. In our systems, the triplet state signal at around 390 nm, characteristic of methoxy substituted chromophores, should be a good monophotonic indicator of those ketones in Figure 5.3 where the triplet is sufficiently long lived to be detected.

Figure 5.5 shows plots of ΔOD_{700} against both percent laser dose and against ΔOD_{400} (due to the triplet state) for compound **III** in cholate micelles. The fits shown correspond to an expression of the type:

$$\text{signal} \propto \text{dose}^{a} \qquad (5.4)$$

Multiple regression led to a values of 2.1 and 1.9 for the top and bottom plots, respectively (see Figure 5.5), indicating that electron photoejection requires two photons. Similar observations were repeated for other compounds in Figure 5.3 with analogous results.

Further evidence that two photons were required for photoionization was obtained using a two-laser two-colour technique. This technique, as the name suggests, is an extension of laser flash photolysis and was developed in the early eighties by Scaiano and coworkers.[119] In this type of experiment two lasers are used in succession to produce, and then excite, the transient intermediate to be studied. The first laser is used to produce the transient to be studied and is dubbed the 'synthesis' laser. At a preset time interval after the synthesis laser has been fired, a second laser, the 'photolysis' laser, is fired into the photolysis cell to excite the transient and produce the desired products. In the present system, a triplet state of ketone **II** is generated using a 266 nm laser and then a 355 nm laser was used to photolyze this triplet state. The object was to test if photoexcitations of the triplet state would produce a solvated electron. Figure 5.6 shows the results of the experiments. Although the signals are weak, it is clear that the second photon generates solvated electron as monitored at 700 nm. Without the second laser, no step is observed thus confirming that the triplet state is being photoionized specifically by the second laser. Photolysis of the the solution with the 355 nm laser alone does not generate any

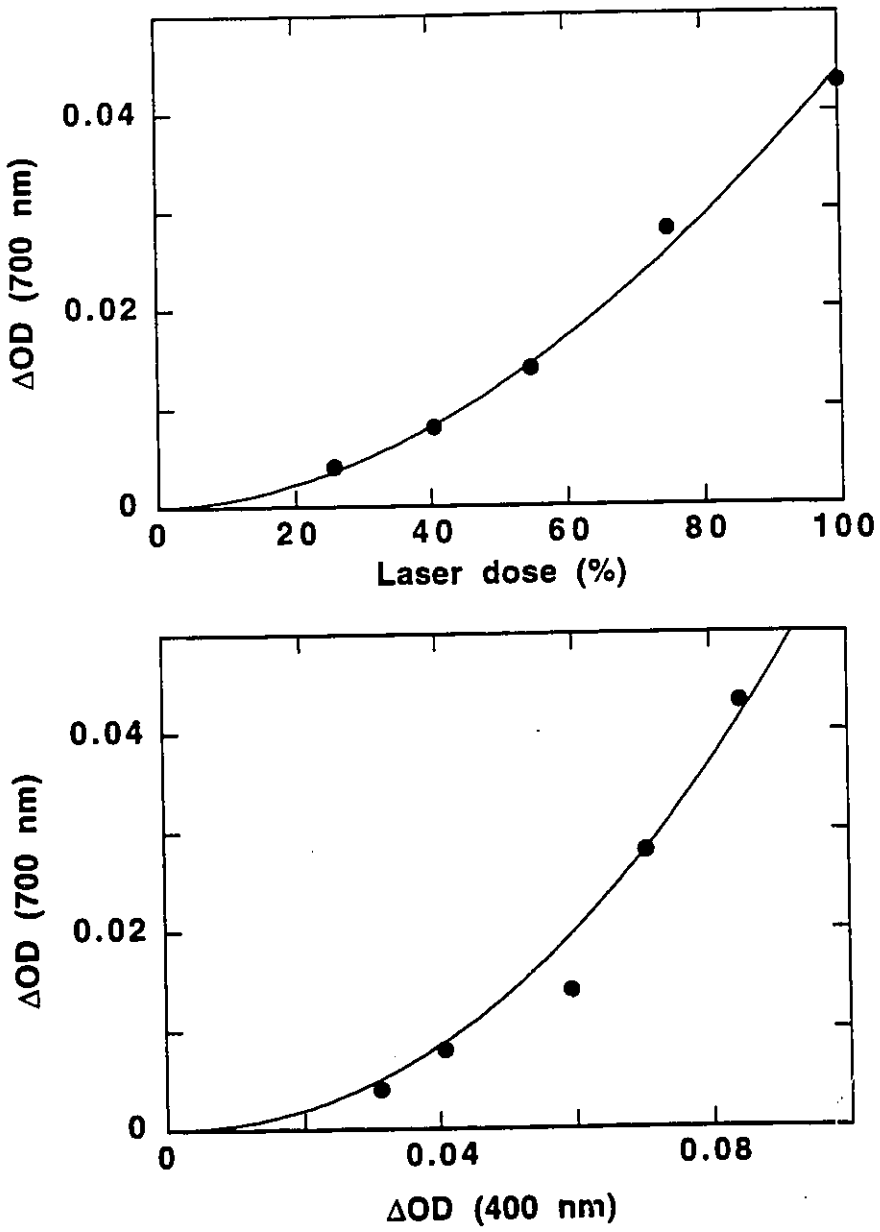

Figure 5.5. Plots of ΔOD recorded at 700 nm against percent laser dose (top) and ΔOD at 400 nm for compound **I** in 30 mM sodium cholate. Note that 100% laser dose corresponds to ca. 18 mJ incident on the sample.

solvated electron since the starting material (the ground state of **II**) does not absorb due to the low extinction coefficient by the ground state at 355 nm. Photolysis with 266 nm laser excitation does generate some solvated electron as seen in Figure 5.6 which is probably biphotonic.

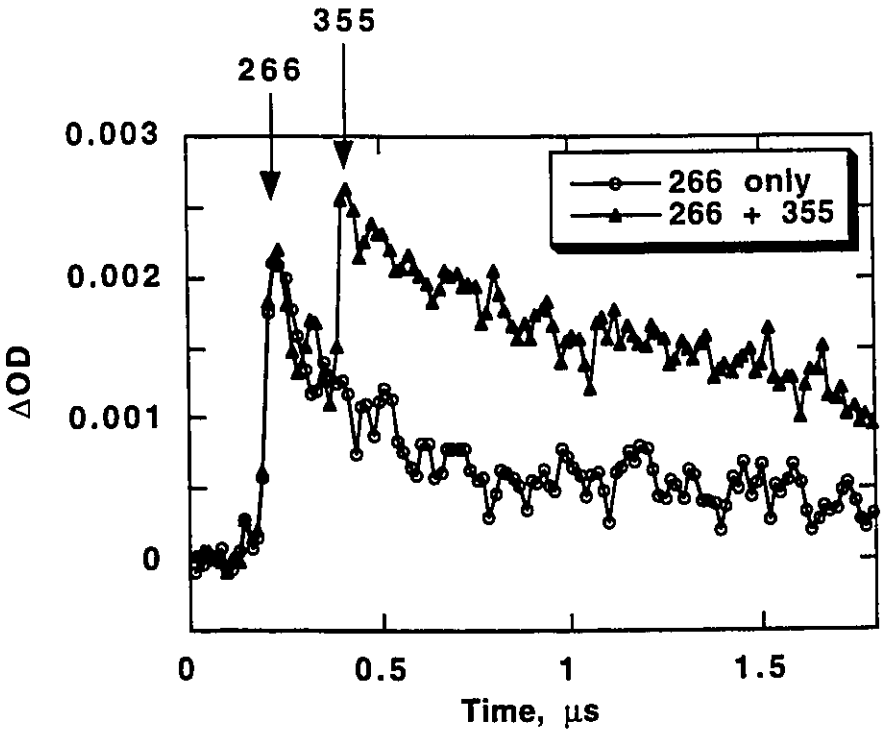

Figure 5.6. Transient absorption decays of solvated electrons generated from photolysis of **II** in sodium cholate solutions (monitored at 700 nm). The signals were monitored after 266 nm irradiation alone (O) and then with 355 nm irradition ~0.5 μs later (▲). The arrows in the figure show the times where the lasers were fired.

Clearly, electron photoejection must yield the ketone radical cation as the second product of the reaction. This cation must be very unstable under our experimental conditions, since all attempts to detect this intermediate

were unsuccessful. Most carbonyl radical cations have high ionization potentials and their derived cations are highly reactive making direct observation of these species difficult.[120] Radical cations of acetophenones and benzophenones generated by paraquat oxidation of their triplets in aqueous acetonitrile have been shown to decompose too rapidly to be detected.[120,121]

In the case of **XIII** earlier studies have shown quite clearly that multiphoton processes are involved in its photochemistry in homogeneous solution.[115] The results reported here suggest that those observations may reflect electron photoejection, a process that must be most facile in electron-rich molecules such as **XIII** and **XIV**.

We have observed wide variations in the lifetimes for e^-_{aq} depending on the precursor employed. The lifetimes are systematically shorter than the value ~10 μs reported in the literature.[122] Similarly *anomalous* lifetimes have also been reported by Kuwata et al.[114] although no interpretation was provided. We believe that these short lifetimes reflect differences both in the rate constants for electron scavenging and the ketone concentration available in the aqueous phase in each case. Rapid electron scavenging by aromatic ketones is well known; for example acetophenone reacts with e^-_{aq} with a rate constant[118] of 2.8×10^{10} M^{-1} s^{-1} according to reaction 5.5.

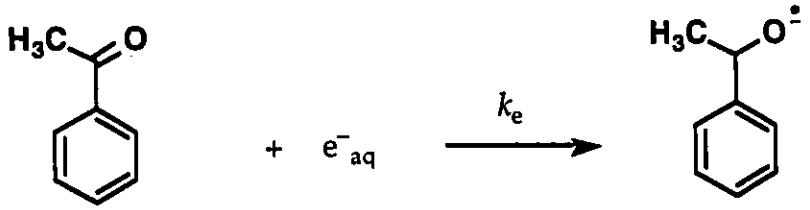

(5.5)

VII

Note that the relevant ketone concentration is not the bulk value, but rather the free concentration in equilibrium with micellized ketone, i.e.:

$$KM \underset{}{\overset{K_{diss}}{\rightleftharpoons}} K + M \qquad (5.6)$$

where K and M represent the ketone and the micelles, while KM represents micelle-incorporated ketone. The equilibrium constant K_{diss} has been shown to be larger for the more hydrophilic ketones which will exit the micelle most readily.[123,124] Thus, reaction will be favored for acetophenone and less favorable for the other ketones used, in agreement with our experimental observations. Note also that the *p*-methoxybenzoyl chromophore has a stronger UV absorption than the unsubstituted benzoyl chromophore and that therefore higher substrate concentrations are required in the cases of **VII**, **IX** and **XI**.

The anionic charge in SDS and cholate micelles is believed to promote the yield of e_{aq}^- by promoting charge separation as a result of coulombic repulsion.[109] However, the lifetimes of e_{aq}^- generated in the larger SDS micelles are generally longer than those in the smaller cholate micelles (see Table 5.1). This difference can be attributed to a more extensive dissociation (i.e. more aqueous probe) in the case of the cholate micelles. This leads to faster electron scavenging in this case. In the case of **XIII** and **XIV** in SDS micelles (approximately matched substrate concentration) the e^-_{aq} lifetime is much shorter in the case of **XIV** (see Table 5.1). We believe this reflects easier exit into the aqueous phase induced by the $-CH_2OH$ substituent.

We were surprised by the report on the absence of detectable solvated electrons in the case of benzil (**XV**).[114] The observation is particularly interesting in view of earlier studies from our laboratory that show that

doubly-excited benzil undergoes fragmentation to yield two benzoyl radicals in a process described as a "reluctant" Norrish Type I reaction.[125] However, in our hands, benzil in SDS micelles led to readily detectable signals from hydrated electrons. The lifetime of these electrons showed the concentration dependence expected from the equilibrium of equation 5.7, i.e.:

$$k_{obs} = \frac{K_{diss} \cdot k_e \cdot [K]_{total}}{[M]} \qquad (5.7)$$

which includes the implicit assumption of $[K]_{aqueous} << [KM]$. The plot of Figure 5.7 leads to $k_{obs} = 9.9 \times 10^8\ M^{-1}\ s^{-1}$. Given the reported value of electron scavenging by benzil (k_e) of $3.6 \times 10^{10}\ M^{-1}\ s^{-1}$,[118] one can estimate a K_{diss} value of 5.5×10^{-5} M. Note that these measurements were carried out at 750 nm, rather than our usual electron monitoring wavelength of 700 nm. This is done in order to minimize interference from from benzil anions, presumably formed by protonation following electron capture. The radicals show λ_{max} ~600 nm, but the absorption extends to 700 nm.[126] The insert in Figure 5.7 shows that even in the presence of N_2O, small amounts of this radical are also formed. We believe that the failure of Kuwata et al.[114] to detect electrons reflects a reduced electron lifetime due to the use of high benzil concentrations, combined with the limited time resolution of ESR techniques. In this sense, there is no conflict with the results reported here and those recently published.[114]

Further support for this simple model for the interpretation of solvated electron lifetimes can be derived from an analysis of the case of acetophenone, where all the information is available to allow for the calculation of a "predicted" electron lifetime. The reported value of K_{diss} is

4.9×10^{-4} M,[124] while k_e is 2.8×10^{10} M^{-1} s^{-1}.[118] For an SDS concentration of 0.1 M (i.e. [M] ~ 1.5 mM) and acetophenone 2.43 mM, this corresponds to an expected lifetime of 45 ns (according to equation 5.7) in good agreement with the experimental value of 54 ns.

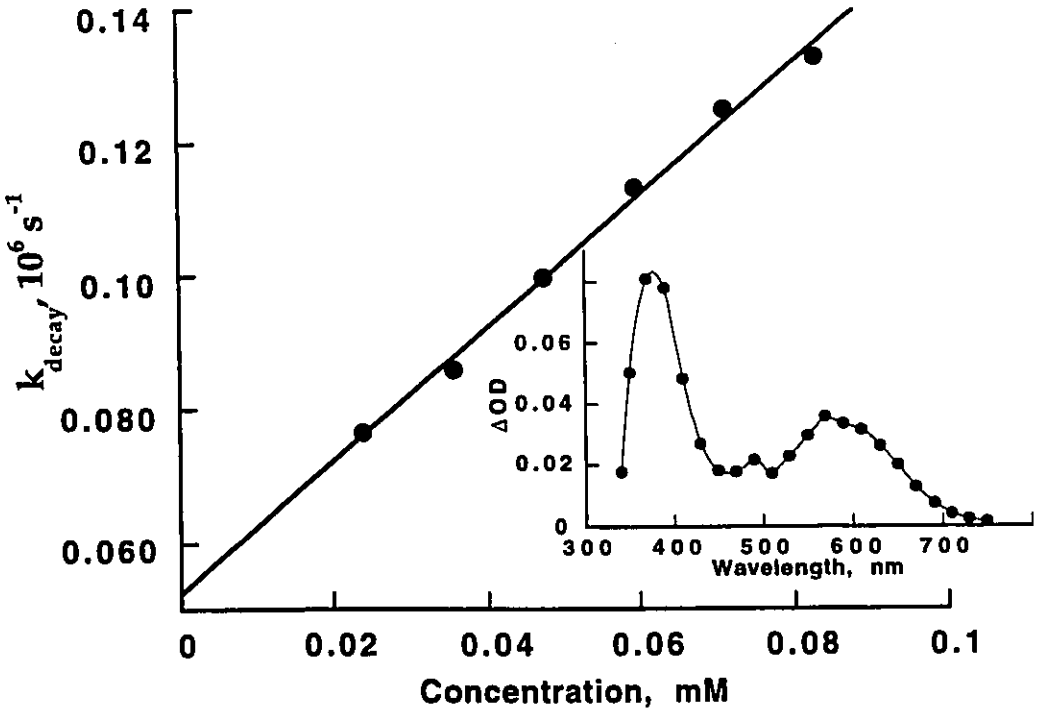

Figure 5.7. Effect of benzil (**XV**) concentration on the decay of solvated electrons in SDS micelles (0.1 M). The inset shows the transient absorption spectrum obtained for benzil (8.3×10^{-5} M) under N_2O, recorded 280 ns after 308 nm laser excitation.

Similarly, in the case of *p*-methoxyacetophenone (**VIII**) it is possible to use the data available to estimate a rate constant for electron capture by **VIII** (k_e). Thus, combining the data for SDS from Table 5.1 with the reported K_{diss} value of 3.3×10^{-4} M we can estimate $k_e \sim 2.3 \times 10^{10}$ M^{-1} s^{-1}.

The value is slightly lower than those for acetophenone and benzophenone,[118] as could be expected for this electron-rich ketone. Similar dependence with ketone concentrations was also observed with other samples used (e.g. **XIII**), although the detailed dynamics were not pursued further.

Finally, we come to the question as to the intermediate involved in the formation of hydrated electrons. In the case of biphenyls, work by Hashimoto and Thomas[109] has shown unequivocally that the intermediate involved is the triplet state. Similar conclusions have been reached by other authors[113,127]. While plots, such as those in Figure 5.5, cannot provide unequivocal proof for the intermediate involved, our results are also consistent with triplet intermediacy and we favor this explanation. In addition, Figure 5.5 provides additional evidence that the triplet state is photoionizing. Aromatic ketones are well known to undergo efficient intersystem crossing in the subnanosecond time scale. Therefore, during a 6 ns pulse, the concentration of singlet state will remain extremely low, while the triplet state is essentially "stable" in this time scale (with the exception of **V** and **VII**). Thus, even this simple argument favors triplet involvement in the reaction.

5.4 Conclusion

Electron photoejection has been shown to be a facile process when aromatic ketones are excited with 308 nm laser pulses in anionic micellar solution. The micellar charge is believed to promote photoionization by promoting charge separation as a result of coulombic repulsion.

The photoionization process requires two-photons, and is believed to involve the intermediacy of the triplet state which is responsible for the absorption of the second photon. Hydrated electron lifetimes show wide variations, reflecting differences in electron trapping rates, as well as variations of the ketone concentration in the aqueous phase.

5.5 Experimental

Compounds **I** and **II** were synthesized as previously described in section 3.4. Acetophenone (**VII**) was purchased from Aldrich and purified by distillation. **IX, X** and **XI** were gifts from J.C. Netto-Ferreira and their synthesis can be found in the literature.[74,82] Compound **XIV** was a generous gift from Dr. N. Weir. **VIII** and **XV** were purchased from Aldrich and recrystallized twice from methanol. Sodium cholate was also from Aldrich and was purified by dissolving in hot methanol and precipitated by slow addition of ethyl acetate until formation of a precipitate occurred whereby the mixture was allowed to cool, then filtered and vacuum dried. Sodium dodecyl sulfate (SDS) was purchased from BDH (specially pure) and used without further purification. Taurocholic acid (disodium salt) was purchased from Aldrich and used as received. Solvents (BDH) were Omnisolve grade and the water used was purified by a Millipore filtration device. Nitrous oxide (N_2O) was from Matheson (CP grade).

XII was prepared by reaction of α-bromo-*p*-methoxyacetophenone with *p*-methoxyphenol using dry acetone as solvent in alkaline media.[128] The most favourable method of preparation involved stirring the phenol in

the basic solution for 2 h, followed by dropwise addition of an acetone solution of the ketone. The mixture was then refluxed until a GC trace showed >95% conversion to the required product. Workup involved removal of any excess phenol followed by purification of the ketone by recrystallization from methanol. ^{13}C NMR ($CDCl_3$) δ 56.12 (OCH_3), 56.27 (OCH_3), 72.20 (CH_2), 40.22, 114.57 (CH), 115.27 (CH), 116.52 (CH), 128.26 (C), 131.11 (CH), 152.89 (C), 164.59 (C), 194.01 (CO); ^1H NMR ($CDCl_3$) δ 3.7 (s, 3H), 3.9 (s, 3H), 5.1 (s,2H), 6.7-7.0 (m, 6H), 7.9 (s, 1H), 8.0 (s , 1H).

XIII was synthesized as previously described by Adler *et al.*[129] and verified by other accounts.[36,72,73,115,128] Anhydrous potassium carbonate (36 g) was added to a solution of α-bromoacetoveratrone (Aldrich) and guaiacol (Aldrich) in dry acetone and the mixture was heated on a water bath with vigorous stirring for 45 min., then filtered, diluted with water and extracted into chloroform. The excess of guaiacol was removed by extraction with sodium hydroxide solution. The remaining chloroform layer was then washed with water, dried over magnesium sulfate and evaporated to give a solid which was recrystallized three times from ethanol.[73] The sample was >99.8% pure by gas chromatography and identified by GC-MS and its melting point (85-86 °C). ^{13}C NMR ($CDCl_3$) δ 56.46 (OCH_3), 56.57 (OCH_3), 56.69 (OCH_3), 72.53 (CH_2), 110.72 (CH), 110.96 (CH), 112.70 (CH), 115.20 (CH), 121.37 (CH), 122.91 (CH), 123.35 (CH), 128.39 (C), 148.14 (C), 149.76 (C), 150.27 (C), 154.38 (C), 193.82 (CO); ^1H NMR ($CDCl_3$) δ 3.8 (s, 3H), 3.9 (s, 3H), 3.95 (s, 3H), 5.3 (s, 2H), 6.8-7.0 (m, 4H), 7.5-7.7 (m, 3H).

The samples were prepared by slowly injecting a portion of stock solution of known concentration of ketone contained in methanol into a micellar solution until an absorption of 0.2-0.3 at the laser wavelength was attained.

The laser flash photolysis system, including the two laser experiments are described in detail in Chapter 2.

Chapter 6. α-Terthienyl (α-T) in a Protein Environment

6.1 Introduction

In this chapter, the investigation of the triplet state of α-terthienyl (α-T) was studied in a protein environment. These studies were carried out to better understand the behavior of a protein conjugated photosensitizer and the singlet oxygen it produces after light irradiation. The purpose of these experiments was to characterize and evaluate the feasibility of using α-terthienyl as a viable antibody conjugated photosensitizer to selectively destroy particular membrane bound proteins thought to be responsible for insect resistance to pesticides.

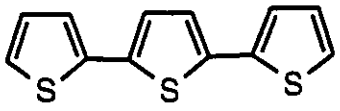

α-terthienyl

α-Terthienyl (α-T) is a member a large group of naturally occurring compounds from the plant family Asteraceae.[130] These compounds are produced as potent phototoxic secondary metabolites and play a role in plant chemical defense against herbivorous insects and fungi.[131] α-Terthienyl has been shown to be an excellent sensitizer of singlet molecular oxygen, O_2 ($^1\Delta_g$)[132] which is thought to be responsible for the phototoxicity of these compounds.[111]

As a photosensitizer, α-T generates a triplet excited state upon light activation and can be readily monitored using laser flash photolysis

techniques.[110,111,132-134] A very high intersystem crossing quantum yield, Φ_{isc} from the singlet state has been measured in the range of 0.9-1.0.[111] α-T has a triplet energy of 39.7 ± 1.5 kcal/mol which was determined by heavy atom-induced optical absorption.[111] A sample triplet absorption spectrum of α-T is shown in Figure 6.1. The spectrum is dominated by the strong triplet absorption at 460 nm (ε = 26000 $M^{-1}cm^{-1}$) with a lifetime of about 27 μs in nitrogen saturated acetonitrile solution.[110,133] In the presence of oxygen, the triplet is readily quenched by oxygen (k_{O_2} = 2 x 10^9 $M^{-1}s^{-1}$)[133] to give singlet oxygen, O_2 ($^1\Delta_g$).

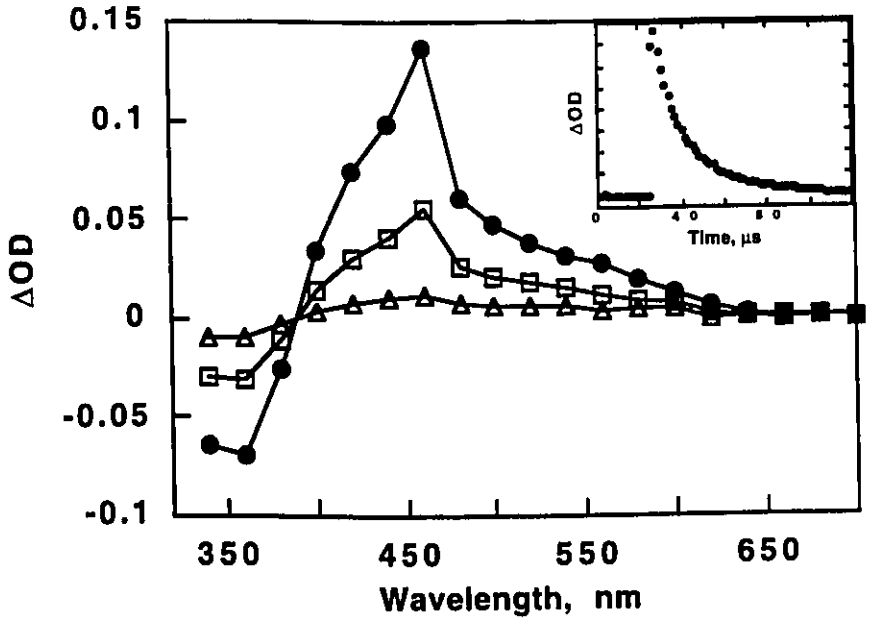

Figure 6.1. Transient absorption spectrum of α-T (2 x 10^{-5} M) in nitrogen saturated acetonitrile recorded 4 (●), 20 (□) and 50 μs (Δ) after 355 nm laser excitation. Note the photobleaching of starting material at ~ 360 nm. The inset shows a typical triplet decay trace collected at 450 nm.

Photosensitization can be viewed as a collisional energy transfer process between an excited triplet state and quencher (ground state oxygen). At a geometry, r_c, the triplet excited state/ground state oxygen surface intersects with that of the ground state/singlet oxygen surface and an intersystem crossing to the lower state occurs resulting in singlet oxygen formation and ground state (S_0) α-T. The value of Φ_Δ represents the quantum yield of singlet oxygen generation under conditions where all the triplets are quenched by oxygen. The quantum yield of singlet oxygen generation by α-T has been determined using laser flash photolysis techniques[132] including time-resolved measurements of singlet oxygen IR phosphorescence[111] and is in the range of 0.70-0.89 in a variety of solvents.[111] At most, 1% of the quenching events (quantum yield between 0.001-0.01) lead to radical cation generation through electron transfer to O_2.[134] Radiationless decay accounts for the difference between the singlet oxygen yield (0.70-0.89) and Φ_{isc} (0.9-1.0).

Electron transfer can be facilitated in the presence of good electron acceptors such as benzyl viologen, resulting in the formation of α-T radical cation (reaction 6.1).[110,133,134]

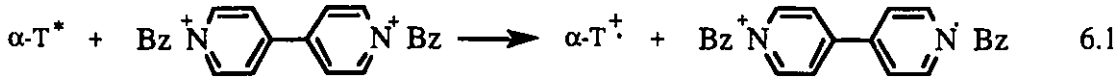

Benzyl viologen

6.1

The α-T radical cation can also be readily detected by its distinct absorption with λ_{max} = 530 nm (ε = 29000 $M^{-1}cm^{-1}$) which is red shifted compared to the triplet absorption spectrum.[135] Figure 6.2 shows a typical

absorption spectrum of the α-T radical cation generated by electron transfer to benzyl viologen (reaction 6.1) in a micellar environment.

α-T is also a fluorescent molecule which facilitates its detection in solution even at extremely low concentrations. Fluorescence quantum yields of a-T (Φ_f) are in the range of 0.05-0.08 in various solvents.[111] This attribute, combined with its ability to produce large amounts of singlet oxygen has made the potential of using α-T as an antibody conjugated photosensitizer the subject of a recent investigation by researchers in the departments of chemistry and biology, here at the University of Ottawa.

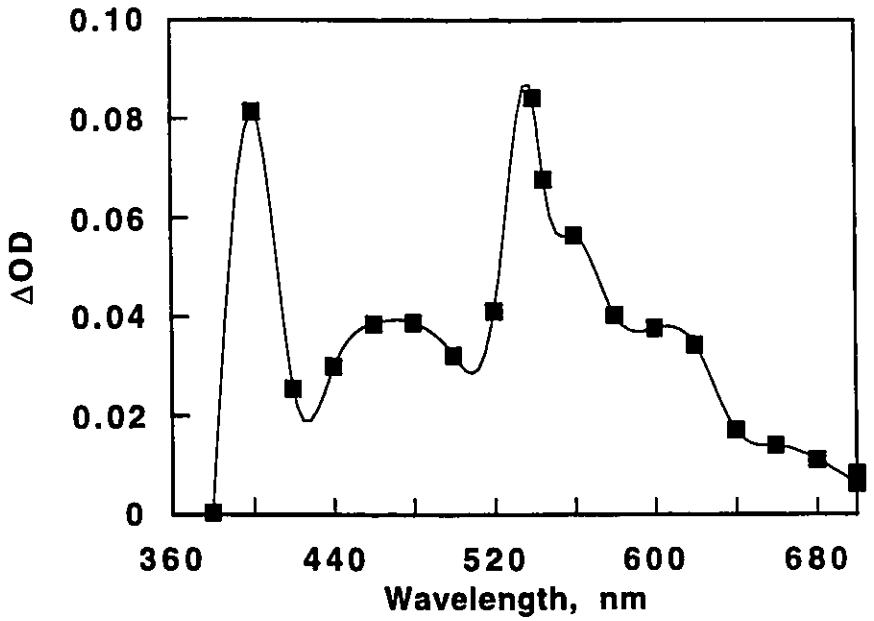

Figure 6.2. Transient absorption spectrum of the α-T radical cation generated from 3 x 10^{-5} M α-T in a 0.2 M SDS solution with 2 mM benzyl viologen monitored 40 ns after 355 laser excitation.

For more than twenty years, antibodies conjugated to fluorescent molecules have been used extensively in molecular biology to detect the presence of various cellular structures and proteins using fluorescent microscopy techniques. However, antibody targeted photolysis is a fairly new concept. Recently, there have been several accounts of conjugating photosensitizers onto antibodies which are specific for a particular cell or cellular structure.[136-140] Conjugating α-T onto an antibody would result in an excellent fluorescent indicator and if desired, a potent photosensitizer capable of destroying the attached antigen. This concept would be useful if the attached antigen is a cancerous cell or cellular component whose function is not desired. The extent of the inactivation would be controlled by the duration of light exposure and particularly the number of conjugated sensitizers attached to the antibody.

The beginning of this investigation arose from two distinct origins. The discovery of P-glycoprotein by Victor Ling (Ontario Cancer Institute) who was looking at tubulin in cancer cells resistant to colchicine, a chemotherapeutic antitubulin alkaloid, and the discovery that an alkaloid pump analogous to P-glycoprotein was present in insects. Ling found that colchicine-resistant cells protected themselves from the chemotherapeutic agent by active alkaloid extrusion. The active pump, P-glycoprotein, was also present in elevated levels in the resistant cells. P-glycoprotein has been assigned as a non-specific carrier which transports a wide variety of drugs and has been implicated as the source of multi-drug resistance in cancer cells.

The xenobiotic pump present in insects is thought to be responsible for insect resistance to pesticides. In addition, it is believed that the pump protects from poisoning in natural feeding patterns in insects such as

tobacco hornworms which feed on tabacco plants high in toxic nicotine. It was found that antibodies which are specific for P-glycoprotein in mammalian cells also bind to the protein pump present in these insects. This would imply that the two proteins are homologous. However, there was no other evidence to confirm this preliminary observation. It was the initial goal of this highly collaborative project to provide evidence assigning P-glycoprotein as the source of insect resistance to pesticides. The approach selected was to use antibody-targeted photolysis in which α-T was conjugated to an antibody specific for P-glycoprotein. Insects, such as tobacco hormworms would then be incubated with the antibody conjugate. In this way the localization of P-glycoprotein in the insect could be facilitated through fluorescence microscopy and upon further light irradiation, the pump could be distroyed, causing mortality of the insect from nicotine poisoning upon consumption of the tabacco. This would provide evidence for the localization of the pump in the insects and a means of selectively destroying their ability to feed. The long term goal of this project was to understand insect resistance at a molecular level and perhaps provide a new approach to the development of new insecticides which function by obstructing the pump responsible for insect resistance to pesticides.

The above approach posed many potential questions that would have to be addressed before experiments of such an advanced nature with antibodies were to be performed. The preliminary investigations were to analyze the triplet state of α-T in a protein environment and relate it to previous solution experiments. In addition, the quantification of phototoxic singlet oxygen was to be carried out in a protein environment and the effect that conjugation would have compared to freely associated protein-α-T

complexes would be examined. Bovine serum albumin (BSA) was chosen as a model for a typical protein adduct having a size comparable to antibody proteins.

6.2. α-T in a Protein Environment: Triplet Behavior and Singlet Oxygen Yields

6.2.1. Results

The synthesis of the conjugates was performed by Y. Lear, a graduate student working in the Department of Chemistry, University of Ottawa under the supervision of Prof. T. Durst. The synthesis involves the mixed anhydride procedure[141] in which α-T is converted to an acid anhydride intermediate through its corresponding carboxylic acid[142] and reacted with the amino groups of bovine serum albumin (primarily lysine groups) to give the amide linked photosensitizer. The synthetic process is outlined in Scheme 6.1.

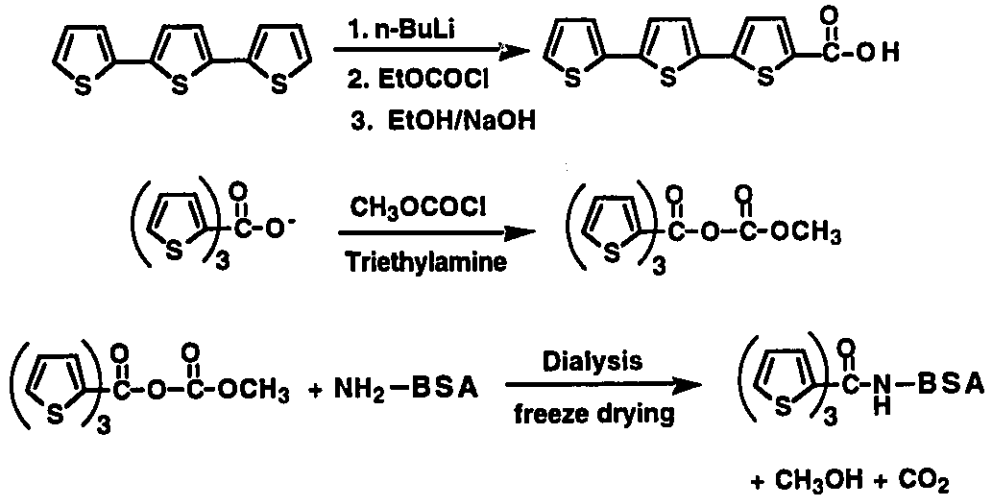

Scheme 6.1. Synthetic scheme of α-T-bovine serum albumin conjugate.

The conjugates were synthesized with varying number of conjugated α-T sensitizers so that comparisons could be made between singlet oxygen

yield and the number of α-T's attached to the protein. Typically, conjugates consisting of under 12 α-T's/BSA were prepared. A list of the various conjugates employed in this study are shown in Table 6.1. The extent of conjugation was verified by calculating the α-T concentration in a known amount of conjugate through its absorption at 374 nm. The measured extinction coefficient of the amide substituted α-T at 374 nm was used in the calculations (ε = 24500 $M^{-1}cm^{-1}$). Denaturing the protein conjugate with urea and subsequent washing with ethyl acetate revealed no α-T absorption in the solvent wash, showing that the conjugation was fulfilled.

Table 6.1. α-T-BSA conjugates and the number of α-T's attached to the protein.

Conjugate	α-T / BSA ratio[a]
1	12
2	7
3	5
4	4
5	1

[a] ±0.5

The conjugates proved to be very fluorescent. As an example, the fluorescence emission spectra collected from 10 ppm α-T and 1 ppm α-T-BSA conjugate (**2**) are shown in Figure 6.3. The fluorescence from the conjugates is red shifted approximately 50 nm compared to α-T alone in solution. Part of this shift is attributed to the amide linkage which

increases the π conjugation in the chromophore and shifts both the absorption and emission to higher wavelengths.

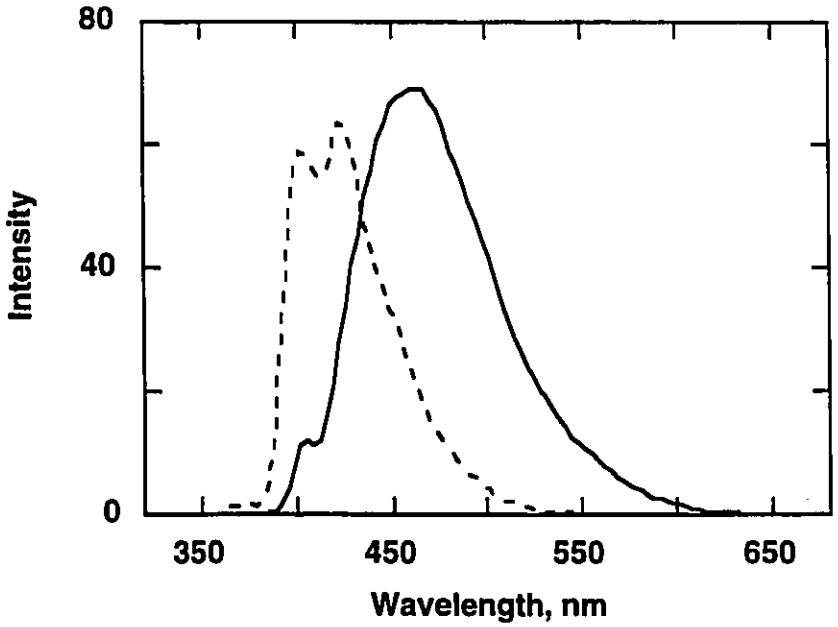

Figure 6.3. Fluorescence emission spectra collected from α-T (-----) and α-T-BSA conjugate (**2**) (——) solutions at 10 ppm (3.7×10^{-7} M) and 1 ppm (1.5×10^{-8} M) in methanol and pH 7 buffered aqueous solution, respectively, after 355 nm excitation.

The transient absorption spectra recorded for the conjugates were all very similar and red-shifted compared to α-T. Figure 6.4 shows the transient absorption spectra of α-T-BSA conjugate (**3**) compared to α-T recorded after 355 nm laser excitation under nitrogen saturated conditions. The shift in triplet absorption observed parallels the shift found with the fluorescence spectra shown in Figure 6.3. In addition, some photoionization may result in α-T radical cation formation which absorbs at

higher wavelengths (Figure 6.2). The photoionization of α-T in a micelle was reported in Chapter 5. The absence of solvated electron absorption at wavelengths >650 nm suggests that the electrons are reacting with the protein and therefore are not observed.

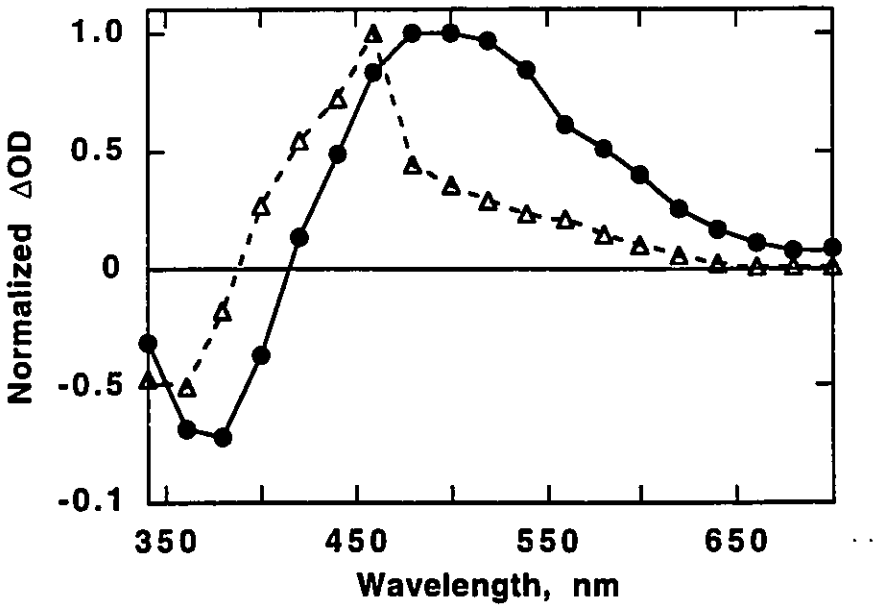

Figure 6.4. Transient absorption spectra of α-T-BSA conjugate (3) in pH 7 buffered water (●) and α-T (Δ) in acetonitrile under nitrogen saturated conditions at 7.27 x 10^{-6} and 2 x 10^{-5} M α-T, respectively, collected 4 μs after 355 laser excitation.

The triplet decay of protein conjugated α-T was significantly longer compared to protein-free α-T in homogeneous solution. Figure 6.5 shows a comparison between the transient triplet decays of α-T in methanol and α-T-BSA conjugate (5) under nitrogen saturated conditions. The first order

decay of α-T in methanol has a lifetime close to 25 μs while when conjugated, this increases to around 100 μs.

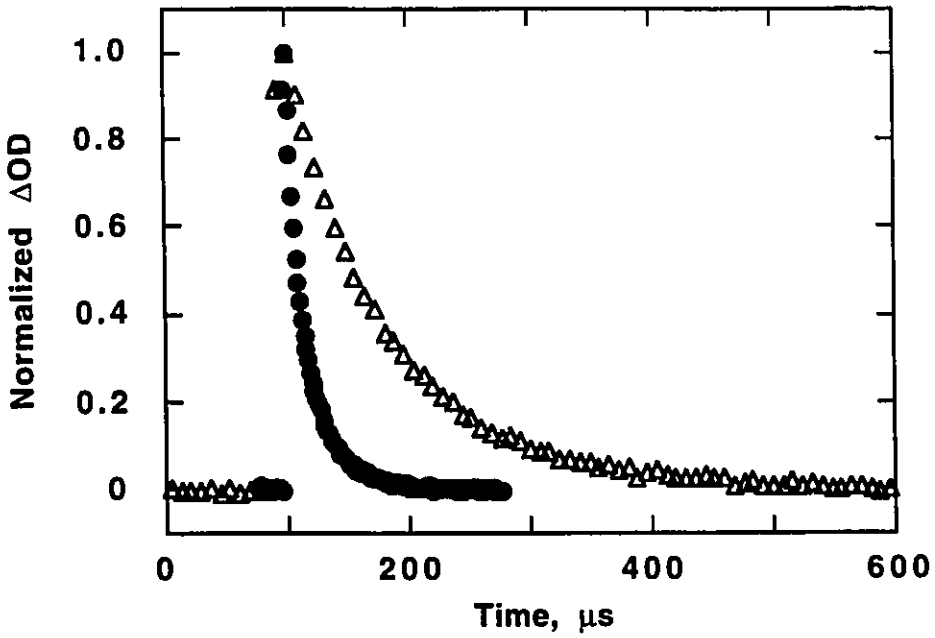

Figure 6.5. Triplet decay traces of α-T in methanol (●) and α-T-BSA conjugate (**5**) in pH 7 buffered aqueous solution (Δ) at 1.9 x 10^{-5} and 1.5 x 10^{-5} M, respectively, recorded at 450 nm after 355 nm laser excitation under nitrogen saturated conditions.

Oxygen readily quenches the triplet of α-T in methanol solution (k_{O_2} = 2 x 10^9 $M^{-1}s^{-1}$).[133] However, α-T conjugated to BSA shows a rate constant of oxygen quenching about an order of magnitude slower (k_{O_2} = 3.6 x 10^8 $M^{-1}s^{-1}$). Figure 6.6 shows the effect of oxygen on the triplet signals of α-T-BSA conjugate (**5**) observed under nitrogen and oxygen saturated conditions, while Figure 6.7 shows a representative quenching plot obtained. Varying the conjugation did not affect the triplet lifetimes observed or the rates of

oxygen quenching. With the addition of oxygen, the triplet lifetime changes from 93 to 3 μs representing about 97% triplet quenching by the addition of oxygen.

For comparison, a freely associated complex of α-T and BSA was prepared by injection of a stock solution of α-T in methanol into a BSA solution so that both the protein concentration and the absorbance at the laser wavelength matched the conjugated sample (**5**) used. Figure 6.7 shows that the rate of oxygen quenching between the two samples is approximately the same at ~3.6 x 10^8 $M^{-1}s^{-1}$.

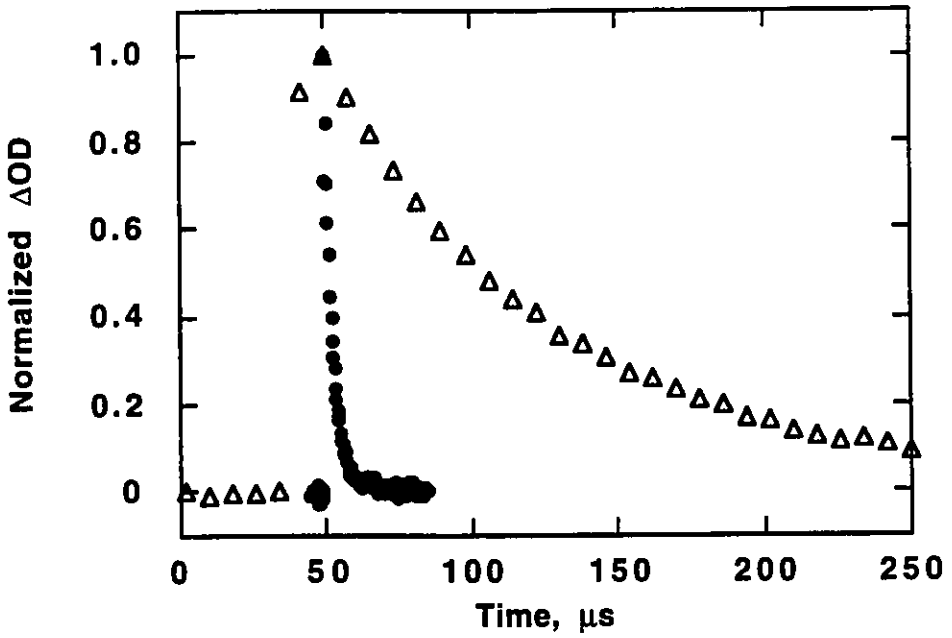

Figure 6.6. Triplet decay traces of α-T-BSA conjugate (**5**) in pH 7 buffered water (1.5 x 10^{-5} M) collected after 355 nm laser excitation under nitrogen (Δ) and oxygen (●) saturated conditions.

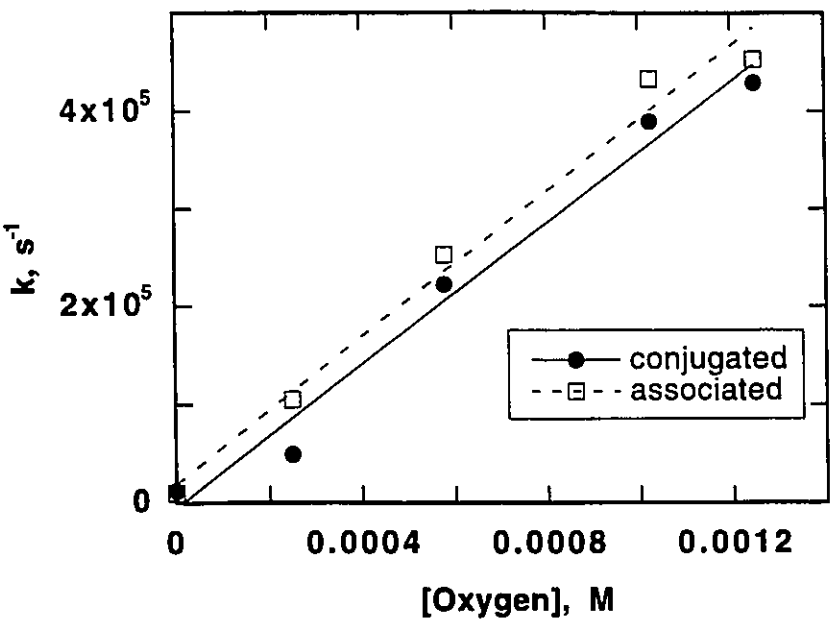

Figure 6.7. Oxygen quenching plot of α-T-BSA conjugate (**5**) in water (1.5 x 10^{-5} M) at pH 7 and an optically matched freely associated complex of α-T and BSA (1.5 x 10^{-5} M) giving rate constants of oxygen quenching of 3.6 x 10^8 and 3.7 x 10^8 $M^{-1}s^{-1}$, respectively.

Although the conjugated α-T shows a slower rate constant of oxygen quenching compared to homogeneous solution, a significant amount of singlet oxygen was observed. Using the apparatus described in Chapter 2, the time-resolved luminescence of singlet oxygen at 1.27 μm produced from sensitization of ground state oxygen by the triplet state of the conjugated α-T can be readily monitored.[35,40-42] It is necessary to use deuterated water (D_2O) as the solvent in these experiments to increase the lifetime of singlet oxygen so that its detection is possible with the detector-amplifier system used to detect the singlet oxygen luminescence (Chapter 2). D_2O also absorbs less of the infrared luminescence produced by the singlet oxygen.

Figure 6.8 shows a time-resolved singlet oxygen decay generated by α-T-BSA conjugate (**1**) in oxygen saturated D_2O.

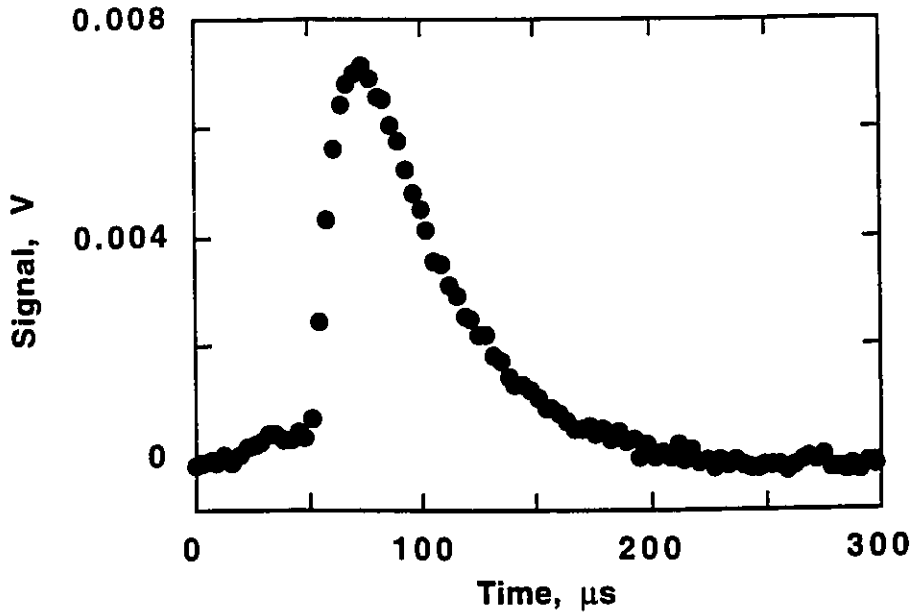

Figure 6.8. Singlet oxygen ($^1\Delta_g$) luminescence decay trace centered at 1.27 μm generated from α-T-BSA conjugate (**1**) under oxygen saturated conditions in D_2O solution.

To measure quantum yields (Φ_Δ) of singlet oxygen production from the samples, a comparison method is used (see Chapter 2) whereby the energy dependence of the initial O_2 ($^1\Delta_g$) luminescence intensity (I_0) was measured for optically matched samples under study and for a reference compound for which the Φ_Δ is accurately known in the same solvent. In this case, Rose Bengal is used as the reference (Φ_Δ = 0.80 in D_2O).[46,47] By direct comparison of the slopes of the power dependence plots, the Φ_Δ value for the sample may be obtained. In many cases, curved lines result due to competitive absorption by the sensitizer triplet states formed during the

laser pulse. In these cases, a second order polynomial fit was employed to determine the slope at zero dose. Figure 6.9 shows the power dependence plots of conjugates 1 and 4 compared to Rose Bengal. The resulting quantum yields calculated from the slopes of the lines are 0.2 and 0.1 for the two conjugates, respectively.

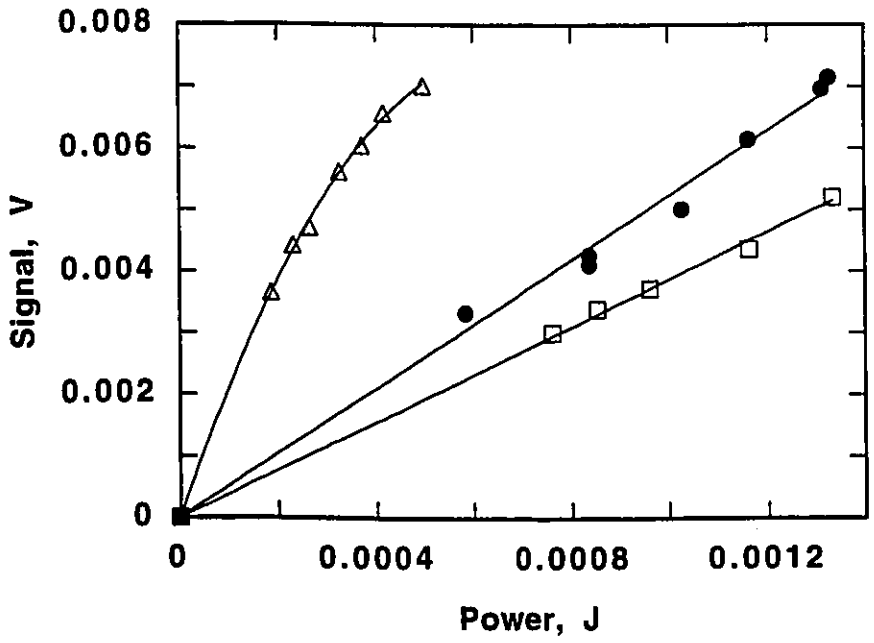

Figure 6.9. Power dependence plots in deuterated water for Rose Bengal (Δ), an α-T conjugate having 12 α-T's/BSA (**1**) (●) and 4 α-T's/BSA (**4**) (□). The resulting quantum yields calculated from the slopes of the lines are 0.2 and 0.1 for the two conjugates, respectively using a yield of 0.80 for Rose Bengal.[46,47]

6.2.2. Discussion.

The purpose of these experiments was to spectroscopically characterize the transient behavior of protein conjugated α-T and to quantify the amount of singlet oxygen produced upon photosensitization.

The protein chosen for conjugation was bovine serum albumin (BSA) which would serve as a model protein environment for future antibody conjugates. The results of these studies would evaluate the potential of using α-T as viable photosensitizer in antibody-targeted photolysis.

In addition to using α-T as a potent photosensitizer, it can also be used as a fluorescent indicator. The detection of fluorescence would serve to localize the antibody conjugates *in vivo*. Figure 6.2 shows a sample fluorescence emission spectrum recorded from conjugate **2** compared to α-T in methanol. The emission from conjugated α-T is readily detectable even at a concentration of 1 ppm protein and shows a shift to higher wavelengths by about 50 nm compared to unconjugated α-T. Fluorescence microscopy using antibodies tagged with fluorescent indicators such as fluorescein are typically used at these concentrations in determining the locations of antigens in cellular media. In this respect, the use of α-T as a fluorescent indicator would be an excellent alternative.

Triplet signals generated by the conjugates are readily detectable and show a broadening and a red shift in λ_{max} by approximately 40 nm and are approximately 5 times longer lived compared to unconjugated α-T (Figure 6.4). This increase represents a restriction of triplet deactivation pathways present in homogeneous solution and is beneficial in allowing more photosensitization to occur.

The triplets of the conjugated photosensitizers readily sensitize the formation of singlet oxygen. The triplet lifetime of conjugated α-T decreases from 93 μs under nitrogen to under 3 μs in oxygen saturated solution (Figure 6.5). This shows that about 97% of the triplets are quenched by oxygen. The oxygen quenching rate constant determined was 3.6×10^8 $M^{-1}s^{-1}$ for conjugated α-T and was independent of the amount of

conjugation (Figure 6.7). This represents a slower rate of oxygen quenching by approximately an order of magnitude compared to unconjugated α-T in homogeneous solution. Lissi *et al.*[143] had determined that oxygen had little restriction on its diffusion in a protein environment when studying the luminescence quenching of amino acid residues in various proteins. Our results show a substantial restriction of oxygen diffusion which reduces the oxygen quenching rate constant by about an order of magnitude compared to homogeneous solution. Although the amide linkages joining the photosensitizers to the protein are part of surface exposed lysine residues, it is reasonable to assume that the addition of highly hydrophobic photosensitizers such as α-T drastically rearrange the protein to a more stable conformation thereby effectively burying the α-T molecules deep into the protein's interior, thus restricting the access of oxygen. An optically matched freely associated complex of α-T and BSA shows a similar oxygen quenching rate constant compared to the conjugated sample (Figure 6.7). Both samples were also matched for BSA concentration. Hydrophobic molecules such as α-T would localize in regions of the protein isolated from the surrounding aqueous environment. It is apparent from the oxygen quenching rates of the associated complex and the conjugated samples, that the α-T is not near the surface of the protein in either sample and access by oxygen is substantially restricted by the surrounding protein.

The luminescence generated by singlet oxygen was readily detected at 1.27 μm in D_2O (Figure 6.9). The lifetime of the Rose Bengal generated singlet oxygen is around 60 μs which corresponds to the reported lifetime of singlet oxygen in D_2O.[144,145] However, the lifetime of singlet oxygen generated from the conjugate is substantially shorter, at around 40 μs. In

addition, the size of the signal monitored is significantly smaller compared to Rose Bengal. Both α-T and Rose Bengal have similar quantum yields of singlet oxygen production (~0.8); therefore, any significant difference in the signals observed should be attributed to reaction with the surrounding protein environment. The shorter lifetime corresponds to a scavenging of singlet oxygen by the protein while the initially smaller signal represents a geminate reaction with the protein. Feitelson *et al.*[146] have measured the rate constants of singlet oxygen reaction with tryptophan, tyrosine, histidine, methionine and cysteine to be between 2×10^6 to 5×10^7 $M^{-1}s^{-1}$. Other amino acids show much slower rates. These five amino acids are all present in bovine serum albumin in varying amounts and locations due to their hydrophilicity. It would be reasonable to assume that the conjugated α-T is randomly distributed in the protein making reaction with all these amino acids possible.

Even though geminate and non-geminate reactions do occur between singlet oxygen and the protein, a significant amount does escape into solution. From the plots shown in Figure 6.9, the quantum yields of two representative conjugates (**1** and **4**) were calculated (compared to Rose Bengal) to be 0.2 and 0.1 for conjugates of 12 and 4 α-T's per BSA, respectively. Interestingly, the conjugation in **4** is three times lower than **1** but the singlet oxygen yield only drops by half. Analogous values of singlet oxygen yields were recently reported by Rakestraw *et al.*[140] for a series of clorin e6 immunoconjugates having similar photosensitizer ratios. The sensitizers were attached to the antibody by a dextran carrier and localized in a region of the antibody known as the Fc oligosaccaride. The authors also reported that the singlet oxygen yield *decreased* with increased conjugation and attributed the decline to photosensitizer aggregation which

increases with conjugation thereby lowering the triplet and singlet oxygen yields. In addition, absorption band broadening was reported which resulted from sensitizer aggregation. Compared to chlorin e6, α-T is considerably more hydrophobic and likely to aggregate in aqueous media. Although the triplet spectra observed for our conjugates showed some spectrum broadening which may result from aggregation, this process would be limited due to the random distribution of the attached sensitizers throughout the protein. In our system, it is more likely that increasing the conjugation of highly hydrophobic sensitizers such as α-T, would result in more protein rearrangement, thus further burying the sensitizers deeper into the protein. This in turn leads to more geminate protein-singlet oxygen reactions which lowers the observed yield.

6.2.3. Conclusion

In this chapter, I have described preliminary experiments designed to characterize the triplet excited state behavior of α-T conjugated to a protein. In addition, the measurement of oxygen quenching of the triplet state was carried out and the corresponding Φ_Δ of singlet oxygen was measured for conjugates having varying numbers of α-T's attached. It was found that the triplets were readily generated in the protein environment and were quenched by oxygen with a rate constant approximately ten times slower than in homogeneous solution. The singlet oxygen luminescence resulting from the triplet quenching was monitored at 1.27 μm. It was found that a significant amount of singlet oxygen is unaccounted for and most likely decays by rapid reaction with the protein. Despite this, a significant amount of singlet oxygen is released into the surrounding

solution and its amount can be controlled by the degree of conjugation. In terms of singlet oxygen production and detection through fluorescence, α-T would be an excellent candidate for an antibody conjugated photosensitizer. However, the large amount of geminate reaction of singlet oxygen with the protein may represent a deeply buried photosensitizer and subsequent change of protein conformation. A dramatic rearrangement of the protein of this nature would not be desirable in an antibody conjugate as loss of structure and antigenic specificity may result. The choice of a more water soluble α-T analog would be a prudent step in the next phase of this project to maintain protein conformation and decrease geminate singlet oxygen reactions.

6.3. Experimental

The conjugates used in this study were a generous gift from Y. Lear. The degree of conjugation was calculated using the extinction coefficient of the amide substituted α-T at 374 nm (ε_{355}= 24500 $M^{-1}cm^{-1}$) and from the absorption of a known concentration of conjugate at that wavelength. The conjugates were freeze dried before use. Acetonitrile and methanol were from BDH (Omnisolve). Rose Bengal was purchased from Aldrich and filtered through Sephadex G25 (superfine column Pharmacia, 2.5/45 cm) in 50 mM NH_4OH[147] and its purity verified by its extinction coefficient at 550 nm (ε_{550} = 99000 $M^{-1}cm^{-1}$). α-Terthienyl and the amide substituted α-T were generous gifts from Prof. J.T. Arnason. Associated complexes were prepared by injecting a deaerated stock solution of α-T in methanol (5 mg / mL) into a BSA solution in buffer (pH 7, 0.1 M phosphate buffer made with

Millipore filtered water; 1 mg / mL) until an optical density matching that of the conjugate was achieved at the laser wavelength.

For the transient experiments, solutions of conjugate were prepared in specially designed laser cells having a separate chamber to isolate the protein from bubbling the solvent with either nitrogen, oxygen or a combination of the two prior to mixing. Oxygen quenching experiments were carried out with five individually prepared solutions of protein that were each bubbled for 30 minutes with the appropriate mixture of nitrogen/oxygen using a calibrated Air Products gas mixer.

The laser flash photolysis system including time-resolved singlet oxygen detection is described in detail in Chapter 2.

Fluorescence spectra were recorded using a Perkin Elmer LS50 luminescence spectrometer using an excitation wavelength of 355 nm in order to produce data that would be readily comparable with those obtained under laser excitation.

Chapter 7. Final Comments and New Directions

This thesis has presented research on the investigation of triplet excited states as probes in organized media in solution and in the solid state with comparisons to experiments in homogeneous solution. Chapters 3, 4 and 5 presented results based on triplet probes which deactivated by an intramolecular charge transfer deactivation process. As a result, they were extremely sensitive to substituent effects, and particularly, restrictions to mobility imposed by their surrounding environment. Laser flash photolysis (LFP) studies demonstrated the importance of conformational and redox properties in determining the kinetics for the intramolecular charge transfer quenching in these molecules which were confirmed with molecular modeling calculations and cyclic voltammetry techniques. Two years later, another group verified our results confirming that the triplet lifetimes of these derivatives can be controlled by the redox properties of the β-aryl ring.[84] The results also confirm that in the absence of a *p*-methoxy substituent, the lifetimes are too short to be amenable for direct study with nanosecond techniques and are largely controlled by bond rotation.

We successfully measured the triplet lifetimes of several of these β-aryl ketones in the solid state using laser flash photolysis diffuse reflectance techniques. The results show that these ketones would be excellent mobility probes in the solid state as well as in solution. Their triplet lifetimes in the solid state are determined by the position of the β-phenyl ring in relation to the carbonyl. Small changes in the position of the deactivating β-phenyl ring resulted in measurable changes in triplet lifetime. In addition, small packing differences in the unit cells are

manifested in a change in triplet lifetime as seen by comparing racemic to enantiomerically pure crystals. This represented the first example of chiral recognition measured by triplet lifetimes in crystals.

Excited triplet probe molecules can be successfully employed to study a variety of properties in organized systems that cannot be measured easily by fluorescence techniques. The unique intramolecular triplet quenching mechanism of these probes provides information on specific stereochemical constraints in cyclodextrin solutions (Chapter 4). Experiments using a variety of substituted ketones helped confirm earlier proposals on the conformation of β-aryl ketone-CD complexes. Solid state CD inclusion complexes show chiral recognition through preferential incorporation of one enantiomer of chiral probe over the other. However, triplet decay kinetics in solid CD complexes reveal complex decay patterns possibly due to reaction with the CD host. Although some evidence of chiral selection was manifested in differing triplet decay kinetics of the two enantiomers incorporated into the CDs, confirming these results has been difficult due the complex nature of the decay routes of the triplets inside the CD cavity. With today's sophisticated analysis programs, one may be able to differentiate the various triplet decay components of the two enantiomers allowing comparisons to be made.

The focus of the research carried out in the preliminary stages of this thesis was to demonstrate chiral selectivity through monitoring the triplet decay kinetics of chiral probes incorporated into chiral hosts. In Chapter 5, sodium cholate micelles were chosen as a chiral micellar host environment. The triplet lifetimes of the probes increased significantly when incorporated into this environment as expected from the decrease in rate of intramolecular quenching. Although no difference in triplet

lifetimes of the two enantiomers was observed (similar results were seen in cyclodextrin solutions), a new absorption corresponding to solvated electrons appeared which was unique to anionic micellar environments. The photoionization process requires two photons and involves the intermediacy of the triplet state, which is responsible for the absorption of the second photon. A small equilibrium concentration of ketone resides in the aqueous phase which reacts with the solvated electrons; it is this concentration which determines the electron lifetime. It is conceivable that if chiral selection was occurring in these micelles, that this would be manifested in a lower concentration of ketone in the aqueous phase, thus giving a longer solvated electron lifetime for this enantiomer. Although preliminary experiments with the chiral ketones described in this thesis were carried out with this intention, it became obvious that a larger equilibrium difference would have to be established between the two enantiomers before a difference in solvated electron lifetime could be observed.

β-phenyl ketones, such as the ones presented in this thesis are extremely sensitive to changes in conformation. Most chiral biological environments are selective through hydrogen bonding interactions which stereochemically select one enantiomer over the other. In this regard, the continuation of the experiments presented in this thesis with other chiral substituted β-phenyl ketones could be potentially rewarding. Bulkier hydrogen bonding substitution in the α- or β-positions may result in conformational differences which may be detectable though LFP techniques. However, large equilibrium constants would have to be present to make the system as heterogeneous as possible, thus exposing the potential differences in observed lifetimes. Ketone **VI** (a chiral alcohol

substituted in the α-position) was synthesized in both pure D and L forms for this purpose. However, preliminary solution experiments using this probe in cyclodextrin, cholate micelle and protein solutions did not reveal any triplet lifetime differences for the two enantiomers. Studies in solid state complexes were not carried due to its tendency for cleavage.

In Chapter 6, the analysis of protein conjugated α-terthienyl complexes were investigated in order to characterize the triplet behavior of α-T attached to a protein. Bovine serum albumin (BSA) was used as a model for antibody conjugates that are being developed. The conjugated triplets were much longer lived in the protein, and were partially protected from reactions with quenchers such as oxygen. The goal of these investigations was to evaluate α-T as a potential photosensitizer candidate for antibody targeted photolysis. Some of the singlet oxygen generated in the protein conjugates reacted geminately but a significant amount escaped into the surrounding solution. This amount of singlet oxygen can be controlled by the amount of conjugated sensitizer. In this respect, α-T is an excellent choice as a conjugated photosensitizer, however, its hydrophobic nature will likely rearrange the protein into a more stable, soluable form. Although, in the case of BSA this is not a serious problem, for antibody conjugates it may be. Other examples of photosensitizers used in antibody targeted photolysis were more water soluble so that conjugation to the antibody did not result in significant denaturation and loss of specificity.[140] For this reason, the use of more water soluble derivatives of α-T would be a prudent choice when preparing the antibody conjugates. In addition, the method of chemical attachment to the protein may not be appropriate for antibodies. In particular, the synthetic method attaches the photosensitizer onto the hydrophilic lysine amino acids, which participate in important

hydrogen bonding usually associated with the antigen specific end of an antibody. Conjugating the photosensitizer onto this area may result in a loss of specificity. Although the analysis of antibody conjugates is beyond the scope of this thesis, the next natural step in this project is the evaluation of these conjugates. Due to the very small antibody concentrations available, the experiments would entail working with extremely small volumes of sample in specially designed quartz cells.

Claims to Original Research

(1) The importance of conformational properties in determining the kinetics of intramolecular quenching in *p*-methoxy substituted β-phenyl ketone mobility probes. Molecular modeling calculations demonstrated that conformational preferences imposed by added substituents determine the triplet lifetimes in these ketones.

(2) β-aryl substitution in these ketones affects the redox properties of the deactivating ring which resulted in a change in the kinetics for intramolecular charge transfer. This provided convincing evidence for a charge transfer interaction.

(3) Establishing the importance of steric factors in the formation and stability of cyclodextrin complexes with β-phenylpropiophenone derivatives, thereby providing information on intracavity mobility and inclusion geometries.

(4) Establishing the role of substituents and crystal packing on the triplet lifetimes of β-aryl ketones in the solid state using laser flash photolysis diffuse reflectance techniques. The first example of chiral recognition in a crystal by observing triplet lifetimes.

(5) Aromatic ketones incorporating the benzoyl and *p*-methoxybenzoyl moieties were shown to photoionize under conditions of pulsed laser excitation in anionic micelles. The lifetimes of the resulting solvated electrons are determined by small concentrations of aromatic ketone

present in the aqueous phase thus providing an explanation for the anomalous short solvated electron lifetimes reported in the literature.

(6) The first investigation of α-terthienyl's (α-T) photosensitizing ability when conjugated to a protein through directly monitoring the generated singlet oxygen in solution using laser flash photolysis techniques. These experiments were used in evaluating α-T as a viable photosensitizer for antibody targeted photolysis.

Publications Resulting from the Research Described in this Thesis

1. R. Boch, M. K. Whittlesey and J. C. Scaiano; "Laser-Induced Photoionization of Aromatic Ketones in Anionic Micellar Solutions", **1994**, *J. Phys. Chem.*, **98**, 7854-7857.

2. C. Bohne, M. Barra, R. Boch, E. B. Abuin, J. C. Scaiano; "Excited Triplet States as Probes in Organized Systems. An Overview of Recent Results", **1992**, *J.Photochem. Photobiol. A: Chem.*, **65**, 249-265.

3. R. Boch, C. Bohne, J. C. Netto-Ferreira, J. C. Scaiano; "Effect of Methyl Substitution on the Intramolecular Triplet Deactivation of *p*-Methoxy-β-phenylpropiophenone", **1991**, *Can. J. Chem.*, **69**, 2053-2060.

4. R. Boch, B. Mehta, T. Connolly, T. Durst, J. T. Arnason, R. W. Redmond, J. C. Scaiano; "Singlet Oxygen Yields from Bithiophene and

Trithiophene Derivatives", **1995**, *J. Photochem Photobiol. A: Chem.*, accepted February 9, 1995.

5. R. Boch, C. Bohne, J. C. Scaiano; "Time-Resolved Diffuse Reflectance Studies of β-Phenyl Ketones in the Solid State: Conformational and Chiral Control of Triplet Lifetimes", **1995**, submitted to *J. Org. Chem.*

6. R. Boch, Y. Lear, N. Mohtat, J. T. Arnason, T. Durst, J. C. Scaiano; "Laser Flash Photolysis Studies of α-Terthienyl Conjugated to Bovine Serum Albumin", **1995**, manuscript in preparation.

References

(1) *Photochemistry in Organized and Constrained Media*; Ramamurthy, V., Ed.; VCH Publishers: New York, 1991.

(2) *Organic Phototransformations in Nonhomogeneous Media*; Fox, M. A., Ed.; American Chemical Society: Washington, D.C., 1985; Vol. 278.

(3) Thomas, J. K. *Chem. Rev.* **1980**, *80*, 283-299.

(4) Reddy, G. D.; Usha, G.; Ramanathan, K. V.; Ramamurthy, V. *J. Org. Chem.* **1986**, *51*, 3085-3093.

(5) Reddy, G. D.; Ramamurthy, V. *J. Org. Chem.* **1987**, *52*, 5521-5528.

(6) Scheffer, J. R. *Acc. Chem. Res.* **1980**, *13*, 283-290.

(7) Liu, Y. S.; Ware, W. R. *J. Phys. Chem.* **1993**, *97*, 5080-5986.

(8) Siemiarczuk, A.; Ware, W. R.; Liu, Y. S. *J. Phys. Chem.* **1993**, *97*, 8082-8091.

(9) Gratzel, M.; Thomas, J. K. *J. Am. Chem. Soc.* **1973**, *95*, 6885-6889.

(10) Wallace, S. C.; Thomas, J. K. *Radiat. Res.* **1973**, *54*, 49-62.

(11) Patterson, L. K.; Vieil, E. *J. Phys. Chem.* **1972**, *77*, 1191-1192.

(12) Winnik, F. M. *Chem. Rev.* **1993**, *93*, 587-614.

(13) Almgren, M.; Grieser, F.; Thomas, J. K. *J. Am. Chem. Soc.* **1979**, *101*, 279-291.

(14) Kalyanasundaram, K. In *Photochemistry in Organized and Constrained Media*; V. Ramamurthy, Ed.; VCH Publishers: New York, 1991; pp 39-78.

(15) Hamai, S. *J. Am. Chem. Soc.* **1989**, *111*, 3954-3957.

(16) Porter, G.; Topp, M. R. *Proc. Roy. Soc. London, Ser. A* **1970**, *315*, 163-184.

(17) Kosonocky, W. F.; Harrison, S. E.; Stander, R. *J. Chem. Phys.* **1965**, *43*, 831-833.

(18) Infelta, P. P.; Gratzel, M.; Thomas, J. K. *J. Phys. Chem.* **1974**, *78*, 190-195.

(19) Bohne, C.; Fan, M. G.; Li, Z. J.; Lusztyk, J.; Scaiano, J. C. *J. Chem. Soc., Chem. Commun.* **1990**, 571-572.

(20) Bohne, C.; Abuin, E. B.; Scaiano, J. C. *Langmuir* **1992**, *8*, 469-474.

(21) Barancyk, S. V. *Dissertation Abstracts International* **1990**, *50*, 3470.

(22) Barra, M.; Bohne, C.; Scaiano, J. C. *Photochem. Photobiol.* **1991**, *54*, 1-5.

(23) Levin, P. P.; Ferreira, L. F. V.; Costa, S. M. B. *Langmuir* **1993**, *9*, 1001-1008.

(24) Berinstain, A. B.; Scaiano, J. C.; Bohne, C.; Malenfant, P. R. L.; Sprott, G. D. *Photochem. Photobiol.* **1992**, *56*, 423-426.

(25) Berinstain, A. B.; English, A. M.; Hill, B. C.; Sharma, D. *J. Am. Chem. Soc.* **1990**, *112*, 9649-9651.

(26) Redmond, R. W.; Srichai, M. B.; Bilitz, J. M.; Schlomer, D. D.; Krieg, M. *Photochem. Photobiol.* **1994**, *60*, 348-355.

(27) Dolphin, D. *Can. J. Chem.* **1994**, *72*, 1005-1013.

(28) Moan, J. *Photochem. Photobiol.* **1986**, *43*, 681-690.

(29) Dougherty, T. J. *Photochem. Photobiol.* **1993**, *58*, 895-900.

(30) Levin, P. P.; Malkin, Y. N.; Kuzmin, V. A. *Chem. Phys. Lett.* **1990**, *175*, 74-78.

(31) Lindqvist, L. *Hebd. Seances Acad. Sci., Ser. C* **1966**, *263*, 852-854.

(32) Danziger, R. M.; Bar-Eli, K. H.; Weiss, K. *J. Phys. Chem.* **1967**, *71*, 2633-2640.

(33) Asmus, K. D.; Janata, E. In *The Study of Fast Processes and Transient Species by Electron Pulse Radiolysis*; J. Basendale and F. Busi, Eds.; Reidal Publishing: Boston, 1982; pp 91-113.

(34) Wilkinson, F.; Willsher, C. J.; Casal, H. L.; Johnston, L. J.; Scaiano, J. C. *Can. J. Chem.* **1986**, *64*, 539-544.

(35) Rodgers, M. A. J.; Snowden, P. T. *J. Am. Chem. Soc.* **1982**, *104*, 5541-5543.

(36) Scaiano, J. C.; Chen, C.; McGarry, P. *J. Photochem. Photobiol.* **1991**, *62*, 75-81.

(37) Wilkinson, F.; Kelly, G. In *Handbook of Organic Photochemistry*; J. C. Scaiano, Ed.; CRC Press: Boca Raton, Florida, 1989; Vol. II; pp 293-247.

(38) Kubelka, P. *J. Opt. Soc. Am.* **1948**, *38*, 448.

(39) Turro, N. J. *Modern Molecular Photochemistry*; University Science Books: Mill Valley, 1991.

(40) Hurst, J. R.; Schuster, G. B. *J. Am. Chem. Soc.* **1983**, *105*, 5756-5760.

(41) Parker, J. G.; Stanbro, W. D. *J. Am. Chem. Soc.* **1982**, *104*, 2067-2069.

(42) Ogilby, P. R.; Foote, C. S. *J. Am. Chem. Soc.* **1982**, *104*, 2069-2070.

(43) Redmond, R. W.; Braslavsky, S. E. In *Photosensitization: Molecular, Cellular and Medical Aspects*; G. Moreno, R. H. Pottier and T. G. Truscott, Eds.; Springer-Verlag: Berlin, 1988; Vol. NATO ASI Series, H15; pp 93-95.

(44) Redmond, R. W.; Braslavsky, S. E. *Chem. Phys. Lett.* **1988**, *148*, 523-529.

(45) Barra, M.; Calbrese, G. S.; Allen, M. T.; Redmond, R. W.; Sinta, R.; Lamola, R. D.; Scaiano, J. C. *Chem. Mater.* **1991**, *3*, 610-616.

(46) Redmond, R. W. *Photochem. Photobiol.* **1991**, *54*, 547-556.

(47) Gandin, E.; Lion, Y.; Van de Vorst, A. *Photochem. Photobiol.* **1983**, *37*, 271-278.

(48) Demas, J. N.; McBride, R. P.; Harris, E. W. *J. Phys. Chem.* **1976**, *80*, 2248-2253.

(49) Ciamician, G.; Silber, P. *Ber.* **1901**, *34*, 1530.

(50) Wagner, P. J. *Acc. Chem. Res.* **1971**, *4*, 168-177.

(51) Johnston, L. J.; Scaiano, J. C. *Chem. Rev.* **1989**, *89*, 521-547.

(52) Cohen, S. G.; Parola, A.; Parsons, G. *Chem. Rev.* **1973**, *73*, 141-161.

(53) Whitten, D. G.; Punch, W. E. *Mol. Photochem.* **1970**, *2*, 77-80.

(54) Wagner, P. J.; Kelso, P. A.; Kemppainen, A. E. *Mol. Photochem.* **1970**, *2*, 81-85.

(55) Stermitz, F. R.; Nicodem, D. E. *Mol. Photochem.* **1970**, *2*, 87-89.

(56) Bergmann, F.; Hirshberg, Y. *J. Am. Chem. Soc.* **1943**, *65*, 1429.

(57) Wagner, P. J.; Hammond, G. S. *J. Am. Chem. Soc.* **1966**, *88*, 1245-1251.

(58) Bell, J. A.; Linschitz, H. *J. Am. Chem. Soc.* **1963**, *85*, 528-532.

(59) Schuster, D. I.; Brizzolara, D. F. *J. Am. Chem. Soc.* **1970**, *92*, 4357-4365.

(60) Saltiel, J.; Curtis, H. C.; Metts, L.; Miley, J. W.; Winterle, J.; Wrighton, M. *J. Am. Chem. Soc.* **1969**, *92*, 410-411.

(61) Giering, L.; Berger, M.; Steel, C. *J. Am. Chem. Soc.* **1974**, *96*, 953-958.

(62) Wolf, M. W.; Brown, R. E.; Singer, L. A. *J. Am. Chem. Soc.* **1977**, *99*, 526-531.

(63) Wagner, P. J.; Leavitt, R. A. *J. Am. Chem. Soc.* **1970**, *95*, 3669-3677.

(64) Wagner, P. J.; Leavitt, R. A. *J. Am. Chem. Soc.* **1970**, *92*, 5806-5807.

(65) Small, R. D., Jr.; Scaiano, J. C. *J. Phys. Chem.* **1978**, *82*, 2064-2066.

(66) Scaiano, J. C.; Perkins, M. J.; Sheppard, J. W.; Platz, M. S.; Barcus, R. L. *J. Photochem.* **1983**, *21*, 137-147.

(67) Netto-Ferreira, J. C.; Leigh, W. J.; Scaiano, J. C. *J. Am. Chem. Soc.* **1985**, *107*, 2617-2622.

(68) Wagner, P. J.; Kemppainen, A. E.; Schott, H. N. *J. Am. Chem. Soc.* **1973**, *95*, 5604-5614.

(69) Wismontski Knittel, T.; Kilp, T. *J. Phys. Chem.* **1984**, *88*, 110-115.

(70) Ariel, S.; Evans, S. V.; Garcia-Garibay, M.; Harkness, B. R.; Omkaram, N.; Scheffer, J. R.; Trotter, J. *J. Am. Chem. Soc.* **1988**, *110*, 5591-5592.

(71) Ariel, S.; Ramamurthy, V.; Scheffer, J. R.; Trotter, J. *J. Am. Chem. Soc.* **1983**, *105*, 6959-6960.

(72) Hurrell, L.; Johnston, L. J.; Mathivanan, N.; Vong, D. *Can. J. Chem.* **1993**, *71*, 1340-1348.

(73) Scaiano, J. C.; Berinstain, A. B.; Whittlesey, M. K.; Malenfant, P. R. L.; Bensimon, C. *Chem. Mater.* **1993**, *5*, 700-704.

(74) Netto-Ferreira, J. C.; Scaiano, J. C. *Tett. Lett.* **1989**, *30*, 443-446.

(75) PCMODEL. Molecular Modeling Software, Serena Software, Bloominton, IN. 1990.

(76) Howell, J. O.; Goncalves, J. M.; Amatore, C.; Klasinc, L.; Wrightman, R. M.; Kochi, J. K. *J. Am. Chem. Soc.* **1984**, *106*, 3968-3976.

(77) Encina, M. V.; Lissi, E. A.; Lemp, E.; Zanocco, A.; Scaiano, J. C. *J. Am. Chem. Soc.* **1983**, *105*, 1856-1860.

(78) Scaiano, J. C.; Casal, H. L.; Netto-Ferreira, J. C. *ACS Symp. Ser.* **1985**, *278*, 211-222.

(79) Casal, H. L.; Netto-Ferreira, J. C.; Scaiano, J. C. *J. Inclusion Phenom.* **1985**, *3*, 395-401.

(80) Netto-Ferreira, J. C.; Scaiano, J. C. *J. Photochem. Photobiol. A: Chem.* **1988**, *45*, 109-116.

(81) Scaiano, J. C.; Netto-Ferreira, J. C. *J. Photochem.* **1986**, *32*, 253-259.

(82) Netto-Ferreira, J. C.; Avellar, I. G. J.; Scaiano, J. C. *J. Org. Chem.* **1990**, *55*, 89-92.

(83) Zhou, B.; Wagner, P. J. *J. Am. Chem. Soc.* **1989**, *111*, 6796-6799.

(84) Leigh, W. J.; Banisch, J. H.; Workentin, M. S. *J. Chem. Soc., Chem. Commun.* **1993**, 988-990.

(85) Visser, J. W. *J. Appl. Crystallogr.* **1969**, *2*, 89-95.

(86) Evans, S. V.; Omkaram, N.; Scheffer, J. R.; Trotter, J. *Tet. Lett.* **1986**, *27*, 1419-1422.

(87) Vogel, A. *Textbook of Pratical Organic Chemistry Including Qualitative Organic Analysis;* 4 ed.; Longman Group Limited: Essex, 1978.

(88) Whitmore, F. C.; Weisberger, C. A.; Sttabica, A. C. *J. Am. Chem. Soc.* **1943**, *65*, 1469.

(89) Pratt, E. F.; Evans, A. P. *J. Am. Chem. Soc.* **1956**, *78*, 4950-4952.

(90) Wissner, A.; Grudzinskas, C. V. *J. Org. Chem.* **1978**, *43*, 3972-3974.

(91) Corey, E. J.; Venkateswarlu, A. *J. Am. Chem. Soc.* **1972**, 6190-6191.

(92) Leigh, W. J. *Can. J. Chem.* **1986**, *64*, 1130-1139.

(93) Workentin, M. S.; Leigh, W. J. *J. Phys. Chem.* **1992**, *96*, 9666-9673.

(94) Hemminga, M. A.; De Jager, P. A. *J. Mag. Res.* **1983**, *51*, 339-344.

(95) Alemany, L. B.; Grant, D. M.; Alger, T. D.; Pugmire, R. J. *J. Am. Chem. Soc.* **1983**, *105*, 6697-6704.

(96) Saenger, W. In *Inclusion Compounds*; J. L. Atwood, J. E. D. Davies and D. D. MacNicol, Eds.; Academic Press Inc.: London, 1984; Vol. 2; pp 231-255.

(97) Tabushi, I. *Acc. Chem. Res.* **1982**, *15*, 66-72.

(98) Tabushi, I.; Kuroda, Y. *Adv. Catal.* **1983**, *32*, 417-466.

(99) Bender, M. L.; Komiyama, M. *Cyclodextrin Chemistry*; Springer-Verlag: New York, 1977.

(100) Saenger, W. *Angew. Chem. Int. Ed. Engl.* **1980**, *19*, 344-362.

(101) Sirlin, C. *Bull. Soc. Chim. Fr., Part II* **1984**, *1-2*, 5.

(102) Leigh, W. J. *J. Am. Chem. Soc.* **1985**, *107*, 6114-6116.

(103) Leigh, W. J.; Workentin, M. S.; Andrew, D. *J. Photochem. Photobiol. A: Chem.* **1991**, *57*, 97-109.

(104) Kano, K.; Tatemoto, S.; Hashimoto, S. *J. Phys. Chem.* **1991**, *95*, 966-970.

(105) Iu, K. K.; Thomas, J. K. *J. Phys. Chem.* **1991**, *95*, 506-509.

(106) Piciulo, P. L.; Thomas, J. K. *J. Chem. Phys.* **1978**, *68*, 3260-3264.

(107) Hirata, Y.; Mataga, N. *J. Phys. Chem.* **1985**, *89*, 2439-2442.

(108) Richards, J. T.; West, G.; Thomas, J. K. *J. Phys. Chem.* **1970**, *74*, 4137-4141.

(109) Hashimoto, S.; Thomas, J. K. *J. Photochem. Photobiol. A: Chem.* **1991**, *55*, 377-386.

(110) Evans, C.; Weir, D.; Scaiano, J. C.; Mac Eachern, A.; Arnason, J. T.; Morand, P.; Hollebone, B.; Leitch, L. C.; Philogene, B. J. R. *Photochem. Photobiol.* **1986**, *44*, 441-451.

(111) Scaiano, J. C.; Redmond, R. W.; Mehta, B.; Arnason, J. T. *Photochem. Photobiol.* **1990**, *52*, 655-659.

(112) Hug, G. L. *Optical Spectra of Nonmetallic Inorganic Transient Species in Aqueous Solution*; National Bureau of Standards: Washington, 1981; Vol. NSRDS-NBS 69.

(113) Elisei, F.; Favaro, G.; Görner, H. *J. Photochem. Photobiol. A: Chem.* **1991**, *59*, 243-253.

(114) Ishiwata, N.; Murai, H.; Kuwata, K. *J. Phys. Chem.* **1993**, *97*, 7129-7131.

(115) Berinstain, A. B.; Whittlesey, M. K.; Scaiano, J. C. In *Photochemistry of Lignocellulosic Materials*; C. Heitner and J. C. Scaiano, Eds.; American Chemical Society: Washington, 1993; Vol. 531; pp 111-121.

(116) Leigh, W. J.; Johnston, L. J. In *Handbook of Organic Photochemistry*; J. C. Scaiano, Ed.; CRC Press: Boca Raton, Florida, 1989; Vol. II; pp 401-422.

(117) Nair, P. P.; Kritchevsky, D. *The Bile Acids: Chemistry, Physiology and Metabolism*; Plenum Press: New York, 1971; Vol. 1.

(118) Ross, A. B.; Mallard, W. G.; Helman, W. P.; Bielski, B. H. J.; Buxton, G. V.; Cabelli, D. A.; Greenstock, C. L.; Huie, R. E.; Neta, P. *NRDL/NIST Solution Kinetics Database: Ver. 1;* 1.0 ed.; NIST, U.S. Department of Commerce: Gaithersburg, 1992.

(119) Scaiano, J. C.; Johnston, L. J.; McGimpsey, W. G.; Weir, D. *Acc. Chem. Res.* **1988**, *21*, 22-29.

(120) Wang, Z.; McGimpsey, W. G.; Ren, Y.; Weininger, S. J. *J. Am. Chem. Soc.* **1994**, *116*, 7925-7926.

(121) Baral-Tosh, S.; Chattopadhyay, S. K.; Das, P. K. *J. Phys. Chem.* **1984**, *88*, 1404-1408.

(122) Alkaitis, S. A.; Grätzel, M. *J. Am. Chem. Soc.* **1976**, *98*, 3549-3554.

(123) Scaiano, J. C.; Selwyn, J. C. *Photochem. Photobiol.* **1981**, *34*, 29-32.

(124) Scaiano, J. C.; Selwyn, J. C. *Can. J. Chem.* **1981**, *59*, 2368-2372.

(125) McGimpsey, W. G.; Scaiano, J. C. *J. Am. Chem. Soc.* **1987**, *109*, 2179-2181.

(126) Scaiano, J. C. *J. Phys. Chem.* **1981**, *85*, 2851-2855.

(127) Rahn, R.; Schroeder, J.; Troe, J.; Grellmann, K. H. *J. Phys. Chem.* **1989**, *93*, 7841-7846.

(128) Scaiano, J. C.; Whittlesey, M. K.; Berinstain, A. B.; Malenfant, P. R. L.; Schuler, R. H. *Chem. Mater.* **1994**, *6*, 836-843.

(129) Adler, E.; Lindgren, B. O.; Saedén, U. *Svensk Papperstidning* **1952**, *55*, 245-254.

(130) Weir, D.; Scaiano, J. C.; Arnason, J. T.; Evans, C. *Photochem. Photobiol.* **1985**, *42*, 223-230.

(131) Arnason, J. T.; Philogene, B. J. R.; Morand, P.; Imrie, K.; Iyengar, S.; Duval, F.; Soucy-Breau, C.; Scaiano, J. C.; Werstiuk, N. H.; Hasspieler, B.; Downe, A. E. R. In *Naturally Occurring and Synthetic Thiophenes as Photoactivated Insecticides*; J. T. Arnason, B. J. R. Philogene and P. Morand, Eds.; ACS Symposium Series 387: 1989; pp 165-172.

(132) Scaiano, J. C.; MacEachern, A.; Arnason, J. T.; Morand, P.; Weir, D. *Photochem. Photobiol.* **1987**, *46*, 193-199.

(133) Evans, C.; Scaiano, J. C. *J. Am. Chem. Soc.* **1990**, *112*, 2694-2701.

(134) Scaiano, J. C.; Wintgens, V.; Netto-Ferriera, J. C. *Photochem. Photobiol.* **1989**, *50*, 707-710.

(135) Scaiano, J. C.; Evans, C.; Arnason, J. T. *J. Photochem. Photobiol. B: Biol.* **1989**, *3*, 411-418.

(136) Devanathan, S.; Dahl, T. A.; Midden, W. R.; Neckers, D. C. *Proc. Natl. Acad. Sci. USA* **1990**, *87*, 2980-2984.

(137) Rakestraw, S. L.; Tompkins, R. G.; Yarmush, M. L. *Proc. Natl. Acad. Sci. USA* **1990**, *87*, 4217-4221.

(138) Vilaseca, L. A.; Rose, K.; Werlen, R.; Meunier, A.; Offord, R. E.; Nichols, C. L.; Scott, W. L. *Bioconj. Chem.* **1993**, *4*, 515-520.

(139) Morgan, J.; Lottman, H.; Abbou, C. C.; Chopin, D. K. *Photochem. Photobiol.* **1994**, *60*, 486-496.

(140) Rakestraw, S. L.; Ford, W. E.; Tompkins, R. G.; Rodgers, M. A. J.; Thorpe, W. P.; Yarmush, M. L. *Biotechnol. Prog.* **1992**, *8*, 30-39.

(141) Erlanger, B. F. *Methods in Enzymology* **1980**, *70*, 85-107.

(142) Kagan, J.; Arora, S. K.; Ustunol, A. *J. Org. Chem.* **1983**, *48*, 4076-4078.

(143) Abuin, E. B.; Lissi, E. A. *Prog. Reaction Kinetics* **1991**, *16*, 1-33.

(144) Gorman, A. A.; Rodgers, M. A. J. In *Handbook of Organic Photochemistry*; J. C. Scaiano, Ed.; CRC Press: Boca Raton, Florida, 1989; Vol. II; pp 229-247.

(145) Rodgers, M. A. J. *J. Am. Chem. Soc.* **1983**, *105*, 6201-6205.

(146) Michaeli, A.; Feitelson, J. *Photochem. Photobiol.* **1995**, *61*, 255-260.

(147) Houba-Herin, N.; Calberg-Bacq, C. M.; Piette, J.; Van De Vorst, A. *Photochem. Photobiol.* **1982**, *36*, 297-306.

Supplementary X-ray data for ketones I, IIS and VI.

```
   Space Group and Cell Dimensions     Orthorhombic  P cab
a  10.3193(72)    b  31.0812(90)    c   8.0179(71)
        Volume  2571.63(72)A**3

Empirical formula : O2 C16 H16

Cell dimensions were obtained from  24 reflections with 2Theta angle
in the range  40.00 -  50.00 degrees.

Crystal dimensions :  0.20  X  0.20  X  0.20  mm

FW =    240.30     Z =    8     F(000) =    1024.38

Dcalc  1.241Mg.m-3, mu   0.08mm-1, lambda 0.70930A, 2Theta(max)  49.9

The intensity data were collected on a Rigaku   diffractometer,
using the theta/2theta scan mode.
The h,k,l ranges used during structure solution and refinement are :--
Hmin,max    0  12;  Kmin,max    0  36;  Lmin,max   0   9
No. of reflections measured                    2262
No. of unique reflections                      2262
No. of reflections with Inet > 2.5sigma(Inet)  1178
Merging R-value on intensities  0.000
No correction was made for absorption


The last least squares cycle was calculated with
 34 atoms, 140 parameters and 1178 out of 2262 reflections.
Weights based on counting-statistics were used.
The weight modifier K in KFo**2 is 0.000300

The residuals are as follows :--
For significant reflections,  RF 0.154, Rw 0.201 GoF  8.57
For all reflections,          RF 0.173, Rw 0.201.
where RF = Sum(Fo-Fc)/Sum(Fo),
      Rw = Sqrt[Sum(w(Fo-Fc)**2)/Sum(wFo**2)] and
     GoF = Sqrt[Sum(w(Fo-Fc)**2)/(No. of reflns - No. of params.)]
The maximum shift/sigma ratio was  0.087.

In the last D-map, the deepest hole was  -0.780e/A**3,
and the highest peak   0.820e/A**3.

Secondary ext. coeff.   14.153257      sigma    1.915764
```

The following references are relevant to the NRCVAX System.

1. Full System Reference :
   Gabe, E.J., Le Page, Y., Charland,.J.-P., Lee, F.L. and White, P.S.
   (1989) J. Appl. Cryst., 22, 384-387.

2. Scattering Factors from Int. Tab. Vol. 4 :
   International Tables for X-ray Crystallography, Vol. IV, (1974)

Kynoch Press, Birmingham, England.

The following references may also be relevant.

3. ORTEP Plotting :
Johnson, C.K., (1976) ORTEP - A Fortran Thermal Ellipsoid Plot Program, Technical Report ORNL-5138, Oak Ridge

4. Pluto Plotting :
S. Motherwell, University Chemical Laboratory, Cambridge, 1978

5. Missing Symmetry Treatment by MISSYM :
Le Page, Y., (1988) J. Appl. Cryst., 21, 983-984.

7. Extinction Treatment :
Larson, A.C., (1970) p.293, Crystallographic Computing, Munksgaard, Copenhagen.

Table of Atomic Parameters x,y,z and Biso.
E.S.Ds. refer to the last digit printed.

	x	y	z	Biso
O2	0.9041(20)	0.3865(5)	0.187(3)	4.5(9)
O1	0.7668(22)	0.5805(5)	0.023(3)	5.3(10)
C2	0.935 (3)	0.5977(8)	0.211(3)	3.8(11)
C1	0.848 (3)	0.5665(7)	0.111(4)	4.4(12)
C3	0.908 (3)	0.6449(8)	0.178(4)	4.6(13)
C16	1.000 (4)	0.3684(8)	0.288(4)	5.1(14)
H2A	1.039	0.592	0.170	3.2
H2B	0.932	0.592	0.342	3.2
H3A	0.807	0.652	0.208	3.5
H3B	0.922	0.653	0.045	3.5
H5	0.812	0.704	0.380	3.9
H6	0.936	0.755	0.571	2.4
H7	1.171	0.752	0.576	1.9
H8	1.303	0.703	0.389	3.4
H9	1.168	0.649	0.199	2.7
H11	0.698	0.505	-0.021	3.1
H12	0.731	0.423	0.019	2.7
H14	1.059	0.444	0.347	3.2
H15	1.043	0.526	0.296	2.9
H16C	1.002	0.334	0.292	3.7
H16A	1.100	0.379	0.246	3.7
H16B	0.995	0.380	0.419	3.7
C4	0.983 (3)	0.6746(7)	0.282(3)	3.4(10)
C5	0.920 (3)	0.7038(8)	0.385(4)	4.3(12)
C6	0.988 (3)	0.7317(7)	0.490(3)	3.8(11)
C7	1.121 (3)	0.7303(7)	0.489(3)	3.7(11)
C8	1.190 (3)	0.7023(9)	0.388(4)	5.1(14)
C9	1.118 (3)	0.6734(7)	0.284(3)	3.7(11)
C10	0.868 (3)	0.5191(6)	0.142(4)	3.8(11)
C11	0.784 (3)	0.4915(8)	0.058(4)	4.5(13)
C12	0.798 (3)	0.4472(7)	0.082(4)	4.6(13)
C13	0.8965(23)	0.4308(6)	0.178(3)	3.2(9)
C14	0.982 (3)	0.4576(7)	0.262(4)	4.0(12)
C15	0.967 (3)	0.5036(7)	0.242(4)	3.7(11)

Biso is the Mean of the Principal Axes of the Thermal Ellipsoid

Table of u(i,j) or U values *100.
E.S.Ds. refer to the last digit printed

	u11(U)	u22	u33	u12	u13	u23
O2	7.7(13)	1.6(7)	7.8(13)	-0.6(8)	-0.5(11)	0.3(8)
O1	8.0(14)	2.7(8)	9.6(16)	0.5(9)	-3.8(13)	0.7(10)
C2	7.7(18)	3.4(12)	3.4(13)	-0.2(12)	-1.5(13)	-0.7(10)
C1	6.8(18)	1.7(10)	8.3(20)	-0.3(11)	-2.0(17)	1.3(12)
C3	8.5(21)	2.8(12)	6.3(18)	2.0(13)	0.7(17)	1.0(12)
C16	10.4(25)	2.9(12)	6.0(18)	0.4(15)	-2.4(18)	1.1(12)
C4	7.1(17)	1.9(10)	3.7(13)	-0.6(11)	0.9(12)	0.0(9)
C5	5.7(16)	3.0(12)	7.6(19)	2.3(12)	0.0(15)	2.6(13)
C6	8.4(19)	1.8(10)	4.2(13)	-0.1(12)	-0.7(14)	-0.8(10)
C7	8.0(19)	1.9(10)	4.1(13)	-0.7(11)	0.6(13)	-0.1(10)
C8	7.3(20)	4.3(15)	7.7(21)	-1.2(14)	-0.2(18)	1.0(15)
C9	6.5(16)	2.0(10)	5.8(16)	0.1(11)	0.8(14)	-0.4(11)
C10	7.1(18)	1.3(9)	6.2(16)	-1.4(11)	-0.7(15)	-0.7(10)
C11	6.1(18)	3.4(13)	7.8(20)	-1.0(12)	-1.6(16)	2.1(13)
C12	7.3(19)	1.7(10)	8.3(20)	-0.2(11)	-2.1(17)	1.5(12)
C13	4.6(13)	1.1(9)	6.2(15)	-1.1(9)	-0.7(12)	1.6(10)
C14	5.8(16)	1.9(10)	7.6(19)	0.4(11)	-1.3(15)	0.6(12)
C15	7.1(18)	1.1(9)	5.8(15)	0.8(10)	-1.4(14)	1.2(10)

Anisotropic Temperature Factors are of the form
Temp=-2*Pi*Pi*(h*h*u11*astar*astar+---+2*h*k*u12*astar*bstar+---)

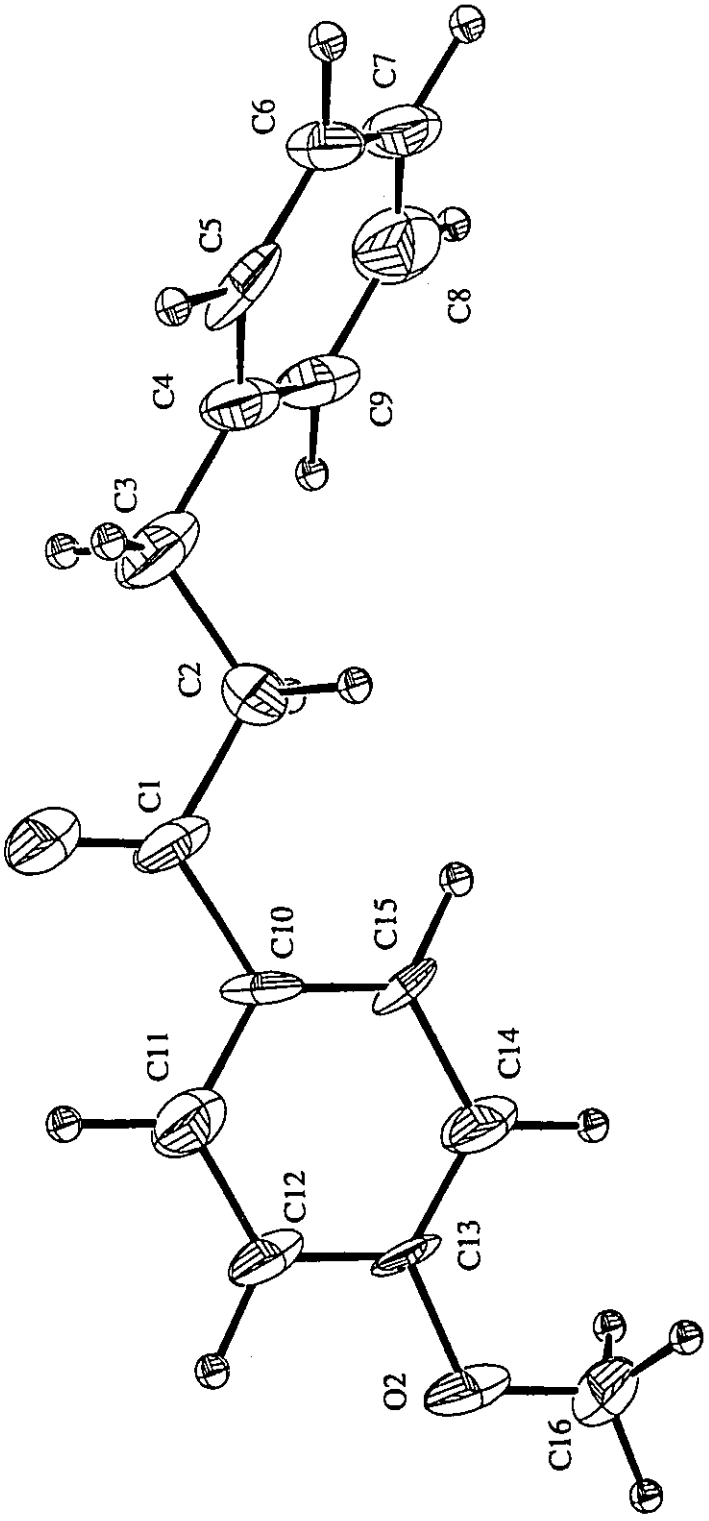
C6
C7
C5
C8
C4
C9
C3
C2
C1
C10
C15
C11
C14
C12
C13
O2
C16

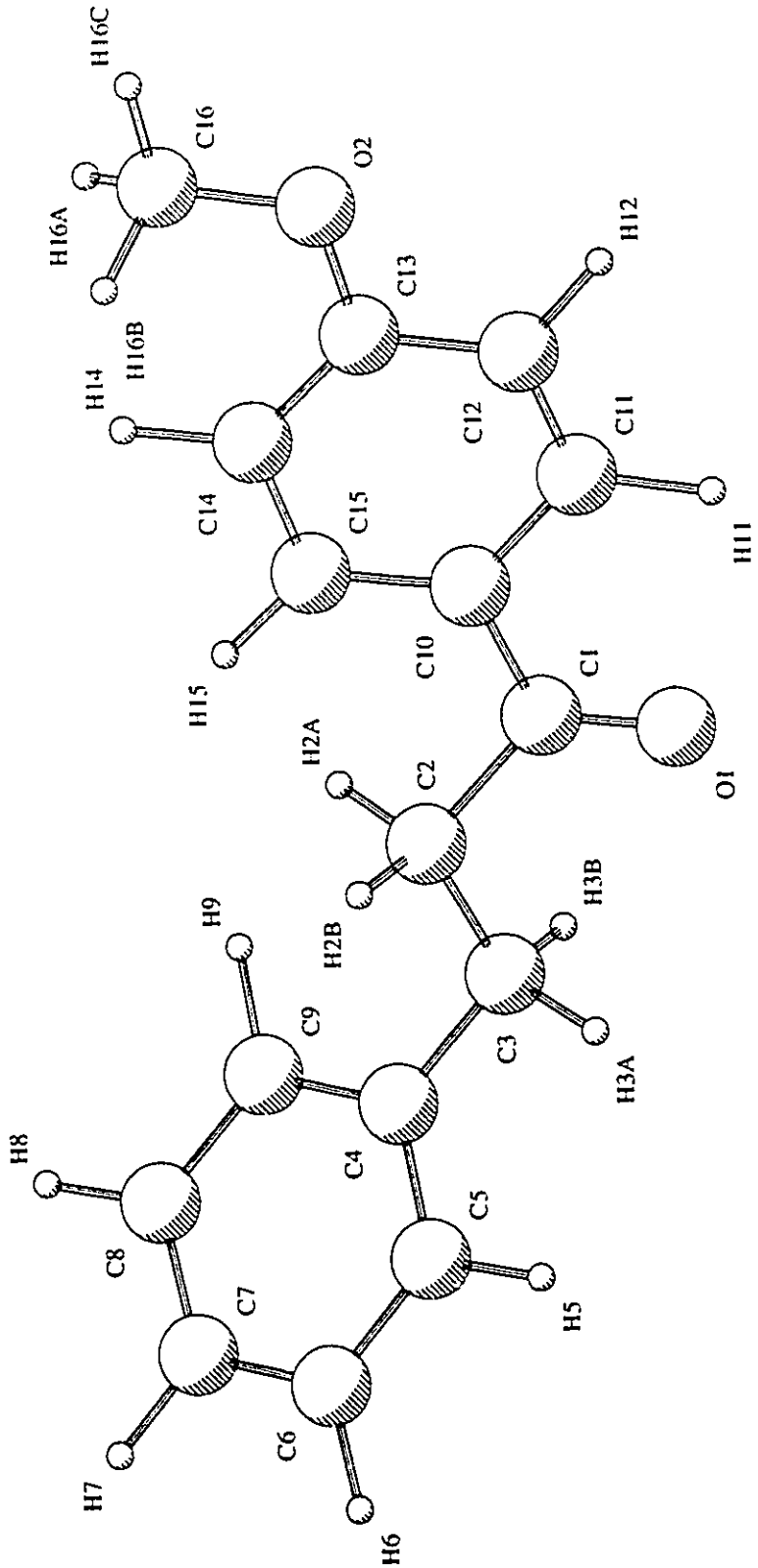
H16C
C16
H16A
O2
H16B
C13
H12
H14
C12
C11
C14
C15
H11
H15
C10
C1
H2A
C2
O1
H2B
H3B
H9
C9
C3
H3A
H8
C4
C5
C8
C7
H5
C6
H7
H6

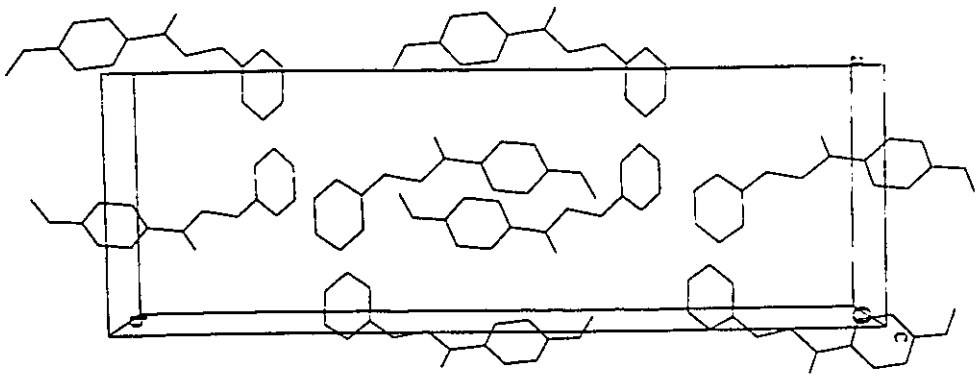

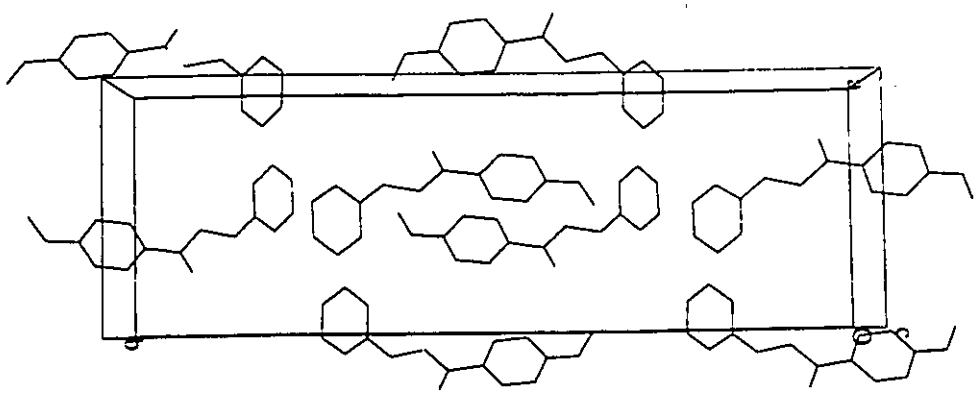

Table of Atomic Bond Distances in Angstroms

O2-C16	1.39(4)	H9-C9	1.136(24)
O2-C13	1.380(24)	H11-C11	1.17(3)
O1-C1	1.18(3)	H12-C12	1.13(3)
C2-C1	1.55(4)	H14-C14	1.13(3)
C2-C3	1.52(3)	H15-C15	1.14(3)
C2-H2A	1.13(3)	C4-C5	1.39(4)
C2-H2B	1.066(25)	C4-C9	1.39(4)
C1-C10	1.51(3)	C5-C6	1.39(4)
C3-H3A	1.09(3)	C6-C7	1.38(4)
C3-H3B	1.10(3)	C7-C8	1.39(4)
C3-C4	1.47(4)	C8-C9	1.43(4)
C16-H16C	1.077(25)	C10-C11	1.39(4)
C16-H16A	1.14(4)	C10-C15	1.38(4)
C16-H16B	1.11(3)	C11-C12	1.40(3)
H5-C5	1.12(3)	C12-C13	1.38(4)
H6-C6	1.11(3)	C13-C14	1.39(3)
H7-C7	1.090(25)	C14-C15	1.45(3)
H8-C8	1.17(3)		

Table of Atomic Bond Angles in Degrees

C16-O2-C13	118.2(20)	H6-C6-C7	120.5(22)
C1-C2-C3	113.8(22)	C5-C6-C7	118.6(23)
C1-C2-H2A	107.5(21)	H7-C7-C6	116.7(23)
C1-C2-H2B	112.6(23)	H7-C7-C8	121(3)
C3-C2-H2A	106.2(23)	C6-C7-C8	122.0(24)
C3-C2-H2B	109.7(21)	H8-C8-C7	119(3)
H2A-C2-H2B	106.6(22)	H8-C8-C9	122(3)
O1-C1-C2	119.7(20)	C7-C8-C9	118(3)
O1-C1-C10	123.9(24)	H9-C9-C4	117.5(23)
C2-C1-C10	116.2(22)	H9-C9-C8	121(3)
C2-C3-H3A	109.4(25)	C4-C9-C8	120.5(24)
C2-C3-H3B	111.8(23)	C1-C10-C11	115.6(24)
C2-C3-C4	114.0(24)	C1-C10-C15	122.6(21)
H3A-C3-H3B	107(3)	C11-C10-C15	121.7(21)
H3A-C3-C4	104.7(23)	H11-C11-C10	120.8(22)
H3B-C3-C4	109.3(24)	H11-C11-C12	120.5(24)
O2-C16-H16C	115(3)	C10-C11-C12	118(3)
O2-C16-H16A	111.1(23)	H12-C12-C11	121.5(25)
O2-C16-H16B	112(3)	H12-C12-C13	117.4(19)
H16C-C16-H16A	105(3)	C11-C12-C13	121.1(24)
H16C-C16-H16B	107.4(23)	O2-C13-C12	116.1(20)
H16A-C16-H16B	103(3)	O2-C13-C14	122.5(21)
C3-C4-C5	120(3)	C12-C13-C14	121.3(19)
C3-C4-C9	121.4(22)	H14-C14-C13	120.9(19)
C5-C4-C9	118.6(23)	H14-C14-C15	120.9(23)
H5-C5-C4	116(3)	C13-C14-C15	118.1(23)
H5-C5-C6	121(3)	H15-C15-C10	121.0(18)
C4-C5-C6	122(3)	H15-C15-C14	119.4(22)
H6-C6-C5	120(3)	C10-C15-C14	119.2(23)

Torsion angles

C13	O2	C16	H16C	179.7(35)	C13	O2	C16	H16A	-59.9(19)
C13	O2	C16	H16B	55.5(19)	C16	O2	C13	C12	-177.9(30)
C16	O2	C13	C14	1.5(17)	C3	C2	C1	O1	-2.1(16)
C3	C2	C1	C10	-178.4(32)	H2A	C2	C1	O1	-119.4(34)
H2A	C2	C1	C10	64.3(21)	H2B	C2	C1	O1	123.6(36)
H2B	C2	C1	C10	-52.7(19)	C1	C2	C3	H3A	58.7(21)
C1	C2	C3	H3B	-59.7(21)	C1	C2	C3	C4	175.6(33)
H2A	C2	C3	H3A	176.7(40)	H2A	C2	C3	H3B	58.3(20)
H2A	C2	C3	C4	-66.4(22)	H2B	C2	C3	H3A	-68.5(23)
H2B	C2	C3	H3B	173.1(41)	H2B	C2	C3	C4	48.4(18)
O1	C1	C10	C11	0.4(16)	O1	C1	C10	C15	177.9(37)
C2	C1	C10	C11	176.5(33)	C2	C1	C10	C15	-5.9(15)
C2	C3	C4	C5	-121.4(30)	C2	C3	C4	C9	56.9(20)
H3A	C3	C4	C5	-1.8(12)	H3A	C3	C4	C9	176.5(37)
H3B	C3	C4	C5	112.6(32)	H3B	C3	C4	C9	-69.1(23)
C3	C4	C5	H5	-1.6(12)	C3	C4	C5	C6	177.9(33)
C9	C4	C5	H5	-180.0(36)	C9	C4	C5	C6	-0.5(15)
C3	C4	C9	H9	1.6(12)	C3	C4	C9	C8	-179.2(33)
C5	C4	C9	H9	179.9(34)	C5	C4	C9	C8	-0.9(17)
H5	C5	C6	H6	-1.0(0)	H5	C5	C6	C7	-179.6(37)
C4	C5	C6	H6	179.5(36)	C4	C5	C6	C7	0.9(15)
H6	C6	C7	H7	3.5(1)	H6	C6	C7	C8	-178.6(36)
C5	C6	C7	H7	-177.9(36)	C5	C6	C7	C8	0.0(17)
H7	C7	C8	H8	-4.1(2)	H7	C7	C8	C9	176.5(39)
C6	C7	C8	H8	178.1(38)	C6	C7	C8	C9	-1.3(15)
H8	C8	C9	H9	1.5(1)	H8	C8	C9	C4	-177.6(38)
C7	C8	C9	H9	-179.1(39)	C7	C8	C9	C4	1.8(14)
C1	C10	C11	H11	-5.4(12)	C1	C10	C11	C12	180.0(34)
C15	C10	C11	H11	177.0(37)	C15	C10	C11	C12	2.4(16)
C1	C10	C15	H15	-5.5(12)	C1	C10	C15	C14	-178.4(32)
C11	C10	C15	H15	171.9(35)	C11	C10	C15	C14	-0.9(16)
H11	C11	C12	H12	4.0(2)	H11	C11	C12	C13	-178.2(38)
C10	C11	C12	H12	178.6(38)	C10	C11	C12	C13	-3.6(14)
H12	C12	C13	O2	0.6(9)	H12	C12	C13	C14	-178.8(35)
C11	C12	C13	O2	-177.3(33)	C11	C12	C13	C14	3.3(16)
O2	C13	C14	H14	-2.6(9)	O2	C13	C14	C15	178.9(31)
C12	C13	C14	H14	176.8(35)	C12	C13	C14	C15	-1.7(16)
H14	C14	C15	H15	9.1(3)	H14	C14	C15	C10	-177.9(36)
C13	C14	C15	H15	-172.4(35)	C13	C14	C15	C10	0.6(14)

Columns are 10Fo 10Fc 10Sig, * for Insignificant

l	kFo	Fc	Sig	l	kFo	Fc	Sig	l	kFo	Fc	Sig	l	kFo	Fc	Sig
	0, 0, 1			4	596	509	4	4	302	329	6		0, 29, 1		
2	1010	1113	2	6	180	122	8	6	169	131	8	2	9	82	262*
4	615	621	4	8	44	64	39*	8	52	22	35*	4	192	141	9
6	91	98	6		0, 10, 1				0, 19, 1				0, 30, 1		
8	119	64	7	0	453	455	3	2	186	189	7	0	243	276	8
	0, 1, 1			2	178	111	5	4	443	425	5	2	9	101	181*
2	677	628	2	4	133	169	5	6	621	571	6	4	116	135	8
4	6	14	123*	6	30	69	23*	8	10	70	187*		0, 31, 1		
6	12	30	85*	8	9	38	166*		0, 20, 1			2	170	230	7
8	49	11	31*		0, 11, 1			0	74	143	7	4	10	7	176*
	0, 2, 1			2	677	627	3	2	145	185	6		0, 32, 1		
2	654	682	2	4	294	262	5	4	283	300	7	0	453	578	7
4	6	50	124*	6	189	149	8	6	302	315	10	2	9	87	211*
6	239	174	6	8	9	6	163*	8	82	49	11	4	51	55	16*
8	97	94	8		0, 12, 1				0, 21, 1				0, 33, 1		
	0, 3, 1			0	440	472	3	2	256	266	6	2	208	225	10
2	764	734	2	2	283	239	4	4	154	137	7	4	85	68	11
4	103	110	4	4	667	575	4	6	28	11	64*		0, 34, 1		
6	62	62	9	6	139	70	6		0, 22, 1			0	208	257	8
8	88	53	9	8	9	16	166*	0	42	57	23*	2	10	30	221*
	0, 4, 1				0, 13, 1			2	43	29	29*		0, 35, 1		
0	176	152	2	2	265	282	4	4	782	724	5	2	37	105	50*
2	1594	1611	2	4	297	298	5	6	159	105	8		0, 36, 1		
4	6	8	121*	6	307	260	7		0, 23, 1			0	147	155	7
6	276	137	6	8	88	48	9	2	222	247	7	2	59	61	33*
8	346	256	7		0, 14, 1			4	489	454	7		1, 1, 1		
	0, 5, 1			0	614	647	3	6	124	81	7	1	3	591	546*
2	226	163	4	2	759	725	4		0, 24, 1			2	1499	1560	3
4	140	66	6	4	300	225	5	0	8	27	136*	3	547	468	3
6	131	108	5	6	110	70	7	2	179	210	9	4	98	57	5
8	148	101	6	8	47	44	37*	4	204	120	8	5	57	59	7
	0, 6, 1				0, 15, 1			6	312	337	8	6	189	140	7
0	195	239	3	2	526	520	4		0, 25, 1			7	59	28	11
2	1449	1459	2	4	381	398	5	2	109	132	7	8	9	1	164*
4	101	57	4	6	153	145	6	4	267	241	8	9	118	59	8
6	454	320	5	8	10	22	172*	6	116	94	9		1, 2, 1		
8	33	18	24*		0, 16, 1				0, 26, 1			0	28	36	4
	0, 7, 1			0	506	543	4	0	89	137	7	1	213	312	4
2	391	422	3	2	100	212	6	2	322	303	6	2	370	354	3
4	187	79	6	4	90	120	6	4	273	252	8	3	234	148	4
6	260	199	6	6	195	154	9	6	182	215	8	4	65	78	6
8	269	235	8	8	75	44	12		0, 27, 1			5	29	4	31*
	0, 8, 1				0, 17, 1			2	129	196	7	6	118	23	6
0	145	123	4	2	195	245	6	4	181	149	8	7	95	43	7
2	135	119	5	4	57	59	10	6	58	97	16*	8	158	49	8
4	463	430	4	6	42	47	36*		0, 28, 1			9	10	1	204*
6	218	167	7	8	10	1	173*	0	8	83	158*		1, 3, 1		
8	63	27	13*		0, 18, 1			2	447	548	6	1	697	795	3
	0, 9, 1			0	284	410	5	4	94	49	9	2	218	242	4
2	1007	903	3	2	267	274	5	6	55	114	17*	3	137	131	5

Columns are 10Fo 10Fc 10Sig, * for Insignificant

l	kFo	Fc	Sig	l	kFo	Fc	Sig	l	kFo	Fc	Sig	l	kFo	Fc	Sig
	1, 3, 1			0	135	101	5	8	31	35	50*	1	7	72	239*
4	435	332	4	1	673	71	3		1, 13, 1			2	7	96	172*
5	34	38	24*	2	298	238	3	1	755	48	4	3	118	93	6
6	62	90	9	3	109	179	4	2	169	194	6	4	165	214	8
7	80	62	8	4	301	206	5	3	492	478	4	5	247	203	8
8	38	31	40*	5	287	188	5	4	168	162	7	6	112	74	7
9	233	135	10	6	182	142	8	5	176	159	7	7	170	107	8
	1, 4, 1			7	150	72	6	6	76	91	9	8	164	82	7
0	630	619	2	8	46	29	16*	7	124	121	6		1, 19, 1		
1	1204	1261	2	9	10	28	187*	8	86	65	10	1	186	192	7
2	280	306	3		1, 9, 1				1, 14, 1			2	7	67	147*
3	239	222	4	1	692	541	3	0	505	547	4	3	37	30	27*
4	155	114	6	2	137	113	6	1	906	982	4	4	8	30	164*
5	164	108	6	3	635	685	4	2	6	59	149*	5	377	388	6
6	81	30	7	4	99	58	5	3	416	449	5	6	37	24	41*
7	8	26	155*	5	327	229	5	4	132	122	6	7	191	132	8
8	238	103	9	6	108	57	6	5	163	179	6	8	24	92	84*
9	10	0	193*	7	335	255	7	6	38	10	35*		1, 20, 1		
	1, 5, 1			8	74	42	11	7	138	102	7	0	294	331	5
1	993	985	2	9	10	26	185*	8	10	20	175*	1	7	27	258*
2	5	13	125*		1, 10, 1				1, 15, 1			2	12	8	84*
3	494	436	3	0	441	476	3	1	674	339	7	3	62	45	9
4	257	176	5	1	997	711	3	2	349	320	4	4	133	114	6
5	401	385	5	2	725	665	3	3	228	217	6	5	60	87	14*
6	106	101	5	3	599	555	4	4	176	152	7	6	10	27	149*
7	76	65	9	4	275	209	5	5	248	265	7	7	299	210	8
8	32	8	50*	5	259	187	6	6	32	71	29*		1, 21, 1		
9	145	117	7	6	8	34	154*	7	52	65	14*	1	7	171	229*
	1, 6, 1			7	97	82	8	8	40	11	29*	2	7	130	199*
0	584	558	2	8	9	37	168*		1, 16, 1			3	72	73	8
1	4	552	601*	9	101	77	9	0	765	865	4	4	127	169	6
2	241	195	3		1, 11, 1			1	377	348	6	5	9	5	170*
3	303	253	4	1	973	442	3	2	6	56	204*	6	75	31	10
4	158	132	6	2	6	51	235*	3	254	195	6	7	172	215	7
5	154	47	5	3	277	303	5	4	115	92	5		1, 22, 1		
6	111	63	5	4	13	2	69*	5	253	220	7	0	199	186	7
7	24	37	54*	5	304	249	5	6	136	103	6	1	150	261	7
8	103	19	8	6	143	109	7	7	133	107	6	2	411	439	6
9	10	29	187*	7	9	67	158*	8	92	46	9	3	56	37	11*
	1, 7, 1			8	9	24	164*		1, 17, 1			4	107	88	7
1	354	591	9	9	134	87	7	1	178	131	8	5	49	58	15*
2	209	264	4		1, 12, 1			2	184	207	6	6	53	46	30*
3	179	193	5	0	158	84	5	3	207	212	7	7	57	59	31*
4	218	210	5	1	683	511	3	4	46	0	23*		1, 23, 1		
5	28	8	23*	2	75	69	5	5	354	359	6	1	8	165	351*
6	8	6	141*	3	348	344	4	6	90	65	8	2	8	221	413*
7	223	197	8	4	56	43	8	7	43	26	18*	3	474	480	6
8	34	13	47*	5	7	4	156*	8	85	48	11	4	109	146	7
9	10	12	191*	6	43	46	28*		1, 18, 1			5	204	213	6
	1, 8, 1			7	116	104	7	0	105	93	6	6	131	54	7

Columns are 10Fo 10Fc 10Sig, * for Insignificant

l	kFo	Fc	Sig
	1, 23, 1		
7	118	169	8
	1, 24, 1		
0	75	99	8
1	256	368	9
2	130	263	10
3	334	341	8
4	35	17	39*
5	19	3	57*
6	154	110	7
7	88	43	11
	1, 25, 1		
1	8	173	386*
2	8	98	287*
3	8	81	233*
4	84	94	9
5	118	76	7
6	46	14	37*
	1, 26, 1		
0	135	142	6
1	8	27	254*
2	26	77	57*
3	9	38	174*
4	139	154	6
5	9	38	173*
6	119	94	8
	1, 27, 1		
1	8	144	253*
2	8	10	174*
3	228	283	8
4	83	97	10
5	88	119	9
6	35	27	26*
	1, 28, 1		
0	46	72	14*
1	202	298	8
2	9	23	161*
3	9	45	208*
4	85	120	9
5	46	4	35*
6	84	41	11
	1, 29, 1		
1	9	38	338*
2	9	3	171*
3	28	78	55*
4	111	137	8
5	70	34	12
	1, 30, 1		
0	48	76	28*
1	65	89	12
2	106	134	7
3	9	45	173*
4	56	49	30*
5	40	57	29*
	1, 31, 1		
1	9	99	206*
2	9	104	193*
3	9	36	165*
4	39	32	41*
5	51	53	34*
	1, 32, 1		
0	81	75	9
1	101	136	9
2	9	83	187*
3	78	69	11
4	10	35	162*
	1, 33, 1		
1	9	94	227*
2	53	67	33*
3	10	59	182*
4	10	11	171*
	1, 34, 1		
0	10	56	170*
1	10	22	199*
2	46	49	19*
3	33	24	54*
	1, 35, 1		
1	41	152	36*
2	10	40	173*
	1, 36, 1		
0	133	160	7
1	156	272	8
2	10	45	186*
	2, 0, 1		
0	1132	1320	2
1	1236	1882	4
2	634	2061	12
3	5	231	334*
4	648	626	4
5	336	235	5
6	39	27	27*
7	94	63	7
8	115	34	7
9	61	48	31*
	2, 1, 1		
1	198	374	7
2	5	130	185*
3	80	211	7
4	37	34	22*
5	131	179	6
6	72	60	8
7	44	5	30*
8	83	46	9
9	106	66	9
	2, 2, 1		
0	596	683	3
1	561	1073	6
2	5	1292	1183*
3	84	73	5
4	35	82	24*
5	77	71	6
6	170	134	8
7	31	26	28*
8	93	18	8
9	50	33	27*
	2, 3, 1		
1	116	168	4
2	79	101	5
3	6	12	124*
4	82	92	5
5	313	208	5
6	164	144	6
7	67	31	10
8	139	83	6
9	148	50	7
	2, 4, 1		
0	450	490	3
1	236	295	4
2	269	403	5
3	165	199	7
4	333	307	5
5	158	102	8
6	38	21	20*
7	252	165	7
8	283	171	8
9	149	56	7
	2, 5, 1		
1	97	126	5
2	15	23	22*
3	233	273	5
4	36	16	23*
5	98	76	5
6	41	9	27*
7	169	117	7
8	135	88	7
9	171	69	7
	2, 6, 1		
0	484	466	3
1	485	469	3
2	275	306	4
3	226	219	5
4	295	265	5
5	54	18	8
6	135	132	6
7	49	10	27*
8	150	48	7
9	183	90	8
	2, 7, 1		
1	19	19	30*
2	44	157	22*
3	573	549	4
4	365	343	5
5	80	51	6
6	38	83	30*
7	9	5	158*
8	111	118	8
9	10	34	185*
	2, 8, 1		
0	965	941	3
1	372	335	3
2	165	193	7
3	337	334	6
4	112	113	5
5	30	13	16*
6	48	45	12*
7	113	60	6
8	45	52	34*
9	10	5	188*
	2, 9, 1		
1	221	216	4
2	329	263	4
3	292	350	7
4	7	1	123*
5	9	41	76*
6	209	130	8
7	174	118	7
8	9	20	168*
9	102	60	9
	2, 10, 1		
0	266	253	3
1	254	260	4
2	466	360	4
3	42	200	36*
4	129	119	5
5	79	39	7
6	95	64	7
7	32	2	44*
8	11	10	136*
9	10	33	183*
	2, 11, 1		

Columns are 10Fo 10Fc 10Sig, * for Insignificant

l	kFo	Fc	Sig	l	kFo	Fc	Sig	l	kFo	Fc	Sig	l	kFo	Fc	Sig
	2, 11, 1			2	300	274	5	6	122	85	7		2, 28, 1		
1	266	291	4	3	7	135	342*	7	87	22	10	0	151	194	7
2	443	209	4	4	81	114	8		2, 22, 1			1	122	149	6
3	6	9	270*	5	33	5	38*	0	397	397	5	2	204	234	10
4	55	60	8	6	9	8	157*	1	359	334	5	3	9	75	242*
5	31	54	25*	7	9	26	167*	2	277	270	7	4	49	2	29*
6	142	110	6	8	38	21	47*	3	54	126	27*	5	37	19	45*
7	9	36	163*		2, 17, 1			4	229	305	10	6	141	122	7
8	9	27	177*	1	162	93	6	5	215	176	9		2, 29, 1		
	2, 12, 1			2	273	56	6	6	107	41	8	1	136	148	6
0	322	324	4	3	7	111	214*	7	56	66	30*	2	9	46	271*
1	6	106	273*	4	8	11	155*		2, 23, 1			3	9	22	177*
2	441	367	4	5	211	197	8	1	357	128	6	4	119	106	7
3	27	13	15*	6	45	27	29*	2	270	253	9	5	55	35	32*
4	149	124	7	7	111	74	7	3	213	226	10		2, 30, 1		
5	51	34	11*	8	10	3	177*	4	8	17	248*	0	288	341	7
6	130	71	6		2, 18, 1			5	220	180	9	1	81	15	10
7	34	17	39*	0	303	389	5	6	146	70	7	2	9	39	165*
8	10	30	165*	1	147	86	7	7	10	46	185*	3	20	35	77*
	2, 13, 1			2	63	20	7		2, 24, 1			4	199	222	8
1	6	157	292*	3	7	16	187*	0	8	6	176*	5	53	9	33*
2	447	235	4	4	280	273	6	1	313	311	6		2, 31, 1		
3	232	224	5	5	119	123	6	2	403	445	7	1	32	21	44*
4	106	84	5	6	77	64	10	3	8	2	311*	2	33	12	25*
5	98	93	6	7	9	30	174*	4	20	10	69*	3	9	74	179*
6	91	92	7	8	137	76	7	5	190	144	8	4	10	4	241*
7	54	58	13*		2, 19, 1			6	252	174	9		2, 32, 1		
8	52	58	32*	1	166	42	7	7	73	54	13	0	23	24	64*
	2, 14, 1			2	230	210	6		2, 25, 1			1	37	22	22*
0	647	672	4	3	218	179	6	1	293	162	7	2	43	52	35*
1	410	328	5	4	268	295	8	2	115	202	15	3	48	71	36*
2	264	128	5	5	212	216	9	3	209	264	8	4	10	11	179*
3	7	95	306*	6	68	83	11	4	35	37	41*		2, 33, 1		
4	223	160	6	7	118	117	8	5	214	164	9	1	47	29	33*
5	8	31	163*	8	98	93	10	6	128	51	8	2	63	81	13*
6	20	16	67*		2, 20, 1				2, 26, 1			3	10	8	182*
7	20	5	72*	0	73	84	7	0	32	16	35*		2, 34, 1		
8	46	32	35*	1	228	211	6	1	167	128	7	0	94	96	9
	2, 15, 1			2	190	73	8	2	54	39	40*	1	35	31	47*
1	505	365	4	3	8	159	280*	3	9	221	294*	2	10	44	190*
2	145	68	7	4	8	102	225*	4	9	14	161*	3	43	6	23*
3	203	262	9	5	225	237	9	5	9	11	194*		2, 35, 1		
4	179	170	8	6	49	18	31*	6	54	27	33*	1	32	4	52*
5	105	123	6	7	43	9	40*		2, 27, 1			2	40	38	45*
6	74	66	9		2, 21, 1			1	96	63	8		2, 36, 1		
7	98	58	8	1	341	216	5	2	104	108	7	0	149	207	7
8	42	20	23*	2	168	146	8	3	9	209	278*	1	10	76	181*
	2, 16, 1			3	8	60	227*	4	9	8	161*		3, 1, 1		
0	99	77	4	4	214	205	8	5	51	74	32*	1	721	886	4
1	397	182	4	5	175	187	7	6	48	28	35*	2	179	307	8

Columns are 10Fo 10Fc 10Sig, * for Insignificant

l	kFo	Fc	Sig	l	kFo	Fc	Sig	l	kFo	Fc	Sig	l	kFo	Fc	Sig
	3, 1, 1				3, 6, 1			8	10	8	175*	1	7	249	309*
3	6	302	293*	0	394	387	3		3, 11, 1			2	353	288	5
4	6	702	840*	1	200	170	5	1	153	185	6	3	244	196	6
5	7	41	134*	2	154	177	7	2	41	103	11*	4	200	115	9
6	8	70	147*	3	34	61	23*	3	324	213	5	5	112	125	6
7	37	33	21*	4	358	406	7	4	159	169	7	6	9	9	159*
8	49	21	29*	5	122	121	5	5	89	81	7	7	9	4	171*
9	10	8	187*	6	77	77	9	6	8	2	113*	8	22	33	82*
	3, 2, 1			7	169	84	7	7	135	80	6		3, 17, 1		
0	23	52	23*	8	9	25	168*	8	169	123	7	1	103	267	12
1	293	389	5	9	118	39	9		3, 12, 1			2	355	217	5
2	5	37	127*		3, 7, 1			0	201	198	5	3	234	57	6
3	29	18	25*	1	31	62	19*	1	266	244	4	4	8	67	265*
4	6	239	369*	2	374	414	5	2	159	129	7	5	39	69	41*
5	37	22	27*	3	207	252	7	3	335	232	5	6	40	23	36*
6	202	154	8	4	36	26	13*	4	132	79	5	7	74	72	11
7	141	71	6	5	42	45	12*	5	77	97	9	8	42	14	30*
8	38	34	42*	6	79	68	8	6	20	31	65*		3, 18, 1		
9	89	29	10	7	9	50	116*	7	37	18	28*	0	494	498	4
	3, 3, 1			8	9	11	169*	8	52	58	35*	1	225	66	8
1	354	411	5	9	59	9	31*		3, 13, 1			2	247	108	5
2	39	92	9*		3, 8, 1			1	312	258	4	3	154	171	6
3	6	6	130*	0	523	504	3	2	6	104	253*	4	8	8	189*
4	7	94	151*	1	426	415	4	3	265	77	5	5	136	187	7
5	254	275	8	2	377	374	5	4	77	86	7	6	176	116	7
6	325	243	7	3	308	325	7	5	56	60	13*	7	56	6	29*
7	100	91	7	4	62	33	7	6	157	109	7		3, 19, 1		
8	9	13	168*	5	53	52	10	7	115	92	7	1	183	125	7
9	37	48	49*	6	250	195	8	8	10	6	187*	2	186	126	7
	3, 4, 1			7	28	45	48*		3, 14, 1			3	160	106	6
0	488	559	3	8	9	23	177*	0	75	118	5	4	122	131	6
1	25	59	23*	9	10	1	196*	1	238	258	6	5	9	167	247*
2	37	46	19*		3, 9, 1			2	456	443	4	6	131	151	7
3	15	135	76*	1	212	198	4	3	149	126	7	7	65	25	13
4	30	63	14*	2	37	26	21*	4	7	44	150*		3, 20, 1		
5	26	22	38*	3	59	170	34*	5	80	123	10	0	74	91	7
6	178	127	6	4	157	156	7	6	46	30	16*	1	211	199	6
7	134	69	7	5	82	32	7	7	9	41	174*	2	399	418	5
8	9	9	171*	6	128	83	6	8	94	72	10	3	230	238	7
9	128	51	8	7	100	89	8		3, 15, 1			4	8	19	208*
	3, 5, 1			8	70	10	12	1	6	90	236*	5	125	153	9
1	168	205	5		3, 10, 1			2	479	210	5	6	113	121	9
2	460	584	6	0	479	415	3	3	177	92	6	7	57	10	29*
3	69	67	7	1	356	325	4	4	149	107	6		3, 21, 1		
4	171	245	7	2	114	94	5	5	8	6	188*	1	184	81	7
5	7	36	135*	3	272	196	5	6	41	55	33*	2	414	236	5
6	40	36	30*	4	87	3	6	7	61	45	13*	3	260	215	7
7	9	10	115*	5	8	14	156*	8	44	59	42*	4	29	75	48*
8	91	101	9	6	8	18	168*		3, 16, 1			5	9	38	241*
9	89	22	11	7	9	17	165*	0	573	561	4	6	9	54	188*

Columns are 10Fo 10Fc 10Sig, * for Insignificant

l	kFo	Fc	Sig
	3, 21, 1		
7	43	22	42*
	3, 22, 1		
0	564	649	5
1	128	128	6
2	153	39	7
3	153	44	6
4	37	11	19*
5	194	149	9
6	37	44	41*
7	38	32	32*
	3, 23, 1		
1	130	83	6
2	216	272	8
3	63	65	10
4	106	93	7
5	9	33	233*
6	10	76	173*
7	102	79	10
	3, 24, 1		
0	395	451	6
1	129	85	6
2	226	89	8
3	167	149	7
4	9	68	216*
5	57	60	15*
6	97	54	9
	3, 25, 1		
1	153	120	6
2	224	249	8
3	182	159	8
4	9	18	191*
5	96	74	10
6	10	5	180*
	3, 26, 1		
0	141	196	7
1	118	27	6
2	201	41	10
3	158	153	7
4	56	91	13*
5	9	45	205*
6	90	35	10
	3, 27, 1		
1	67	52	10
2	218	230	9
3	9	15	200*
4	56	77	28*
5	10	26	172*
6	25	14	76*
	3, 28, 1		

l	kFo	Fc	Sig
0	241	242	8
1	82	102	8
2	201	49	10
3	118	125	7
4	9	16	174*
5	10	15	171*
	3, 29, 1		
1	88	57	8
2	33	43	45*
3	9	50	190*
4	25	81	65*
5	35	31	51*
	3, 30, 1		
0	38	93	28*
1	38	50	38*
2	91	99	8
3	9	23	162*
4	10	41	188*
5	10	1	177*
	3, 31, 1		
1	82	64	9
2	39	20	40*
3	49	11	32*
4	84	151	12
	3, 32, 1		
0	9	13	154*
1	101	84	8
2	10	17	164*
3	13	2	125*
4	10	63	225*
	3, 33, 1		
1	78	20	11
2	38	19	30*
3	40	45	42*
	3, 34, 1		
0	109	130	8
1	61	64	13*
2	32	35	52*
	3, 35, 1		
1	29	38	58*
2	10	65	177*
	4, 0, 1		
0	41	68	7
1	827	830	4
2	250	280	6
3	354	524	9
4	271	543	13
5	7	106	239*
6	8	216	369*
7	9	0	160*

l	kFo	Fc	Sig
8	43	31	26*
9	10	33	196*
	4, 1, 1		
1	353	418	5
2	108	168	5
3	42	87	24*
4	7	126	209*
5	7	98	176*
6	8	96	206*
7	84	77	9
8	9	2	162*
	4, 2, 1		
0	387	383	4
1	67	85	5
2	71	119	6
3	46	559	91*
4	7	315	467*
5	46	81	24*
6	8	137	240*
7	27	13	51*
8	20	17	53*
	4, 3, 1		
1	144	121	6
2	31	115	24*
3	41	31	10*
4	7	212	287*
5	7	96	207*
6	115	209	12
7	125	134	7
8	67	19	11
	4, 4, 1		
0	294	288	4
1	271	365	5
2	201	333	9
3	46	108	12*
4	7	105	186*
5	7	42	112*
6	46	54	30*
7	185	175	9
8	97	26	9
	4, 5, 1		
1	150	206	6
2	152	180	6
3	20	85	49*
4	7	61	149*
5	8	44	153*
6	40	71	25*
7	150	95	7
8	9	48	187*
	4, 6, 1		

l	kFo	Fc	Sig
0	152	129	5
1	6	53	130*
2	333	402	6
3	6	80	148*
4	7	25	130*
5	8	12	149*
6	98	128	9
7	145	93	7
8	40	21	26*
	4, 7, 1		
1	201	243	5
2	334	374	6
3	102	127	5
4	50	64	10*
5	39	31	21*
6	42	35	30*
7	9	14	169*
8	25	8	70*
	4, 8, 1		
0	72	40	5
1	145	143	6
2	119	98	6
3	103	146	5
4	7	41	155*
5	37	24	15*
6	101	101	7
7	9	4	159*
8	46	18	26*
	4, 9, 1		
1	488	488	4
2	309	328	5
3	107	132	5
4	7	32	140*
5	60	23	10
6	28	24	47*
7	53	70	28*
8	174	113	7
	4, 10, 1		
0	6	30	128*
1	504	488	4
2	202	227	6
3	88	107	6
4	7	6	133*
5	45	12	13*
6	25	21	53*
7	146	134	7
8	10	51	194*
	4, 11, 1		
1	78	39	5
2	68	66	6

Columns are 10Fo 10Fc 10Sig, * for Insignificant

l	kFo	Fc	Sig
	4, 11, 1		
3	190	195	8
4	37	19	28*
5	139	106	6
6	8	4	160*
7	9	9	191*
8	131	73	8
	4, 12, 1		
0	206	194	5
1	70	56	6
2	345	316	5
3	148	270	8
4	128	84	6
5	128	80	6
6	31	28	46*
7	16	11	88*
8	10	5	180*
	4, 13, 1		
1	108	77	4
2	67	92	10
3	7	80	365*
4	141	97	5
5	61	32	10
6	9	46	169*
7	20	17	51*
8	53	12	32*
	4, 14, 1		
0	80	74	5
1	34	25	23*
2	98	125	6
3	127	70	6
4	253	181	7
5	82	50	8
6	9	42	161*
7	46	31	33*
8	40	15	31*
	4, 15, 1		
1	51	73	8
2	189	197	9
3	207	146	7
4	337	238	6
5	163	122	7
6	9	7	160*
7	62	46	12
8	10	14	177*
	4, 16, 1		
0	54	12	8
1	118	63	6
2	7	13	297*
3	266	189	6
4	252	73	7
5	118	71	7
6	9	63	166*
7	49	11	34*
	4, 17, 1		
1	143	170	6
2	123	108	6
3	209	156	7
4	86	20	7
5	25	27	58*
6	101	62	8
7	10	25	176*
	4, 18, 1		
0	113	100	5
1	7	36	209*
2	124	61	6
3	339	286	6
4	151	166	7
5	37	51	39*
6	9	61	215*
7	10	1	176*
	4, 19, 1		
1	7	9	255*
2	45	30	26*
3	406	262	6
4	240	208	8
5	228	209	9
6	9	90	218*
7	69	67	12
	4, 20, 1		
0	79	146	7
1	257	257	6
2	139	154	7
3	265	148	7
4	215	95	9
5	9	25	263*
6	9	42	210*
7	135	59	8
	4, 21, 1		
1	216	41	8
2	194	146	8
3	238	220	7
4	109	107	7
5	138	114	6
6	9	52	185*
7	53	23	40*
	4, 22, 1		
0	587	674	5
1	189	6	7
2	316	284	6
3	283	225	7
4	74	34	10
5	9	87	230*
6	40	45	31*
	4, 23, 1		
1	353	372	6
2	381	268	6
3	266	156	7
4	38	47	37*
5	9	6	198*
6	10	48	193*
	4, 24, 1		
0	497	599	6
1	364	85	6
2	274	149	7
3	169	70	7
4	71	57	11
5	9	39	166*
6	10	13	191*
	4, 25, 1		
1	165	137	7
2	122	58	6
3	32	44	25*
4	9	36	181*
5	10	33	172*
6	45	17	41*
	4, 26, 1		
0	111	150	6
1	162	156	7
2	62	71	12
3	30	24	48*
4	9	40	167*
5	40	0	42*
6	10	49	191*
	4, 27, 1		
1	139	65	6
2	91	70	8
3	9	3	156*
4	42	25	26*
5	96	130	9
	4, 28, 1		
0	56	72	13*
1	153	187	6
2	45	15	24*
3	87	66	9
4	56	44	30*
5	10	70	198*
	4, 29, 1		
1	178	50	7
2	42	20	25*
3	52	14	16*
4	35	37	28*
5	93	95	11
	4, 30, 1		
0	9	17	163*
1	152	91	6
2	172	154	7
3	39	17	20*
4	47	34	35*
	4, 31, 1		
1	147	82	7
2	168	84	8
3	34	61	48*
4	107	84	9
	4, 32, 1		
0	44	45	36*
1	108	72	8
2	141	130	7
3	98	105	10
	4, 33, 1		
1	95	62	9
2	112	38	8
	4, 34, 1		
0	39	49	46*
1	114	97	8
2	42	54	29*
	5, 1, 1		
1	71	53	6
2	129	109	5
3	380	505	10
4	7	85	133*
5	8	215	335*
6	8	145	337*
7	9	25	161*
8	39	4	44*
	5, 2, 1		
0	457	413	4
1	102	69	5
2	32	41	12*
3	7	30	137*
4	7	233	301*
5	8	132	195*
6	8	18	183*
7	9	61	194*
8	52	19	32*
	5, 3, 1		
1	300	305	5
2	6	29	122*
3	43	117	12*
4	16	57	63*

Columns are 10Fo 10Fc 10Sig, * for Insignificant

l	kFo	Fc	Sig
	5, 3, 1		
5	8	105	184*
6	8	52	215*
7	9	113	243*
8	56	46	33*
	5, 4, 1		
0	493	460	4
1	22	59	20*
2	139	174	6
3	53	101	11*
4	7	130	227*
5	8	165	273*
6	8	54	203*
7	9	109	232*
8	68	71	15*
	5, 5, 1		
1	104	108	5
2	205	232	8
3	163	276	7
4	7	92	166*
5	8	126	234*
6	8	86	174*
7	9	123	243*
8	10	24	182*
	5, 6, 1		
0	75	40	5
1	129	119	5
2	172	189	8
3	65	83	8
4	30	41	31*
5	8	76	191*
6	39	59	37*
7	9	42	186*
8	43	23	20*
	5, 7, 1		
1	169	170	6
2	182	185	7
3	7	49	137*
4	7	44	141*
5	8	33	164*
6	36	61	41*
7	9	38	182*
8	51	38	36*
	5, 8, 1		
0	548	497	4
1	437	425	5
2	156	175	5
3	17	11	52*
4	66	49	9
5	8	32	147*
6	22	57	31*
7	9	55	186*
8	10	35	193*
	5, 9, 1		
1	129	124	5
2	114	78	5
3	80	102	7
4	86	102	9
5	8	2	85*
6	9	126	192*
7	9	15	173*
8	103	100	11
	5, 10, 1		
0	276	269	5
1	233	189	6
2	144	187	5
3	36	25	25*
4	8	67	196*
5	32	31	26*
6	44	14	31*
7	9	41	171*
8	10	64	217*
	5, 11, 1		
1	143	119	5
2	17	82	52*
3	33	7	14*
4	8	126	190*
5	123	148	7
6	99	92	8
7	9	4	169*
8	10	6	184*
	5, 12, 1		
0	47	55	9
1	150	112	7
2	253	228	6
3	53	41	9
4	8	41	174*
5	145	46	7
6	148	144	7
7	9	1	168*
8	10	24	184*
	5, 13, 1		
1	138	104	5
2	40	62	24*
3	7	18	138*
4	8	46	154*
5	102	91	7
6	128	69	7
7	9	62	185*
8	10	7	180*
	5, 14, 1		
0	235	267	5
1	59	33	8
2	34	34	28*
3	8	4	147*
4	293	252	7
5	155	87	6
6	43	13	25*
7	61	52	15*
	5, 15, 1		
1	59	46	8
2	128	94	6
3	154	127	6
4	299	24	7
5	156	41	7
6	144	72	7
7	10	35	183*
	5, 16, 1		
0	80	58	6
1	133	78	6
2	8	48	171*
3	8	20	215*
4	8	12	155*
5	122	81	6
6	130	78	7
7	105	77	9
	5, 17, 1		
1	7	7	150*
2	8	6	154*
3	38	17	31*
4	31	28	29*
5	197	121	9
6	108	147	8
7	10	36	215*
	5, 18, 1		
0	118	135	6
1	249	256	6
2	8	8	145*
3	172	174	6
4	305	300	7
5	143	6	7
6	60	4	15*
7	10	6	199*
	5, 19, 1		
1	8	105	261*
2	61	67	10
3	200	92	8
4	355	135	6
5	75	68	10
6	46	21	25*
7	90	58	10
	5, 20, 1		
0	202	147	7
1	264	326	8
2	153	170	7
3	330	294	6
4	130	10	6
5	97	45	8
6	82	49	11
	5, 21, 1		
1	8	127	359*
2	253	214	7
3	312	147	7
4	101	60	7
5	64	20	12
6	58	24	32*
	5, 22, 1		
0	57	82	11*
1	8	63	221*
2	230	132	8
3	186	159	9
4	98	31	8
5	9	41	166*
6	10	54	178*
	5, 23, 1		
1	189	169	9
2	196	127	8
3	188	101	9
4	99	105	8
5	9	44	166*
6	102	85	9
	5, 24, 1		
0	101	89	7
1	373	322	6
2	264	178	7
3	116	36	7
4	96	53	8
5	10	12	172*
6	10	68	220*
	5, 25, 1		
1	313	46	7
2	212	115	9
3	74	53	10
4	29	29	53*
5	64	51	13*
	5, 26, 1		
0	48	83	31*
1	156	162	7
2	95	55	8
3	35	41	44*

Columns are 10Fo 10Fc 10Sig, * for Insignificant

l	kFo	Fc	Sig
5, 26, 1			
4	83	71	10
5	76	13	12
5, 27, 1			
1	147	90	7
2	117	139	7
3	124	94	7
4	10	11	185*
5	40	21	45*
5, 28, 1			
0	45	20	24*
1	106	58	8
2	203	152	9
3	139	77	6
4	14	0	113*
5, 29, 1			
1	126	93	6
2	170	111	8
3	84	13	10
4	10	19	175*
5, 30, 1			
0	42	100	38*
1	79	36	10
2	67	44	13
3	58	9	14*
5, 31, 1			
1	29	23	39*
2	10	17	170*
3	94	124	10
5, 32, 1			
0	10	26	164*
1	45	11	26*
2	10	23	172*
5, 33, 1			
1	10	18	171*
6, 0, 1			
0	127	140	5
1	203	199	6
2	29	25	29*
3	145	189	6
4	8	95	164*
5	195	357	12
6	9	112	348*
7	9	23	159*
8	10	84	282*
6, 1, 1			
1	160	145	7
2	52	94	9
3	50	89	11*
4	8	75	167*
5	8	56	195*
6	9	69	192*
7	9	12	161*
8	10	6	194*
6, 2, 1			
0	114	103	5
1	7	10	122*
2	143	132	6
3	35	33	27*
4	34	89	35*
5	8	172	369*
6	9	85	248*
7	9	59	191*
8	10	27	204*
6, 3, 1			
1	143	168	5
2	148	178	6
3	86	91	7
4	44	180	39*
5	8	343	464*
6	9	35	171*
7	9	27	175*
8	70	8	12
6, 4, 1			
0	510	439	5
1	136	103	6
2	88	81	6
3	30	7	19*
4	8	110	182*
5	8	149	303*
6	9	99	232*
7	9	4	166*
8	10	6	163*
6, 5, 1			
1	276	241	6
2	103	113	5
3	62	136	10
4	8	90	188*
5	8	149	274*
6	9	63	216*
7	9	75	189*
8	10	9	167*
6, 6, 1			
0	345	306	5
1	322	289	6
2	193	218	9
3	121	164	7
4	8	153	252*
5	8	145	226*
6	9	20	185*
7	9	32	175*
8	10	37	176*
6, 7, 1			
1	193	142	7
2	55	54	9
3	158	190	7
4	8	95	191*
5	8	46	172*
6	9	28	164*
7	9	100	216*
8	10	9	176*
6, 8, 1			
0	77	42	6
1	53	40	8
2	134	143	6
3	96	107	7
4	71	84	11
5	8	38	154*
6	9	62	185*
7	35	20	33*
8	10	23	169*
6, 9, 1			
1	347	323	6
2	44	26	11*
3	30	69	38*
4	8	15	152*
5	8	58	164*
6	55	125	37*
7	10	87	199*
6, 10, 1			
0	411	367	5
1	40	30	12*
2	61	68	8
3	87	78	7
4	91	71	8
5	8	69	167*
6	114	74	7
7	47	23	36*
6, 11, 1			
1	7	9	135*
2	94	101	6
3	78	58	8
4	8	26	167*
5	9	11	161*
6	25	82	68*
7	10	82	211*
6, 12, 1			
0	157	167	8
1	231	194	6
2	76	73	7
3	119	139	6
4	114	108	7
5	93	124	9
6	55	31	28*
7	115	5	7
6, 13, 1			
1	22	22	46*
2	91	98	7
3	8	107	179*
4	8	62	251*
5	109	82	7
6	9	76	187*
7	41	5	20*
6, 14, 1			
0	108	123	5
1	185	152	7
2	69	64	8
3	36	92	40*
4	8	18	206*
5	91	37	8
6	104	26	8
7	28	14	59*
6, 15, 1			
1	27	15	38*
2	44	86	28*
3	8	91	189*
4	97	44	8
5	90	18	8
6	79	52	11
7	57	62	16*
6, 16, 1			
0	126	75	6
1	43	21	25*
2	8	6	150*
3	8	2	164*
4	90	16	8
5	112	84	7
6	94	65	9
7	76	48	12
6, 17, 1			
1	33	37	34*
2	121	133	5
3	147	104	7
4	60	99	11
5	113	19	7
6	55	18	30*
7	56	48	31*
6, 18, 1			
0	113	99	6
1	279	250	6

Columns are 10Fo 10Fc 10Sig, * for Insignificant

l	kFo	Fc	Sig
	6, 18, 1		
2	98	147	9
3	8	33	207*
4	95	48	7
5	139	85	6
6	30	20	53*
	6, 19, 1		
1	186	248	9
2	125	201	9
3	52	39	12*
4	124	97	7
5	144	53	6
6	53	37	29*
	6, 20, 1		
0	105	116	7
1	8	138	301*
2	8	76	301*
3	23	49	58*
4	149	44	6
5	9	4	167*
6	38	22	21*
	6, 21, 1		
1	8	62	258*
2	79	105	10
3	100	72	8
4	78	41	10
5	172	120	8
6	10	2	166*
	6, 22, 1		
0	232	216	8
1	298	392	11
2	148	131	7
3	104	32	7
4	150	133	7
5	176	69	8
6	46	41	36*
	6, 23, 1		
1	9	293	507*
2	221	166	10
3	104	77	7
4	231	134	9
5	64	59	13*
	6, 24, 1		
0	40	13	36*
1	293	286	10
2	339	277	7
3	132	70	6
4	186	65	7
5	51	8	32*
	6, 25, 1		

l	kFo	Fc	Sig
1	220	67	10
2	281	99	8
3	153	191	7
4	91	65	9
5	10	3	169*
	6, 26, 1		
0	103	150	8
1	70	27	10
2	49	32	31*
3	130	9	7
4	85	52	10
	6, 27, 1		
1	73	46	11
2	9	33	165*
3	140	85	6
4	112	103	8
	6, 28, 1		
0	114	113	7
1	125	83	6
2	48	30	33*
3	195	102	7
4	133	17	7
	6, 29, 1		
1	88	60	10
2	68	38	12
3	151	96	7
	6, 30, 1		
0	141	131	7
1	74	26	11
2	10	26	169*
3	149	105	7
	6, 31, 1		
1	54	22	31*
2	66	67	13*
	6, 32, 1		
0	82	72	10
1	17	8	97*
	7, 1, 1		
1	234	170	7
2	145	184	7
3	65	54	9
4	161	142	7
5	111	173	13
6	9	94	201*
7	10	104	306*
	7, 2, 1		
0	84	98	6
1	29	48	33*
2	249	235	8
3	88	93	7

l	kFo	Fc	Sig
4	30	64	33*
5	45	35	33*
6	23	40	69*
7	10	0	182*
	7, 3, 1		
1	7	22	129*
2	7	22	145*
3	162	175	7
4	78	121	11
5	55	223	43*
6	9	122	279*
7	10	33	181*
	7, 4, 1		
0	133	60	6
1	62	69	8
2	72	59	7
3	281	326	11
4	141	258	10
5	9	123	252*
6	9	77	207*
7	10	46	188*
	7, 5, 1		
1	64	74	8
2	172	154	8
3	148	187	7
4	8	6	170*
5	35	21	39*
6	9	6	172*
7	10	8	204*
	7, 6, 1		
0	185	106	7
1	156	90	6
2	71	41	8
3	8	44	168*
4	8	64	167*
5	18	32	71*
6	9	82	207*
7	10	46	194*
	7, 7, 1		
1	29	37	33*
2	131	122	6
3	205	190	10
4	50	16	12*
5	9	123	233*
6	9	91	267*
7	10	79	200*
	7, 8, 1		
0	184	139	7
1	129	110	6
2	8	38	154*

l	kFo	Fc	Sig
3	81	97	9
4	45	13	14*
5	9	11	165*
6	9	119	257*
7	51	29	34*
	7, 9, 1		
1	120	88	6
2	8	8	137*
3	81	123	8
4	38	108	43*
5	9	50	175*
6	9	76	208*
7	10	31	173*
	7, 10, 1		
0	90	104	6
1	154	117	6
2	324	298	7
3	158	74	7
4	57	85	13*
5	9	28	180*
6	9	29	190*
7	10	57	218*
	7, 11, 1		
1	84	44	7
2	8	26	156*
3	8	16	148*
4	8	70	152*
5	9	7	166*
6	36	15	23*
7	87	78	11
	7, 12, 1		
0	31	19	33*
1	61	45	9
2	183	159	8
3	89	109	7
4	57	71	12*
5	32	16	47*
6	9	68	187*
7	34	36	57*
	7, 13, 1		
1	233	195	7
2	108	124	6
3	199	159	9
4	40	93	27*
5	9	57	183*
6	44	3	37*
7	91	84	12
	7, 14, 1		
0	149	154	6
1	87	91	7

Columns are 10Fo 10Fc 10Sig, * for Insignificant

l	kFo	Fc	Sig	l	kFo	Fc	Sig	l	kFo	Fc	Sig	l	kFo	Fc	Sig
	7, 14, 1				7, 21, 1			1	104	36	9	6	10	11	170*
2	36	32	35*	1	9	143	329*		8, 0, 1			7	10	64	208*
3	8	9	187*	2	9	99	270*	0	296	195	6		8, 6, 1		
4	9	77	193*	3	9	2	167*	1	81	59	7	0	43	16	24*
5	55	6	14*	4	37	80	48*	2	34	57	33*	1	203	139	8
6	77	27	12	5	62	75	14*	3	210	154	9	2	306	243	8
	7, 15, 1				7, 22, 1			4	201	199	9	3	216	205	11
1	170	156	6	0	65	56	11	5	9	94	223*	4	44	52	30*
2	134	58	6	1	9	38	259*	6	66	72	17*	5	9	23	166*
3	8	54	153*	2	126	101	8	7	10	95	342*	6	10	56	200*
4	9	43	189*	3	175	129	8		8, 1, 1			7	10	19	190*
5	41	66	18*	4	157	83	7	1	8	13	143*		8, 7, 1		
6	100	0	9	5	102	78	9	2	92	66	7	1	141	100	7
	7, 16, 1				7, 23, 1			3	106	117	7	2	144	82	6
0	444	346	6	1	134	121	6	4	83	106	10	3	107	92	8
1	134	91	6	2	74	16	12	5	9	101	218*	4	38	67	39*
2	8	40	160*	3	212	105	9	6	9	119	253*	5	9	47	190*
3	21	20	62*	4	151	52	7	7	10	1	196*	6	10	40	186*
4	9	34	171*	5	92	26	10		8, 2, 1				8, 8, 1		
5	54	0	28*		7, 24, 1			0	8	47	141*	0	8	29	141*
6	128	80	8	0	27	34	54*	1	92	44	6	1	90	63	7
	7, 17, 1			1	17	27	111*	2	74	55	8	2	135	103	6
1	184	177	9	2	40	24	28*	3	24	74	43*	3	8	10	147*
2	75	86	9	3	177	76	8	4	167	195	8	4	73	108	12
3	9	39	145*	4	126	71	7	5	47	29	33*	5	9	37	165*
4	104	95	8		7, 25, 1			6	9	53	167*	6	10	29	174*
5	9	20	159*	1	9	49	176*	7	10	68	304*		8, 9, 1		
6	171	44	8	2	95	52	9		8, 3, 1			1	9	6	122*
	7, 18, 1			3	177	41	8	1	99	85	6	2	8	19	145*
0	414	376	6	4	107	71	9	2	59	3	9	3	128	114	7
1	385	338	7		7, 26, 1			3	129	166	7	4	49	169	33*
2	150	142	6	0	192	196	7	4	92	139	10	5	24	44	64*
3	12	27	116*	1	96	56	9	5	9	24	158*	6	27	51	71*
4	119	88	7	2	15	21	84*	6	9	49	180*		8, 10, 1		
5	33	38	33*	3	89	19	9	7	10	16	210*	0	267	188	7
6	49	17	36*	4	10	67	180*		8, 4, 1			1	27	40	44*
	7, 19, 1				7, 27, 1			0	27	8	39*	2	112	86	6
1	9	61	290*	1	87	77	10	1	285	191	7	3	53	84	14*
2	57	113	37*	2	172	121	8	2	20	31	62*	4	9	48	182*
3	91	91	9	3	39	61	32*	3	184	159	8	5	9	29	171*
4	98	46	8		7, 28, 1			4	20	39	49*	6	10	5	205*
5	142	102	7	0	54	62	29*	5	9	12	169*		8, 11, 1		
6	51	51	17*	1	93	39	10	6	30	77	64*	1	135	103	6
	7, 20, 1			2	156	47	7	7	31	14	55*	2	186	193	9
0	170	199	7	3	77	33	11		8, 5, 1			3	17	8	55*
1	265	213	7		7, 29, 1			1	119	95	5	4	9	85	174*
2	32	212	38*	1	112	109	8	2	151	81	7	5	9	88	199*
3	47	28	35*	2	59	23	14*	3	181	199	9	6	32	29	58*
4	43	2	26*		7, 30, 1			4	37	30	21*		8, 12, 1		
5	142	40	6	0	42	62	41*	5	9	24	176*	0	220	160	7

Columns are 10Fo 10Fc 10Sig, * for Insignificant

l	kFo	Fc	Sig	l	kFo	Fc	Sig	l	kFo	Fc	Sig	l	kFo	Fc	Sig
	8, 12, 1			1	139	100	6	5	9	4	165*	2	54	31	12*
1	136	98	6	2	9	43	167*	6	56	54	20*	3	41	37	37*
2	131	86	6	3	87	75	12		9, 2, 1			4	9	17	165*
3	35	35	36*	4	49	42	32*	0	147	77	7	5	60	66	30*
4	25	84	65*	5	31	15	57*	1	198	138	8	6	10	30	186*
5	9	6	207*		8, 20, 1			2	36	53	39*		9, 9, 1		
6	10	0	191*	0	559	408	6	3	41	12	22*	1	50	11	12*
	8, 13, 1			1	9	57	215*	4	9	31	161*	2	23	26	39*
1	81	72	8	2	9	17	165*	5	9	30	166*	3	74	74	11
2	158	117	6	3	139	109	8	6	42	14	39*	4	9	8	163*
3	9	43	156*	4	41	37	40*		9, 3, 1			5	29	46	64*
4	9	21	187*	5	64	16	13*	1	111	102	6	6	10	6	187*
5	20	7	75*		8, 21, 1			2	121	68	6		9, 10, 1		
6	23	78	101*	1	240	183	9	3	9	29	160*	0	85	46	8
	8, 14, 1			2	131	77	7	4	32	79	63*	1	91	60	8
0	75	69	8	3	33	13	63*	5	40	75	44*	2	46	18	14*
1	105	93	6	4	47	36	37*	6	10	8	177*	3	41	72	42*
2	117	93	6		8, 22, 1				9, 4, 1			4	9	16	154*
3	9	3	163*	0	121	110	7	0	213	135	8	5	10	76	227*
4	9	3	176*	1	9	157	347*	1	246	210	8		9, 11, 1		
5	40	13	27*	2	9	37	219*	2	154	98	7	1	150	93	7
6	151	50	8	3	202	157	7	3	84	75	10	2	68	65	10
	8, 15, 1			4	131	56	7	4	40	100	53*	3	136	142	7
1	77	69	9		8, 23, 1			5	19	9	90*	4	35	2	43*
2	74	105	10	1	9	24	282*	6	10	30	183*	5	10	16	218*
3	9	21	161*	2	10	47	188*		9, 5, 1				9, 12, 1		
4	53	15	28*	3	271	137	9	1	8	12	148*	0	51	40	26*
5	79	49	11	4	140	12	7	2	94	66	8	1	39	54	34*
6	98	6	9		8, 24, 1			3	31	33	33*	2	9	67	173*
	8, 16, 1			0	81	81	10	4	42	107	26*	3	9	1	169*
0	36	65	20*	1	121	105	7	5	93	100	13	4	9	10	112*
1	9	10	154*	2	120	107	8	6	29	13	40*	5	18	40	94*
2	140	118	6	3	277	172	9		9, 6, 1				9, 13, 1		
3	40	40	24*		8, 25, 1			0	144	65	7	1	9	10	148*
4	29	10	52*	1	47	24	25*	1	19	5	33*	2	82	43	9
5	64	46	13*	2	63	101	18*	2	96	62	8	3	46	25	30*
	8, 17, 1			3	269	130	9	3	75	63	11	4	35	24	25*
1	79	56	9		8, 26, 1			4	25	46	76*	5	10	1	184*
2	89	105	11	0	58	47	29*	5	10	23	167*		9, 14, 1		
3	54	58	14*	1	10	52	178*	6	47	0	35*	0	47	24	27*
4	70	64	11	2	188	172	8		9, 7, 1			1	119	87	7
5	60	22	14*		8, 27, 1			1	30	27	21*	2	33	15	29*
	8, 18, 1			1	46	44	35*	2	20	30	66*	3	9	8	160*
0	9	49	116*		8, 28, 1			3	9	51	160*	4	39	9	28*
1	23	50	72*	0	42	16	19*	4	9	46	166*	5	10	9	174*
2	9	46	200*		9, 1, 1			5	41	31	38*		9, 15, 1		
3	90	88	10	1	166	113	7	6	10	16	174*	1	162	131	8
4	38	33	31*	2	38	18	33*		9, 8, 1			2	25	18	56*
5	47	33	18*	3	36	2	19*	0	46	30	26*	3	9	26	152*
	8, 19, 1			4	45	63	34*	1	154	108	7	4	10	2	169*

Columns are 10Fo 10Fc 10Sig, * for Insignificant

l	kFo	Fc	Sig
9, 15, 1			
5	114	113	10
9, 16, 1			
0	67	50	11
1	20	41	75*
2	38	12	25*
3	9	4	160*
4	10	28	163*
9, 17, 1			
1	123	71	7
2	34	45	45*
3	46	58	24*
4	48	34	37*
9, 18, 1			
0	358	259	7
1	9	39	173*
2	118	95	8
3	92	44	9
4	10	35	177*
9, 19, 1			
1	9	69	175*
2	10	50	209*
3	10	19	183*
4	77	35	11
9, 20, 1			
0	256	151	8
1	59	64	14*
2	10	78	210*
3	104	88	9
9, 21, 1			
1	52	44	33*
2	75	64	15
3	36	8	39*
9, 22, 1			
0	10	12	169*
1	10	29	132*
2	10	42	229*
3	44	29	23*
9, 23, 1			
1	48	43	36*
2	10	23	179*
9, 24, 1			
0	10	16	164*
1	58	87	15*
10, 0, 1			
0	303	223	8
1	100	47	8
2	75	56	10
3	49	9	28*
4	10	34	159*

l	kFo	Fc	Sig
5	73	45	14
10, 1, 1			
1	23	47	62*
2	146	114	7
3	34	15	44*
4	10	3	170*
5	10	1	172*
10, 2, 1			
0	93	63	8
1	164	126	7
2	9	9	165*
3	9	15	156*
4	10	8	163*
5	10	32	185*
10, 3, 1			
1	44	20	33*
2	172	108	8
3	9	45	170*
4	10	30	162*
5	43	16	38*
10, 4, 1			
0	70	44	10
1	222	124	10
2	186	131	8
3	40	37	38*
4	33	8	46*
5	10	25	173*
10, 5, 1			
1	54	35	28*
2	189	126	8
3	31	30	27*
4	49	20	16*
5	10	22	171*
10, 6, 1			
0	48	50	15*
1	135	67	6
2	19	18	78*
3	9	1	152*
4	10	9	168*
5	48	25	26*
10, 7, 1			
1	34	10	29*
2	18	41	86*
3	89	48	10
4	55	22	31*
5	10	6	120*
10, 8, 1			
0	19	20	68*
1	31	21	44*
2	42	66	40*

l	kFo	Fc	Sig
3	47	44	31*
4	35	18	45*
5	46	10	37*
10, 9, 1			
1	48	41	15*
2	151	112	7
3	98	66	9
4	52	49	18*
10, 10, 1			
0	80	38	9
1	44	29	31*
2	62	63	13*
3	55	34	31*
4	87	62	11
10, 11, 1			
1	9	17	154*
2	9	17	149*
3	119	90	8
4	10	11	187*
10, 12, 1			
0	176	92	7
1	9	0	158*
2	9	19	157*
3	48	50	35*
4	10	13	173*
10, 13, 1			
1	40	4	36*
2	16	14	67*
3	10	27	165*
4	91	53	11
10, 14, 1			
0	9	18	158*
1	39	17	19*
2	32	16	46*
3	10	8	162*
4	10	36	223*
10, 15, 1			
1	59	38	13*
2	10	32	161*
3	37	13	30*
10, 16, 1			
0	103	80	8
1	10	59	170*
2	10	26	155*
3	10	12	172*
10, 17, 1			
1	10	14	117*
2	94	55	9
3	10	19	167*
10, 18, 1			

l	kFo	Fc	Sig
0	10	38	167*
1	10	38	163*
2	10	18	193*
10, 19, 1			
1	10	5	176*
2	133	61	8
10, 20, 1			
0	18	9	93*
1	25	11	67*
2	10	82	263*
10, 21, 1			
1	61	44	14*
11, 1, 1			
1	123	50	7
2	10	34	185*
3	10	35	175*
4	61	2	14*
11, 2, 1			
0	263	146	9
1	85	44	10
2	12	34	141*
3	10	21	177*
4	29	14	59*
11, 3, 1			
1	9	16	183*
2	36	3	22*
3	55	4	30*
4	10	9	174*
11, 4, 1			
0	211	105	7
1	211	99	10
2	47	43	35*
3	78	35	12
4	44	19	41*
11, 5, 1			
1	110	56	8
2	138	68	7
3	136	69	8
11, 6, 1			
0	196	121	7
1	37	18	43*
2	28	3	41*
3	52	22	32*
11, 7, 1			
1	72	26	11
2	10	9	166*
3	10	11	167*
11, 8, 1			
0	76	40	11
1	10	3	169*

Columns are 10Fo 10Fc 10Sig, * for Insignificant

l	kFo	Fc	Sig
11, 8, 1			
2	49	9	16*
3	10	15	182*
11, 9, 1			
1	10	40	174*
2	10	26	167*
3	41	14	20*
11, 10, 1			
0	55	45	29*
1	46	17	17*
2	26	24	64*
3	84	38	10
11, 11, 1			

l	kFo	Fc	Sig
1	87	50	10
2	10	8	169*
3	10	0	170*
11, 12, 1			
0	41	42	23*
1	10	19	172*
2	10	2	179*
11, 13, 1			
1	47	9	24*
2	55	8	30*
11, 14, 1			
0	79	56	11

l	kFo	Fc	Sig
1	16	15	103*
2	10	19	171*
11, 15, 1			
1	54	38	16*
11, 16, 1			
0	49	9	32*
12, 0, 1			
0	31	5	57*
1	96	44	9
12, 1, 1			
1	48	15	37*
12, 2, 1			

l	kFo	Fc	Sig
0	179	64	7
1	60	38	15*
12, 3, 1			
1	175	68	8
12, 4, 1			
0	236	82	10
1	40	8	45*
12, 5, 1			
1	126	41	8
12, 6, 1			
0	157	58	8
1	25	3	73*

Space Group and Cell Dimensions Orthorhombic P 212121
a 8.028(3) b 31.240(14) c 5.681(4)
Volume 1424.7(12)A**3

Empirical formula : O2 C17 H18

Cell dimensions were obtained from 24 reflections with 2Theta angle in the range 40.00 - 50.00 degrees.

Crystal dimensions : 0.20 X 0.05 X 0.20 mm

FW = 254.33 Z = 4 F(000) = 544.20

Dcalc 1.186Mg.m-3, mu 0.06mm-1, lambda 0.70930A, 2Theta(max) 47.0

The intensity data were collected on a Rigaku diffractometer, using the theta/2theta scan mode.
The h,k,l ranges are :-- 0 9, 0 35, 0 6
No. of reflections measured 4495
No. of unique reflections 2116
No. of reflections with Inet > 2.5sigma(Inet) 1262
No correction was made for absorption

The last least squares cycle was calculated with
37 atoms, 149 parameters and 1260 out of 2116 reflections.
Weights based on counting-statistics were used.

The residuals are as follows :--
For significant reflections, RF 0.120, Rw 0.086 GoF 9.44
For all reflections, RF 0.169, Rw 0.086.
where RF = Sum(Fo-Fc)/Sum(Fo),
Rw = Sqrt[Sum(w(Fo-Fc)**2)/Sum(wFo**2)] and
GoF = Sqrt[Sum(w(Fo-Fc)**2)/(No. of reflns - No. of params.)]
The maximum shift/sigma ratio was 0.050.

In the last D-map, the deepest hole was -0.270e/A**3,
and the highest peak 0.300e/A**3.

Secondary ext. coeff. = 1.634664 sigma = 0.191026

EXPERIMENTAL

1. Data Collection

A plate crystal of O2C17H18 having approximate dimensions of .2,.05,.2 was mounted on a glass capillary. All the measurements were made on a Rigaku diffractometer with Mo Kalpha radiation.

Cell constants and an orientation matrix for data collection, were obtained from least-squares refinement using the setting angles of 25 reflections in the range 25<2theta<35 corresponded to a orthorombic cell with dimensions:

a = 8.0283(26)
b = 31.2398(143)
c = 5.6805(35)

For Z= 4 and FW= 254.33 , the calculated density is 1.186g/cm3. Based on the systematic absences, the space group was determined to be P 21 21 21.

The data was collected at a temperature of -100 degrees using the omega-2theta scan technique to a maximum 2theta value of 47.

2. Data reduction

A total of 4495 reflections was measured. Th unique set contains only 2216 reflections. The standards were measured after every 150 reflections. No crystal decay was noticed. The data were collected for Lorentz and polarisation effects (1).

3. Solution and refinement:

The structure was solved by direct methods. All the atoms were refined anisotropically except the hydrogen. The hydrogen atoms were calculated. The phe nyls were refined as rigid groups. Because of the sm
refinement was based on 1260 observed reflections (I>2.5 sigma(I)) and 149 variable parameters. Weights based on counting statistics were used. The maximum and minimum peaks on the final differences Fourier map corresponded to -.270 and .300 e/a3, respectively.

All the calculations were performed using the NRCVAX crystallographic software package (2).

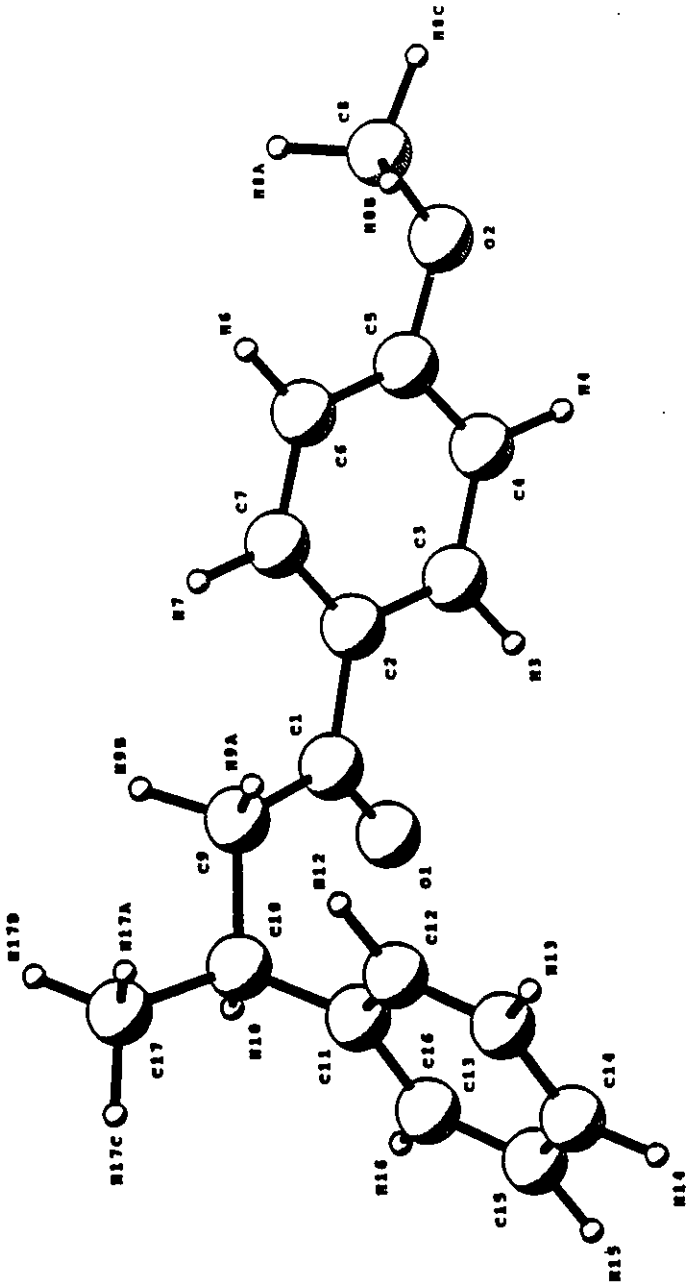
H1C
C8
H8A
H8B
O2
C5
H6
H4
C6
C4
C7
C3
H7
H3
C2
C1
H9B
H9A
C9
O1
H12
C10
C12
H19
H17A
H13
C17
O10
C11
C16
C13
C14
H17C
H18
H16
C15
H15

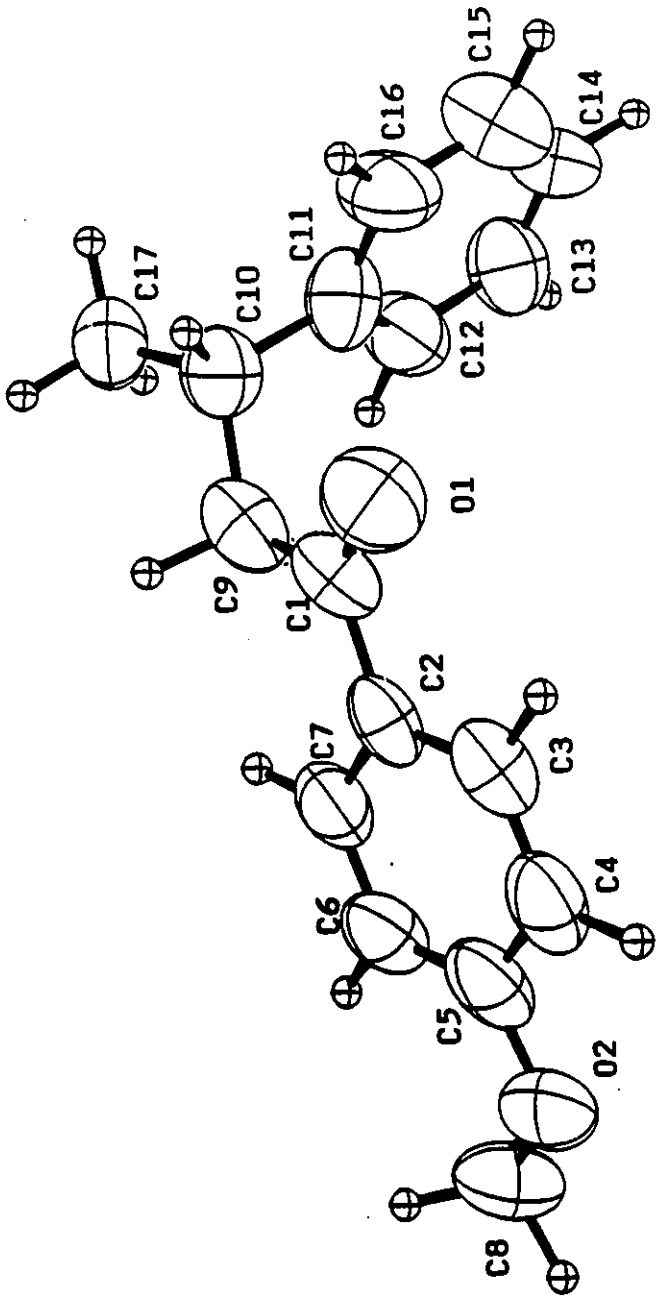
C15
C14
C16
C11
C17
C10
C13
C12
O1
C9
C1
C2
C7
C3
C6
C4
C5
O2
C8

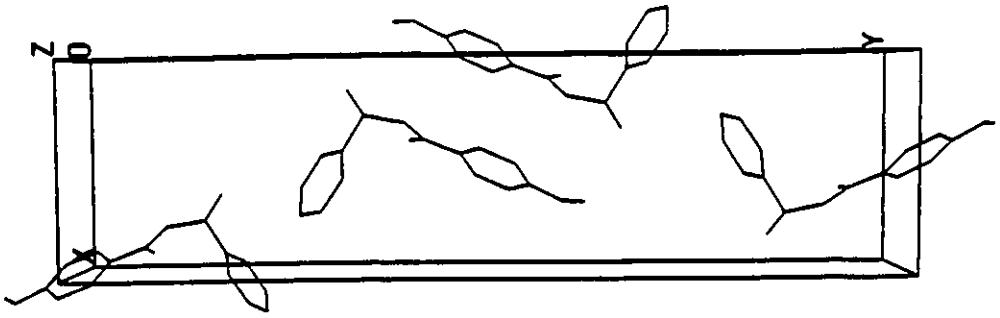
Z
O
Y
X

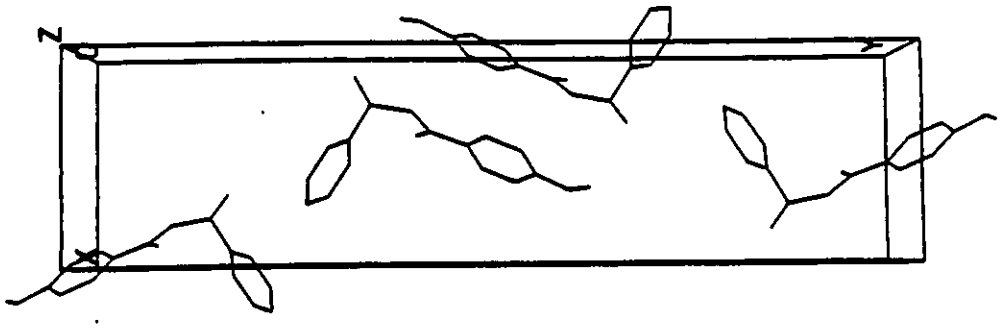
Z
Y
X

References

1. D.F. Grant and E.J. Gabe
J. Appl. Crystallogr., 11, 114 (1978)
2. E.J. Gabe, F.L. Lee and Y. Lepage
J. Appl. Crystallogr., 22, 384 (1989)

Table of Contents

EXPERIMENTAL DETAILS

Empirical formula	O2C17H18
Formula weight	254.33
Crystal shape	plate
Crystal dimensions (mm)	.2,.05,.2
Crystal system	orthorombic
No. Reflection used for unit cell dimension (2theta range)	25 25-35
Lattice parameters	a=8.0283 b=31.2398 c=5.6805
Space group	P 21 21 21
Z value	4
Dcalc (g.cm-3)	1.186
F(000)	544.20
mu (mm-1)	.06
No of reflection measured	4495
No of reflection unique	2116
No of reflection observed	1260
No of atoms	37
No of variables	149
Rf (sign refl)	.12
Rw (sign refl)	.086
Rf (all refl)	.169
Rw (all refl)	.086
Goodness of fit	9.44
Last difference fourier map	
max peak	.300
min peak	-.270

Table of Atomic Parameters x,y,z and Biso.
E.S.Ds. refer to the last digit printed.

	x	y	z	Biso
O1	0.0999(10)	0.59424(24)	0.9800(14)	7.8(4)
O2	-0.1633(10)	0.41104(21)	1.2686(15)	7.7(4)
C1	0.1124(13)	0.5762 (3)	1.1705(18)	5.6(4)
C8	-0.1559(17)	0.3880 (3)	1.4833(24)	8.4(7)
C9	0.1949(14)	0.5970 (4)	1.3696(21)	6.8(5)
C10	0.2283(13)	0.6456 (4)	1.3354(24)	7.3(6)
C17	0.3439(13)	0.6618 (3)	1.536 (3)	8.2(7)
H3	-0.076	0.533	0.864	6.9
H4	-0.198	0.461	0.910	6.8
H6	0.035	0.449	1.587	6.4
H7	0.157	0.522	1.540	7.2
H8C	-0.222	0.357	1.471	9.0
H8A	-0.026	0.381	1.531	9.0
H8B	-0.211	0.406	1.629	9.0
H9A	0.119	0.595	1.531	7.0
H9B	0.315	0.582	1.411	7.0
H10	0.297	0.651	1.167	7.8
H12	-0.027	0.648	1.661	7.8
H13	-0.283	0.692	1.650	8.4
H14	-0.334	0.741	1.315	7.6
H15	-0.128	0.746	0.992	10.5
H16	0.128	0.702	1.003	8.1
H17C	0.373	0.695	1.518	8.4
H17A	0.279	0.657	1.703	8.4
H17B	0.458	0.643	1.540	8.4
C2	0.0481(8)	0.53191(17)	1.2004(12)	5.3(4)
C3	-0.0519(9)	0.51466(22)	1.0234(10)	6.4(5)
C4	-0.1203(8)	0.47390(23)	1.0504(11)	6.9(5)
C5	-0.0887(8)	0.45040(17)	1.2544(14)	6.6(5)
C6	0.0113(9)	0.46765(19)	1.4314(10)	6.2(5)
C7	0.0797(8)	0.50841(21)	1.4044(11)	6.4(5)
C11	0.0672(7)	0.67169(23)	1.3308(14)	6.6(6)
C12	-0.0499(9)	0.66904(24)	1.5116(12)	8.2(7)
C13	-0.1933(8)	0.6942 (3)	1.5040(14)	8.6(7)
C14	-0.2197(8)	0.72201(22)	1.3156(17)	7.4(6)
C15	-0.1026(12)	0.72466(22)	1.1347(14)	9.4(8)
C16	0.0408(10)	0.6995 (3)	1.1423(12)	7.8(6)

Biso is the Mean of the Principal Axes of the Thermal Ellipsoid

Table of u(i,j) or U values *100.
E.S.Ds. refer to the last digit printed

	u11(U)	u22	u33	u12	u13	u23
O1	10.9(6)	10.4(5)	8.5(5)	0.6(5)	-0.1(5)	0.8(5)
O2	10.6(6)	6.5(4)	12.0(6)	1.7(4)	-1.0(5)	-1.9(4)
C1	8.1(7)	7.5(6)	5.6(5)	2.6(5)	0.3(5)	0.6(5)
C8	14.4(11)	5.9(6)	11.4(10)	0.8(7)	0.0(9)	2.4(7)
C9	8.0(7)	9.3(7)	8.7(8)	2.6(6)	0.3(6)	0.7(6)
C10	6.4(6)	8.9(7)	12.3(10)	0.6(5)	1.5(7)	1.0(7)
C17	6.8(7)	8.5(7)	15.8(12)	0.2(6)	-2.3(8)	-0.9(8)
C2	5.5(5)	8.0(6)	6.7(6)	2.9(5)	0.3(5)	-0.6(5)
C3	7.6(7)	8.7(7)	8.2(7)	2.7(6)	-0.6(6)	0.3(6)
C4	7.1(7)	9.6(8)	9.3(8)	3.1(6)	-1.2(6)	-2.1(7)
C5	8.5(7)	7.9(7)	8.6(7)	3.9(6)	-0.8(6)	-1.8(6)
C6	8.7(7)	6.6(6)	8.1(7)	2.6(5)	-0.5(6)	-0.8(5)
C7	6.5(6)	8.1(7)	9.8(8)	2.0(5)	-0.3(6)	1.3(6)
C11	6.2(6)	11.3(8)	7.7(7)	-0.2(6)	0.3(6)	-0.5(7)
C12	7.5(7)	9.5(8)	14.3(12)	1.3(6)	2.4(8)	4.4(8)
C13	6.8(7)	11.1(9)	14.8(12)	1.8(7)	1.4(8)	0.2(9)
C14	10.5(9)	5.6(6)	12.1(10)	0.8(6)	-0.7(9)	1.3(7)
C15	13.7(13)	10.2(9)	11.7(11)	2.5(9)	-0.3(11)	1.9(8)
C16	10.8(9)	8.2(7)	10.5(9)	0.3(7)	1.8(8)	3.5(7)

Anisotropic Temperature Factors are of the form
Temp=-2*Pi*Pi*(h*h*u11*astar*astar+----+2*h*k*u12*astar*bstar+---)

Table of Bond Distances in Angstroms

O1-C1	1.223(13)	H6-C6	1.066(6)
O2-C8	1.418(15)	H7-C7	1.073(6)
O2-C5	1.370(9)	H12-C12	1.097(7)
C1-C9	1.464(16)	H13-C13	1.102(8)
C1-C2	1.487(12)	H14-C14	1.085(7)
C8-H8C	1.097(11)	H15-C15	1.063(8)
C8-H8A	1.096(14)	H16-C16	1.058(7)
C8-H8B	1.092(13)	C2-C3	1.395(9)
C9-C10	1.553(16)	C2-C7	1.395(9)
C9-H9A	1.108(11)	C3-C4	1.395(10)
C9-H9B	1.101(10)	C4-C5	1.395(10)
C10-C17	1.555(18)	C5-C6	1.395(9)
C10-H10	1.116(12)	C6-C7	1.395(9)
C10-C11	1.529(12)	C11-C12	1.395(10)
C17-H17C	1.075(11)	C11-C16	1.395(11)
C17-H17A	1.091(14)	C12-C13	1.395(10)
C17-H17B	1.084(10)	C13-C14	1.395(12)
H3-C3	1.094(6)	C14-C15	1.395(12)
H4-C4	1.087(7)	C15-C16	1.395(12)

Table of Bond Angles in Degrees

C8-O2-C5	119.2(8)	H3-C3-C4	120.4(6)
O1-C1-C9	121.1(10)	C2-C3-C4	120.0(6)
O1-C1-C2	120.1(9)	H4-C4-C3	119.0(6)
C9-C1-C2	118.8(8)	H4-C4-C5	121.0(6)
O2-C8-H8C	111.7(11)	C3-C4-C5	120.0(6)
O2-C8-H8A	110.9(11)	O2-C5-C4	116.2(7)
O2-C8-H8B	112.2(8)	O2-C5-C6	123.8(7)
H8C-C8-H8A	107.1(9)	C4-C5-C6	120.0(5)
H8C-C8-H8B	107.4(11)	H6-C6-C5	119.6(6)
H8A-C8-H8B	107.4(12)	H6-C6-C7	120.4(6)
C1-C9-C10	114.5(9)	C5-C6-C7	120.0(6)
C1-C9-H9A	111.1(10)	H7-C7-C2	119.7(6)
C1-C9-H9B	111.4(9)	H7-C7-C6	120.3(6)
C10-C9-H9A	105.5(9)	C2-C7-C6	120.0(6)
C10-C9-H9B	107.8(10)	C10-C11-C12	121.7(8)
H9A-C9-H9B	106.0(9)	C10-C11-C16	118.3(7)
C9-C10-C17	109.1(10)	C12-C11-C16	120.0(6)
C9-C10-H10	109.4(10)	H12-C12-C11	119.7(7)
C9-C10-C11	112.1(8)	H12-C12-C13	120.3(7)
C17-C10-H10	106.9(9)	C11-C12-C13	120.0(7)
C17-C10-C11	110.1(9)	H13-C13-C12	118.6(7)
H10-C10-C11	109.0(9)	H13-C13-C14	121.4(7)
C10-C17-H17C	111.8(11)	C12-C13-C14	120.0(7)
C10-C17-H17A	107.8(9)	H14-C14-C13	117.7(8)
C10-C17-H17B	110.2(10)	H14-C14-C15	122.3(8)
H17C-C17-H17A	109.0(11)	C13-C14-C15	120.0(6)
H17C-C17-H17B	109.6(9)	H15-C15-C14	118.1(8)
H17A-C17-H17B	108.3(11)	H15-C15-C16	121.9(8)
C1-C2-C3	118.5(6)	C14-C15-C16	120.0(7)
C1-C2-C7	121.5(7)	H16-C16-C11	120.7(7)
C3-C2-C7	120.0(5)	H16-C16-C15	119.3(7)
H3-C3-C2	119.6(6)	C11-C16-C15	120.0(7)

1 Torsion angles

C5	O2	C8	H8C	179.3(14)	C5	O2	C8	H8A	-61.4(8)
C5	O2	C8	H8B	58.7(7)	C8	O2	C5	C4	-171.3(10)
C8	O2	C5	C6	7.4(6)	O1	C1	C9	C10	12.6(6)
O1	C1	C9	H9A	132.0(14)	O1	C1	C9	H9B	-110.1(13)
C2	C1	C9	C10	-169.4(12)	C2	C1	C9	H9A	-50.0(6)
C2	C1	C9	H9B	67.9(8)	O1	C1	C2	C3	-11.5(5)
O1	C1	C2	C7	171.4(11)	C9	C1	C2	C3	170.5(11)
C9	C1	C2	C7	-6.6(5)	C1	C9	C10	C17	-169.7(14)
C1	C9	C10	H10	-53.1(8)	C1	C9	C10	C11	68.0(8)
H9A	C9	C10	C17	67.8(9)	H9A	C9	C10	H10	-175.6(17)
H9A	C9	C10	C11	-54.5(7)	H9B	C9	C10	C17	-45.2(7)
H9B	C9	C10	H10	71.5(10)	H9B	C9	C10	C11	-167.5(15)
C9	C10	C17	H17C	178.6(16)	C9	C10	C17	H17A	-61.6(9)
C9	C10	C17	H17B	56.5(9)	H10	C10	C17	H17C	60.4(9)
H10	C10	C17	H17A	-179.8(17)	H10	C10	C17	H17B	-61.7(9)
C11	C10	C17	H17C	-57.9(8)	C11	C10	C17	H17A	61.9(8)
C11	C10	C17	H17B	180.0(15)	C9	C10	C11	C12	53.9(7)
C9	C10	C11	C16	-127.8(11)	C17	C10	C11	C12	-67.9(8)
C17	C10	C11	C16	110.5(10)	H10	C10	C11	C12	175.1(13)
H10	C10	C11	C16	-6.5(4)	C1	C2	C3	H3	2.8(4)
C1	C2	C3	C4	-177.2(9)	C7	C2	C3	H3	180.0(9)
C7	C2	C3	C4	0.0(4)	C1	C2	C7	H7	-2.9(4)
C1	C2	C7	C6	177.1(8)	C3	C2	C7	H7	180.0(9)
C3	C2	C7	C6	0.0(4)	H3	C3	C4	H4	0.2(0)
H3	C3	C4	C5	-180.0(9)	C2	C3	C4	H4	-179.9(9)
C2	C3	C4	C5	0.0(4)	H4	C4	C5	O2	-1.4(3)
H4	C4	C5	C6	179.9(9)	C3	C4	C5	O2	178.7(9)
C3	C4	C5	C6	0.0(4)	O2	C5	C6	H6	1.6(3)
O2	C5	C6	C7	-178.6(9)	C4	C5	C6	H6	-179.8(9)
C4	C5	C6	C7	0.0(4)	H6	C6	C7	H7	-0.2(0)
H6	C6	C7	C2	179.8(9)	C5	C6	C7	H7	-180.0(9)
C5	C6	C7	C2	0.0(4)	C10	C11	C12	H12	-0.4(5)
C10	C11	C12	C13	178.3(10)	C16	C11	C12	H12	-178.7(10)
C16	C11	C12	C13	0.0(4)	C10	C11	C16	H16	2.2(5)
C10	C11	C16	C15	-178.4(10)	C12	C11	C16	H16	-179.5(10)
C12	C11	C16	C15	0.0(4)	H12	C12	C13	H13	-0.8(0)
H12	C12	C13	C14	178.6(10)	C11	C12	C13	H13	-179.4(10)
C11	C12	C13	C14	0.0(4)	H13	C13	C14	H14	-1.3(0)
H13	C13	C14	C15	179.4(11)	C12	C13	C14	H14	179.3(11)
C12	C13	C14	C15	0.0(4)	H14	C14	C15	H15	-0.5(0)
H14	C14	C15	C16	-179.3(11)	C13	C14	C15	H15	178.7(11)
C13	C14	C15	C16	0.0(4)	H15	C15	C16	H16	0.8(0)
H15	C15	C16	C11	-178.7(11)	C14	C15	C16	H16	179.5(11)
C14	C15	C16	C11	0.0(4)					

1 Table . Distances(A) to the least-squares planes.

Plane no. 1

Equation of the plane :- 6.492(14)X + 12.51(8)Y + 2.447(15)Z = 9.28(4)

Distances(A) to the plane from the atoms in the plane.

C2	0.000(8)	C3	0.000(9)
C4	0.000(9)	C5	0.000(9)
C6	0.000(8)	C7	0.000(8)

Chi squared for this plane 0.000

Plane no. 2

Equation of the plane : 3.830(25)X + 22.69(8)Y + 2.812(17)Z = 19.24(4)

Distances(A) to the plane from the atoms in the plane.

C11	0.000(10)	C12	0.000(9)
C13	0.000(10)	C14	0.000(12)
C15	0.000(11)	C16	0.000(10)

Chi squared for this plane 0.000

1 Dihedral angle between planes A and B

A	B	Angle(deg)
1	2	83.2(3)

BIVOET -- Best Measurable Bijvoet Differences

This routine selects reflections for which the Bijvoet difference is
MOST significant, i.e. (Fc+ - Fc-)/Sigma(Fo) is largest.
If Fo- is available (Fc+ - Fc-) is compared to (Fo+ - Fo-).
Before running the routine Structure Factors must be calculated with :--
(1) A refined structure
(2) The dispersion flag "Yes" for all atoms
(3) An ETA parameter of 1.0.
If this has not been done, abort the run by requesting 0 reflections.

	h	k	l	Fc+		Fc-	Del/Sig	Fo+		Fo-	Sense
1	1	2	1	35.428	<	35.445	-0.142	31.326	>	30.104	-
2	2	5	1	35.330	<	35.348	-0.136	33.996	>	32.974	-
3	2	1	1	29.991	>	29.973	0.129	28.540	>	28.460	+
4	1	5	2	29.998	<	30.017	-0.126	31.189	>	29.228	-
5	1	7	1	24.883	>	24.869	0.116	24.123	>	22.664	+
6	1	2	2	9.470	<	9.490	-0.106	8.953	>	6.820	-
7	2	6	1	25.956	<	25.969	-0.093	26.046	>	24.835	-
8	2	7	1	28.106	<	28.119	-0.091	28.436	>	27.378	-
9	1	4	1	25.826	<	25.837	-0.090	24.929	>	23.784	-
10	1	1	1	24.758	<	24.770	-0.090	21.395	>	19.724	-
11	1	1	2	11.392	>	11.374	0.090	7.251	>	5.799	+
12	1	6	1	44.885	<	44.894	-0.082	44.300	>	42.181	-
13	2	4	1	67.402	>	67.393	0.074	64.754	>	62.372	+
14	1	8	1	23.194	<	23.204	-0.069	22.165	>	21.620	-
15	2	2	1	34.933	>	34.926	0.068	34.710	>	33.305	+
16	1	10	2	20.317	>	20.306	0.060	21.048	>	19.848	+
17	2	11	1	27.459	>	27.449	0.059	27.944	>	27.318	+
18	2	12	1	19.606	>	19.595	0.058	19.811	>	19.544	+
19	3	4	2	22.720	>	22.709	0.055	24.365	>	23.267	+
20	1	15	1	6.575	>	6.562	0.055	7.326	<	9.245	-
21	1	5	1	4.317	<	4.327	-0.052	3.960	>	3.375	-
22	1	4	2	10.037	>	10.025	0.052	10.176	>	7.022	+
23	1	11	1	7.111	>	7.100	0.051	6.629	>	5.816	+
24	3	8	2	15.587	<	15.599	-0.050	14.912	>	14.705	-
25	3	2	1	21.112	<	21.120	-0.047	21.640	>	20.873	-
26	1	11	2	12.381	>	12.370	0.047	12.794	>	10.412	+
27	2	8	1	30.582	<	30.589	-0.047	30.036	>	28.899	-
28	2	6	2	12.888	>	12.878	0.044	13.706	>	10.710	+
29	1	17	2	6.486	<	6.496	-0.042	6.393	<	6.524	+
30	2	8	2	13.378	>	13.369	0.040	14.808	>	12.658	+
31	3	11	2	9.959	>	9.948	0.039	11.401	>	9.727	+
32	3	2	2	4.479	<	4.489	-0.038	3.948	>	3.740	-
33	2	14	1	6.975	>	6.966	0.038	6.380	<	6.481	-
34	1	3	1	79.104	>	79.100	0.037	72.541	>	69.711	+
35	2	10	1	17.894	<	17.900	-0.036	16.751	>	16.120	-
36	1	8	3	12.076	>	12.067	0.036	14.806	>	12.514	+
37	1	7	3	13.087	>	13.079	0.036	15.082	>	12.437	+
38	3	12	1	16.387	>	16.380	0.033	17.047	>	16.512	+
39	4	13	2	5.305	>	5.296	0.033	5.876	>	5.130	+
40	5	1	1	17.616	>	17.609	0.033	18.511	<	19.046	-
41	4	7	1	28.105	>	28.099	0.032	28.655	>	28.290	+
42	2	12	2	13.206	<	13.214	-0.031	14.687	>	13.416	-
43	1	8	2	22.268	>	22.263	0.031	25.035	>	23.485	+
44	3	18	1	12.574	<	12.584	-0.031	12.060	>	10.871	-
45	3	14	1	11.373	>	11.364	0.031	11.438	>	11.068	+
46	3	10	1	14.923	>	14.916	0.031	14.870	>	14.152	+
47	3	1	2	10.621	>	10.615	0.031	9.281	<	10.113	-

48	4	11	1	13.198	<	13.206	-0.030	13.836	<	14.169	+	
49	1	13	1	18.871	>	18.865	0.029	18.698	<	20.007		-
50	4	1	2	7.074	>	7.066	0.029	7.496	>	7.473	+	
51	3	9	2	8.269	>	8.261	0.028	8.761	>	7.031	+	
52	1	5	3	6.280	<	6.287	-0.028	7.403	>	5.564		-
53	3	7	2	14.152	<	14.159	-0.028	14.549	>	12.255		-
54	1	13	3	8.466	<	8.473	-0.027	8.916	<	9.160	+	
55	3	5	1	27.700	<	27.704	-0.027	27.771	>	27.284		-
56	1	19	1	19.942	>	19.935	0.027	19.534	>	19.394	+	
57	3	2	3	4.201	<	4.210	-0.027	3.905	<	4.515	+	
58	3	7	1	31.181	>	31.177	0.027	32.218	>	31.740	+	
59	4	2	1	12.178	>	12.172	0.027	13.115	<	13.365		-
60	6	6	2	6.657	<	6.664	-0.026	8.133	>	7.546		-
61	2	4	2	14.974	>	14.969	0.026	13.753	>	12.128	+	
62	5	5	1	7.205	>	7.199	0.025	7.711	>	7.580	+	
63	1	6	2	10.192	>	10.187	0.025	11.112	>	9.461	+	
64	2	11	2	23.716	>	23.712	0.025	23.244	>	22.351	+	
65	4	15	2	6.599	<	6.605	-0.025	6.683	>	5.882		-
66	2	16	1	5.051	<	5.063	-0.024	3.391	<	4.154	+	
67	3	4	1	31.975	<	31.979	-0.024	32.879	>	32.064		-
68	6	4	1	5.867	>	5.861	0.024	5.714	>	5.259	+	
69	3	6	1	29.509	<	29.513	-0.024	29.160	>	28.674		-
70	4	1	3	5.398	>	5.390	0.023	5.841	>	4.796	+	
71	1	4	3	13.483	<	13.488	-0.023	14.349	>	10.749		-
72	4	8	1	9.458	<	9.465	-0.023	8.679	<	8.811	+	
73	1	9	2	6.458	<	6.463	-0.023	5.949	>	4.044		-
74	1	18	2	2.499	<	2.507	-0.023	6.556	>	4.976		-
75	2	16	2	12.415	>	12.409	0.023	10.292	<	11.342		-
76	1	12	3	7.059	<	7.065	-0.022	5.892	<	6.796	+	
77	2	3	4	8.423	>	8.416	0.021	6.656	<	6.829		-
78	6	8	1	5.703	>	5.697	0.021	6.224	>	5.724	+	
79	1	20	2	4.872	>	4.862	0.021	5.416	<	7.646		-
80	2	20	1	8.137	>	8.130	0.021	7.511	<	8.749		-
81	2	1	3	11.181	>	11.175	0.021	8.432	<	8.494		-
82	3	18	2	11.940	<	11.947	-0.021	9.335	>	8.827		-
83	4	3	1	1.694	>	1.685	0.020	2.844	>	0.384	+	
84	3	6	3	5.875	<	5.880	-0.020	5.186	>	5.037		-
85	3	5	2	19.458	>	19.454	0.020	19.554	>	19.163	+	
86	2	26	1	7.391	<	7.398	-0.020	6.913	<	7.564	+	
87	1	17	1	19.073	>	19.069	0.020	21.184	<	21.913		-
88	5	3	1	5.662	<	5.667	-0.020	5.532	>	5.025		-
89	1	18	3	6.087	<	6.093	-0.020	6.643	>	6.116		-
90	3	5	3	5.974	>	5.969	0.019	5.209	<	6.089		-
91	4	3	3	3.672	<	3.679	-0.019	3.735	>	3.718		-
92	2	3	1	13.625	<	13.628	-0.018	14.228	>	13.717		-
93	3	10	2	7.152	<	7.157	-0.018	8.496	>	7.224		-
94	1	21	1	1.731	<	1.738	-0.018	8.583	>	5.123		-
95	2	7	3	4.235	>	4.230	0.018	4.516	>	4.436	+	
96	1	10	3	7.659	>	7.652	0.018	8.158	<	8.786		-
97	1	9	1	22.922	<	22.924	-0.018	21.833	>	21.227		-
98	3	22	1	9.073	>	9.067	0.018	6.753	>	6.459	+	
99	1	22	1	5.855	<	5.860	-0.018	5.627	<	5.708	+	
100	2	2	3	18.156	<	18.161	-0.018	16.407	>	12.309		-
101	2	19	1	13.277	>	13.272	0.018	13.644	<	14.730		-
102	1	21	2	7.552	<	7.558	-0.017	7.763	>	7.431		-
103	1	3	2	6.099	>	6.096	0.017	5.188	>	4.547	+	
104	1	2	4	8.176	<	8.181	-0.017	7.878	>	6.929		-
105	1	12	1	6.760	>	6.753	0.017	4.967	<	7.565		-
106	1	14	3	5.058	<	5.063	-0.017	5.753	<	6.515	+	
107	4	6	3	5.239	>	5.234	0.017	5.820	>	5.567	+	

108	2	9	4	2.959	<	2.969	-0.017	3.342	>	3.321		-
109	5	13	1	4.298	<	4.304	-0.017	4.470	>	2.658		-
110	2	1	4	7.484	>	7.478	0.017	5.392	<	5.398		-
111	2	22	2	7.756	>	7.751	0.017	7.816	>	7.540	+	
112	2	14	2	12.322	<	12.326	-0.016	13.419	>	11.972		-
113	4	19	1	5.730	<	5.734	-0.016	6.175	>	5.472		-
114	1	24	1	5.045	<	5.050	-0.016	6.361	>	5.754		-
115	1	18	1	5.221	<	5.225	-0.016	12.828	>	12.663		-
116	1	13	2	18.803	<	18.807	-0.016	21.543	<	22.030	+	
117	6	2	2	5.598	<	5.603	-0.016	5.836	<	5.875	+	
118	6	7	1	5.295	>	5.290	0.015	5.867	>	5.559	+	
119	4	13	1	6.107	<	6.111	-0.015	5.847	<	6.105	+	
120	3	20	2	13.399	>	13.394	0.015	13.148	>	11.685	+	
121	4	16	1	6.209	>	6.205	0.015	7.093	>	7.076	+	
122	4	14	1	4.557	>	4.550	0.015	3.764	<	4.083		-
123	3	9	1	26.023	<	26.026	-0.015	26.931	>	26.480		-
124	5	1	2	10.397	>	10.393	0.015	10.837	<	10.912		-
125	1	7	2	25.007	>	25.004	0.015	26.130	>	24.512	+	
126	4	4	1	19.181	>	19.178	0.015	21.791	<	21.878		-
127	2	6	5	5.940	>	5.936	0.015	6.700	<	6.919		-
128	4	5	1	15.176	>	15.173	0.015	15.217	>	14.821	+	
129	3	28	1	7.437	<	7.442	-0.014	6.785	<	6.865	+	
130	4	7	2	17.243	>	17.240	0.014	18.711	>	17.835	+	
131	2	9	1	12.893	>	12.890	0.014	12.751	>	11.913	+	
132	2	3	2	16.341	<	16.344	-0.014	16.102	>	13.498		-
133	2	6	3	3.769	<	3.773	-0.014	4.467	<	4.542	+	
134	3	4	3	7.473	>	7.469	0.014	6.302	<	6.428		-
135	1	23	2	11.619	<	11.624	-0.014	10.072	>	9.302		-
136	1	12	2	7.888	<	7.895	-0.014	4.953	<	9.133	+	
137	3	3	4	7.157	>	7.153	0.013	7.239	>	6.516	+	
138	2	9	3	5.652	>	5.649	0.013	5.630	>	4.625	+	
139	1	17	3	3.084	>	3.079	0.013	5.362	>	1.854	+	
140	3	22	3	4.227	<	4.232	-0.013	5.241	>	4.964		-
141	3	12	2	9.283	>	9.279	0.013	10.141	>	9.020	+	
142	3	8	3	5.178	<	5.181	-0.013	4.919	<	5.344	+	
143	2	12	3	8.206	<	8.209	-0.013	8.641	>	7.231		-
144	3	8	1	3.613	>	3.609	0.013	4.009	>	3.150	+	
145	2	5	3	3.058	<	3.062	-0.013	4.013	<	4.080	+	
146	1	15	2	10.000	<	10.004	-0.013	9.308	<	11.291	+	
147	2	15	1	11.479	<	11.483	-0.013	11.428	>	10.812		-
148	6	4	3	5.918	>	5.915	0.013	7.254	>	6.884	+	
149	3	16	3	10.165	>	10.160	0.013	8.370	>	8.003	+	
150	2	22	1	3.885	<	3.888	-0.013	5.996	<	7.343	+	
151	4	4	2	7.775	<	7.778	-0.013	8.759	>	7.520		-
152	5	11	2	9.128	<	9.132	-0.012	8.923	>	7.858		-
153	5	7	3	5.545	>	5.541	0.012	5.920	>	5.841	+	
154	2	2	2	15.322	>	15.319	0.012	12.474	>	10.823	+	
155	1	25	3	7.199	>	7.195	0.012	7.841	>	7.009	+	
156	1	19	3	5.476	>	5.472	0.012	6.196	<	6.944		-
157	5	7	1	19.316	<	19.319	-0.012	19.157	<	19.203	+	
158	3	4	4	7.457	<	7.461	-0.012	6.809	<	6.822	+	
159	2	5	4	7.326	>	7.322	0.012	7.701	>	6.973	+	
160	2	7	2	32.065	<	32.067	-0.012	34.691	>	32.244		-
161	7	3	1	7.236	<	7.240	-0.012	8.263	>	8.018		-
162	5	16	1	11.736	>	11.732	0.012	11.599	<	11.932		-
163	4	9	1	19.600	<	19.603	-0.012	20.013	>	19.617		-
164	4	5	2	6.345	>	6.343	0.012	6.155	>	5.949	+	
165	4	11	3	5.145	<	5.149	-0.012	4.961	<	5.380	+	
166	5	3	2	5.933	<	5.936	-0.012	6.004	<	6.234	+	
167	3	3	1	12.506	>	12.503	0.011	11.810	>	11.129	+	

168	5	11	1	2.406	>	2.400	0.011	3.320	>	2.069	+	
169	3	1	3	8.833	<	8.836	-0.011	6.475	<	6.728	+	
170	6	10	2	9.758	>	9.755	0.011	9.654	>	9.650	+	
171	6	4	2	2.523	>	2.517	0.011	3.102	<	3.185		-
172	4	6	1	17.795	<	17.797	-0.011	18.560	<	18.847	+	
173	3	7	4	4.191	<	4.195	-0.011	5.446	>	4.339		-
174	4	24	2	6.679	>	6.675	0.011	6.586	>	6.226	+	
175	3	15	2	5.393	<	5.396	-0.011	4.821	>	4.699		-
176	2	21	2	4.990	<	4.994	-0.011	5.763	<	6.227	+	
177	2	10	2	5.715	>	5.712	0.011	5.843	>	5.423	+	
178	4	15	3	9.170	<	9.173	-0.011	10.316	>	8.091		-
179	1	5	5	3.271	>	3.267	0.011	5.706	>	5.450	+	
180	4	8	2	10.389	>	10.386	0.010	9.854	>	8.984	+	
181	1	14	2	7.600	>	7.596	0.010	4.926	<	8.721		-
182	3	16	1	8.693	>	8.690	0.010	8.891	>	8.351	+	
183	6	14	1	6.420	<	6.423	-0.010	7.014	>	7.005		-
184	5	8	2	4.550	<	4.553	-0.010	4.689	>	4.688		-
185	4	18	2	9.041	<	9.044	-0.010	7.728	>	7.669		-
186	4	5	3	6.385	<	6.388	-0.009	6.605	>	6.116		-
187	3	24	1	4.942	>	4.936	0.009	3.914	<	5.725		-
188	4	10	2	5.879	>	5.877	0.009	6.050	>	5.848	+	
189	3	2	4	13.146	<	13.149	-0.009	9.866	<	9.869	+	
190	1	26	2	10.446	>	10.443	0.009	9.116	>	8.652	+	
191	1	6	3	18.058	>	18.056	0.009	20.206	>	16.847	+	
192	4	2	2	9.161	>	9.158	0.009	9.785	>	8.789	+	
193	4	19	2	8.852	>	8.850	0.009	8.867	>	7.444	+	
194	2	13	3	8.557	<	8.560	-0.009	7.986	>	7.254		-
195	6	2	1	11.106	<	11.108	-0.009	12.122	>	11.774		-
196	4	9	2	15.731	<	15.733	-0.009	16.138	>	15.417		-
197	4	2	3	6.796	<	6.798	-0.009	6.346	>	6.198		-
198	3	24	3	5.796	>	5.793	0.008	6.693	<	7.092		-
199	2	28	1	3.784	>	3.781	0.008	6.149	<	6.233		-
200	5	10	1	9.184	<	9.187	-0.008	8.910	<	9.254	+	

Out of 200 TOTAL measurements, (Fo+ - Fo-) has the SAME sign as (Fc+ - Fc-) in 103 cases and the OPPOSITE sign in 97 cases.

Cumulative Binomial Distribution

The Absolute Structure of the Model is CONFIRMED
Based on 200 Measurements, 103 of which Support the Model
The Probability that the Above Statement is WRONG is 0.3619E+00

Columns are 10Fo 10Fc 1000Sig, * for Insignificant

l	kFo	Fc	Sig
	0, 0, 1		
2	276	351	216
4	91	87	274
6	49	46	507
	0, 1, 1		
1	223	209	82
2	154	128	148
4	49	54	239
	0, 2, 1		
1	327	336	74
2	85	96	171
3	52	43	166
4	77	91	222
5	161	137	304
	0, 3, 1		
1	417	424	73
2	29	10	205
3	116	96	213
4	95	105	238
5	112	105	289
6	47	33	400
	0, 4, 1		
0	21	17	205
1	551	513	77
2	41	32	137
3	49	62	159
4	46	42	223
6	43	28	501
	0, 5, 1		
1	637	645	80
2	210	203	109
3	125	123	171
4	55	56	202
5	79	57	269
	0, 6, 1		
0	273	253	90
1	276	254	103
2	413	376	111
3	34	21	279
5	46	45	310
	0, 7, 1		
1	621	616	86
2	230	210	127
3	272	223	156
4	71	51	203
5	74	48	248
6	59	28	345
	0, 8, 1		
0	232	221	112
1	307	153	110
2	228	216	131
3	202	171	150
4	32	3	358
	0, 9, 1		
1	94	69	138
2	92	111	173
3	79	69	186
	0, 10, 1		
0	465	457	114
1	227	218	132
2	290	265	130
3	134	105	172
5	39	22	411
	0, 11, 1		
1	387	360	119
2	107	94	191
3	44	44	255
5	57	33	237
	0, 12, 1		
0	262	267	140
1	258	136	178
2	74	60	220
3	46	45	197
4	42	9	278
5	31	4	545
	0, 13, 1		
1	40	68	511
2	125	68	219
3	82	75	173
4	54	31	274
5	58	45	246
	0, 14, 1		
0	216	215	169
1	146	132	185
2	199	205	175
4	87	70	193
5	52	29	279
	0, 15, 1		
1	34	40	591
2	159	120	215
3	26	8	470
5	33	25	495
	0, 16, 1		
0	578	614	158
1	69	84	155
2	75	29	295
3	45	27	293
4	29	28	488
	0, 17, 1		
2	48	33	209
3	67	79	177
4	37	45	401
5	35	6	590
	0, 18, 1		
1	72	114	241
1	68	91	196
5	39	25	562
	0, 19, 1		
2	77	81	167
5	39	15	465
	0, 20, 1		
1	56	84	314
	0, 21, 1		
2	66	80	268
3	41	28	349
	0, 22, 1		
0	76	60	220
2	87	136	242
3	89	106	213
	0, 23, 1		
2	66	66	347
3	89	99	290
	0, 24, 1		
3	94	90	251
	0, 25, 1		
2	61	58	288
4	58	64	270
	0, 26, 1		
1	72	92	192
3	80	78	220
4	36	26	693
	0, 27, 1		
4	33	27	533
	0, 28, 1		
0	35	44	466
3	49	42	329
	0, 29, 1		
3	41	47	480
	0, 30, 1		
1	34	36	591
	0, 32, 1		
1	51	58	284
	1, 0, 1		
1	911	1203	140
2	107	134	248
3	46	44	253
4	69	83	286
	1, 1, 1		
0	91	95	101
1	214	248	137
2	73	114	205
3	55	50	291
4	102	107	269
5	84	73	368
6	42	23	589
	1, 2, 1		
0	480	491	70
1	313	354	120
2	90	95	182
3	104	97	220
4	79	82	280
5	79	71	398
6	69	45	381
	1, 3, 1		
0	181	182	88
1	725	791	108
2	52	61	214
3	72	78	235
4	55	64	287
5	105	85	345
6	37	19	595
	1, 4, 1		
0	575	577	79
1	249	258	119
2	102	100	220
3	143	135	243
4	76	67	249
5	61	44	342
6	44	26	662
	1, 5, 1		
0	375	369	89
1	40	43	190
2	312	300	150
3	74	63	247
4	87	78	245
5	57	33	336
6	51	26	455
	1, 6, 1		
0	348	355	98
1	443	449	109
2	111	102	222
3	202	181	206
4	78	77	233
5	57	41	333
6	59	34	505
	1, 7, 1		
0	498	502	99
1	241	249	126
2	261	250	156
3	151	131	236
5	38	14	635
6	36	21	605
	1, 8, 1		
0	279	275	115
1	222	232	133
2	250	223	159
3	148	121	232
4	31	34	484

Columns are 10Fo 10Fc 1000Sig, * for Insignificant

l	kFo	Fc	Sig
	1, 8, 1		
5	69	47	385
	1, 9, 1		
0	374	381	116
1	218	229	137
2	59	65	203
3	83	65	272
5	60	38	331
6	48	28	582
	1, 10, 1		
0	158	147	157
1	83	89	234
2	210	203	179
3	82	77	349
4	65	55	270
5	42	34	581
	1, 11, 1		
0	240	248	158
1	66	71	219
2	128	124	244
3	151	144	259
4	59	54	295
5	35	23	677
6	36	11	723
	1, 12, 1		
0	175	200	233
1	50	68	419
2	50	79	528
3	59	71	280
4	56	39	288
5	49	38	391
	1, 13, 1		
0	210	232	221
1	187	189	204
2	215	188	201
3	89	85	256
	1, 14, 1		
0	271	291	212
1	86	123	422
2	49	76	398
3	58	51	264
4	52	40	414
	1, 15, 1		
0	45	39	739
1	73	66	243
2	93	100	286
3	58	44	250
4	61	57	289
	1, 16, 1		
0	172	177	201
1	183	159	215
2	59	40	261

l	kFo	Fc	Sig
5	42	19	597
	1, 17, 1		
0	154	133	227
1	212	191	212
2	64	65	231
3	54	31	346
5	45	36	458
	1, 18, 1		
0	154	130	226
1	128	52	288
2	66	25	368
3	66	61	278
4	39	24	462
	1, 19, 1		
0	75	54	258
1	195	199	226
2	77	64	242
3	62	55	318
4	38	28	481
	1, 20, 1		
0	82	64	224
1	142	131	238
2	54	49	436
3	64	62	302
	1, 21, 1		
0	57	35	282
1	86	17	370
2	78	76	316
3	78	56	434
	1, 22, 1		
0	47	37	384
1	56	59	274
2	96	105	311
3	76	78	286
	1, 23, 1		
0	46	45	440
1	61	48	290
2	101	116	344
3	50	25	526
	1, 24, 1		
0	74	69	240
1	64	50	277
2	133	145	351
3	72	56	404
	1, 25, 1		
0	63	30	367
1	63	52	352
2	99	71	553
3	78	72	316
	1, 26, 1		
1	44	31	499
2	91	104	338

l	kFo	Fc	Sig
3	51	27	560
	1, 27, 1		
1	33	39	526
2	75	51	408
3	62	51	373
	1, 28, 1		
3	46	44	604
	1, 29, 1		
0	72	80	287
1	41	42	614
	1, 30, 1		
0	67	27	391
	1, 32, 1		
0	59	60	357
	1, 33, 1		
1	42	36	474
	2, 0, 1		
0	296	278	147
1	203	221	147
2	122	168	232
3	83	125	310
5	70	89	417
	2, 1, 1		
0	235	250	112
1	285	300	136
2	175	211	231
3	84	112	278
4	54	75	348
5	83	93	381
	2, 2, 1		
0	576	580	98
1	347	349	131
2	125	153	212
3	164	182	299
4	46	68	427
	2, 3, 1		
0	1182	1244	97
1	142	136	167
2	161	163	212
4	67	84	303
	2, 4, 1		
0	620	626	103
1	648	674	124
2	138	150	216
3	214	205	240
4	55	44	304
	2, 5, 1		
0	455	470	108
1	340	353	132
2	51	50	198
3	40	31	306
4	77	73	306

l	kFo	Fc	Sig
5	50	42	387
	2, 6, 1		
0	483	473	112
1	260	260	138
2	137	129	227
3	45	38	271
5	67	59	308
	2, 7, 1		
0	268	268	127
1	284	281	137
2	347	321	171
3	45	42	264
4	79	74	290
6	38	19	586
	2, 8, 1		
0	130	110	169
1	300	306	141
2	148	134	218
4	68	53	270
	2, 9, 1		
0	274	289	137
1	128	129	203
2	140	142	219
3	56	57	230
4	33	30	568
	2, 10, 1		
0	103	92	220
1	168	179	183
2	58	57	225
3	45	42	286
4	43	30	488
	2, 11, 1		
0	200	221	163
1	279	275	160
2	232	237	192
3	56	64	247
4	69	65	253
5	52	38	402
	2, 12, 1		
0	43	58	279
1	198	196	185
2	147	132	232
3	86	82	268
	2, 13, 1		
0	317	313	164
3	80	86	297
	2, 14, 1		
0	214	202	191
1	64	70	226
2	134	123	249
3	111	109	327
5	39	26	539

Columns are 10Fo 10Fc 1000Sig, * for Insignificant

l	kFo	Fc	Sig
	2, 15, 1		
0	45	48	267
1	114	115	258
5	38	24	559
	2, 16, 1		
0	54	60	209
1	34	51	457
2	103	124	273
3	32	32	550
4	40	53	758
5	41	34	680
	2, 17, 1		
2	67	67	325
3	43	46	472
4	102	87	308
5	48	25	445
	2, 18, 1		
0	61	25	418
1	86	73	282
3	110	101	328
	2, 19, 1		
0	188	203	233
1	136	133	300
2	49	37	412
3	48	44	548
4	46	26	515
	2, 20, 1		
0	93	105	333
1	75	81	345
2	66	54	278
3	91	77	298
	2, 21, 1		
0	67	32	361
1	63	62	286
2	58	50	350
3	73	59	292
	2, 22, 1		
0	54	71	276
1	60	39	298
2	78	78	281
3	64	49	312
	2, 23, 1		
0	63	19	362
1	67	58	268
2	81	48	305
3	42	30	577
4	33	17	583
	2, 24, 1		
0	76	72	251
1	69	67	312
2	108	99	352
3	43	17	566

l	kFo	Fc	Sig
	2, 25, 1		
0	65	52	327
1	71	75	321
2	81	77	322
3	54	34	480
	2, 26, 1		
0	46	8	485
1	69	74	324
2	62	54	355
3	38	35	728
	2, 27, 1		
1	56	29	434
2	51	44	390
3	48	29	548
	2, 28, 1		
1	61	38	329
3	39	39	545
	2, 29, 1		
0	37	21	644
1	81	83	297
	2, 30, 1		
0	42	54	618
1	65	19	414
	2, 31, 1		
0	41	5	628
	2, 32, 1		
0	36	27	571
	3, 0, 1		
1	225	228	159
2	72	71	242
3	46	49	347
4	80	103	321
	3, 1, 1		
0	111	121	186
1	149	157	179
2	93	106	225
3	65	88	303
4	35	46	644
	3, 2, 1		
0	226	221	140
1	216	211	157
2	39	45	256
3	39	42	341
4	99	131	331
	3, 3, 1		
0	89	94	222
1	118	125	208
2	65	69	217
3	63	69	272
4	72	72	310
	3, 4, 1		
0	35	38	246

l	kFo	Fc	Sig
1	329	320	147
2	244	227	201
3	63	75	305
4	68	75	310
	3, 5, 1		
0	87	70	234
1	278	277	156
2	196	195	220
3	52	60	283
4	83	78	303
	3, 6, 1		
0	53	54	185
1	292	295	156
2	158	147	225
3	52	59	265
	3, 7, 1		
0	277	278	149
1	322	312	158
2	145	142	232
4	54	42	305
	3, 8, 1		
0	241	234	160
1	40	36	285
2	149	156	236
3	49	52	281
	3, 9, 1		
0	72	94	209
1	269	260	172
2	88	83	259
4	50	43	331
5	49	41	431
	3, 10, 1		
0	121	116	236
1	149	149	218
2	85	72	256
3	42	42	425
	3, 11, 1		
0	299	287	170
1	82	71	226
2	114	100	275
	3, 12, 1		
0	131	121	253
1	170	164	211
2	101	93	300
	3, 13, 1		
0	30	31	394
1	103	93	275
2	63	62	216
4	64	56	401
	3, 14, 1		
0	114	121	264
1	114	114	274

l	kFo	Fc	Sig
3	75	74	290
4	83	69	309
	3, 15, 1		
0	44	45	271
1	151	142	243
2	48	54	292
3	77	77	424
4	45	40	452
	3, 16, 1		
1	89	87	248
2	57	61	268
3	84	102	370
	3, 17, 1		
0	51	56	252
3	82	93	320
4	50	46	541
5	39	22	669
	3, 18, 1		
0	39	31	433
1	121	126	314
2	93	119	324
4	71	61	309
	3, 19, 1		
0	44	53	414
1	40	50	559
2	74	77	399
3	38	32	653
	3, 20, 1		
0	65	89	248
1	79	82	308
2	131	134	379
3	39	25	487
	3, 21, 1		
1	64	83	385
2	97	136	515
4	43	25	605
	3, 22, 1		
1	68	91	309
3	52	42	381
	3, 23, 1		
1	79	91	330
3	41	17	685
	3, 24, 1		
0	38	33	466
1	39	49	633
2	31	13	578
3	67	58	335
	3, 25, 1		
0	60	42	313
1	54	48	358
	3, 26, 1		
0	64	64	305

Columns are 10Fo 10Fc 1000Sig, * for Insignificant

l	kFo	Fc	Sig
	3, 27, 1		
0	51	27	465
1	67	23	358
	3, 28, 1		
0	43	29	436
1	68	74	309
2	49	34	520
	3, 29, 1		
0	57	32	353
1	62	41	454
2	39	41	689
	3, 30, 1		
1	47	43	586
	3, 32, 1		
0	43	35	615
	3, 33, 1		
0	41	13	651
	4, 0, 1		
0	213	216	249
1	129	131	232
2	60	68	233
3	58	66	258
4	56	54	418
	4, 1, 1		
0	111	106	239
1	166	158	203
2	75	71	264
3	58	54	312
	4, 2, 1		
0	174	167	191
1	131	122	229
2	98	92	299
3	63	68	264
	4, 3, 1		
0	156	147	197
1	28	17	435
3	37	37	374
4	42	52	444
5	37	24	652
	4, 4, 1		
0	72	59	228
1	218	192	187
2	88	78	270
3	45	51	411
4	62	77	333
	4, 5, 1		
0	71	61	221
1	152	152	221
2	62	63	230
3	66	64	283
4	61	60	333
	4, 6, 1		

l	kFo	Fc	Sig
0	262	268	176
1	186	178	207
2	63	62	235
3	58	52	283
	4, 7, 1		
0	316	300	174
1	287	281	184
2	187	172	235
3	48	55	316
4	49	36	347
	4, 8, 1		
0	39	52	327
1	87	95	283
2	99	104	278
	4, 9, 1		
0	76	62	244
1	200	196	208
2	161	157	256
3	53	50	380
	4, 10, 1		
0	127	128	246
1	92	91	266
2	61	59	249
	4, 11, 1		
1	138	132	259
2	102	100	277
3	50	51	346
4	44	26	397
	4, 12, 1		
0	186	190	218
2	38	34	494
3	85	78	267
	4, 13, 1		
0	97	102	262
1	58	61	232
2	59	53	258
3	54	44	429
4	61	55	347
	4, 14, 1		
1	38	46	443
2	36	34	544
	4, 15, 1		
0	82	67	253
2	67	66	253
3	103	92	303
4	40	36	695
	4, 16, 1		
1	71	62	244
2	70	74	264
4	55	41	524
	4, 17, 1		
1	59	58	289

l	kFo	Fc	Sig
2	59	68	343
3	53	55	529
4	45	41	489
	4, 18, 1		
0	52	39	289
1	76	81	294
2	77	90	357
3	71	66	301
	4, 19, 1		
1	62	57	304
2	89	89	293
4	48	41	506
	4, 20, 1		
3	43	34	471
4	46	39	495
	4, 21, 1		
1	59	60	327
	4, 22, 1		
3	49	52	438
	4, 23, 1		
0	40	45	508
1	48	65	406
	4, 24, 1		
2	66	67	333
	4, 25, 1		
1	36	15	647
	4, 26, 1		
2	44	20	464
	4, 27, 1		
0	41	32	537
2	61	54	358
	4, 28, 1		
0	42	49	583
2	41	33	533
	4, 29, 1		
1	49	43	434
	4, 30, 1		
1	44	42	634
	5, 0, 1		
2	59	53	253
	5, 1, 1		
0	133	123	251
1	185	176	232
2	108	104	269
4	39	37	471
	5, 2, 1		
0	47	62	271
1	109	93	301
2	37	36	370
3	53	48	407
	5, 3, 1		
0	35	32	350

l	kFo	Fc	Sig
1	55	57	239
2	60	59	250
4	40	40	481
	5, 4, 1		
0	122	114	255
1	110	98	282
2	89	94	298
3	65	70	357
4	49	47	553
	5, 5, 1		
1	77	72	239
2	48	50	319
3	76	76	307
4	77	72	362
	5, 6, 1		
0	43	49	288
2	67	68	245
3	91	95	301
4	66	58	355
	5, 7, 1		
1	192	193	240
2	125	116	332
3	59	55	322
	5, 8, 1		
0	46	41	279
1	66	72	238
2	47	46	347
3	68	55	279
4	45	47	475
	5, 9, 1		
0	54	53	253
1	125	125	286
2	92	87	285
3	71	72	289
	5, 10, 1		
0	77	61	240
1	89	92	303
2	59	48	284
3	101	96	289
	5, 11, 1		
0	29	12	560
1	33	24	528
2	89	91	273
3	77	68	279
	5, 12, 1		
2	101	112	340
3	55	49	362
	5, 13, 1		
0	90	95	250
1	45	43	336
2	87	86	262
3	60	56	437

Columns are 10Fo 10Fc 1000Sig, * for Insignificant

l	kFo	Fc	Sig
	5, 14, 1		
0	114	114	359
3	55	45	366
	5, 15, 1		
1	87	83	275
2	55	50	328
	5, 16, 1		
1	116	117	273
2	43	41	444
3	59	52	345
	5, 17, 1		
0	71	80	259
1	76	75	274
2	38	35	632
	5, 18, 1		
1	73	59	271
2	50	51	397
	5, 19, 1		
0	36	36	478
1	39	35	593
	5, 22, 1		
0	59	61	344
1	37	42	498
	5, 24, 1		
1	39	39	506
	5, 29, 1		
0	43	37	495
	6, 0, 1		
0	83	81	401
2	54	42	314
	6, 1, 1		
1	92	93	276
2	68	57	263
3	44	35	527
	6, 2, 1		
0	44	43	332
1	121	111	328
2	58	56	295
	6, 3, 1		
0	38	37	384
2	53	60	328
	6, 4, 1		
0	74	69	240
1	57	59	278
2	31	25	539
3	73	59	295
	6, 5, 1		
0	79	76	264
1	31	37	620
2	63	54	279
3	49	48	390
	6, 6, 1		

l	kFo	Fc	Sig
0	61	68	266
2	81	67	274
3	49	34	481
4	47	44	460
	6, 7, 1		
1	59	53	279
2	112	111	322
	6, 8, 1		
0	33	26	432
1	62	57	272
2	61	61	310
3	84	72	295
	6, 9, 1		
1	72	75	246
2	57	55	333
	6, 10, 1		
0	39	35	403
2	97	98	326
3	43	35	582
4	59	45	488
	6, 11, 1		
2	88	88	309
	6, 12, 1		
1	53	56	333
2	76	81	283
3	39	42	513
4	39	24	555
	6, 13, 1		
0	44	43	395
1	55	44	345
2	94	86	302
3	35	21	541
	6, 14, 1		
0	74	60	259
1	70	64	287
2	52	44	383
	6, 15, 1		
0	40	40	462
1	36	31	698
	6, 16, 1		
0	56	48	324
	6, 17, 1		
0	53	58	363
1	42	33	543
	6, 18, 1		
0	63	68	317
	6, 19, 1		
0	56	66	364
	6, 22, 1		
0	38	32	497
	7, 0, 1		
1	90	84	294

l	kFo	Fc	Sig
	7, 1, 1		
2	63	53	303
	7, 2, 1		
0	147	140	327
2	42	19	537
	7, 3, 1		
0	54	52	361
1	83	72	278
	7, 4, 1		
0	43	36	425
1	78	72	275
	7, 5, 1		
0	67	52	278
2	44	40	433
	7, 6, 1		
1	57	58	330
2	45	42	420
	7, 7, 1		
1	37	28	611
	7, 8, 1		
0	54	63	340
2	41	40	473
3	52	43	425
	7, 9, 1		
3	52	52	570
	7, 10, 1		
3	85	69	314
	7, 11, 1		
0	72	64	295
1	52	54	386
	7, 12, 1		
0	46	42	583
2	42	38	475
3	53	49	439
	7, 13, 1		
0	54	38	405
2	44	38	576
	7, 14, 1		
0	80	71	286
1	43	45	585
	7, 19, 1		
1	47	30	538
	8, 0, 1		
0	70	64	416
1	42	34	572
	8, 1, 1		
1	36	33	699
	8, 3, 1		
0	56	46	365
	8, 5, 1		
1	44	40	463
	8, 6, 1		

l	kFo	Fc	Sig
0	48	48	429
1	52	50	400
	8, 7, 1		
0	46	36	573
	8, 8, 1		
1	37	27	680
	8, 9, 1		
1	40	43	611
	8, 10, 1		
0	47	34	458
	8, 11, 1		
0	47	31	476
	8, 12, 1		
1	47	30	588
	8, 13, 1		
1	36	26	613
	9, 1, 1		
0	43	6	575
	-1, -1, 1		
-1	197	248	152
-2	58	114	259
-3	39	50	285
-4	87	107	300
-5	80	73	345
-6	33	23	779*
	-1, -2, 1		
-1	301	354	129
-2	68	95	223
-3	74	97	286
-4	69	82	278
-5	61	71	525
-6	64	45	525
	-1, -3, 1		
-1	697	791	120
-2	45	61	225
-3	63	78	274
-4	66	64	376
-5	77	85	437
-6	47	19	592
	-1, -4, 1		
-1	238	258	134
-2	70	100	209
-3	107	135	219
-4	73	67	371
-5	72	44	414
-6	42	26	584
	-1, -5, 1		
-1	34	43	220
-2	292	300	175
-3	56	63	270
-4	72	78	479
-5	55	33	347

Friedel Pair Columns are 10Fo 10Fc 1000Sig, * for Insignificant

l	kFo	Fc	Sig	l	kFo	Fc	Sig	l	kFo	Fc	Sig	l	kFo	Fc	Sig
	-1, -5, 1			-2	87	76	204	-1	35	31	640	-2	127	134	225
-6	41	26	669	-3	65	51	249	-2	87	104	329	-4	70	53	405
	-1, -6, 1			-4	44	40	360	-3	64	27	474		-2, -9, 1		
-1	422	449	126		-1,-15, 1				-1,-27, 1			-1	119	129	218
-2	95	102	222	-1	92	66	200	-1	36	39	616	-2	136	142	243
-3	168	181	228	-2	113	100	266	-2	76	51	429	-3	46	56	272
-4	81	77	330	-3	57	44	283	-3	58	51	383	-4	33	30	570
-5	60	41	399	-4	56	57	300		-1,-28, 1				-2,-10, 1		
-6	54	34	529		-1,-16, 1			-3	49	44	603	-1	161	179	199
	-1, -7, 1			-1	189	159	201		-1,-29, 1			-2	54	57	227
-1	227	249	145	-2	67	40	247	-1	41	42	614	-3	39	42	325
-2	245	250	183	-5	12	19	2900*		-1,-33, 1			-4	38	30	522
-3	124	131	254		-1,-17, 1			-1	37	36	630		-2,-11, 1		
-5	33	14	676*	-1	219	191	203		-2, -1, 1			-1	273	274	169
-6	44	21	630	-2	65	65	232	-1	285	300	139	-2	224	237	218
	-1, -8, 1			-3	19	31	1175*	-2	152	211	222	-3	50	64	267
-1	216	232	148	-5	37	36	700	-3	85	112	251	-4	59	65	298
-2	235	223	187		-1,-18, 1			-4	54	75	348	-5	55	38	491
-3	125	121	244	-1	127	52	267	-5	72	93	415		-2,-12, 1		
-4	33	34	546	-2	50	25	289		-2, -2, 1			-1	195	196	194
-5	63	47	325	-3	61	61	276	-1	333	349	140	-2	134	132	267
	-1, -9, 1			-4	33	24	652	-2	108	153	215	-3	72	82	287
-1	212	229	150		-1,-19, 1			-3	123	182	293		-2,-13, 1		
-2	40	65	353	-1	194	199	226	-4	37	68	441	-3	73	86	283
-3	70	65	236	-2	79	64	243		-2, -3, 1				-2,-14, 1		
-5	59	38	369	-3	69	55	363	-1	137	136	178	-1	65	70	224
-6	43	28	632	-4	25	28	1416*	-2	135	163	216	-2	120	123	295
	-1,-10, 1				-1,-20, 1			-4	68	84	395	-3	53	109	406
-1	74	89	230	-1	144	131	230		-2, -4, 1			-5	37	26	560
-2	198	203	202	-2	76	49	357	-1	624	674	135		-2,-15, 1		
-3	88	77	246	-3	62	62	298	-2	121	150	209	-1	108	115	279
-4	61	55	373		-1,-21, 1			-3	173	205	259	-5	6	24	7131*
-5	45	34	514	-1	51	17	351	-4	51	44	413		-2,-16, 1		
	-1,-11, 1			-2	74	76	277		-2, -5, 1			-1	42	51	373
-1	58	71	298	-3	68	56	373	-1	330	353	145	-2	113	124	338
-2	104	124	289		-1,-22, 1			-2	44	50	249	-3	35	32	433
-3	156	144	256	-1	57	59	264	-3	41	31	355	-4	63	53	388
-4	59	54	350	-2	97	105	326	-4	70	73	309	-5	44	34	595
-5	38	23	594	-3	71	78	328	-5	52	42	457		-2,-17, 1		
-6	24	11	1640*		-1,-23, 1				-2, -6, 1			-2	65	67	377
	-1,-12, 1			-1	64	48	344	-1	248	260	154	-3	53	45	325
-1	76	68	288	-2	93	116	357	-2	107	129	221	-4	79	87	342
-2	91	79	241	-3	68	25	405	-3	45	38	264	-5	42	25	635
-3	68	71	270		-1,-24, 1			-5	69	59	369		-2,-18, 1		
-4	62	39	330	-1	58	51	302		-2, -7, 1			-1	87	73	244
-5	34	38	715*	-2	130	145	367	-1	274	281	153	-3	92	101	307
	-1,-13, 1			-3	51	56	557	-2	322	321	198		-2,-19, 1		
-1	200	189	189		-1,-25, 1			-3	44	42	339	-1	147	133	282
-2	220	188	202	-1	49	52	359	-4	58	74	400	-2	55	37	353
-3	92	85	276	-2	79	71	737	-6	6	19	7174*	-3	74	44	394
	-1,-14, 1			-3	70	72	371		-2, -8, 1			-4	23	26	1351*
-1	147	123	228		-1,-26, 1			-1	289	306	155		-2,-20, 1		

Friedel Pair Columns are 10Fo 10Fc 1000Sig, * for Insignificant

l	kFo	Fc	Sig	l	kFo	Fc	Sig	l	kFo	Fc	Sig	l	kFo	Fc	Sig
	-2,-20, 1			-2	60	69	235	-4	5	40	8170*	-1	134	122	223
-1	87	81	286	-3	58	69	292		-3,-16, 1			-2	88	92	275
-2	67	54	274	-4	65	72	346	-1	84	87	239	-3	62	68	248
-3	72	77	341		-3, -4, 1			-2	53	61	283		-4, -3, 1		
	-2,-21, 1			-1	321	320	155	-3	80	102	318	-1	4	17	5783*
-1	71	62	272	-2	233	227	216		-3,-17, 1			-3	37	37	370
-2	62	50	348	-3	64	75	271	-3	47	93	634	-4	49	52	489
-3	66	59	360	-4	68	75	386	-4	48	46	524	-5	22	24	1128*
	-2,-22, 1				-3, -5, 1			-5	39	22	693		-4, -4, 1		
-1	73	39	381	-1	273	277	164		-3,-18, 1			-1	219	192	188
-2	75	78	305	-2	192	195	228	-1	109	126	355	-2	75	78	252
-3	71	49	416	-3	61	60	286	-2	98	119	288	-3	48	51	376
	-2,-23, 1			-4	93	78	375	-4	39	61	821*	-4	75	77	443
-1	64	58	309		-3, -6, 1				-3,-19, 1				-4, -5, 1		
-2	64	48	390	-1	287	295	166	-1	46	50	474	-1	148	152	227
-3	65	30	383	-2	135	147	230	-2	40	77	717	-2	59	63	236
-4	6	17	5260*	-3	50	59	289	-3	5	32	7749*	-3	61	64	300
	-2,-24, 1				-3, -7, 1				-3,-20, 1			-4	64	60	311
-1	66	67	317	-1	317	312	165	-1	73	82	341		-4, -6, 1		
-2	99	99	331	-2	123	142	239	-2	117	134	363	-1	188	178	209
-3	38	17	653	-4	43	42	373	-3	5	25	7291*	-2	58	62	236
	-2,-25, 1				-3, -8, 1				-3,-21, 1			-3	56	52	291
-1	78	75	279	-1	32	36	476	-1	68	83	360		-4, -7, 1		
-2	75	77	374	-2	147	156	252	-2	96	136	400	-1	283	281	189
-3	45	34	535	-3	53	52	250	-4	26	25	1553*	-2	178	172	252
	-2,-26, 1				-3, -9, 1				-3,-22, 1			-3	42	55	358
-1	76	74	277	-1	265	260	179	-1	65	91	326	-4	40	36	430
-2	74	54	412	-2	70	83	258	-3	50	42	391		-4, -8, 1		
-3	56	35	475	-4	48	43	437		-3,-23, 1			-1	88	95	244
	-2,-27, 1			-5	57	41	456	-1	83	91	283	-2	90	104	265
-1	60	30	404		-3,-10, 1			-3	48	17	538		-4, -9, 1		
-2	52	44	387	-1	142	149	237		-3,-24, 1			-1	196	196	212
-3	50	29	534	-2	72	72	222	-1	57	49	430	-2	154	157	284
	-2,-28, 1			-3	44	42	387	-2	22	13	1059*	-3	55	50	326
-1	62	38	316		-3,-11, 1			-3	71	58	394		-4,-10, 1		
-3	52	39	519	-1	83	71	221		-3,-25, 1			-1	91	91	236
	-2,-29, 1			-2	97	99	271	-1	63	48	384	-2	58	59	258
-1	77	83	294		-3,-12, 1				-3,-27, 1				-4,-11, 1		
	-2,-30, 1			-1	165	164	220	-1	59	23	423	-1	142	132	251
-1	67	19	414	-2	90	93	246		-3,-28, 1			-2	90	100	280
	-3, -1, 1				-3,-13, 1			-1	69	74	302	-3	54	51	402
-1	149	157	183	-1	94	93	253	-2	23	34	1123*	-4	5	26	6804*
-2	101	106	235	-2	58	62	241		-3,-29, 1				-4,-12, 1		
-3	67	88	266	-4	60	56	413	-1	63	41	444	-2	37	34	374
-4	35	46	585		-3,-14, 1			-2	55	41	476	-3	69	78	359
	-3, -2, 1			-1	111	114	285		-3,-30, 1				-4,-13, 1		
-1	209	211	165	-3	62	74	343	-1	51	43	529	-1	61	61	218
-2	37	45	270	-4	61	69	389		-4, -1, 1			-2	51	53	292
-3	45	42	375		-3,-15, 1			-1	166	158	203	-3	49	44	461
-4	99	131	327	-1	149	142	245	-2	75	71	269	-4	61	55	437
	-3, -3, 1			-2	47	54	295	-3	48	54	302		-4,-14, 1		
-1	111	125	226	-3	68	77	307		-4, -2, 1			-1	41	46	310

Friedel Pair Columns are 10Fo 10Fc 1000Sig, * for Insignificant

l	kFo	Fc	Sig	l	kFo	Fc	Sig	l	kFo	Fc	Sig	l	kFo	Fc	Sig
-4,-14, 1				-2	29	36	604*	-2	47	51	392	-6,-11, 1			
-2	18	34	1391*	-3	49	48	364	-5,-16, 1				-2	81	88	308
-4,-15, 1				-5, -3, 1				-1	119	117	368	-6,-12, 1			
-2	59	66	286	-1	50	57	260	-2	38	41	614	-1	52	56	337
-3	81	92	322	-2	62	59	234	-3	56	52	368	-2	77	81	277
-4	6	36	7687*	-4	39	40	614	-5,-17, 1				-3	9	42	4724*
-4,-16, 1				-5, -4, 1				-1	75	75	279	-4	26	24	1343*
-1	71	62	239	-1	105	98	298	-2	31	35	743*	-6,-13, 1			
-2	61	74	298	-2	88	94	263	-5,-18, 1				-1	54	44	344
-4	6	41	6734*	-3	72	70	356	-1	70	59	284	-2	88	86	289
-4,-17, 1				-4	50	47	524	-2	52	51	370	-3	7	21	5716*
-1	65	58	259	-5, -5, 1				-5,-19, 1				-6,-14, 1			
-2	70	68	278	-1	76	72	244	-1	38	35	602	-1	70	64	288
-3	52	55	410	-2	50	50	307	-5,-22, 1				-2	31	44	1314*
-4	44	41	603	-3	73	76	320	-1	5	42	7091*	-6,-15, 1			
-4,-18, 1				-4	72	72	349	-5,-24, 1				-1	29	31	836*
-1	80	81	260	-5, -6, 1				-1	39	39	498	-6,-17, 1			
-2	77	90	301	-2	61	68	291	-6, -1, 1				-1	40	33	458
-3	57	66	389	-3	80	95	318	-1	93	93	247	-7, -1, 1			
-4,-19, 1				-4	65	58	363	-2	59	57	286	-2	61	53	316
-1	55	57	344	-5, -7, 1				-3	24	35	933*	-7, -2, 1			
-2	74	89	310	-1	192	193	240	-6, -2, 1				-2	37	19	492
-4	62	41	471	-2	107	116	276	-1	118	111	341	-7, -3, 1			
-4,-20, 1				-3	58	55	326	-2	59	56	291	-1	80	72	266
-3	35	34	652	-5, -8, 1				-6, -3, 1				-7, -4, 1			
-4	30	39	947*	-1	64	72	248	-2	57	60	300	-1	75	72	266
-4,-21, 1				-2	47	46	444	-6, -4, 1				-7, -5, 1			
-1	56	60	343	-3	64	55	379	-1	53	59	301	-2	49	40	377
-4,-22, 1				-4	58	47	354	-2	32	25	523	-7, -6, 1			
-3	47	52	604	-5, -9, 1				-3	69	59	295	-1	58	58	323
-4,-23, 1				-1	122	125	300	-6, -5, 1				-2	40	42	620
-1	51	65	387	-2	79	87	273	-1	34	37	572	-7, -7, 1			
-4,-24, 1				-3	60	72	339	-2	49	54	455	-1	20	28	1756*
-2	62	67	356	-5,-10, 1				-3	54	48	457	-7, -8, 1			
-4,-25, 1				-1	93	92	252	-6, -6, 1				-2	41	40	473
-1	5	15	6909*	-2	57	48	298	-2	75	67	257	-3	63	43	425
-4,-26, 1				-3	78	96	382	-3	14	34	2744*	-7, -9, 1			
-2	12	20	3424*	-5,-11, 1				-4	52	44	486	-3	50	52	461
-4,-27, 1				-1	21	24	1347*	-6, -7, 1				-7,-10, 1			
-2	53	54	410	-2	79	91	288	-1	56	53	291	-3	79	69	322
-4,-28, 1				-3	71	68	330	-2	112	111	332	-7,-11, 1			
-2	51	33	557	-5,-12, 1				-6, -8, 1				-1	57	54	344
-4,-29, 1				-2	103	112	335	-1	57	57	293	-7,-12, 1			
-1	44	43	480	-3	48	49	536	-2	59	61	322	-2	40	38	617
-4,-30, 1				-5,-13, 1				-3	73	72	318	-3	44	49	655
-1	24	42	1251*	-1	27	43	1104*	-6, -9, 1				-7,-13, 1			
-5, -1, 1				-2	80	86	287	-1	74	75	254	-2	38	38	615
-1	190	176	225	-3	56	56	362	-2	54	55	346	-7,-14, 1			
-2	109	104	323	-5,-14, 1				-6,-10, 1				-1	45	45	573
-4	39	37	588	-3	59	45	434	-2	97	98	294	-7,-19, 1			
-5, -2, 1				-5,-15, 1				-3	51	35	491	-1	6	30	7091*
-1	109	93	296	-1	81	83	274	-4	57	45	492	-8, -1, 1			

Friedel Pair Columns are 10Fo 10Fc 1000Sig, * for Insignificant

l	kFo	Fc	Sig	l	kFo	Fc	Sig	l	kFo	Fc	Sig	l	kFo	Fc	Sig
-8, -1, 1				-8, -6, 1				-8, -9, 1				-1	41	30	680
-1	20	33	1139*	-1	49	50	429	-1	50	43	421	-8,-13, 1			
-8, -5, 1				-8, -8, 1				-8,-12, 1				-1	34	26	745*
-1	52	40	390	-1	33	27	624								

Space Group and Cell Dimensions Monoclinic, C c
a 21.953(8) b 23.183(9) c 10.658(5)
beta 102.793(5)
Volume 5290(4)A**3

Empirical formula : O3 C16 H15

Cell dimensions were obtained from 24 reflections with 2Theta angle
in the range 40.00 - 50.00 degrees.

Crystal dimensions : 0.20 X 0.20 X 0.20 mm

FW = 255.29 Z = 16 F(000) = 2160.90

Dcalc 1.282Mg.m-3, mu 0.04mm-1, lambda 0.70930A, 2Theta(max) 50.0

The intensity data were collected on a Rigaku diffractometer,
using the theta/2theta scan mode.
The h,k,l ranges used during structure solution and refinement are :--
Hmin,max -26 25; Kmin,max 0 27; Lmin,max 0 12
No. of reflections measured 4802
No. of unique reflections 4802
No. of reflections with Inet > 2.5sigma(Inet) 2034
Merging R-value on intensities 0.000
No correction was made for absorption

The last least squares cycle was calculated with
136 atoms, 348 parameters and 1922 out of 4673 reflections.
Weights based on counting-statistics were used.
The weight modifier K in KFo**2 is 0.000150

The residuals are as follows :--
For significant reflections, RF 0.055, Rw 0.073 GoF 3.58
For all reflections, RF 0.103, Rw 0.074.
where RF = Sum(Fo-Fc)/Sum(Fo),
Rw = Sqrt[Sum(w(Fo-Fc)**2)/Sum(wFo**2)] and
GoF = Sqrt[Sum(w(Fo-Fc)**2)/(No. of reflns - No. of params.)]
The maximum shift/sigma ratio was 0.273.

In the last D-map, the deepest hole was -0.270e/A**3,
and the highest peak 0.540e/A**3.

Secondary ext. coeff. 0.729632 sigma 0.016761

The following references are relevant to the NRCVAX System.

1. Full System Reference :
Gabe, E.J., Le Page, Y., Charland, J.-P., Lee, F.L. and White, P.S.
(1989) J. Appl. Cryst., 22, 384-387.

2. Scattering Factors from Int. Tab. Vol. 4 :

International Tables for X-ray Crystallography, Vol. IV, (1974) Kynoch Press, Birmingham, England.

The following references may also be relevant.

3. ORTEP Plotting :
Johnson, C.K., (1976) ORTEP - A Fortran Thermal Ellipsoid Plot Program, Technical Report ORNL-5138, Oak Ridge

4. Pluto Plotting :
S. Motherwell, University Chemical Laboratory, Cambridge, 1978

5. Missing Symmetry Treatment by MISSYM :
Le Page, Y., (1988) J. Appl. Cryst., 21, 983-984.

7. Extinction Treatment :
Larson, A.C., (1970) p.293, Crystallographic Computing, Munksgaard, Copenhagen.

EXPERIMENTAL

1. Data Collection

A crystal of O3C16H15 having approximate dimensions of .2,.2,.2 mm was mounted on a glass capillary. All the measurements were made on a Rigaku diffractometer with Mo Kalpha radiation.

Cell constants and an orientation matrix for data collection, were obtained from least-squares refinement using the setting angles of 25 reflections in the range 40<2theta<50 corresponded to a monoclinic cell with dimensions:

a =21.953(8)
b =23.183(9)
c = 10.658(5)
beta= 102.793(5)

For Z=16 and FW=255.29, the calculated density is 1.282g/cm3. Based on the systematic absences, the space group was determined to be C c or C2/c. In C 2/c, there is a disorder, so the structure was solved in C c.

The data was collected at a temperature of -140 degrees using the omega-2theta scan technique to a maximum 2theta value of 49.9 degrees.

2. Data reduction

A total of 4802 reflections was collected. The unique set contains only 4802 reflections. The standards were measured after every 150 reflections. No crystal decay was noticed. The data were corrected for Lorentz and polarisation effects (1). No absorption correction was made.

3. Solution and refinement:

The structure was solved by direct methods. All the atoms were refined anisotropically except the hydrogen. The hydrogen atoms were calculated. The benzene rings were all refined as rigid group to increase the ratio reflection/parameters. The final cycle of full matrix least-squares refinement was based on 2034 observed reflections (I>2.5 sigma(I)) and 348 variable parameters. Weights based on counting statistics were used. The maximum and minimum peaks on the final differences Fourier map corresponded to .540 and -.270 e/a3, respectively.

All the calculations were performed using the NRCVAX crystallographic software package (2).

EXPERIMENTAL DETAILS

Empirical formula	O3C16H15
Formula weight	255.29
Crystal shape	cube
Crystal dimensions (mm)	.2,.2,.2
Crystal system	monoclinic
No. Reflection used for unit cell dimension (2theta range)	25 40-50
Lattice parameters	a=21.953(8) b=23.183(9) c=10.658(5) beta=102.793(5)
Space group	C c
Z value	16
Dcalc (g.cm-3)	1.282
F(000)	540.22
mu (mm-1)	0.04
No of reflection measured	4802
No of reflection unique	4802
No of reflection observed	2034
No of atoms	136
No of variables	348
Rf (sign refl)	.055
Rw (sign refl)	.073
Rf (all refl)	.103
Rw (all refl)	.074
Goodness of fit	3.58
Last difference fourier map	
max peak	.540
min peak	-.270

References

1. D.F. Grant and E.J. Gabe
J. Appl. Crystallogr., 11, 114 (1978)
2. E.J. Gabe, F.L. Lee and Y. Lepage
J. Appl. Crystallogr., 22, 384 (1989)

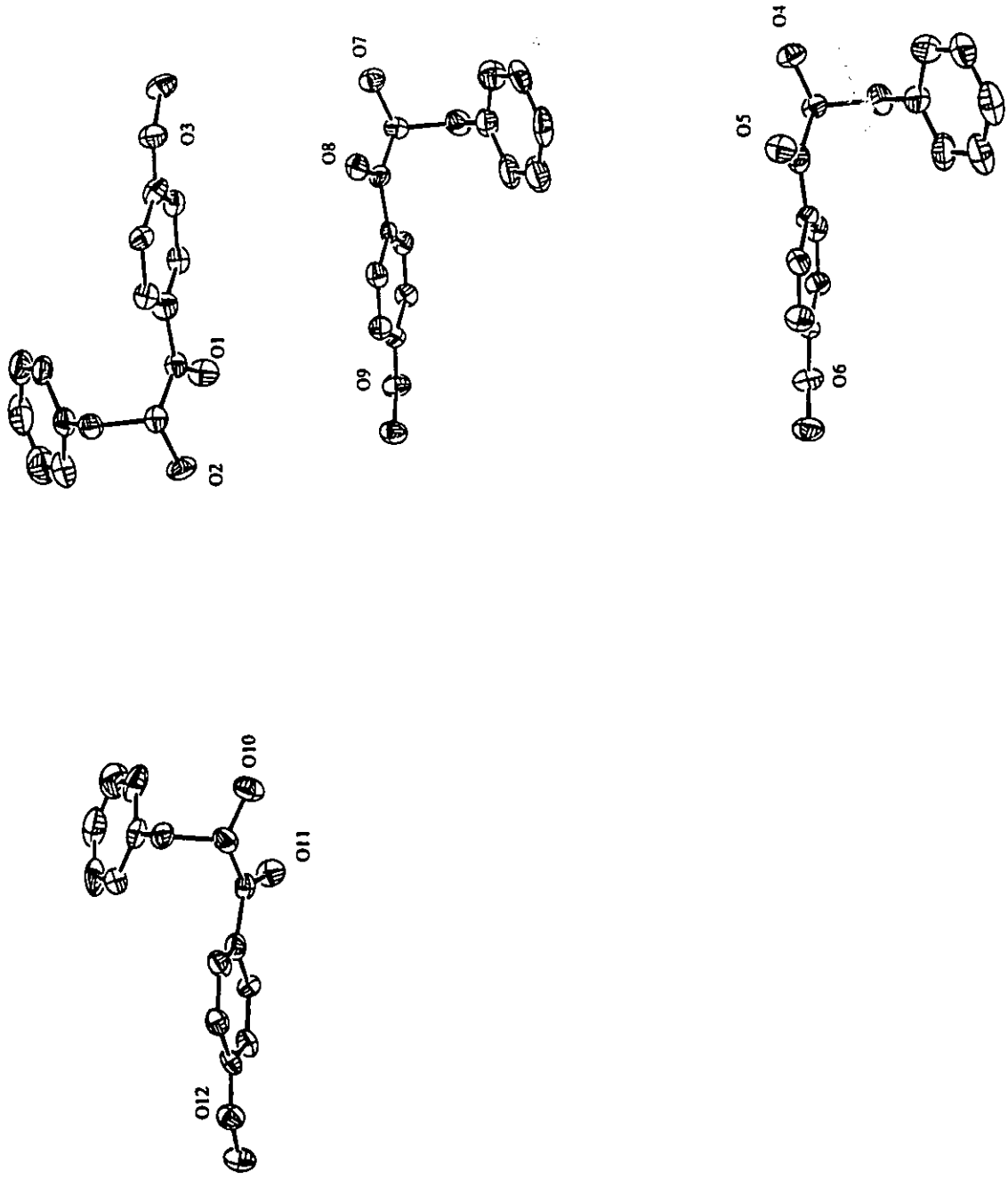
O1
O2
O3
O4
O5
O6
O7
O8
O9
O10
O11
O12

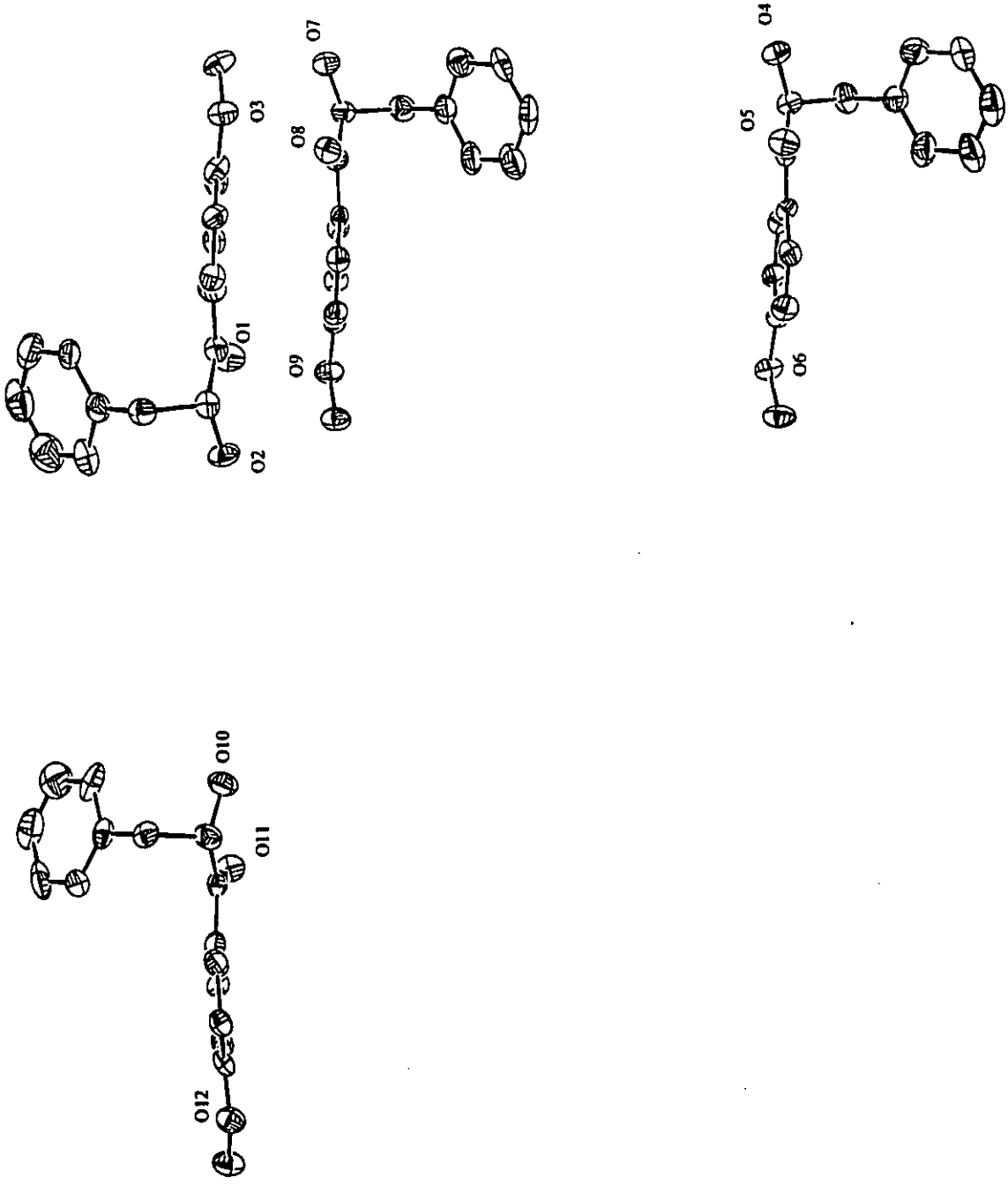
O1
O2
O3
O4
O5
O6
O7
O8
O9
O10
O11
O12

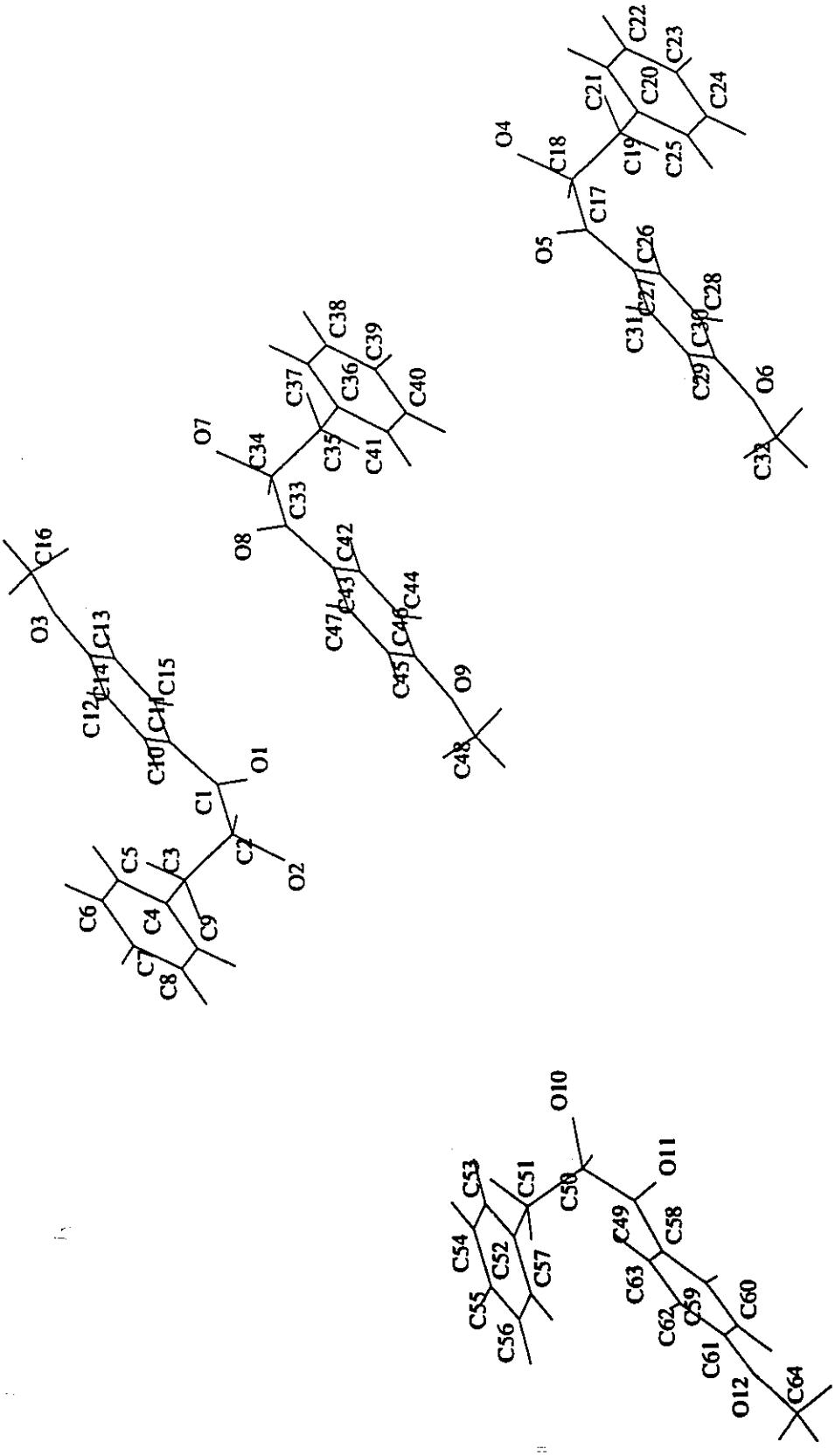
O1
O2
O3
O4
O5
O6
O7
O8
O9
O10
O11
O12
C1
C2
C3
C4
C5
C6
C7
C8
C9
C10
C11
C12
C13
C14
C15
C16
C17
C18
C19
C20
C21
C22
C23
C24
C25
C26
C27
C28
C29
C30
C31
C32
C33
C34
C35
C36
C37
C38
C39
C40
C41
C42
C43
C44
C45
C46
C47
C48
C49
C50
C51
C52
C53
C54
C55
C56
C57
C58
C59
C60
C61
C62
C63
C64

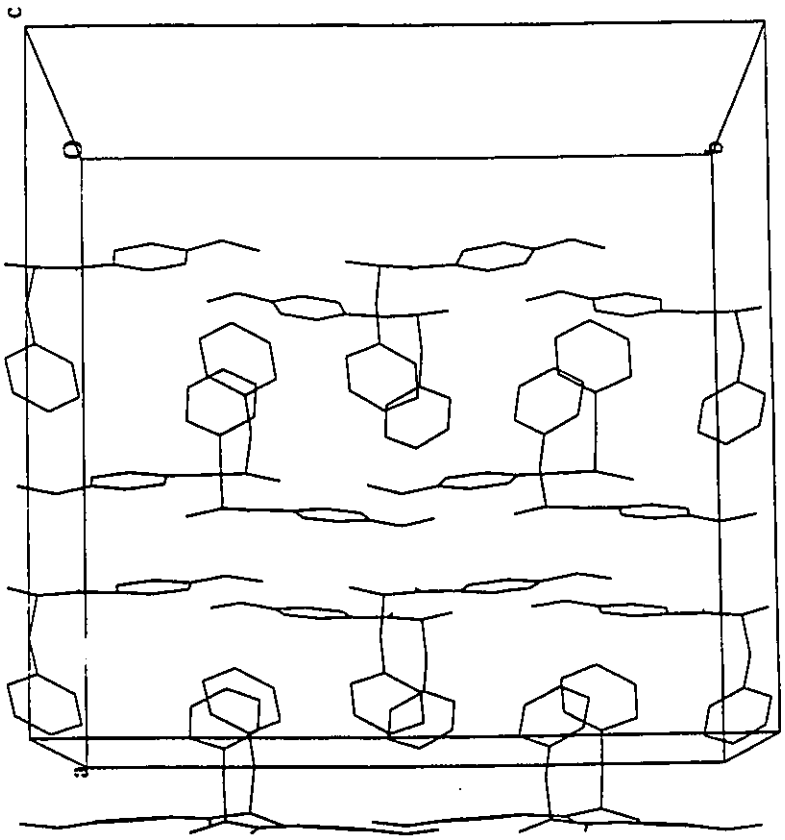
c
a

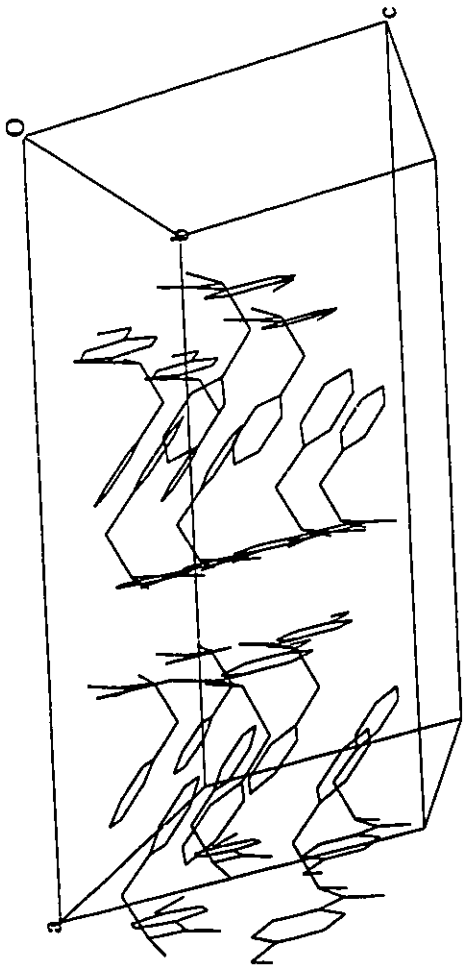
c
o
a

Table of Atomic Parameters x,y,z and Biso.
E.S.Ds. refer to the last digit printed.

	x	y	z	Biso
O1	0.7393 (4)	0.4832 (3)	0.8398 (7)	3.5 (3)
O2	0.7479 (4)	0.5777 (3)	0.9645 (7)	3.4 (3)
O3	0.7464 (3)	0.2511 (3)	1.1542 (6)	3.0 (3)
O4	0.1115 (3)	0.1716 (3)	0.2079 (6)	3.1 (3)
O5	0.1160 (4)	0.2685 (3)	0.3384 (6)	3.2 (3)
O6	0.1098 (3)	0.4995 (3)	0.0209 (7)	3.2 (3)
O7	0.61357	0.1722 (3)	0.20906	3.1 (3)
O8	0.6171 (3)	0.2679 (3)	0.3372 (6)	3.0 (3)
O9	0.6102 (4)	0.4996 (3)	0.0222 (7)	3.3 (3)
O10	0.7470 (4)	0.9224 (3)	0.4643 (8)	3.8 (3)
O11	0.7387 (4)	1.0166 (3)	0.3394 (7)	3.5 (3)
O12	0.7464 (3)	1.2489 (3)	0.6529 (7)	3.2 (3)
C1	0.7543 (4)	0.4751 (4)	0.9559 (9)	2.4 (4)
C2	0.7655 (4)	0.5282 (4)	1.0413 (9)	2.5 (4)
C3	0.8336 (5)	0.5338 (4)	1.1113 (9)	3.0 (4)
C16	0.7484 (5)	0.1999 (4)	1.0750 (11)	3.5 (5)
C17	0.1043 (4)	0.2762 (5)	0.2218 (10)	3.0 (4)
C18	0.0917 (5)	0.2224 (4)	0.1338 (9)	2.6 (4)
C19	0.0228 (5)	0.2163 (5)	0.0597 (10)	3.5 (5)
C32	0.1054 (6)	0.5493 (4)	0.0988 (11)	3.7 (5)
C33	0.6035 (4)	0.2755 (4)	0.2212 (9)	2.4 (4)
C34	0.5927 (5)	0.2224 (4)	0.1336 (9)	2.6 (4)
C35	0.5227 (5)	0.2174 (5)	0.0610 (11)	3.4 (4)
C48	0.6056 (6)	0.5499 (4)	0.0972 (10)	3.3 (4)
C49	0.7544 (4)	1.0247 (4)	0.4563 (9)	2.4 (4)
C50	0.7652 (5)	0.9722 (4)	0.5427 (10)	3.2 (4)
C51	0.8342 (5)	0.9664 (4)	0.6134 (9)	2.9 (4)
C64	0.7483 (6)	1.2997 (5)	0.5728 (12)	3.8 (5)
H2	0.737	0.524	1.113	3.2
H3A	0.845	0.500	1.184	3.0
H3B	0.840	0.575	1.160	3.0
H5	0.900	0.439	1.062	3.5
H6	0.975	0.434	0.920	5.1
H7	0.998	0.522	0.806	5.9
H8	0.946	0.614	0.834	6.0
H9	0.871	0.619	0.976	4.0
H11	0.762	0.444	1.204	3.1
H12	0.757	0.344	1.288	3.2
H14	0.749	0.276	0.911	3.0
H15	0.754	0.375	0.827	3.0
H16C	0.741	0.162	1.129	3.7
H16A	0.708	0.202	0.990	3.7
H16B	0.790	0.197	1.041	3.7
H18	0.120	0.227	0.063	2.8
H19A	0.017	0.174	0.011	3.9
H19B	0.012	0.250	-0.014	3.9
H21	-0.015	0.133	0.215	4.3
H22	-0.092	0.145	0.351	4.2
H23	-0.143	0.239	0.363	5.4
H24	-0.116	0.322	0.239	5.7

H25	-0.039	0.311	0.103	5.0
H27	0.093	0.309	-0.032	2.8
H28	0.097	0.410	-0.109	3.0
H30	0.111	0.472	0.275	3.4
H31	0.106	0.372	0.352	3.8
H32C	0.108	0.589	0.046	4.6
H32A	0.057	0.549	0.120	4.6
H32B	0.138	0.549	0.187	4.6
H34	0.620	0.227	0.062	3.0
H35A	0.516	0.176	0.007	3.9
H35B	0.513	0.252	-0.012	3.9
H37	0.484	0.133	0.215	4.3
H38	0.407	0.145	0.351	4.3
H39	0.357	0.240	0.364	4.8
H40	0.384	0.323	0.241	5.4
H41	0.461	0.311	0.105	4.8
H43	0.593	0.309	-0.032	2.6
H44	0.597	0.410	-0.110	2.8
H46	0.611	0.472	0.274	3.2
H47	0.607	0.372	0.352	3.0
H48C	0.609	0.589	0.043	4.1
H48A	0.558	0.550	0.118	4.1
H48B	0.639	0.550	0.186	4.1
H50	0.736	0.976	0.615	3.9
H51A	0.841	0.924	0.661	3.2
H51B	0.845	1.000	0.686	3.2
H53	0.868	0.882	0.475	5.0
H54	0.943	0.885	0.330	5.9
H55	0.997	0.976	0.303	5.7
H56	0.977	1.064	0.420	5.3
H57	0.903	1.061	0.564	3.7
H59	0.755	1.126	0.326	2.6
H60	0.749	1.224	0.411	3.2
H62	0.756	1.155	0.787	3.2
H63	0.762	1.056	0.702	3.5
H64C	0.742	1.338	0.627	4.0
H64A	0.790	1.302	0.540	4.0
H64B	0.708	1.298	0.489	4.0
C4	0.8806 (3)	0.5295 (3)	1.0283 (6)	3.22(20)
C5	0.9096 (3)	0.4772 (3)	1.0135 (7)	3.22(20)
C6	0.9517 (3)	0.4738 (3)	0.9332 (8)	4.90(20)
C7	0.9649 (3)	0.5227 (4)	0.8677 (7)	5.69(20)
C8	0.9359 (4)	0.5750 (3)	0.8826 (7)	5.86(20)
C9	0.8938 (3)	0.5784 (3)	0.9629 (7)	3.63(21)
C10	0.7584 (3)	0.41560(20)	1.0113 (5)	3.11(15)
C11	0.7596 (3)	0.40619(21)	1.1411 (5)	2.58(16)
C12	0.7569 (3)	0.35009(25)	1.1869 (4)	2.71(15)
C13	0.7529 (3)	0.30341(19)	1.1029 (5)	2.92(16)
C14	0.7517 (3)	0.31283(22)	0.9730 (5)	2.56(16)
C15	0.7544 (3)	0.3689 (3)	0.9273 (4)	2.45(16)
C20	-0.0224 (3)	0.2211 (3)	0.1508 (7)	3.17(22)
C21	-0.0372 (3)	0.17397(25)	0.2199 (7)	3.96(22)
C22	-0.0804 (4)	0.1800 (3)	0.2971 (7)	3.89(22)
C23	-0.1090 (3)	0.2332 (4)	0.3052 (7)	5.02(21)

C24	-0.0943 (3)	0.2804 (3)	0.2362 (9)	5.37(21)
C25	-0.0510 (3)	0.2743 (3)	0.1590 (8)	4.79(21)
C26	0.0993 (3)	0.33393(18)	0.1656 (5)	1.91(15)
C27	0.0973 (3)	0.34404(20)	0.0357 (5)	2.43(15)
C28	0.0999 (3)	0.40038(24)	-0.0088 (4)	2.60(15)
C29	0.1045 (3)	0.44661(18)	0.0766 (6)	2.49(15)
C30	0.1065 (3)	0.43650(21)	0.2064 (5)	3.06(15)
C31	0.1039 (3)	0.38016(25)	0.2510 (4)	3.46(15)
C36	0.4769 (3)	0.2214 (3)	0.1496 (7)	3.41(21)
C37	0.4622 (3)	0.1742 (3)	0.2187 (8)	4.11(21)
C38	0.4194 (3)	0.1804 (3)	0.2970 (7)	4.09(22)
C39	0.3913 (3)	0.2338 (4)	0.3061 (7)	4.64(22)
C40	0.4060 (3)	0.2809 (3)	0.2369 (9)	5.29(21)
C41	0.4488 (3)	0.2747 (3)	0.1587 (8)	4.68(21)
C42	0.6000 (3)	0.33452(18)	0.1654 (5)	1.93(14)
C43	0.5976 (3)	0.34438(20)	0.0352 (4)	2.28(15)
C44	0.6000 (3)	0.40063(24)	-0.0099 (4)	2.50(14)
C45	0.6047 (3)	0.44702(18)	0.0751 (5)	2.42(14)
C46	0.6071 (3)	0.43717(20)	0.2052 (5)	2.85(14)
C47	0.6047 (3)	0.38091(24)	0.2503 (4)	2.73(15)
C52	0.8816 (3)	0.9707 (3)	0.5298 (6)	3.24(21)
C53	0.8933 (3)	0.9215 (3)	0.4634 (8)	4.54(22)
C54	0.9347 (4)	0.9242 (3)	0.3814 (8)	5.73(21)
C55	0.9644 (3)	0.9760 (4)	0.3657 (7)	5.38(21)
C56	0.9527 (3)	1.0252 (3)	0.4321 (8)	4.97(21)
C57	0.9113 (3)	1.0225 (3)	0.5141 (7)	3.36(21)
C58	0.7591 (3)	1.08453(19)	0.5098 (5)	2.87(15)
C59	0.7553 (3)	1.13145(25)	0.4265 (4)	2.08(15)
C60	0.7520 (3)	1.18738(21)	0.4728 (5)	2.71(15)
C61	0.7525 (3)	1.19639(19)	0.6024 (5)	2.51(15)
C62	0.7563 (3)	1.1495 (3)	0.6857 (4)	2.70(15)
C63	0.7596 (3)	1.09354(21)	0.6394 (5)	3.01(15)

Biso is the Mean of the Principal Axes of the Thermal Ellipsoid

Table of u(i,j) or U values *100.
E.S.Ds. refer to the last digit printed

	u11(U)	u22	u33	u12	u13	u23
O1	5.9 (5)	4.3 (4)	3.1 (4)	-0.1 (4)	1.2.(3)	0.2 (3)
O2	5.4 (5)	2.8 (4)	4.4 (4)	0.7 (3)	0.5 (3)	1.0 (3)
O3	4.9 (4)	2.9 (3)	3.5 (4)	0.3 (3)	0.5 (3)	0.0 (3)
O4	4.8 (4)	3.2 (4)	3.3 (4)	0.7 (3)	0.5 (3)	0.3 (3)
O5	5.5 (4)	4.2 (4)	2.4 (3)	-0.2 (3)	0.6 (3)	0.4 (3)
O6	5.2 (4)	2.9 (4)	4.0 (4)	0.6 (3)	1.2 (3)	0.1 (3)
O7	4.9 (4)	3.5 (4)	3.2 (4)	0.3 (3)	0.7 (3)	0.2 (3)
O8	4.2 (4)	4.3 (4)	2.3 (3)	-0.3 (3)	-0.5 (3)	0.2 (3)
O9	5.5 (5)	3.3 (4)	3.8 (4)	0.2 (3)	1.3 (3)	0.8 (3)
O10	5.5 (5)	3.3 (4)	6.0 (5)	-1.0 (3)	1.8 (4)	-0.2 (4)
O11	5.6 (5)	4.3 (4)	3.6 (4)	0.4 (4)	1.1 (3)	0.2 (3)
O12	4.9 (4)	3.2 (4)	3.7 (4)	-0.5 (3)	0.7 (3)	0.6 (3)
C1	2.9 (5)	3.7 (5)	2.4 (4)	-0.1 (4)	0.5 (4)	0.4 (4)
C2	3.1 (5)	3.8 (5)	2.5 (4)	0.0 (4)	0.7 (4)	0.1 (4)
C3	4.3 (6)	3.5 (5)	2.9 (5)	-0.2 (5)	-0.3 (4)	-0.3 (4)
C16	5.4 (7)	3.1 (5)	4.8 (6)	1.7 (5)	1.5 (5)	-0.2 (5)
C17	2.6 (5)	4.5 (6)	4.1 (6)	0.0 (4)	0.8 (4)	-1.0 (5)
C18	3.8 (5)	3.2 (5)	2.5 (5)	0.3 (4)	0.3 (4)	-0.1 (4)
C19	3.9 (6)	5.6 (7)	3.7 (6)	-0.7 (5)	0.7 (5)	-0.9 (5)
C32	6.2 (7)	3.0 (5)	4.1 (6)	-0.2 (5)	-0.6 (5)	-0.4 (5)
C33	3.2 (5)	2.9 (5)	2.7 (5)	0.3 (4)	0.1 (4)	0.1 (4)
C34	3.8 (5)	3.0 (5)	3.4 (5)	-0.1 (4)	1.2 (4)	0.0 (4)
C35	4.4 (6)	4.3 (6)	4.2 (6)	-0.4 (5)	0.5 (5)	-0.5 (5)
C48	5.8 (7)	3.3 (5)	3.1 (5)	-0.2 (5)	0.0 (5)	-0.6 (4)
C49	2.4 (4)	4.1 (5)	2.7 (4)	0.3 (4)	0.9 (4)	-0.3 (4)
C50	4.4 (6)	3.7 (6)	3.8 (5)	-0.6 (5)	0.1 (4)	-0.6 (5)
C51	4.0 (6)	3.8 (6)	2.9 (5)	0.5 (5)	0.0 (4)	0.2 (4)
C64	6.1 (7)	3.1 (5)	5.4 (7)	-0.7 (5)	1.6 (6)	0.1 (5)
C4	3.22(24)	4.6 (3)	3.8 (3)	-0.27(22)	-0.46(20)	0.15(23)
C5	2.44(24)	4.7 (3)	4.8 (3)	0.08(22)	0.16(20)	0.86(23)
C6	3.68(24)	7.1 (3)	7.3 (3)	1.37(22)	-0.12(20)	-2.38(23)
C7	4.43(24)	10.0 (3)	6.4 (3)	-1.63(22)	-0.55(20)	1.20(23)
C8	6.51(24)	8.4 (3)	6.5 (3)	-1.03(22)	-0.21(20)	-0.01(23)
C9	3.30(24)	7.1 (3)	3.4 (3)	-1.23(22)	0.56(20)	-0.08(23)
C10	4.23(20)	4.32(21)	3.27(20)	-0.21(17)	0.85(16)	0.84(16)
C11	3.29(20)	3.86(21)	2.84(20)	0.19(17)	1.10(16)	-0.07(16)
C12	3.35(20)	2.99(21)	3.88(20)	0.54(17)	0.66(16)	-0.01(16)
C13	3.32(20)	4.06(21)	3.80(20)	1.28(17)	0.96(16)	0.30(16)
C14	2.91(20)	3.74(21)	2.92(20)	0.11(17)	0.30(16)	0.01(16)
C15	2.69(20)	4.28(21)	2.56(20)	-0.06(17)	1.02(16)	-0.09(16)
C20	3.45(24)	3.9 (3)	4.4 (3)	0.04(22)	0.31(21)	-0.09(24)
C21	4.85(24)	4.3 (3)	5.7 (3)	-0.03(22)	0.76(21)	-0.55(24)
C22	3.48(24)	6.9 (3)	4.5 (3)	-0.90(22)	0.95(21)	0.40(24)
C23	3.36(24)	9.9 (3)	5.8 (3)	-1.19(22)	1.09(21)	-3.21(24)
C24	3.57(24)	8.8 (3)	7.8 (3)	-1.89(22)	0.85(21)	-1.18(24)
C25	3.12(24)	7.3 (3)	7.4 (3)	-0.01(22)	0.38(21)	-2.22(24)
C26	2.65(20)	2.62(19)	1.88(20)	0.49(16)	0.26(16)	-0.62(16)
C27	2.84(20)	3.82(19)	2.50(20)	0.36(16)	0.47(16)	-0.40(16)
C28	3.62(20)	3.30(19)	3.10(20)	0.05(16)	1.01(16)	-0.71(16)

C29	2.75(20)	2.08(19)	4.37(20)	-0.30(16)	0.24(16)	0.36(16)
C30	4.55(20)	3.95(19)	3.12(20)	-0.05(16)	0.86(16)	-1.07(16)
C31	2.90(20)	3.90(19)	6.17(20)	-0.54(16)	0.62(16)	-0.83(16)
C36	3.15(23)	5.0 (3)	4.7 (3)	-0.16(22)	0.69(21)	-0.7 (3)
C37	4.95(23)	5.7 (3)	4.9 (3)	-0.29(22)	1.10(21)	0.4 (3)
C38	3.06(23)	7.1 (3)	5.4 (3)	-1.98(22)	1.01(21)	0.6 (3)
C39	2.04(23)	9.4 (3)	6.1 (3)	-0.09(22)	0.73(21)	-2.8 (3)
C40	4.04(23)	7.9 (3)	7.6 (3)	-1.53(22)	0.12(21)	0.9 (3)
C41	2.55(23)	6.8 (3)	8.1 (3)	-0.64(22)	0.45(21)	-1.9 (3)
C42	1.86(19)	2.84(19)	2.49(18)	0.03(16)	0.15(15)	-0.71(16)
C43	3.01(19)	3.46(19)	2.01(18)	0.26(16)	0.17(15)	-0.19(16)
C44	3.89(19)	3.53(19)	2.10(18)	0.00(16)	0.68(15)	-0.74(16)
C45	3.06(19)	2.67(19)	3.17(18)	0.05(16)	0.05(15)	0.19(16)
C46	3.52(19)	3.56(19)	3.75(18)	0.38(16)	0.84(15)	-1.20(16)
C47	3.34(19)	4.10(19)	2.90(18)	-0.17(16)	0.63(15)	-0.77(16)
C52	2.74(24)	5.2 (3)	4.0 (3)	0.71(22)	-0.03(21)	0.77(24)
C53	3.77(24)	8.6 (3)	4.9 (3)	2.77(22)	1.02(21)	-0.24(24)
C54	6.84(24)	8.1 (3)	5.9 (3)	0.54(22)	-0.50(21)	-0.32(24)
C55	4.10(24)	10.5 (3)	5.5 (3)	1.71(22)	0.22(21)	-1.15(24)
C56	2.37(24)	8.0 (3)	8.1 (3)	-1.35(22)	0.35(21)	2.68(24)
C57	3.25(24)	4.1 (3)	5.0 (3)	-0.26(22)	0.07(21)	-0.38(24)
C58	2.55(19)	4.49(21)	3.75(20)	0.36(16)	0.42(16)	-1.04(16)
C59	3.10(19)	2.76(21)	2.23(20)	0.32(16)	1.01(16)	0.52(16)
C60	2.92(19)	4.47(21)	2.81(20)	-0.69(16)	0.40(16)	-0.45(16)
C61	2.72(19)	3.53(21)	3.25(20)	-1.28(16)	0.60(16)	-0.21(16)
C62	3.06(19)	3.74(21)	3.58(20)	-0.67(16)	1.01(16)	0.13(16)
C63	3.32(19)	4.00(21)	4.24(20)	-0.72(16)	0.82(16)	-0.58(16)

Anisotropic Temperature Factors are of the form
Temp=-2*Pi*Pi*(h*h*u11*astar*astar+---+2*h*k*u12*astar*bstar+---)

Table of Atomic Bond Distances in Angstroms

O1-C1	1.223(11)	H27-C27	1.072(5)
O2-C2	1.413(11)	H28-C28	1.079(5)
O3-C16	1.462(12)	H30-C30	1.089(5)
O3-C13	1.350(8)	H31-C31	1.082(4)
O4-C18	1.432(11)	H37-C37	1.076(6)
O5-C17	1.224(12)	H38-C38	1.072(8)
O6-C32	1.437(13)	H39-C39	1.078(8)
O6-C29	1.379(8)	H40-C40	1.085(7)
O7-C34	1.431(11)	H41-C41	1.088(7)
O8-C33	1.219(11)	H43-C43	1.074(5)
O9-C48	1.428(12)	H44-C44	1.072(4)
O9-C45	1.360(8)	H46-C46	1.087(5)
O10-C50	1.429(12)	H47-C47	1.089(4)
O11-C49	1.230(11)	H53-C53	1.093(7)
O12-C64	1.461(13)	H54-C54	1.096(8)
O12-C61	1.349(9)	H55-C55	1.084(8)
C1-C2	1.520(13)	H56-C56	1.068(8)
C1-C10	1.494(10)	H57-C57	1.065(7)
C2-C3	1.520(14)	H59-C59	1.074(5)
C2-H2	1.099(9)	H60-C60	1.070(5)
C3-H3A	1.093(10)	H62-C62	1.087(5)
C3-H3B	1.087(10)	H63-C63	1.091(5)
C3-C4	1.503(13)	C4-C5	1.395(9)
C16-H16C	1.086(11)	C4-C9	1.395(10)
C16-H16A	1.120(12)	C5-C6	1.395(12)
C16-H16B	1.050(11)	C6-C7	1.395(12)
C17-C18	1.547(14)	C7-C8	1.395(12)
C17-C26	1.461(12)	C8-C9	1.395(12)
C18-C19	1.551(14)	C10-C11	1.395(8)
C18-H18	1.081(10)	C10-C15	1.395(7)
C19-H19A	1.095(11)	C11-C12	1.395(8)
C19-H19B	1.090(12)	C12-C13	1.395(7)
C19-C20	1.539(13)	C13-C14	1.395(8)
C32-H32C	1.078(11)	C14-C15	1.395(8)
C32-H32A	1.139(13)	C20-C21	1.395(10)
C32-H32B	1.048(11)	C20-C25	1.395(10)
C33-C34	1.532(13)	C21-C22	1.395(12)
C33-C42	1.487(10)	C22-C23	1.395(11)
C34-C35	1.565(15)	C23-C24	1.395(12)
C34-H34	1.070(9)	C24-C25	1.395(13)
C35-H35A	1.102(11)	C26-C27	1.395(7)
C35-H35B	1.105(11)	C26-C31	1.395(7)
C35-C36	1.526(14)	C27-C28	1.395(7)
C48-H48C	1.080(11)	C28-C29	1.395(7)
C48-H48A	1.119(12)	C29-C30	1.395(8)
C48-H48B	1.056(10)	C30-C31	1.395(8)
C49-C50	1.513(14)	C36-C37	1.395(10)
C49-C58	1.495(11)	C36-C41	1.395(10)
C50-C51	1.541(15)	C37-C38	1.395(12)
C50-H50	1.103(11)	C38-C39	1.395(11)
C51-H51A	1.089(10)	C39-C40	1.395(12)
C51-H51B	1.082(10)	C40-C41	1.395(13)

C51-C52	1.516(13)	C42-C43	1.395(7)
C64-H64C	1.092(11)	C42-C47	1.395(7)
C64-H64A	1.052(12)	C43-C44	1.395(7)
C64-H64B	1.108(12)	C44-C45	1.395(7)
H5-C5	1.066(7)	C45-C46	1.395(8)
H6-C6	1.070(7)	C46-C47	1.395(7)
H7-C7	1.084(8)	C52-C53	1.395(10)
H8-C8	1.094(8)	C52-C57	1.395(10)
H9-C9	1.090(6)	C53-C54	1.395(13)
H11-C11	1.091(5)	C54-C55	1.395(12)
H12-C12	1.084(5)	C55-C56	1.395(12)
H14-C14	1.070(5)	C56-C57	1.395(12)
H15-C15	1.077(5)	C58-C59	1.395(7)
H21-C21	1.070(6)	C58-C63	1.395(8)
H22-C22	1.066(8)	C59-C60	1.395(7)
H23-C23	1.076(8)	C60-C61	1.395(8)
H24-C24	1.090(7)	C61-C62	1.395(7)
H25-C25	1.095(7)	C62-C63	1.395(8)

Table of Atomic Bond Angles in Degrees

C16-O3-C13	118.4(7)	O3-C13-C14	124.2(5)
C32-O6-C29	116.3(7)	C12-C13-C14	120.0(4)
C48-O9-C45	118.4(7)	H14-C14-C13	118.6(5)
C64-O12-C61	118.5(7)	H14-C14-C15	121.4(5)
O1-C1-C2	117.0(8)	C13-C14-C15	120.0(5)
O1-C1-C10	121.3(8)	H15-C15-C10	121.0(5)
C2-C1-C10	121.6(7)	H15-C15-C14	119.0(5)
O2-C2-C1	108.9(7)	C10-C15-C14	120.0(4)
O2-C2-C3	109.2(8)	C19-C20-C21	122.3(7)
O2-C2-H2	110.3(8)	C19-C20-C25	117.7(8)
C1-C2-C3	111.9(8)	C21-C20-C25	120.0(7)
C1-C2-H2	107.6(8)	H21-C21-C20	120.6(8)
C3-C2-H2	108.8(8)	H21-C21-C22	119.4(7)
C2-C3-H3A	109.4(9)	C20-C21-C22	120.0(6)
C2-C3-H3B	108.9(9)	H22-C22-C21	121.4(7)
C2-C3-C4	115.7(7)	H22-C22-C23	118.6(8)
H3A-C3-H3B	108.0(8)	C21-C22-C23	120.0(7)
H3A-C3-C4	107.2(8)	H23-C23-C22	121.9(8)
H3B-C3-C4	107.3(8)	H23-C23-C24	118.1(8)
O3-C16-H16C	109.7(9)	C22-C23-C24	120.0(8)
O3-C16-H16A	108.2(8)	H24-C24-C23	121.7(8)
O3-C16-H16B	112.5(10)	H24-C24-C25	118.2(7)
H16C-C16-H16A	106.2(10)	C23-C24-C25	120.0(7)
H16C-C16-H16B	111.3(9)	H25-C25-C20	119.0(8)
H16A-C16-H16B	108.7(10)	H25-C25-C24	121.0(6)
O5-C17-C18	117.9(9)	C20-C25-C24	120.0(7)
O5-C17-C26	121.9(8)	C17-C26-C27	123.0(6)
C18-C17-C26	120.1(8)	C17-C26-C31	116.6(6)
O4-C18-C17	109.7(7)	C27-C26-C31	120.0(4)
O4-C18-C19	110.4(8)	H27-C27-C26	121.5(4)
O4-C18-H18	108.9(8)	H27-C27-C28	118.5(5)
C17-C18-C19	113.9(8)	C26-C27-C28	120.0(4)
C17-C18-H18	106.9(8)	H28-C28-C27	121.8(5)
C19-C18-H18	106.9(8)	H28-C28-C29	118.2(5)
C18-C19-H19A	109.0(9)	C27-C28-C29	120.0(4)
C18-C19-H19B	109.5(9)	O6-C29-C28	113.8(6)
C18-C19-C20	111.4(8)	O6-C29-C30	126.1(5)
H19A-C19-H19B	107.6(9)	C28-C29-C30	120.0(4)
H19A-C19-C20	109.4(9)	H30-C30-C29	121.2(4)
H19B-C19-C20	109.9(9)	H30-C30-C31	118.8(5)
O6-C32-H32C	111.0(10)	C29-C30-C31	120.0(4)
O6-C32-H32A	107.3(8)	H31-C31-C26	119.1(5)
O6-C32-H32B	113.1(9)	H31-C31-C30	120.9(5)
H32C-C32-H32A	105.3(9)	C26-C31-C30	120.0(4)
H32C-C32-H32B	112.1(10)	C35-C36-C37	122.7(7)
H32A-C32-H32B	107.4(10)	C35-C36-C41	117.3(7)
O8-C33-C34	118.2(8)	C37-C36-C41	120.0(7)
O8-C33-C42	121.2(8)	H37-C37-C36	120.9(8)
C34-C33-C42	120.6(7)	H37-C37-C38	119.1(7)
O7-C34-C33	108.9(7)	C36-C37-C38	120.0(6)
O7-C34-C35	112.0(7)	H38-C38-C37	121.2(7)

O7-C34-H34	108.8(7)	H38-C38-C39	118.8(8)
C33-C34-C35	111.3(8)	C37-C38-C39	120.0(7)
C33-C34-H34	108.6(8)	H39-C39-C38	121.5(8)
C35-C34-H34	107.2(8)	H39-C39-C40	118.4(8)
C34-C35-H35A	109.1(9)	C38-C39-C40	120.0(7)
C34-C35-H35B	108.5(9)	H40-C40-C39	121.5(8)
C34-C35-C36	113.5(8)	H40-C40-C41	118.5(7)
H35A-C35-H35B	106.1(9)	C39-C40-C41	120.0(6)
H35A-C35-C36	109.8(9)	H41-C41-C36	118.9(8)
H35B-C35-C36	109.5(9)	H41-C41-C40	121.1(6)
O9-C48-H48C	110.7(9)	C36-C41-C40	120.0(7)
O9-C48-H48A	107.8(8)	C33-C42-C43	122.4(5)
O9-C48-H48B	111.9(9)	C33-C42-C47	117.4(5)
H48C-C48-H48A	106.6(9)	C43-C42-C47	120.0(4)
H48C-C48-H48B	111.3(9)	H43-C43-C42	121.2(4)
H48A-C48-H48B	108.3(9)	H43-C43-C44	118.8(4)
O11-C49-C50	117.7(9)	C42-C43-C44	120.0(4)
O11-C49-C58	120.5(8)	H44-C44-C43	121.6(5)
C50-C49-C58	121.7(7)	H44-C44-C45	118.3(5)
O10-C50-C49	107.9(8)	C43-C44-C45	120.0(4)
O10-C50-C51	109.5(8)	O9-C45-C44	115.0(6)
O10-C50-H50	110.1(9)	O9-C45-C46	124.9(5)
C49-C50-C51	111.9(8)	C44-C45-C46	120.0(4)
C49-C50-H50	108.7(9)	H46-C46-C45	121.8(4)
C51-C50-H50	108.7(8)	H46-C46-C47	118.2(5)
C50-C51-H51A	108.9(9)	C45-C46-C47	120.0(4)
C50-C51-H51B	109.3(8)	H47-C47-C42	118.6(5)
C50-C51-C52	115.8(8)	H47-C47-C46	121.4(5)
H51A-C51-H51B	108.6(8)	C42-C47-C46	120.0(4)
H51A-C51-C52	106.7(8)	C51-C52-C53	118.2(7)
H51B-C51-C52	107.3(8)	C51-C52-C57	121.8(7)
O12-C64-H64C	109.3(9)	C53-C52-C57	120.0(7)
O12-C64-H64A	112.2(10)	H53-C53-C52	118.9(8)
O12-C64-H64B	108.5(9)	H53-C53-C54	121.1(7)
H64C-C64-H64A	110.6(10)	C52-C53-C54	120.0(6)
H64C-C64-H64B	106.6(10)	H54-C54-C53	118.0(7)
H64A-C64-H64B	109.5(10)	H54-C54-C55	122.0(8)
C3-C4-C5	120.9(7)	C53-C54-C55	120.0(7)
C3-C4-C9	119.1(7)	H55-C55-C54	117.4(8)
C5-C4-C9	120.0(7)	H55-C55-C56	122.5(8)
H5-C5-C4	121.5(7)	C54-C55-C56	120.0(8)
H5-C5-C6	118.5(6)	H56-C56-C55	117.7(8)
C4-C5-C6	120.0(6)	H56-C56-C57	122.3(7)
H6-C6-C5	122.2(7)	C55-C56-C57	120.0(7)
H6-C6-C7	117.8(8)	H57-C57-C52	121.4(7)
C5-C6-C7	120.0(7)	H57-C57-C56	118.6(6)
H7-C7-C6	122.4(8)	C52-C57-C56	120.0(6)
H7-C7-C8	117.6(8)	C49-C58-C59	119.4(6)
C6-C7-C8	120.0(8)	C49-C58-C63	120.1(5)
H8-C8-C7	121.8(8)	C59-C58-C63	120.0(4)
H8-C8-C9	118.1(7)	H59-C59-C58	121.3(5)
C7-C8-C9	120.0(7)	H59-C59-C60	118.7(5)
H9-C9-C4	118.9(7)	C58-C59-C60	120.0(4)
H9-C9-C8	121.1(6)	H60-C60-C59	121.8(5)

C4-C9-C8	120.0(6)	H60-C60-C61	118.2(4)
C1-C10-C11	121.5(5)	C59-C60-C61	120.0(4)
C1-C10-C15	118.2(6)	O12-C61-C60	123.4(5)
C11-C10-C15	120.0(4)	O12-C61-C62	116.5(5)
H11-C11-C10	118.4(4)	C60-C61-C62	120.0(4)
H11-C11-C12	121.6(5)	H62-C62-C61	122.2(5)
C10-C11-C12	120.0(4)	H62-C62-C63	117.8(5)
H12-C12-C11	118.0(5)	C61-C62-C63	120.0(4)
H12-C12-C13	122.0(5)	H63-C63-C58	118.3(4)
C11-C12-C13	120.0(5)	H63-C63-C62	121.7(5)
O3-C13-C12	115.7(6)	C58-C63-C62	120.0(4)

Torsion angles

C13	O3	C16	H16C	-178.6(12)	C13	O3	C16	H16A	-63.2(6)
C13	O3	C16	H16B	56.9(6)	C16	O3	C13	C12	-173.9(8)
C16	O3	C13	C14	10.4(5)	C29	O6	C32	H32C	-177.2(12)
C29	O6	C32	H32A	-62.6(6)	C29	O6	C32	H32B	55.8(6)
C32	O6	C29	C28	171.1(8)	C32	O6	C29	C30	-12.3(5)
C45	O9	C48	H48C	-178.3(12)	C45	O9	C48	H48A	-62.1(6)
C45	O9	C48	H48B	56.9(6)	C48	O9	C45	C44	170.5(8)
C48	O9	C45	C46	-13.2(5)	C61	O12	C64	H64C	179.1(12)
C61	O12	C64	H64A	-57.9(6)	C61	O12	C64	H64B	63.2(7)
C64	O12	C61	C60	-9.1(5)	C64	O12	C61	C62	174.2(8)
O1	C1	C2	O2	7.3(4)	O1	C1	C2	C3	-113.6(10)
O1	C1	C2	H2	126.9(11)	C10	C1	C2	O2	-169.8(10)
C10	C1	C2	C3	69.4(7)	C10	C1	C2	H2	-50.1(5)
O1	C1	C10	C11	-163.3(10)	O1	C1	C10	C15	10.1(4)
C2	C1	C10	C11	13.6(4)	C2	C1	C10	C15	-173.0(9)
O2	C2	C3	H3A	169.1(12)	O2	C2	C3	H3B	51.2(6)
O2	C2	C3	C4	-69.7(7)	C1	C2	C3	H3A	-70.2(8)
C1	C2	C3	H3B	171.9(12)	C1	C2	C3	C4	51.0(6)
H2	C2	C3	H3A	48.6(6)	H2	C2	C3	H3B	-69.3(8)
H2	C2	C3	C4	169.8(12)	C2	C3	C4	C5	-95.3(8)
C2	C3	C4	C9	82.9(7)	H3A	C3	C4	C5	27.0(4)
H3A	C3	C4	C9	-154.7(11)	H3B	C3	C4	C5	142.8(10)
H3B	C3	C4	C9	-38.9(5)	O5	C17	C18	O4	-14.2(4)
O5	C17	C18	C19	110.0(10)	O5	C17	C18	H18	-132.1(12)
C26	C17	C18	O4	168.4(11)	C26	C17	C18	C19	-67.3(7)
C26	C17	C18	H18	50.5(6)	O5	C17	C26	C27	168.0(10)
O5	C17	C26	C31	-4.8(4)	C18	C17	C26	C27	-14.7(4)
C18	C17	C26	C31	172.5(9)	O4	C18	C19	H19A	-48.0(6)
O4	C18	C19	H19B	-165.4(13)	O4	C18	C19	C20	72.9(7)
C17	C18	C19	H19A	-171.9(13)	C17	C18	C19	H19B	70.7(8)
C17	C18	C19	C20	-51.0(6)	H18	C18	C19	H19A	70.3(8)
H18	C18	C19	H19B	-47.1(6)	H18	C18	C19	C20	-168.8(13)
C18	C19	C20	C21	-84.3(8)	C18	C19	C20	C25	98.3(8)
H19A	C19	C20	C21	36.3(5)	H19A	C19	C20	C25	-141.1(11)
H19B	C19	C20	C21	154.2(11)	H19B	C19	C20	C25	-23.1(4)
O8	C33	C34	O7	-11.6(3)	O8	C33	C34	C35	112.3(10)
O8	C33	C34	H34	-130.0(12)	C42	C33	C34	O7	165.9(10)
C42	C33	C34	C35	-70.2(7)	C42	C33	C34	H34	47.5(5)
O8	C33	C42	C43	166.3(9)	O8	C33	C42	C47	-8.1(4)
C34	C33	C42	C43	-11.2(4)	C34	C33	C42	C47	174.4(9)
O7	C34	C35	H35A	-51.8(6)	O7	C34	C35	H35B	-167.0(13)
O7	C34	C35	C36	71.1(7)	C33	C34	C35	H35A	-174.0(13)
C33	C34	C35	H35B	70.8(8)	C33	C34	C35	C36	-51.1(6)
H34	C34	C35	H35A	67.5(8)	H34	C34	C35	H35B	-47.7(6)
H34	C34	C35	C36	-169.7(13)	C34	C35	C36	C37	-82.4(8)
C34	C35	C36	C41	98.4(8)	H35A	C35	C36	C37	40.1(5)
H35A	C35	C36	C41	-139.1(11)	H35B	C35	C36	C37	156.2(11)
H35B	C35	C36	C41	-23.0(4)	O11	C49	C50	O10	-6.5(4)
O11	C49	C50	C51	113.9(10)	O11	C49	C50	H50	-125.9(12)

C58	C49	C50	O10	170.2(11)	C58	C49	C50	C51	-69.3(7)
C58	C49	C50	H50	50.8(6)	O11	C49	C58	C59	-10.1(4)
O11	C49	C58	C63	162.1(9)	C50	C49	C58	C59	173.2(9)
C50	C49	C58	C63	-14.5(4)	O10	C50	C51	H51A	-50.6(6)
O10	C50	C51	H51B	-169.1(13)	O10	C50	C51	C52	69.6(7)
C49	C50	C51	H51A	-170.2(13)	C49	C50	C51	H51B	71.3(8)
C49	C50	C51	C52	-50.0(6)	H50	C50	C51	H51A	69.7(8)
H50	C50	C51	H51B	-48.8(6)	H50	C50	C51	C52	-170.1(12)
C50	C51	C52	C53	-82.0(7)	C50	C51	C52	C57	95.4(8)
H51A	C51	C52	C53	39.4(5)	H51A	C51	C52	C57	-143.2(10)
H51B	C51	C52	C53	155.7(11)	H51B	C51	C52	C57	-27.0(4)
C3	C4	C5	H5	-1.1(4)	C3	C4	C5	C6	178.2(8)
C9	C4	C5	H5	-179.3(9)	C9	C4	C5	C6	0.0(4)
C3	C4	C9	H9	2.2(4)	C3	C4	C9	C8	-178.2(8)
C5	C4	C9	H9	-179.6(9)	C5	C4	C9	C8	0.0(4)
H5	C5	C6	H6	-0.9(0)	H5	C5	C6	C7	179.3(9)
C4	C5	C6	H6	179.8(9)	C4	C5	C6	C7	0.0(4)
H6	C6	C7	H7	-1.0(0)	H6	C6	C7	C8	-179.8(10)
C5	C6	C7	H7	178.7(10)	C5	C6	C7	C8	0.0(4)
H7	C7	C8	H8	-0.1(0)	H7	C7	C8	C9	-178.8(10)
C6	C7	C8	H8	178.7(10)	C6	C7	C8	C9	0.0(4)
H8	C8	C9	H9	0.9(0)	H8	C8	C9	C4	-178.7(9)
C7	C8	C9	H9	179.6(10)	C7	C8	C9	C4	0.0(4)
C1	C10	C11	H11	-6.0(3)	C1	C10	C11	C12	173.3(7)
C15	C10	C11	H11	-179.4(7)	C15	C10	C11	C12	0.0(3)
C1	C10	C15	H15	7.6(3)	C1	C10	C15	C14	-173.5(7)
C11	C10	C15	H15	-178.9(7)	C11	C10	C15	C14	0.0(3)
H11	C11	C12	H12	1.1(0)	H11	C11	C12	C13	179.3(7)
C10	C11	C12	H12	-178.3(7)	C10	C11	C12	C13	0.0(3)
H12	C12	C13	O3	2.3(3)	H12	C12	C13	C14	178.2(7)
C11	C12	C13	O3	-175.9(7)	C11	C12	C13	C14	0.0(3)
O3	C13	C14	H14	-4.4(3)	O3	C13	C14	C15	175.6(7)
C12	C13	C14	H14	-180.0(7)	C12	C13	C14	C15	0.0(3)
H14	C14	C15	H15	-1.1(0)	H14	C14	C15	C10	180.0(7)
C13	C14	C15	H15	178.9(7)	C13	C14	C15	C10	0.0(3)
C19	C20	C21	H21	3.6(4)	C19	C20	C21	C22	-177.3(9)
C25	C20	C21	H21	-179.1(9)	C25	C20	C21	C22	0.0(4)
C19	C20	C25	H25	-1.9(4)	C19	C20	C25	C24	177.4(9)
C21	C20	C25	H25	-179.3(9)	C21	C20	C25	C24	0.0(4)
H21	C21	C22	H22	-0.3(0)	H21	C21	C22	C23	179.1(9)
C20	C21	C22	H22	-179.4(9)	C20	C21	C22	C23	0.0(4)
H22	C22	C23	H23	-0.9(0)	H22	C22	C23	C24	179.4(10)
C21	C22	C23	H23	179.6(10)	C21	C22	C23	C24	0.0(4)
H23	C23	C24	H24	-0.7(0)	H23	C23	C24	C25	-179.7(10)
C22	C23	C24	H24	179.0(10)	C22	C23	C24	C25	0.0(4)
H24	C24	C25	H25	0.3(0)	H24	C24	C25	C20	-179.0(9)
C23	C24	C25	H25	179.3(10)	C23	C24	C25	C20	0.0(4)
C17	C26	C27	H27	8.6(4)	C17	C26	C27	C28	-172.5(7)
C31	C26	C27	H27	-178.9(7)	C31	C26	C27	C28	0.0(3)
C17	C26	C31	H31	-5.9(4)	C17	C26	C31	C30	173.0(7)
C27	C26	C31	H31	-178.9(7)	C27	C26	C31	C30	0.0(3)
H27	C27	C28	H28	0.4(0)	H27	C27	C28	C29	178.9(7)
C26	C27	C28	H28	-178.5(7)	C26	C27	C28	C29	0.0(3)
H28	C28	C29	O6	-4.6(3)	H28	C28	C29	C30	178.6(7)

C27	C28	C29	O6	176.8(7)
O6	C29	C30	H30	2.8(3)
C28	C29	C30	H30	179.3(7)
H30	C30	C31	H31	-0.4(0)
C29	C30	C31	H31	178.9(7)
C35	C36	C37	H37	2.6(4)
C41	C36	C37	H37	-178.2(9)
C35	C36	C41	H41	-1.2(4)
C37	C36	C41	H41	179.6(9)
H37	C37	C38	H38	-1.7(0)
C36	C37	C38	H38	180.0(9)
H38	C38	C39	H39	-1.6(0)
C37	C38	C39	H39	178.4(10)
H39	C39	C40	H40	0.2(0)
C38	C39	C40	H40	178.7(10)
H40	C40	C41	H41	1.7(0)
C39	C40	C41	H41	-179.5(9)
C33	C42	C43	H43	7.2(3)
C47	C42	C43	H43	-178.5(7)
C33	C42	C47	H47	-4.6(3)
C43	C42	C47	H47	-179.1(7)
H43	C43	C44	H44	0.2(0)
C42	C43	C44	H44	-178.3(7)
H44	C44	C45	O9	-5.1(3)
C43	C44	C45	O9	176.5(7)
O9	C45	C46	H46	3.1(3)
C44	C45	C46	H46	179.3(7)
H46	C46	C47	H47	-0.2(0)
C45	C46	C47	H47	179.1(7)
C51	C52	C53	H53	-0.8(4)
C57	C52	C53	H53	-178.2(9)
C51	C52	C57	H57	3.1(4)
C53	C52	C57	H57	-179.6(9)
H53	C53	C54	H54	-1.5(0)
C52	C53	C54	H54	-179.6(10)
H54	C54	C55	H55	-1.8(0)
C53	C54	C55	H55	178.5(10)
H55	C55	C56	H56	-0.3(0)
C54	C55	C56	H56	178.2(10)
H56	C56	C57	H57	1.6(0)
C55	C56	C57	H57	179.6(9)
C49	C58	C59	H59	-8.2(3)
C63	C58	C59	H59	179.5(7)
C49	C58	C63	H63	6.8(3)
C59	C58	C63	H63	179.0(7)
H59	C59	C60	H60	0.5(0)
C58	C59	C60	H60	180.0(7)
H60	C60	C61	O12	3.4(3)
C59	C60	C61	O12	-176.6(7)
O12	C61	C62	H62	-1.6(3)
C60	C61	C62	H62	-178.5(7)
H62	C62	C63	H63	-0.4(0)
C61	C62	C63	H63	-178.9(7)

C27	C28	C29	C30	0.0(3)
O6	C29	C30	C31	-176.4(7)
C28	C29	C30	C31	0.0(3)
H30	C30	C31	C26	-179.3(7)
C29	C30	C31	C26	0.0(3)
C35	C36	C37	C38	-179.2(9)
C41	C36	C37	C38	0.0(4)
C35	C36	C41	C40	179.3(9)
C37	C36	C41	C40	0.0(4)
H37	C37	C38	C39	178.3(9)
C36	C37	C38	C39	0.0(4)
H38	C38	C39	C40	-180.0(10)
C37	C38	C39	C40	0.0(4)
H39	C39	C40	C41	-178.5(10)
C38	C39	C40	C41	0.0(4)
H40	C40	C41	C36	-178.7(9)
C39	C40	C41	C36	0.0(4)
C33	C42	C43	C44	-174.3(7)
C47	C42	C43	C44	0.0(3)
C33	C42	C47	C46	174.5(7)
C43	C42	C47	C46	0.0(3)
H43	C43	C44	C45	178.6(7)
C42	C43	C44	C45	0.0(3)
H44	C44	C45	C46	178.4(7)
C43	C44	C45	C46	0.0(3)
O9	C45	C46	C47	-176.1(7)
C44	C45	C46	C47	0.0(3)
H46	C46	C47	C42	-179.3(7)
C45	C46	C47	C42	0.0(3)
C51	C52	C53	C54	177.4(9)
C57	C52	C53	C54	0.0(4)
C51	C52	C57	C56	-177.3(8)
C53	C52	C57	C56	0.0(4)
H53	C53	C54	C55	178.1(10)
C52	C53	C54	C55	0.0(4)
H54	C54	C55	C56	179.6(10)
C53	C54	C55	C56	0.0(4)
H55	C55	C56	C57	-178.5(10)
C54	C55	C56	C57	0.0(4)
H56	C56	C57	C52	-178.1(9)
C55	C56	C57	C52	0.0(4)
C49	C58	C59	C60	172.2(7)
C63	C58	C59	C60	0.0(3)
C49	C58	C63	C62	-172.2(7)
C59	C58	C63	C62	0.0(3)
H59	C59	C60	C61	-179.5(7)
C58	C59	C60	C61	0.0(3)
H60	C60	C61	C62	-180.0(7)
C59	C60	C61	C62	0.0(3)
O12	C61	C62	C63	176.9(7)
C60	C61	C62	C63	0.0(3)
H62	C62	C63	C58	178.5(7)
C61	C62	C63	C58	0.0(3)